RECENT ADVANCES IN CONTINUOUS CULTIVATION

EDITED BY: Manfred Zinn, Thomas Egli, Christoph Herwig and Atul Narang
PUBLISHED IN: Frontiers in Bioengineering and Biotechnology

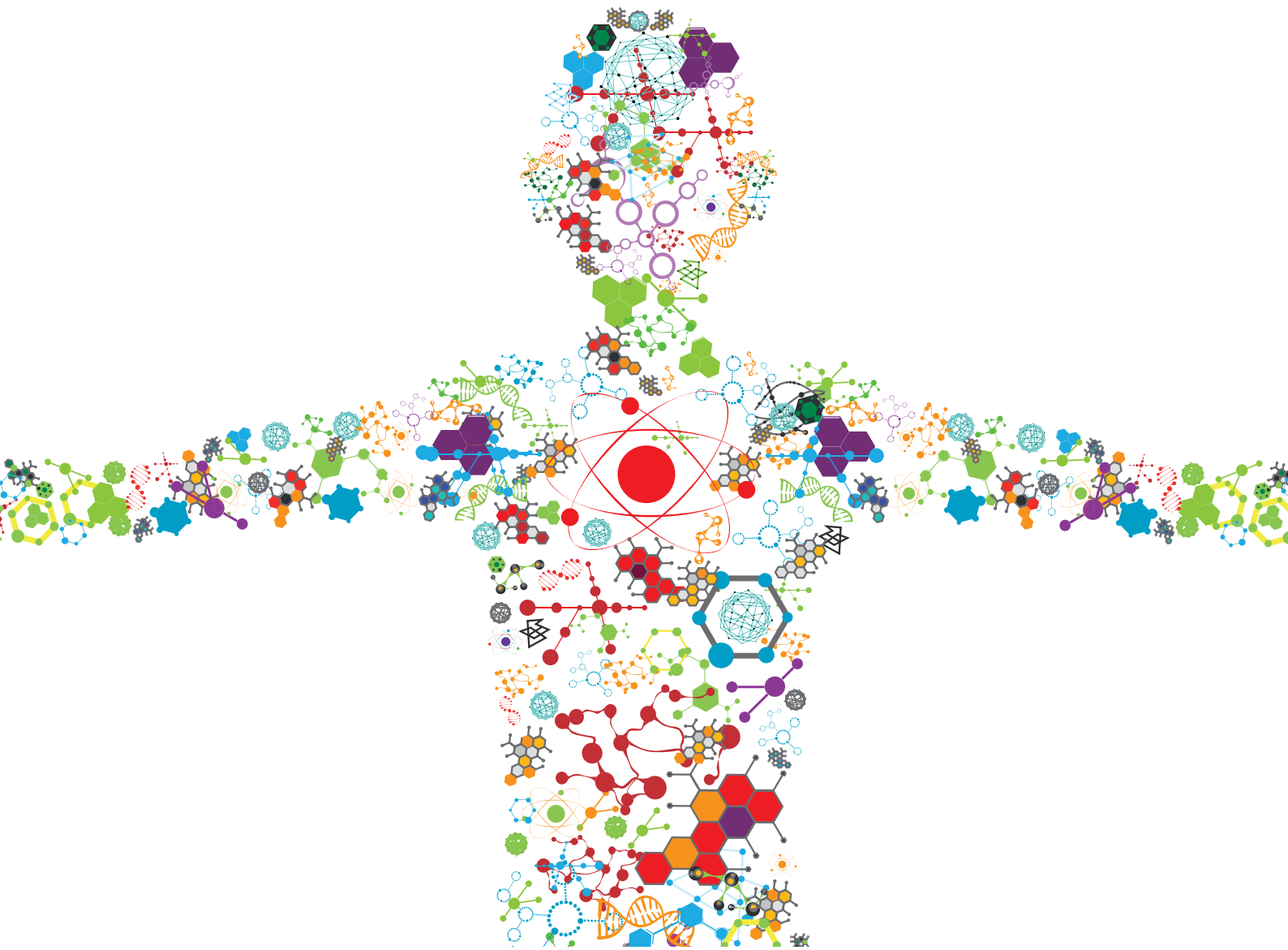

frontiers Research Topics

frontiers

ISSN 1664-8714
ISBN 978-2-88966-649-2
DOI 10.3389/978-2-88966-649-2

About Frontiers

Frontiers is more than just an open-access publisher of scholarly articles: it is a pioneering approach to the world of academia, radically improving the way scholarly research is managed. The grand vision of Frontiers is a world where all people have an equal opportunity to seek, share and generate knowledge. Frontiers provides immediate and permanent online open access to all its publications, but this alone is not enough to realize our grand goals.

Frontiers Journal Series

The Frontiers Journal Series is a multi-tier and interdisciplinary set of open-access, online journals, promising a paradigm shift from the current review, selection and dissemination processes in academic publishing. All Frontiers journals are driven by researchers for researchers; therefore, they constitute a service to the scholarly community. At the same time, the Frontiers Journal Series operates on a revolutionary invention, the tiered publishing system, initially addressing specific communities of scholars, and gradually climbing up to broader public understanding, thus serving the interests of the lay society, too.

Dedication to Quality

Each Frontiers article is a landmark of the highest quality, thanks to genuinely collaborative interactions between authors and review editors, who include some of the world's best academicians. Research must be certified by peers before entering a stream of knowledge that may eventually reach the public - and shape society; therefore, Frontiers only applies the most rigorous and unbiased reviews.
Frontiers revolutionizes research publishing by freely delivering the most outstanding research, evaluated with no bias from both the academic and social point of view. By applying the most advanced information technologies, Frontiers is catapulting scholarly publishing into a new generation.

What are Frontiers Research Topics?

Frontiers Research Topics are very popular trademarks of the Frontiers Journals Series: they are collections of at least ten articles, all centered on a particular subject. With their unique mix of varied contributions from Original Research to Review Articles, Frontiers Research Topics unify the most influential researchers, the latest key findings and historical advances in a hot research area! Find out more on how to host your own Frontiers Research Topic or contribute to one as an author by contacting the Frontiers Editorial Office: frontiersin.org/about/contact

RECENT ADVANCES IN CONTINUOUS CULTIVATION

Topic Editors:
Manfred Zinn, HES-SO Valais-Wallis, Switzerland
Thomas Egli, ETH Zürich, Switzerland
Christoph Herwig, Vienna University of Technology, Austria
Atul Narang, Indian Institute of Technology Delhi, India

Citation: Zinn, M., Egli, T., Herwig, C., Narang, A., eds. (2021). Recent Advances in Continuous Cultivation. Lausanne: Frontiers Media SA.
doi: 10.3389/978-2-88966-649-2

Table of Contents

frontiers in Bioengineering and Biotechnology

EDITORIAL
published: 22 February 2021
doi: 10.3389/fbioe.2021.641249

Editorial: Recent Advances in Continuous Cultivation

Manfred Zinn[1]*, *Thomas Egli*[2,3], *Christoph Herwig*[4,5,6] *and Atul Narang*[7]

[1] Institute of Life Technology, School of Engineering, University of Applied Sciences Western Switzerland, Sion, Switzerland, [2] Department of Environmental Systems Science, Swiss Federal Institute of Technology, Zurich, Switzerland, [3] Microbes-in-Water GmbH, Feldmeilen, Switzerland, [4] Christian Doppler Laboratory for Mechanistic and Physiological Methods for Improved Bioprocesses, Vienna, Austria, [5] Competence Center CHASE GmbH, Linz, Austria, [6] Research Area Biochemical Engineering, Institute of Chemical Engineering, Vienna, Austria, [7] Department of Biochemical Engineering and Biotechnology, Indian Institute of Technology Delhi, New Delhi, India

Keywords: chemostat, continuous culture, cell physiology, growth conditions, cultivation, growth medium, process analytical technology, growth kinetics

Editorial on the Research Topic

Recent Advances in Continuous Cultivation

The scientific work by Monod (1950) and Novick and Szilard (1950a,b) on continuous cultivation in the 1950s and their early analyses and applications by the "Porton" and the "Prague" groups (Herbert et al., 1956; Malek et al., 1958; Pirt and Callow, 1960; Herbert, 1961) evened the path toward a better understanding of the cell physiology of microorganisms. The chemostat, where all physicochemical growth conditions can be kept constant, soon became a very important research tool to study the nutritional needs as a function of the specific growth rate of microorganisms. The recent evolution of new disciplines in systems biology offering a plethora of novel, scientific methods (e.g., transcriptional analysis, proteomics, metabolomics, and detailed metabolic flux analysis) played an important role in gaining a better understanding of the influence of the cell physiology and product formation.

To date, industry is investing in the development of continuous production processes, because of their better volumetric productivity and hence lower equipment cost. Moreover, powerful methods have been developed for continuous medium preparation and product purification (e.g., isolation of recombinant proteins in simulated moving bed chromatography). Finally, a continuous process can be run for an extended period and thus results in a more desired, ideally time invariant, and reproducible product quality. In future, more continuous bioprocesses will be used to produce pharmaceuticals, since the American Food and Drug Administration recently approved drugs produced by continuous cultivation (Matsunami et al., 2018). This change has been made possible because of the good experiences with their initiative Quality by Design (QbD) and the real-time control of cultivations using Process Analytical Technology (PAT).

The goal of this electronic article collection is to give an overview on recent scientific advances in continuous cultivation. In their review article, Nieto-Taype et al. summarize the potential of continuous cultivations of *Pichia pastoris* (*Komagataella phaffii*) with a particular focus on closed feed-back loop control using PAT. Typical examples are the turbidostat (cell density controlled), nutristat (nutrient concentration controlled), and among others, the pH-auxostat, where the substrate consumption changes the pH and thus triggers a pH changing substrate feed. In general, the cells cultured under these conditions are growing at almost maximum specific growth rate (μ_{max}). Other interesting applications of continuous cultivation are changestats, where the dilution rate is continuously increased (accelerostats or A-stats), decreased (deceleration-stats or De-stats), or kept constant with a continuous change of another parameter (e.g., medium composition). A large potential of producing secondary metabolites and products is the retentostat, where all biomass is retained in a bioreactor and where the specific growth rate is practically zero.

Edited and reviewed by:
Eugénio Campos Ferreira, University of Minho, Portugal

***Correspondence:**
Manfred Zinn
manfred.zinn@hevs.ch

Specialty section:
This article was submitted to Bioprocess Engineering, a section of the journal Frontiers in Bioengineering and Biotechnology

Received: *13 December 2020*
Accepted: *19 January 2021*
Published: *22 February 2021*

Citation:
Zinn M, Egli T, Herwig C and Narang A (2021) Editorial: Recent Advances in Continuous Cultivation. Front. Bioeng. Biotechnol. 9:641249. doi: 10.3389/fbioe.2021.641249

Adamberg et al. applied the above described changestat approach to assess the adaptation of a human gut microbiota in A-stats and D-stats. The influence of the dilution rate (D) was tested either starting with steady-states at $D = 0.05\ h^{-1}$ or $D = 0.2\ h^{-1}$ and increasing or decreasing the dilution rate to $D = 0.05\ h^{-1}$ or $D = 0.2\ h^{-1}$, respectively. Interestingly, the detected population distribution was consistent and confirmed the fact that in continuous cultivation the Monod constant (Ks) plays a decisive role in the population dynamics. Finally, this finding is important to enable an industrial cultivation of multi-strain probiotics and fecal transplantation mixtures.

Barbera et al. describe the powerful approach of the chemostat cultivation to determine the necessary growth kinetics of the diazotrophic cyanobacterium *Anabaena* PCC7122 t model growth. The traditional batch approach was not appropriate, since along with the increase of the cell density, the average illumination is reduced and thus the metabolism is significantly affected. However, using small photobioreactors operated in a continuous mode, Barbera et al. were able to determine μ_{max} and the half saturation constant for nitrogen (K_N). They also could show that the specific maintenance rate was influenced by the medium composition and the illumination intensity supplied to the culture.

Velu et al. investigated the potential of continuous outdoor cultures of the cyanobacterium *Tolypothrix* sp. by experimentally simulating the remediation of waste carbon dioxide (flue gas) and metal containing ash dam water from coal-fired power plants that are typically found in Australia. The entire process was economically feasible when the remediation was combined with the production of food-grade phycocyanin alone or in combination with biomass production as biofertilizer using either vertical or raceway suspension cultures.

The potential of the acetogenic bacterium *Clostridium autoethanogenum* to generate biofuel and chemicals from CO_2 and H_2 was assessed by Heffernan et al. using chemostat cultivations. The authors combined their experimental approach with a metabolic flux model and were thus able to optimize the conversion efficiency by supplementing the culture with CO. In future, this data set may be used to favor biosynthesis of a particular cell product.

Many physiological studies have shown that recombinant plasmids containing antibiotic resistance as selection marker may get lost without antibiotic selection, which renders this expression system failure prone and more expensive because of the need for continuous addition of antibiotics. However, new techniques, like CRISPR/CAS9 and related methods guarantee a better genetic stability. Nevertheless, the natural selection of better adapted cells (natural mutants; Novick and Szilard, 1950b) is leading to change in population distribution favoring the cells with a lower genetic burden. Because of such a population shift, the productivity may significantly be reduced or even lost completely. Kopp, Slouka et al. propose to evaluate the dynamic feeding and selection that takes place in the recently developed segregostat and also give an overview on existing online monitoring tools for *Escherichia coli*.

In industry, the product synthesis is frequently done in fed-batch cultivations in a phase separated manner, meaning the biomass formation is followed by the induction of genes of interest during the production phase. This set-up can also be established in a continuous manner by using two-stage chemostats. Kopp, Kolkmann et al. exemplified such recombinant protein production (RPP) in *Escherichia coli* in a two-stage chemostat using glycerol as a carbon source in the first stage and glycerol and lactose as inducers replacing IPTG in the second stage. The space-time-yield could be increased by a factor of 100 in comparison to a single-stage chemostat cultivation.

This continuous two-stage cultivation technique has also been implemented in research studies. Hanik et al. reported the production of tailor-made medium chain length poly(3-hydroxyalkanoate) (mcl-PHA) in two-stage, parallel chemostat cultivations. In the first stage (one bioreactor) *Pseudomonas putida* was grown and in the second chemostat stage consisting of 4 parallel chemostats the substrates for mcl-PHA production (phenylvaleric and decanoic acids) were added. This approach allowed a faster identification of the design window for tailor-made PHA production.

Tapia et al. developed a two-stage chemostat cultivation technique in order to assess the viral dynamics and the interaction of defective interfering particles (DIPs) of influenza A virus with the canine cell line MDCK.SU2. The design of a mathematical model enabled the interpretation of the observed cell and viral oscillations in the second chemostat stage. It was concluded that continuous two-stage cultivations could be efficiently used to produce DIPs.

AUTHOR CONTRIBUTIONS

MZ has drafted the manuscript and submitted in final form. TE, CH, and AN have revised the manuscript draft. All authors contributed to the article and approved the submitted version.

FUNDING

This work was financed by the University of Applied Sciences and Arts Western Switzerland, the Swiss Universities, the Christian Doppler Society, Austria, Microbes-in-water, Switzerland, and by the Department of Science and Technology, India.

ACKNOWLEDGMENTS

The Editors thank all authors who have contributed to this special issue. We are happy for being able to document with this collection of articles the latest promising scientific advancement to leverage the large potential of continuous cultivation and to finally assess, control, and optimize product formation in bioprocesses.

REFERENCES

Herbert, D. (1961). A theoretical analysis of continuous culture systems. *Soc. Chem. Industry Monogr.* 12, 21–53.

Herbert, D., Elsworth, R., and Telling, R. C. (1956). The continuous culture of bacteria; a theoretical and experimental study. *Microbiology* 14, 601–622. doi: 10.1099/00221287-14-3-601

Malek, I. (1958) "The physiological state of microorganisms during continuous culture" in *Continuous Cultivation of Microorganisms: A Symposium* (Prague: Publishing House of the Czechoslovak Academy of Sciences).

Matsunami, K., Miyano, T., Arai, H., Nakagawa, H., Hirao, M., and Sugiyama, H. (2018). Decision support method for the choice between batch and continuous technologies in solid drug product manufacturing. *Ind. Eng. Chem. Res*. 57, 9798–9809. doi: 10.1021/acs.iecr.7b05230

Monod, J. (1950). La technique de culture continue; théorie et applications. *Ann. Inst. Pasteur* 79, 390–410.

Novick, A., and Szilard, L. (1950a). Description of the chemostat. *Science* 112, 715–716. doi: 10.1126/science.112.2920.715

Novick, A., and Szilard, L. (1950b). Experiments with the chemostat on spontaneous mutations of bacteria. *Proc. Natl. Acad. Sci*. 36, 708–719. doi: 10.1073/pnas.36.12.708

Pirt, S. J., and Callow, D. S. (1960). Studies of the growth of *Penicillium chrysogenum* in continuous flow culture with reference to penicillin production. *J. Appl. Bacteriol.* 23, 87–98. doi: 10.1111/j.1365-2672.1960.tb00181.x

Conflict of Interest: The authors declare that the research was conducted in the absence of any commercial or financial relationships that could be construed as a potential conflict of interest.

frontiers in Bioengineering and Biotechnology

ORIGINAL RESEARCH
published: 17 October 2019
doi: 10.3389/fbioe.2019.00274

Continuous Cultivation as a Method to Assess the Maximum Specific Growth Rate of Photosynthetic Organisms

Elena Barbera[1,2], *Alessia Grandi*[1], *Lisa Borella*[2], *Alberto Bertucco*[2] *and Eleonora Sforza*[1]*

[1] *Interdepartmental Center Giorgio Levi Cases, University of Padova, Padova, Italy,* [2] *Department of Industrial Engineering DII, University of Padova, Padova, Italy*

Modeling the growth of photosynthetic organisms is challenging, due to the complex role of light, which can be limiting because of self-shading, or photoinhibiting in the case of high intensities. A case of particular interest is represented by nitrogen-fixing cyanobacteria, whose growth is controlled not only by the light intensity, but also by the availability of atmospheric nitrogen in the liquid medium. The determination of the maximum specific growth rate is often affected by many variables that, in batch growth systems, may change significantly. On the other hand, in a continuous system, once the steady state is reached the values of all the process variables remain constant, including the biomass concentration and the specific light supply rate. In this work, the diazotrophic cyanobacterium *Anabaena* PCC 7122 was cultivated in continuous photobioreactors, to investigate the role of nitrogen, light and residence time on growth kinetics, and to retrieve the value of the maximum specific growth rate of this organism. In addition, the kinetic parameters for temperature and the half saturation constant for nitrogen (3 mg L^{-1}) were measured by respirometric tests. Based on the results of continuous experiments, the specific maintenance rate was found to depend on the light intensity supplied to the reactor, ranging between 0.5 and 0.8 d^{-1}. All these parameters were used to develop a kinetic model able to describe the biomass growth in autotrophic conditions. The maximum specific growth rate could hence be determined by applying the kinetic model in the material balances of the continuous photobioreactor, and resulted equal to 8.22 ± 0.69 d^{-1}.

Keywords: cyanobacteria, *Anabaena* PCC7122, kinetic model, respirometry, continuous photobioreactors

OPEN ACCESS

Edited by:
Atul Narang,
Indian Institute of Technology Delhi, India

Reviewed by:
Ernani Pinto,
University of São Paulo, Brazil
Ankush Karemore,
Georgia Institute of Technology, United States

***Correspondence:**
Eleonora Sforza
eleonora.sforza@unipd.it

Specialty section:
This article was submitted to Bioprocess Engineering, a section of the journal Frontiers in Bioengineering and Biotechnology

Received: *09 July 2019*
Accepted: *01 October 2019*
Published: *17 October 2019*

Citation:
Barbera E, Grandi A, Borella L, Bertucco A and Sforza E (2019) Continuous Cultivation as a Method to Assess the Maximum Specific Growth Rate of Photosynthetic Organisms. Front. Bioeng. Biotechnol. 7:274. doi: 10.3389/fbioe.2019.00274

INTRODUCTION

Photosynthetic microorganisms, such as microalgae and cyanobacteria, have recently gained researchers' interest due to their great potentialities. For example, they can double their cells even 100 times faster than terrestrial plants (Lam et al., 2012) and require significantly less area to grow with respect to other crops thanks to their high photosynthetic efficiency per unit surface (Darvehei et al., 2018). Moreover, they offer a large number of potential applications: the biomass can be used directly (e.g., in aquaculture), or in environmental applications (e.g., waste water treatment, CO_2 mitigation and biofuel production), or alternatively high-value compounds can be extracted (e.g., pigments, vitamins) (Fernandes et al., 2015).

Large-scale cultivation of microalgae and cyanobacteria to produce bioproducts and biofuels has greatly increased over the last years (Khan et al., 2018). However, there are still many challenges to face. The most important is represented by the need to increase the process profitability, which is mainly influenced by the biomass productivity. In order to maximize the productivity, the process operating conditions must be optimized and strictly controlled. An important contribution is given by mathematical models that take into account the effect of each process variable (light, temperature, residence time, etc.) for the estimation of key production parameters (biomass growth rate, productivity, etc.) (Darvehei et al., 2018). In addition, they can be used to bridge the existing gap between lab-scale observations, on which prediction of the growth on large scale is based, and the industrial-scale reality (Bernard et al., 2015).

However, modeling the growth of photosynthetic organisms, as well as control and optimization of the process, is challenging, even more than for bacterial or yeast bioprocesses. This is mainly due to higher complexity of their cells and the wide range of mechanisms they use to respond to, or protect themselves from changes in light intensity, temperature and other environmental factors (Bernard et al., 2015).

One of the most important parameters to be determined is the maximum specific growth rate (μ_{max}). In general, it is evaluated by cultivating the microorganism in batch systems and subsequently elaborating the experimental data obtained during the exponential phase of growth. However, it is important to notice that the value of μ_{max} determined this way is affected by the experimental conditions, such as light intensity, temperature, pH and medium composition, which are not constant during the growth since biomass, substrates and products concentrations all change exponentially (Stanbury et al., 2016). In particular, the actual light perceived by the cells drops along with the increase of biomass concentration. In this way, the microorganism cannot adapt to the environment in which it is growing, since the adaptation process is not instantaneous (Trilli, 1990). Therefore, it is very difficult to relate "cause and effect" by growing the microorganism in batch systems.

On the other hand, in a continuous system, the growth rate is controlled by the dilution rate (Stanbury et al., 2016) and, once the steady state is reached, the values of all the process variables remain constant, including the biomass and substrate concentrations, and especially the specific light supply rate. Moreover, the adaptation process is no longer a problem because the microorganism is let to adapt to the growing conditions during the transient phase. This allows a quantitative assessment of the effect of the operating variables on the performances of the culture.

In this work, we propose a new approach that combines the use of cultivation in continuous systems and respirometric tests to determine the kinetic parameters of photosynthetic microorganisms' growth (Sforza et al., 2019). In particular, it was applied to study the growth of the nitrogen-fixing cyanobacterium *Anabaena* PCC 7122, which is not only affected by the light intensity, but also by the liquid solubility of atmospheric nitrogen, that controls its availability in the culture medium. The cultivation of diazotrophic cyanobacteria can find promising applications toward the development of a sustainable agriculture (Singh and Datta, 2007), or in the production of valuable pigments, such as phycocyanin (Moreno et al., 1995, 2003), while not requiring nitrogen fertilizers inputs. However, the approach could be applied to other photosynthetic microorganisms as well.

The cyanobacterium was cultivated in continuous photobioreactors at different incident light intensities with and without additional supply of nitrates, in order to investigate the role of nitrogen, together with light and residence time, on growth kinetics. The experimental results obtained were elaborated to retrieve the value of the specific maintenance rate (Gons and Mur, 1980). The kinetic parameters describing the effect of temperature and the half-saturation constant of nitrogen were instead measured by means of respirometric tests. All these parameters were combined in a comprehensive kinetic model able to describe the biomass growth in autotrophic conditions. The maximum specific growth rate μ_{max} could finally be determined by applying the developed kinetic model in the material balances of the continuous reactor, for all the experimental conditions investigated.

MATERIALS AND METHODS

Experimental Strain and Culture Medium

The photosynthetic organism used in this work is *Anabaena* PCC 7122, purchased from the Pasteur Culture Collection of Cyanobacteria, Paris (France). *Anabaena* PCC 7122, also known as *Anabaena cylindrica*, is a diazotrophic filamentous cyanobacterium forming heterocysts (i.e., specific cells where the nitrogen fixation is performed) (Fogg, 1944; Allen and Arnon, 1955), and which does not produce toxins (Phillips and Roberts, 1985; Quiblier et al., 2013). This strain was selected as, in preliminary screening tests, it showed good growth and N-fixation performances compared to other diazotrophic species. The cyanobacterium was maintained in 250 mL Erlenmeyer flasks placed in an orbital shaker, under a continuous light intensity of 75 μmol m^{-2} s^{-1} and ambient temperature. The culture media used in continuous cultivation experiments were modified BG11 and $BG11_0$ (i.e., without nitrogen salts), with a final composition as reported in the Supplementary materials (**Table S1**). In addition, the media were supplied with 2.5 g L^{-1} of $NaHCO_3$ to obtain a buffered system with the CO_2-air gas mixture (section Experimental Setup) and maintain the pH within the optimal interval of 7.5–8.

Experimental Setup

All the experiments were carried out in vertical flat-panel polycarbonate photobioreactors having a working volume (V_R) of 350 mL and an irradiated surface (A_{PBR}) of 87.5 cm^2. The photobioreactor (PBR) (**Figure 1**) was specifically designed for the cultivation of this filamentous cyanobacterium. Since it has a high tendency to aggregate and to form clusters, a thickness of 4 cm was chosen to allow a better stirring of the culture. A thin

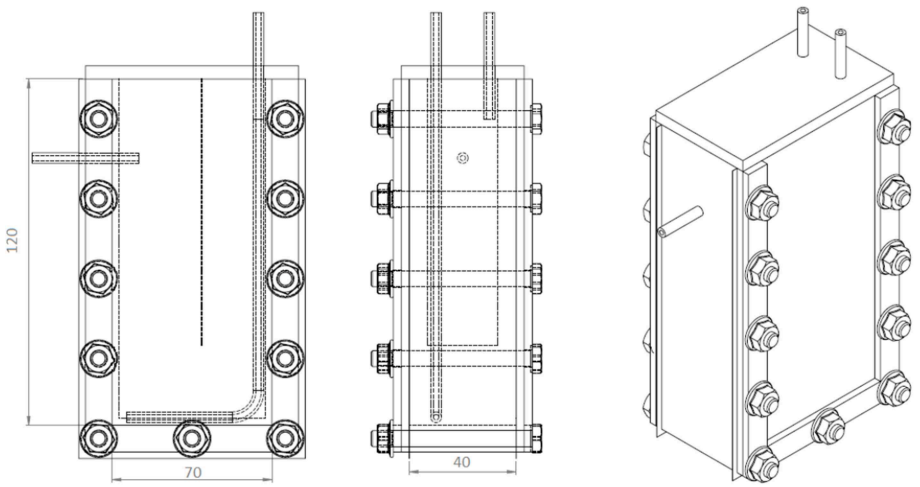

FIGURE 1 | Scheme of the PBR used for the continuous growth experiments. In the first sketch, the dotted vertical line represents the baffle.

baffle was inserted to avoid short-circuiting of the inlet medium flow rate, which was fed from the top.

The mixing was ensured by both a stirring magnet placed at the bottom of the reactor and the bubbling of CO_2-enriched air (5% v/v), sparged from the bottom at a flowrate of 1 L h^{-1}. The mixing condition was checked by means of tracer experiments, that allow to consider such a reactor as a completely stirred tank one (CSTR) (Sforza et al., 2014a, 2015). Accordingly, the specific growth rate μ (d^{-1}) is equal to the dilution rate D, which is the inverse of the residence time τ (d) according to:

$$\mu = D = \frac{1}{\tau} \tag{1}$$

Hence, by changing the residence time, different growth rates can be imposed to the culture.

Fresh inlet BG11 or $BG11_0$ was continuously fed by means of a tunable peristaltic pump (120S, Watson Marlow, USA), that allows regulating the inlet flow rate Q (mL d^{-1}). The reactor volume was kept constant by an overflow tube, from which the biomass was constantly withdrawn. Accordingly, the residence time of the culture inside the PBR was calculated as:

$$\tau = \frac{V_R}{Q} \tag{2}$$

The temperature was kept constant at T = 24 ± 1°C, in a refrigerated incubator. Continuous artificial white light was provided by a LED lamp (Photon System Instruments, SN-SL 3500-22). The light intensities at the front and back surfaces of the PBR were measured with a photoradiometer (HD 2101.1, Delta Ohm), which quantifies the PAR (Photosynthetically Active Radiation, 400–700 nm).

The reactor was started up in batch operation mode, inoculating the cyanobacterium at initial OD_{750} = 0.3 (corresponding to ∼0.1 g L^{-1} dry weight). Once a sufficient biomass concentration was reached (about 1 g L^{-1}) the feed peristaltic pump was switched on. When changing any experimental conditions (i.e., residence time or incident light intensity), a transient period was observed (7–10 d), after which a stable steady-state was reached. For each condition, steady state was maintained for at least 5 days, during which biomass samples were taken twice a day, and the corresponding experimental values were averaged accordingly.

Analytical Procedures and Calculations

The biomass concentration in the PBR was monitored daily by both optical density at 750 nm (OD_{750}) and dry weight (c_x, g L^{-1}) measurements. OD_{750} was measured with a UV-Visible double beam spectrophotometer (UV1900, by Shimadzu, Japan). The dry weight was determined by filtering 10 mL of culture sample on previously dried 0.45 μm nitrocellulose filters. The filters were then dried at 105°C in a laboratory oven for at least 2 h. The biomass volumetric and areal productivities were then calculated according to:

$$P_{x,V}\left(\frac{g}{L{\cdot}d}\right) = \frac{c_x}{\tau} \tag{3}$$

Once the steady-state was reached, the number of heterocysts was experimentally counted with a Bürker chamber, in order to compare their concentration when the cyanobacterium was grown with or without nitrates feed. Moreover, at steady-state, the experimental values of the specific light supply rate I_{sp} (i.e., the amount of light supplied per unit mass of biomass and unit time) were determined according to:

$$I_{sp}\left(\frac{mmol}{g{\cdot}d}\right) = \frac{I_0}{C_x\, W} \tag{4}$$

where I_0 is the incident light intensity at the front of the PBR and W is the PBR width (0.04 m).

Kinetic Model Description

According to the result of elemental analysis performed on dried biomass of *Anabaena* PCC 7122, its chemical formula was determined and, thus, the corresponding autotrophic growth stoichiometry could be written as follows:

$$\begin{aligned} 0.2518\, H_2O \; &+ \; 0.0202\, N_2 + 0.2314\, CO_2 \\ &+ \; 0.0018\, H_2PO_4^- + 0.0018\, HPO_4^{2-} \\ &\rightarrow \; C_{0.2314}H_{0.5036}O_{0.2210}N_{0.0404}P_{0.0036} \\ &+ \; 0.2513\, O_2 + 0.0054\, OH^- \end{aligned}$$

According to photosynthesis and nitrogen-fixation processes, water, atmospheric nitrogen, carbon dioxide and phosphates are consumed to produce new biomass and release oxygen.

The equation describing the autotrophic microalgal growth rate (r_x, g L^{-1} d^{-1}) can be written as a function of biomass concentration (c_x, g L^{-1}), the maximum specific growth rate ($\mu_{\max}$, d^{-1}), temperature ($\Phi(T)$), specific light ($f(I_{sp})$) and the most limiting nutrient that, in this case, is nitrogen ($f(N)$). Moreover, the kinetic model takes into account the specific maintenance rate (μ_e), i.e., the loss of biomass due to turnover of cellular components and cell repair, which represents a negative term, thus reducing the net biomass growth rate, according to Equation (5):

$$r_x = c_x \cdot \mu_{\max} \cdot \Phi(T) \cdot f(N) \cdot f(I_{sp}) - \mu_e \cdot c_x \tag{5}$$

The term accounting for the effect of temperature was calculated according to the model proposed by Bernard et al. (2015) based on the so-called cardinal temperature model with inflection (CTMI) (Rosso et al., 1993):

$$\mu(T) = \begin{cases} 0 & \text{for } T < T_{\min} \\ \mu_{opt} \cdot \Phi(T) & \text{for } T_{\min} < T < T_{\max} \\ 0 & \text{for } T > T_{\max} \end{cases} \tag{6}$$

where

$$\Phi(T) = \frac{(T - T_{\max})(T - T_{\min})^2}{(T_{opt} - T_{\min})\left[(T_{opt} - T_{\min})(T - T_{opt}) - (T_{opt} - T_{\max})(T_{opt} + T_{\min} - 2T)\right]} \tag{7}$$

The function $\Phi(T)$ includes three parameters with a physical meaning: $T_{\min}$, $T_{\max}$ and T_{opt} (°C). $T_{\min}$ and $T_{\max}$ are the temperatures below and above which there is no growth nor respiration, while T_{opt} is the temperature at which the growth rate is maximum. In this way, $\mu(T)$ assumes a typical bell-shaped profile.

The term accounting for the limitation due to the nitrogen concentration (c_N) was represented as a Monod function (Monod, 1949):

$$f(N) = \frac{c_N}{K_N + c_N} \tag{8}$$

where K_N is the half-saturation constant (mg_N L^{-1}).

The term accounting for the effect of light was modeled according to Haldane (1930), in order to consider both the saturation and photoinhibition effects:

$$f(I_{sp}) = \frac{I_{sp}}{K_L + I_{sp} + \frac{{I_{sp}}^2}{K_I}} \tag{9}$$

K_L and K_I are the half-saturation and the inhibition constants (mmol photons g^{-1} d^{-1}) of light, respectively, expressed in terms of specific light supply rate (I_{sp}, mmol photons g^{-1} d^{-1}) in order to account for self-shading effects due to increasing biomass concentration, according to Equation (4).

The specific maintenance rate (μ_e), which was first described for heterotrophic microorganisms by Pirt (1965) as "the energy consumed for functions other than productions of new cell material," was calculated according to the model proposed by Gons and Mur (1980). These authors observed that growth yields decrease at low growth rates as a consequence of a requirement of energy for maintenance of existing cells. Therefore, the growth rate is proportional to the energy absorbed, with the exception of the energy required for the cell maintenance. According to these considerations and to the energy balance, they derived the following equation:

$$\mu = \left(\frac{dE}{dt} \cdot \frac{1}{X}\right) \cdot c - \mu_e \tag{10}$$

where $\frac{dE}{dt}$ is the light energy uptake rate (J d^{-1}), X is the energy stored in the culture biomass (J), and c is the "true" efficiency of light conversion into the chemical energy that is stored in biomass (dimensionless). Gons and Mur (1980) applied the model to the continuous light-limited growth of *Scenedesmus protuberans* and found a linear dependence of the growth rate on the specific light uptake rate $\left(\frac{dE}{dt} \cdot \frac{1}{X}\right)$. Hence, by correlating their data according to Equation (10), they derived c and $\mu_e$values.

In our case, the specific light uptake rate $\frac{dE}{dt} \cdot \frac{1}{X}$ (d^{-1}), which represents the amount of light energy utilized per unit of biomass over time, was hence calculated from the experiments according to:

$$\frac{dE}{dt} \cdot \frac{1}{X} = \frac{I_{abs} \cdot E_p \cdot A_{PBR}}{c_x \cdot LHV \cdot V_R} \tag{11}$$

where I_{abs} is the absorbed photon flux density, calculated by subtracting the irradiance at the back of the PBR from the incident light intensity (μmol photons m^{-2} s^{-1}), E_p is the average energy of a photon (assumed to be 0.223 kJ/mmol), A_{PBR} is the illuminated surface of the PBR (m^2), LHV is the lower heating value of the biomass (assumed to be equal to 18.66 kJ/g Zaimes and Khanna, 2013) and V_R is the PBR volume (m^3).

Respirometric Tests

In order to retrieve the values of the parameters contained in Equations (7–9), respirometric tests were carried out. The experimental apparatus and protocol used were the same described by Sforza et al. (2019).

This technique has already been used to determine kinetic parameters of microalgae growth by Decostere et al. (2013) and to evaluate microalgal performances in wastewater by Rossi et al. (2018). The protocol is based on the measurement of oxygen production or consumption due to the growth and respiration of microalgal biomass, to which it is correlated trough yields factors:

$$Y_{O_2/x} = \frac{\frac{dc_{O_2}}{dt}}{\frac{dc_x}{dt}} = \frac{OPR}{r_x} \tag{12}$$

where $Y_{O_2/x}$ is the oxygen/biomass yield and OPR is the oxygen production rate ($mg_{O2}\ L^{-1}\ d^{-1}$). It follows that the normalized oxygen production rate ($OPR_{sp} = OPR/c_x$) is:

$$\frac{OPR}{c_x} = \mu_{\max} \cdot \Phi(T) \cdot f(N) \cdot f\left(I_{sp}\right) \cdot Y_{O_2/x} - \mu_e \cdot Y_{O_2/x} \tag{13}$$

Each respirometric test started by preparing a cyanobacterium inoculum of about 0.2 g L^{-1} of DW. After having filled a flask with it, the inoculum was exposed to light-dark cycles of 5:5 min each, obtained by means of a digital controller connected to a LED lamp. The concentration of nitrogen (supplied as sodium nitrate) or the experimental conditions (light intensity and temperature) were varied independently to study the effect of these variables on the growth. Each test lasted about 3 h and resulted in dissolved oxygen (DO) concentration profiles along with time. During light phases, a positive increase of DO is measured (i.e. OPR), while a negative one is observed during dark phases (i.e., OCR, oxygen consumption rate).

Experimental DO data, obtained from the oximeter (HD2109.1 DELTA OHM), were corrected by taking into account the occurrence of oxygen mass transfer with the atmosphere and, then, fitted by a straight line.

$$\frac{dC_{O_2}}{dt} = k_L a \left(C^*_{O_2} - C_{O_2}\right) + OPR \tag{14}$$

Where $\frac{dC_{O_2}}{dt}$ is the time derivative of DO concentration ($mg_{O2}\ L^{-1}\ d^{-1}$) that corresponds to the slope of the straight line, $k_L a$ is the global oxygen mass transfer coefficient that was determined experimentally by Sforza et al. (2019) and is equal to 0.0033 min^{-1}, $C^*_{O_2}$ is the oxygen saturation concentration in the liquid ($mg_{O2}\ L^{-1}$) and C_{O_2} is the DO concentration ($mg_{O2}\ L^{-1}$).

At least four measurements were performed and averaged to obtain the OPR value of each condition (i.e., four dark-light cycles of 5:5 min each). The specific OPR_{sp} and OCR_{sp} ($mg_{O2}\ mg_X^{-1}\ d^{-1}$) were then obtained by normalization of OPR and OCR ($mg_{O2}\ L^{-1}\ d^{-1}$) with respect to the initial biomass concentration measured as dry weight ($mg_X\ L^{-1}$).

The value of OPR_{sp} obtained during the light phase represents a net oxygen production rate, because it includes the oxygen consumption, which still occurs even under light exposure. This consumption represents energy loss that is used for maintenance of biological functions, which is mathematically described by the specific rate of maintenance energy μ_e (Equation 5). Accordingly, by summing the absolute values of OCR_{sp} to OPR_{sp}, the actual photosynthetic growth is obtained. Mathematically, this translates to:

$$\frac{OPR}{c_x} + \left|\frac{OCR}{c_x}\right| = \mu_{\max} \cdot \Phi(T) \cdot f(N) \cdot f\left(I_{sp}\right) \cdot Y_{O_2/x} \tag{15}$$

The experiments were performed so that all the operating conditions, except one, were set to their optimal values. In this way, it is possible to study the effect of a single variable. For example, to study the effect of the nitrogen concentration, temperature and light intensities were set to their optimal values and Equation (15) became:

$$\frac{OPR}{c_x} + \left|\frac{OCR}{c_x}\right| = \left(\mu_{\max} \cdot Y_{O_2/x}\right) \cdot \frac{c_N}{K_N + c_N} \tag{16}$$

The same is valid when studying the effects of temperature and light. In these cases, nitrogen was supplied in a non-limiting concentration.

μ_{max} Estimation

The respirometric tests allowed to evaluate all the parameters included in Equations (7–9) (K_N, K_L, K_I, $T_{\min}$, T_{opt}, $T_{\max}$), whereas elaborating the experimental data obtained from continuous cultivation with the model of Gons and Mur (1980) allowed to calculate the value of μ_e. Therefore, $\mu_{\max}$ is the only unknown kinetic parameter in Equation (6) that needs to be estimated.

From the material balance of a CSTR:

$$\frac{dc_x}{dt} = \frac{c_{x,in}}{\tau} - \frac{c_x}{\tau} + r_x \tag{17}$$

at steady state ($\frac{dc_x}{dt} = 0$) and with null inlet biomass concentration, r_x can be calculated by simply dividing the steady-state biomass concentration measured experimentally by the residence time (τ):

$$r_x = \frac{c_x}{\tau} \tag{18}$$

By equaling Equation (18) with Equation (5), i.e., comparing the values of r_x obtained at the different experimental conditions with the kinetic model, the only unknown variable is $\mu_{\max}$, which can hence be calculated as:

$$\mu_{\max} = \frac{1 + \mu_e \cdot \tau}{\tau \cdot \phi(T) \cdot \frac{c_N}{K_N + c_N} \cdot \frac{I^{exp}_{sp}}{I^{exp}_{sp} + K_L + \frac{\left(I^{exp}_{sp}\right)^2}{K_I}}} \tag{19}$$

where c_N is the experimental concentration of nitrogen ($mg_N\ L^{-1}$).

Statistical Significance

T-student tests were applied to ascertain statistical differences in biomass concentration and productivity obtained under cultivation in BG11 and $BG11_0$. The level of statistical significance was assumed for $p\text{-}value < 0.05$.

RESULTS AND DISCUSSION

Continuous Cultivation

Continuous experiments were carried out to assess the effect of operating variables on biomass productivity. The effect of residence time, which is the main operating variable in continuous photobioreactors, was investigated (τ = 1–4.6 d), under constant light intensities of 190 μmol m^{-2} s^{-1} and of 650 μmol m^{-2} s^{-1}, by feeding $BG11_0$ medium, i.e., with no nitrogen salts. In addition, *Anabaena* was also cultivated under a constant light intensity of 650 μmol m^{-2} s^{-1} by feeding BG11 medium with 3 g L^{-1} of sodium nitrate, in order to verify if the concentration of atmospheric nitrogen dissolved in the liquid, determined by its solubility, was limiting the growth of the cyanobacterium.

Figure 2 reports the average biomass concentration (g L^{-1}) obtained at steady-state for each value of residence time at different irradiances and medium fed. It can be seen that it increased along with the residence time, as expected. However, the observed trend is not linear, and it tends to flatten at high residence times as a consequence of self-shading effects between cells (Janssen et al., 2003; Sforza et al., 2014b). Moreover, a higher incident light intensity resulted in an increased biomass concentration, suggesting that, at 190 μmol m^{-2} s^{-1}, the growth of *Anabaena* was limited by light.

The comparison between biomass concentrations obtained when supplying nitrates with respect to the ones obtained under strictly nitrogen-fixing conditions highlights that both optical density and dry weight are slightly higher in the case of biomass cultivated in presence of 3 g L^{-1} of sodium nitrate. However, the difference is not considerable, except for the higher residence time. This suggests that *Anabaena*'s growth is not significantly limited by nitrogen concentration or uptake even under atmospheric nitrogen-fixing conditions.

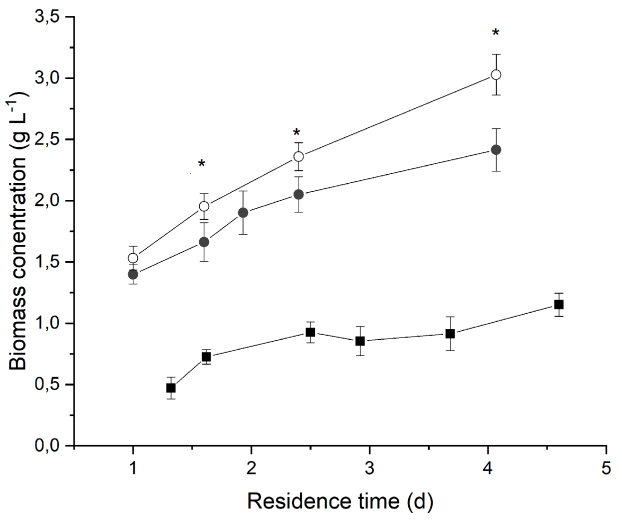

FIGURE 2 | Biomass concentration as a function of residence time at 190 μmol m^{-2} s^{-1} and $BG11_0$ medium (full squares) 650 μmol m^{-2} s^{-1} and $BG11_0$ medium (full circles), and 650 μmol m^{-2} s^{-1} and BG11 medium (open circles). Asterisks mark statistically different results between cultivation in BG11 and $BG11_0$.

By comparing the heterocysts concentration (number of cells per μg of dry weight) in the reactors irradiated at 650 μmol m^{-2} s^{-1} as expected, the value resulted higher in the case of biomass cultivated in nitrogen-fixation conditions, for all the residence times studied (**Figure S1**). However, the presence of heterocysts was noticed also in the case of biomass cultivated with a directly available nitrogen source ($NaNO_3$) in the culture medium.

By observing **Figure 3** it is evident that biomass volumetric productivity increased if the residence time decreased, so that simultaneously the biomass growth rate increased. It is widely acknowledged that when considering continuous autotrophic cultivation of photosynthetic microorganisms in a chemostat reactor, the biomass productivity profile shows a maximum in correspondence of the optimal value of residence time. On the right-hand side, the biomass growth is limited by self-shading effect along the reactor depth; on the left-hand side, when increasing the volumetric flow rate, the biomass removal from the reactor overcomes the biomass growth until the wash-out residence time is reached (Moreno et al., 2003; Takache et al., 2010; Barbera et al., 2015). Clearly, the optimum operating residence time depends on the incident irradiance, and should be assessed accordingly. In fact, in the case of an incident light intensity equal to 190 μmol m^{-2} s^{-1}, the maximum of productivity (0.45 ± 0.04 g L^{-1} d^{-1}) was reached for a residence time of about 1.6 d. Instead, at 650 μmol m^{-2} s^{-1} the maximum was not reached even if the residence time was decreased down to 1 d, suggesting that an even higher biomass growth rate could have been applied. However, a remarkable value of volumetric biomass productivity (1.4 ± 0.1 g L^{-1} d^{-1}) was found at 1 d of residence time when irradiating the photobioreactor with 650 μmol m^{-2} s^{-1}. Reported productivity values of *Anabaena* ATCC 33047 obtained under outdoor cultivation conditions range from 0.06 g L^{-1} d^{-1} in the winter to 0.13 g L^{-1} d^{-1} in the summer season (Moreno et al., 2003).

Maintenance Energy

The evaluation of the maintenance energy requirement in *Anabaena* PCC 7122 was obtained based on the elaboration of experimental data of continuous cultivation at low incident light (I_{in} = 190 μmol m^{-2} s^{-1}) as well as at high light (I_{in} = 650 μmol m^{-2} s^{-1}), both for the growth in presence of nitrates and not, according to the model described in section Kinetic Model Description. The results are reported in **Figure 4**.

Each data set was fitted according to Equation (10) to obtain the values of the "true" efficiency of light conversion into the chemical energy stored in biomass (c) (i.e., the slope of the straight line) and the specific maintenance energy (i.e., the intercept). The values of the regressed parameters and the quality of the fitting are summarized in **Table 1**.

The results obtained are comparable to the values reported by Gons and Mur (1980). In fact, they obtained a value of c that varies between 0.11 and 0.13, which is very similar to our values (0.14–0.16).

On the other hand, by observing the values of μ_E, it can be seen that a higher incident light intensity corresponded to

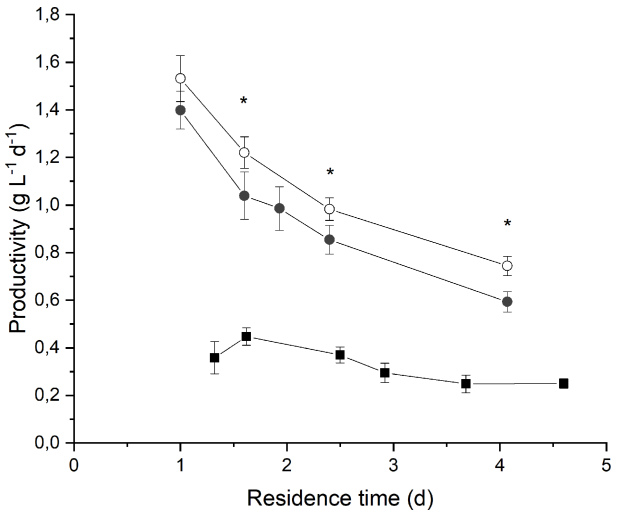

FIGURE 3 | Biomass volumetric productivity as a function of residence time at 190 μmol m^{-2} s^{-1} and $BG11_0$ medium (full squares) 650 μmol m^{-2} s^{-1} and $BG11_0$ medium (full circles), and 650 μmol m^{-2} s^{-1} and BG11 medium (open circles). Asterisks mark statistically different results between cultivation in BG11 and $BG11_0$.

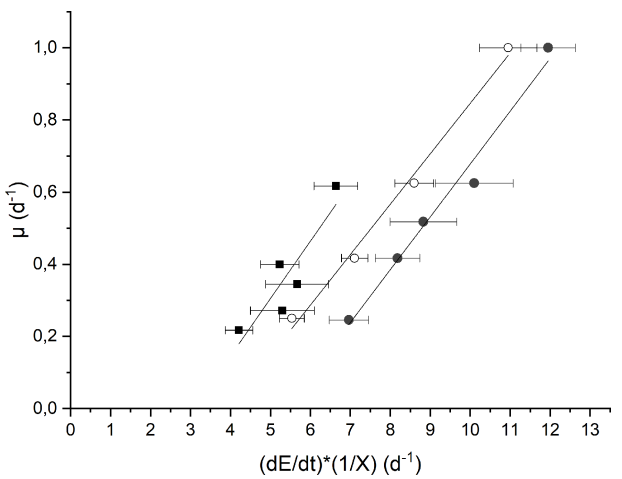

FIGURE 4 | Plot of the growth rate as a function of the specific light supply at 190 μmol m^{-2} s^{-1} and $BG11_0$ medium (full squares) 650 μmol m^{-2} s^{-1} and $BG11_0$ medium (full circles), and 650 μmol m^{-2} s^{-1} and BG11 medium (open circles).

a higher value of specific maintenance rate. For the biomass cultivated in $BG11_0$, a value of 0.49 d^{-1} corresponded to the low incident light of 190 μmol m^{-2} s^{-1}, whereas 0.79 d^{-1} to the higher one (650 μmol m^{-2} s^{-1}). This suggests that, at 650 μmol m^{-2} s^{-1}, a large part of energy was diverted from the biomass growth to cell repair, possibly due to photoinhibition phenomena (Kliphuis et al., 2012).

In addition, it appears that at high light intensity (650 μmol m^{-2} s^{-1}), the specific maintenance rate was slightly lower for the biomass cultivated in presence of sodium nitrate. This is reasonable because the process of atmospheric nitrogen fixation is undoubtedly energy demanding.

TABLE 1 | Parameters of linearization of data reported in **Figure 4**, according to Equation (10).

	I_o(μmol m^{-2} s^{-1})	c (-)	μ_E(d^{-1})	R^2
$BG11_0$	190	0.16 ± 0.04	0.49 ± 0.24	0.81
	650	0.15 ± 0.01	0.79 ± 0.11	0.98
BG11	650	0.14 ± 0.01	0.55 ± 0.07	0.99

Summarizing, our results suggest that irradiation intensity affects the value of the maintenance rate μ_E, according to what already observed also for the microalgae *Scenedesmus obliquus* by Sforza et al. (2015). In particular, μ_E was observed to be strongly increased under inhibiting irradiation. On the contrary, Gons and Mur (1980) found a μ_E independent from the incident light intensity used. However, this can be explained by considering that these authors performed all the experiments at irradiances below the inhibiting value. In fact, other authors (Kliphuis et al., 2012) found that higher light intensities resulted in lower biomass/light yields, suggesting that indeed a larger portion of the incident light was "wasted."

Results of Respirometric Tests

A series of respirometric tests were performed with the aim of retrieving the kinetic parameters to describe the growth of *Anabaena* PCC 7122 in autotrophic conditions. In the following sections, the results obtained for the light, temperature and nitrogen effects are reported and discussed.

Light Effect

The effect of light on growth kinetics was investigated, since it is the main source of energy, essential to support metabolism in autotrophic conditions (Yun and Park, 2003).

The incident light intensity was changed every 4 light-dark cycles and progressively set to values of 50, 75, 100, 150, 450, and 730 μmol m^{-2} s^{-1}.

Respirometric tests were carried out with two different preinocula: one adapted to a low incident light of 150 μmol m^{-2} s^{-1}, the other adapted to a high incident light of 650 μmol m^{-2} s^{-1}. The results obtained experimentally were plotted as a function of the specific light supply rate (I_{sp}) and then fitted with the Haldane model (Equation 9). **Figure 5** shows the experimental data together with the fitting curves for the low light-adapted preincoulum (the high light-adapted one showed a similar trend). As it can be observed, the biomass growth rate, which is correlated to the sum of oxygen production and consumption rates (Equation 15), increased with increasing values of I_{sp} up to a maximum value, and then decreased due to inhibition effects.

The quality of fitting is good and the obtained model parameters together with their standard deviations are summarized in **Table 2**. It can be observed that the values of the half-saturation and inhibition constants are very similar in the two cases, suggesting the reliability of the proposed protocol

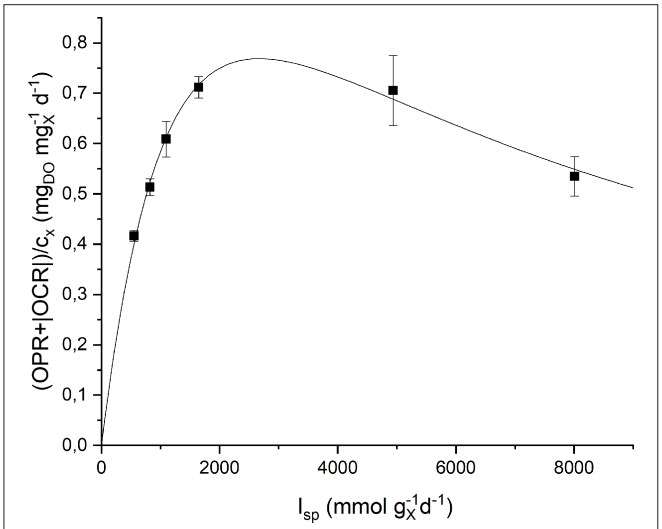

FIGURE 5 | Specific oxygen production rate as a function of specific light supply rate: experimental data (dots) and fitted Haldane model (continuous line).

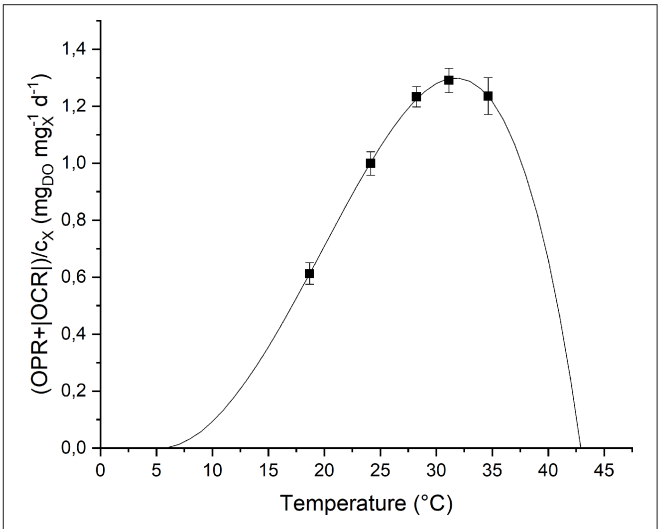

FIGURE 6 | Specific oxygen production rate as a function of temperature: experimental data (dots) and fitted model (continuous line).

TABLE 2 | Summary of the fitted parameters of the Haldane model.

Adaptation	K_L (mmol photons g_x^{-1} d^{-1})	K_L (mmol photons g_x^{-1} d^{-1})
Low light	2,023 ± 515	3,531 ± 958
High light	2,192 ± 575	3,730 ± 1,295

TABLE 3 | Summary of the fitted parameters of the temperature model.

T_{opt} (°C)	T_{min} (°C)	T_{max} (°C)
31.74 ± 0.13	5.29 ± 1.23	42.93 ± 1.19

to assess the effect of light intensity on the growth kinetics, regardless the previous inoculum acclimation.

Temperature Effect

Besides light intensity, temperature is the most important factor influencing the microorganism growth in autotrophic and nutrient unlimited conditions (Bernard and Rémond, 2012).

To study the effect of temperature on the biomass growth, all the other nutrients were supplied in excess, and the light intensity was set to its optimal value, according to the previous results. The investigated values of temperature, changed every 4 light-dark cycles, were: 18, 24, 28, 31, and 35°C. The temperature value was increased progressively by heating up the water bath. The values of T_{opt}, $T_{\min}$ and $T_{\max}$ were hence fitted according to the model by Bernard and Rémond (2012) (Equation 8). **Figure 6** shows the experimental data and the fitting curve.

As expected, according to Bernard and Rémond (2012), the biomass growth rate is null below $T_{\min}$ and above $T_{\max}$, and reaches its maximum value when the temperature is equal to T_{opt}. In particular, for $T > T_{otp}$, the growth rate rapidly decreases because of the heat stress that can affect activities of enzymes (denaturation, inactivation) or modify proteins involved in photosynthesis (Ras et al., 2013).

Moreover, it can be observed that the model (the one represented in **Figure 6** by the solid line) can represent well the experimental points. The model parameters obtained from the fitting procedure together with the standard deviations are summarized in **Table 3**. The value found for T_{opt} is comparable to those reported in literature for microalgae: 20–30°C (Rinanti, 2016).

Nitrogen Effect

Since *Anabaena* PCC 7122 is a nitrogen-fixing cyanobacterium, it is interesting to study its growth in nitrogen limited conditions, in order to determine whether the concentration of atmospheric nitrogen dissolved in the liquid, as supplied in continuous cultivation by means of bubbling CO_2-enriched air, is sufficient or limiting, and to which extent.

The values of nitrogen concentration studied, supplied as sodium nitrate and changed every 4 light-dark cycles, were: 0, 2, 6, 8, and 15 mg L^{-1}. The change in nitrates concentration was obtained by progressive addition of $NaNO_3$ in the sealed flask. Since *Anabaena* is not only capable of using nitrogen in nitrate form, but also atmospheric nitrogen, before each addition of $NaNO_3$, the biomass sample was bubbled with argon in order to strip the dissolved atmospheric nitrogen which could alter the microorganism response to the nutrient supply.

By analyzing the normalized OPR and OCR obtained at each nitrogen concentration (**Figure S2**) it could be noticed that they display a similar trend, since both of them increase (in absolute value) at increasing nitrogen concentration. Moreover, even at 0 mg L^{-1} of N and after stripping with argon, a small rate of oxygen production was detected. This can be explained considering the basal photosynthetic activity of cells: non-growing cells are responsible of a short-term oxygen production rate enhanced by the previous exposure of the preinoculum

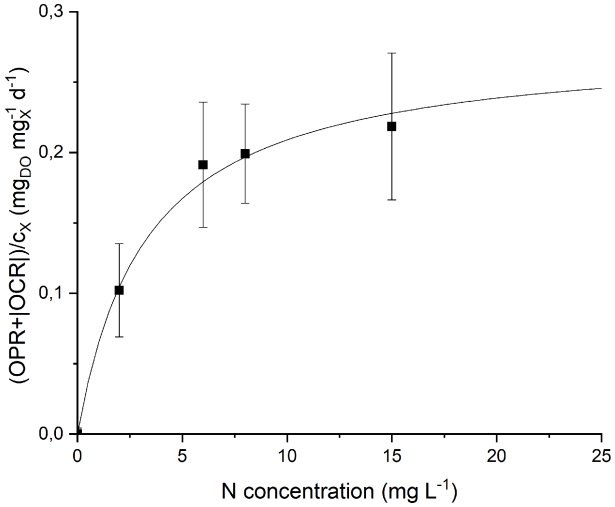

FIGURE 7 | Specific oxygen production rate as a function of nitrogen concentration: experimental data (dots) and fitted Monod model (continuous line).

to light. This phenomenon was taken into account through a further normalization of the data, subtracting the value of $\left(\frac{OPR}{c_x} + \frac{|OCR|}{c_x}\right)$ obtained at 0 mg L^{-1} of N from all the other experimental points. **Figure 7** shows the experimental results together with the fitted Monod model (Equation 9). The value of the half-saturation constant obtained from the regression resulted equal to 2.90 ± 0.67 mg_N L^{-1}.

Note that the obtained value of K_N is much lower than typical values of nitrogen half-saturation constant reported in literature for green microalgae. For example, some authors measured a value of 19.4 mg L^{-1} (Rowley, 2010) and 23.4 mg L^{-1} (Ramos Tercero et al., 2014) for the green microalga *Chlorella protothecoides*. However, specific studies about cyanobacteria confirm the value obtained in our work. Cornet et al. (1992) found a half-saturation constant of 1.2 mg L^{-1} for *Spirulina platensis*, Halterman and Toetz (1984) found a value close to 0 mg L^{-1} for *Anabaena* A7214, while Hattori (1962) reported 0.98 mg L^{-1} for *Anabaena cylindrica*. This is also reasonable considering that nitrogen-fixing organisms should be adapted to the low dissolved nitrogen concentration given by the solubility of this gas in the liquid medium (∼13 mg L^{-1}). In this way, the supply of nitrates at higher concentrations (greater than the saturation one) does not result in improved biomass production rate, as confirmed by the results of our continuous experiments (section Continuous Cultivation).

Maximum Specific Growth Rate μ_{max}

Based on the methodology described in section 2.6, once all the kinetic parameters were determined according to the results presented, the maximum specific growth rate was calculated for each experimental condition investigated. The values obtained for each steady state of the continuous cultivation experiments is reported in **Table 4**. The average μ_{max} resulted equal to 8.22 ± 0.69 d^{-1}.

TABLE 4 | μ_{max} determination results.

Light (μmol m^{-2} s^{-1})	τ (d)	c_x^{exp} (g L^{-1})	μ_{max} (d^{-1})
190	1.32	0.47	7.49
190	1.62	0.73	8.82
190	2.5	0.93	8.51
190	2.92	0.86	7.48
190	3.68	0.91	7.22
190	4.6	1.15	8.09
650	4.1	2.41	7.95
650	2.4	2.05	8.24
650	1.9	1.90	8.50
650	1.6	1.66	8.42
650	1.0	1.40	9.66

The value obtained according to the methodology proposed here appeared slightly higher than what is usually found in the literature, where values around 2.8–3.8 d^{-1} are reported for different cyanobacteria species, such as *Synechocysits* sp. (Kim et al., 2015) and *Cyanothece* sp. (Zhang et al., 2015). On the other hand, Salleh et al. (2017) reported a value of 6 d^{-1} for *Anabaena variabilis*. It should be taken into account that this parameter represents a growth condition that can hardly occur in reality where, even if nutrients are supplied in excess, light will always play an important effect on the actual growth and respiration of the photosynthetic microorganisms. It should be noticed, in addition, that the physical meaning of such a parameter is different from that of the classical Monod function, because the dependence on light intensity is described with a Haldane-like model. Accordingly, the maximum specific growth rate for photosynthetic organisms should be described from a different perspective than for heterotrophic organisms. In fact, it represents an ideal value, useful to correctly describe the growth of the organisms from a mass balance and kinetic point of view, rather than an actual value reachable under specific growth conditions. This different approach appears reasonable when considering the complex metabolisms of photosynthetic organisms. Different metabolic pathways are in fact combined to sustain growth, as a result of complex mechanisms ranging from light capture efficiency, the ratio of the respiration rate, additional effects of light dissipation and energy losses for nitrogen fixation, that are all included in the maintenance term.

CONCLUSIONS

In this work we propose a method to reliably determine kinetic parameters of photosynthetic microorganisms, in particular the maximum specific growth rate. Specifically, the method was applied to describe the behavior of the N-fixing cyanobacterium *Anabaena* PCC7122, whose growth rate is influenced by not only light and temperature, but may also be limited by the reduced concentration of dissolved atmospheric nitrogen. By means of

well-validated respirometric tests, it was possible to measure the kinetic parameters describing the effect of light, temperature and nitrogen on the cyanobacterium growth rate. In particular, the half-saturation of N resulted lower compared to that of green microalagae, but comparable to that of other cyanobacteria. Moreover, the value of 3 mg L^{-1} found here suggests that *Anabaena* growth under N-fixing conditions is not significantly limited by atmospheric nitrogen solubility (about 13 mg L^{-1} at ambient conditions). This was also confirmed by continuous cultivation experiments, which showed only slight differences between the productivities obtained with and without additional supply of nitrates. The evaluation of the specific maintenance rate showed that this parameter is affected by the light intensity, with more energy being dissipated under high light conditions, and by the nitrogen source, with N-fixation requiring more energy for cell maintenance. Finally, the maximum specific growth rate could be determined by applying the comprehensive and fully determined kinetic model in the material balance of the continuous PBR, obtaining a constant value.

The proposed method can be easily applied to any photosynthetic microorganism as a way to quickly quantify the effect of the main process variables on the growth kinetics, and use this to perform process simulations aimed at design and control of large-scale production processes.

DATA AVAILABILITY STATEMENT

The datasets generated for this study are included in the manuscript/**Supplementary Files**.

AUTHOR CONTRIBUTIONS

EB and ES contributed the conception and design of the study. AG and LB performed the experiments. AG and EB wrote the first draft of the manuscript. EB, ES, and AG wrote the sections of the manuscript. ES and AB discussed the results. All authors contributed to manuscript revision, read, and approved the submitted version.

SUPPLEMENTARY MATERIAL

The Supplementary Material for this article can be found online at: https://www.frontiersin.org/articles/10.3389/fbioe.2019.00274/full#supplementary-material

REFERENCES

Allen, M. B., and Arnon, D. J. (1955). Studies on nitrogen-fixing blue-green algae. I. Growth and nitrogen-fixation by *Anabaena cylindrica* Lemn. *Plant Physiol.* 30, 366–372. doi: 10.1104/pp.30.4.366

Barbera, E., Sforza, E., and Bertucco, A. (2015). Maximizing the production of *Scenedesmus obliquus* in photobioreactors under different irradiation regimes: experiments and modeling. *Bioprocess Biosyst. Eng.* 38, 2177–2188. doi: 10.1007/s00449-015-1457-9

Bernard, O., Mairet, F., and Chachuat, B. (2015). "Modelling of microalgae culture systems with applications to control and optimization," in *Advances in Biochemical Engineering Biotechnology*, eds C. Posten and S. Feng Chem (Cham: Springer), 59–87. doi: 10.1007/10_2014_287

Bernard, O., and Rémond, B. (2012). Validation of a simple model accounting for light and temperature effect on microalgal growth. *Bioresour. Technol.* 123, 520–527. doi: 10.1016/j.biortech.2012.07.022

Cornet, J. F., Dussap, C. G., Cluzel, P., and Dubertret, G. (1992). A structured model for simulation of cultures of the Cyanobacterium *Spirulina platensis* in photobioreactors: II. Identification of kinetic parameters under light and mineral limitations. *Biotechnol. Bioeng.* 40, 826–834. doi: 10.1002/bit.260400710

Darvehei, P., Bahri, P. A., and Moheimani, N. R. (2018). Model development for the growth of microalgae: a review. *Renew. Sust. Energy Rev.* 97, 233–258. doi: 10.1016/j.rser.2018.08.027

Decostere, B., Janssens, N., Alvarado, A., Maere, T., Goethals, P., Van Hulle, S. W. H., et al. (2013). A combined respirometer-titrimeter for the determination of microalgae kinetics: experimental data collection and modelling. *Chem. Eng. J.* 222, 85–93. doi: 10.1016/j.cej.2013.01.103

Fernandes, B. D., Mota, A., Teixeira, J. A., and Vicente, A. A. (2015). Continuous cultivation of photosynthetic microorganisms: approaches, applications and future trends. *Biotechnol. Adv.* 33, 1228–1245. doi: 10.1016/j.biotechadv.2015.03.004

Fogg, G. E. (1944). Growth and heterocyst production in *Anabaena cylindrica* Lemm. *New Phytol.* 43, 164–175. doi: 10.1111/j.1469-8137.1944.tb05012.x

Gons, H. J., and Mur, L. R. (1980). Energy requirements for growth and maintenance of *Scenedesmus* protuberans fritsch in light-limited continuous cultures. *Arch. Microbiol.* 125, 9–17. doi: 10.1007/BF00403192

Haldane, J. B. S. (1930). *Enzymes*. London: Longmans.

Halterman, S. G., and Toetz, D. W. (1984). Kinetics of nitrate uptake by freshwater algae. *Hydrobiologia* 114, 209–214. doi: 10.1007/BF00031872

Hattori, A. (1962). Light-induced reduction of nitrate, nitrite and hydroxylamine in a blue-green alga, *Anabaena cylindrica*. *Plant Cell Physiol.* 3, 355–369. doi: 10.1007/BF00446866

Janssen, M., Tramper, J., Mur, L. R., and Wijffels, R. H. (2003). Enclosed outdoor photobioreactors: light regime, photosynthetic efficiency, scale-up, and future prospects. *Biotechnol. Bioeng.* 81, 193–210. doi: 10.1002/bit.10468

Khan, M. I., Shin, J. H., and Kim, J. D. (2018). The promising future of microalgae: current status, challenges, and optimization of a sustainable and renewable industry for biofuels, feed, and other products. *Microb. Cell Fact.* 17, 1–21. doi: 10.1186/s12934-018-0879-x

Kim, H.-W., Park, S., and Rittmann, B. E. (2015). Multi-Component Kinetics for the Growth of the Cyanobacterium *Synechocystis* Sp. PCC6803. *Environ. Eng. Res.* 20, 347–355. doi: 10.4491/eer.2015.033

Kliphuis, A. M., Klok, A. J., Martens, D. E., Lamers, P. P., Janssen, M., and Wijffels, R. H. (2012). Metabolic modeling of *Chlamydomonas reinhardtii*: energy requirements for photoautotrophic growth and maintenance. *J. Appl. Phycol.* 24, 253–266. doi: 10.1007/s10811-011-9674-3

Lam, M. K., Lee, K. T., and Mohamed, A. R. (2012). Current status and challenges on microalgae-based carbon capture. *Int. J. Greenh. Gas Con.* 10, 456–469. doi: 10.1016/j.ijggc.2012.07.010

Monod, J. (1949). The growth of bacterial cultures. *Annu. Rev. Microbiol.* 3, 371–394. doi: 10.1146/annurev.mi.03.100149.002103

Moreno, J., Ángeles Vargas, M., Rodríguez, H., Rivas, J., and Guerrero, M. G. (2003). Outdoor cultivation of a nitrogen-fixing marine Cyanobacterium, *Anabaena* sp. ATCC 33047. *Biomol. Eng.* 20, 191–97. doi: 10.1016/S1389-0344(03)00051-0

Moreno, J., Rodríguez, H., Angeles Vargas, M., Rivas, J., and Guerrero, M. G. (1995). Nitrogen-fixing cyanobacteria as source of phycobiliprotein pigments. Composition and growth performance of ten filamentous heterocystous strains. *J. Appl. Phycol.* 7, 17–23. doi: 10.1007/BF00003545

Phillips, M. J., and Roberts, R. J. (1985). The toxicity of the cyanobacterium *Microcystis aeruginosa* to rainbow trout, *Salmo gairdneri*. *J. Fish Dis.* 8, 339–344. doi: 10.1111/j.1365-2761.1985.tb00953.x

Pirt, S. J. (1965). The maintenance energy of bacteria in growing cultures. *Proc. R. Soc. Lond. Ser. B Biol. Sci.* 163, 224–231. doi: 10.1098/rspb.1965.0069

Quiblier, C., Susanna, W., Isidora, E.-S., Mark, H., Aure, V., and Jean-Franc, H. (2013). A review of current knowledge on toxic benthic freshwater cyanobacteria E ecology, toxin production and risk management. *Water Res.* 47, 5464–5479. doi: 10.1016/j.watres.2013.06.042

Ramos Tercero, E. A., Sforza, E., Morandini, M., and Bertucco, A. (2014). Cultivation of chlorella protothecoides with urban wastewater in continuous photobioreactor: biomass productivity and nutrient removal. *Appl. Biochem. Biotechnol.* 172, 1470–1485. doi: 10.1007/s12010-013-0629-9

Ras, M., Steyer, J. P., and Bernard, O. (2013). Temperature effect on microalgae: a crucial factor for outdoor production. *Rev. Envir. Sci. Biotechnol.* 12, 153–164. doi: 10.1007/s11157-013-9310-6

Rinanti, A. (2016). "Biotechnology carbon capture and storage by microalgae to enhance CO_2 removal efficiency in closed- system photobioreactor," in *Algae–Organisms for Imminent Biotechnology*, eds N. Thajuddin, and D. Dharumadurai (IntechOpen), 133–156. doi: 10.5772/62915

Rossi, S., Bellucci, M., Marazzi, F., Mezzanotte, V., and Ficara, E. (2018). Activity assessment of microalgal-bacterial consortia based on respirometric tests. *Water Sci. Technol.* 78, 207–215. doi: 10.2166/wst.2018.078

Rosso, L., Lobry, J. R., and Flandrois, J. P. (1993). An Unexpected correlation between cardinal temperatures of microbial growth highlighted by a new model. *J. Theor. Biol.* 162, 447–463. doi: 10.1006/jtbi.1993.1099

Rowley, W. M. (2010). *Nitrogen and Phosphorus Biomass-Kinetic Model for Chlorella Vulgaris in a Biofuel Production Scheme*. BiblioScholar. Available online at: https://www.bookdepository.com/Nitrogen-and-Phosphorus-Biomass-Kinetic-Model-for-Chlorella-Vulgaris-in-Biofuel-Production-Scheme-William-M-Rowley/9781249592921

Salleh, S. F., Kamaruddin, A., Uzir, M. H., Mohamed, A. R., and Shamsuddin, A. H. (2017). Modeling the light attenuation phenomenon during photoautotrophic growth of *A. variabilis* ATCC 29413 in a Batch Photobioreactor. *J. Chem. Technol. Biotechnol.* 92, 358–366. doi: 10.1002/jctb.5013

Sforza, E., Enzo, M., and Bertucco, A. (2014a). Design of microalgal biomass production in a continuous photobioreactor: an integrated experimental and modeling approach. *Chem. Eng. Res. Des.* 92, 1153–62. doi: 10.1016/j.cherd.2013.08.017

Sforza, E., Gris, B., De Farias Silva, C. E., Morosinotto, T., and Bertucco, A. (2014b). Effects of light on cultivation of *Scenedesmus obliquus* in batch and continuous flat plate photobioreactor. *Chem. Eng. Trans.* 38, 211–216. doi: 10.3303/CET1438036

Sforza, E., Pastore, M., Barbera, E., and Bertucco, A. (2019). Respirometry as a tool to quantify kinetic parameters of microalgal mixotrophic growth. *Bioprocess Biosyst. Eng.* 42, 839–851. doi: 10.1007/s00449-019-02087-9

Sforza, E., Urbani, S., and Bertucco, A. (2015). Evaluation of maintenance energy requirements in the cultivation of *Scenedesmus obliquus*: effect of light intensity and regime. *J. Appl. Phycol.* 27, 1453–1462. doi: 10.1007/s10811-014-0460-x).

Singh, S., and Datta, P. (2007). Outdoor evaluation of herbicide resistant strains of *Anabaena variabilis* as biofertilizer for rice plants. *Plant Soil* 296, 95–102. doi: 10.1007/s11104-007-9293-6

Stanbury, P. F., Whitaker, A., and Hall, S. J. (2016). "Microbial growth kinetics," in *Principles of Fermentation Technology, 3rd Edn* (Butterworth-Heinemann), 21–74. Available online at: https://www.sciencedirect.com/book/9780080999531/principles-of-fermentation-technology

Takache, H., Cgristophe, G., Cornet, J.-F., and Pruvost, J. (2010). Experimental and theoretical assessment of maximum productivities for the microalgae *Chlamydomonas reinhardtii* in two different geometries of photobioreactors. *Biotechnol. Progress* 26, 431–440. doi: 10.1002/btpr.356.

Trilli, A. (1990). "Kinetics of secondary metabolite production," in *Microbial Growth Dynamics*, eds R. K. Poole, M. J. Bazin, and C. W. Keevil (Oxford: IRL Press), 103–26.

Yun, Y. S., and Park, J. M. (2003). Kinetic modeling of the light-dependent photosynthetic activity of the green microalga *Chlorella vulgaris*. *Biotechnol. Bioeng.* 83, 303–311. doi: 10.1002/bit.10669

Zaimes, G. G., and Khanna, V. (2013). Microalgal biomass production pathways: evaluation of life cycle environmental impacts. *Biotechnol. Biofuels* 6:88. doi: 10.1186/1754-6834-6-88

Zhang, D., Dechatiwongse, P., and Hellgardt, K. (2015). Modelling light transmission, cyanobacterial growth kinetics and fluid dynamics in a laboratory scale multiphase photo-bioreactor for biological hydrogen production. *Algal Res.* 8, 99–107. doi: 10.1016/j.algal.2015.01.006

Conflict of Interest: The authors declare that the research was conducted in the absence of any commercial or financial relationships that could be construed as a potential conflict of interest.

NOMENCLATURE

PBR = photobioreactor
W = width of the photobioreactor, cm
A_{PBR} = irradiated surface of the photobioreactor, cm^2
V_R = volume of the photobioreactor, mL
Q = volumetric flow rate fed to and withdrawn from the photobioreactor, mL d^{-1}
τ = hydraulic residence time, d
μ = apparent growth rate, d^{-1}
μ_{max} = maximum specific growth rate, d^{-1}
OD = optical density, abs
c_X = biomass concentration, g L^{-1}
$P_{x,V}$ = volumetric biomass productivity, g L^{-1} d^{-1}
$P_{x,A}$ = areal biomass productivity, g m^{-2} d^{-1}
I_0 = incident light intensity, μmol photons m^{-2} s^{-1}
BI = back irradiance, μ mol photons m^{-2} s^{-1}
I_{sp}^{exp} = specific light supply rate obtained from continuous cultivations, mmol photons g^{-1} d^{-1}
η_{PAR} = photosynthetic active radiation efficiency, %
LHV = lower heating value of the biomass, MJ kg^{-1}
E_P = average energy of photons, J μmol^{-1}
r_X = biomass growth rate, mg L^{-1} d^{-1}
μ_e = specific maintenance energy, d^{-1}
$\phi(T)$ = limiting factor due to temperature
T = temperature, °C
T_{min} = minimum temperature (kinetic parameter), °C
T_{max} = maximum temperature (kinetic parameter), °C
T_{opt} = optimal temperature (kinetic parameter), °C
μ_{opt} = optimal growth rate at T_{opt} (kinetic parameter), d^{-1}
$f(I_{sp})$ = limiting factor due to specific light supply rate
I_{sp} = specific light supply rate, mmol photons g^{-1} d^{-1}
K_L = half-saturation constant of the specific light supply rate, mmol photons g^{-1} d^{-1}
K_I = inhibition constant of the specific light supply rate, mmol photons g^{-1} d^{-1}
$f(N)$ = limiting factor due to nitrogen
C_N = concentration of nitrogen, mg N L^{-1}
K_N = nitrogen half-saturation constant, mg N L^{-1}
$Y_{O_2/X}$ = yield of oxygen on biomass, mg_{O2} mg_X^{-1}
k_La = oxygen mass transfer coefficient, min^{-1}
OPR = oxygen production rate, mg_{O2} L^{-1} d^{-1}
OCR = oxygen consumption rate, mg_{O2} L^{-1} d^{-1}
C_{O_2} = oxygen concentration, mg_{O2} L^{-1}
$C_{O_2}^*$ = oxygen saturation concentration in the liquid, mg_{O2} L^{-1}

frontiers in Bioengineering and Biotechnology

ORIGINAL RESEARCH
published: 18 October 2019
doi: 10.3389/fbioe.2019.00275

Production of Defective Interfering Particles of Influenza A Virus in Parallel Continuous Cultures at Two Residence Times—Insights From qPCR Measurements and Viral Dynamics Modeling

Felipe Tapia[1*†], *Tanja Laske*[1†], *Milena A. Wasik*[1], *Markus Rammhold*[1], *Yvonne Genzel*[1] and *Udo Reichl*[1,2]

[1] Max Planck Institute for Dynamics of Complex Technical Systems, Magdeburg, Germany, [2] Chair for Bioprocess Engineering, Otto-von-Guericke-University Magdeburg, Magdeburg, Germany

OPEN ACCESS

Edited by:
Christoph Herwig,
Vienna University of Technology, Austria

Reviewed by:
Xiangzhao Mao,
Ocean University of China, China
Roopali Rajput,
LRS Institute of Tuberculosis and Respiratory Diseases, India

***Correspondence:**
Felipe Tapia
tapia@mpi-magdeburg.mpg.de

[†]These authors have contributed equally to this work

Specialty section:
This article was submitted to Bioprocess Engineering, a section of the journal Frontiers in Bioengineering and Biotechnology

Received: 11 July 2019
Accepted: 01 October 2019
Published: 18 October 2019

Citation:
Tapia F, Laske T, Wasik MA, Rammhold M, Genzel Y and Reichl U (2019) Production of Defective Interfering Particles of Influenza A Virus in Parallel Continuous Cultures at Two Residence Times—Insights From qPCR Measurements and Viral Dynamics Modeling. Front. Bioeng. Biotechnol. 7:275. doi: 10.3389/fbioe.2019.00275

Defective interfering particles (DIPs) are a natural byproduct of influenza A virus (IAV) replication. DIPs interfere with the propagation and spread of infectious standard virus (STV), reduce virus yields by competing for viral and cellular resources, and induce antiviral responses. These properties open exciting possibilities for the development of DIP-based antivirals. Exploring options for cell culture-based DIP production, we have established a fully continuous cultivation process, where one bioreactor is used to grow cells that are fed to two bioreactors operated in parallel for virus production. This system allows head-to-head comparisons of STV and DIP replication dynamics over extended time periods. Cultivations were performed at two residence times (RT, 22 and 36 h) using MDCK suspension cells grown in a fully defined medium. For infection, we used a virus seed generated by reverse genetics containing STVs and a known DIP carrying a deletion in segment 1 (delS1(1)). Four days post infection, DIPs achieved maximum concentrations of $7.0{\cdot}10^9$ virions/mL and $8.4{\cdot}10^9$ virions/mL for RTs of 22 and 36 h, respectively. Furthermore, oscillations in virus titers with two to three maxima were found for DIP accumulation at 36 and 22 h RT, respectively. To complement the study, a basic mathematical model using simple kinetics and a reasonable number of parameters to describe DIP-propagation in continuous cultures was established. Upon fitting the model individually to each of the two data sets, oscillations in the viral dynamics and the cell population dynamics were described well. Modeling suggests that both STV inactivation and virus degradation have to be taken into account to achieve good agreement of simulations and experimental data for longer RTs. Together, the high DIP titers obtained, and the successful simulation of the experimental data showed that the combination of continuous bioreactors and mathematical models can enable studies regarding DIP dynamics over extended time periods and allow large scale manufacturing of DIP-based antivirals.

Keywords: influenza A virus, continuous virus production, suspension MDCK cells, defective interfering particles, mathematical model, virus evolution, antiviral

INTRODUCTION

Viruses are a major threat to human health and significant efforts have been made over the last century to prevent and treat viral diseases. A huge success was the development of potent, safe and affordable viral human and veterinary vaccines using egg- and cell-based production systems (Aubrit et al., 2015; Genzel, 2015; Barrett et al., 2017; Volz and Sutter, 2017). In addition, novel approaches toward vaccination are under development, i.e., DNA and RNA vaccines (Kutzler and Weiner, 2008; De Gregorio and Rappuoli, 2014; Ahmed et al., 2017). In addition, for various viruses such as HIV, IAV, or herpes virus, potent antivirals are available for treatment [e.g., for influenza virus (Samson et al., 2013; Simonsen et al., 2018)]. Despite this, significant challenges remain. On the one hand, humans are constantly challenged by new viruses including Zika virus, MERS-coronavirus, or Ebola virus. On the other hand, most viruses change rapidly in the face of selective pressure and emergence of antiviral drug resistance is of major concern [e.g., for influenza virus (Samson et al., 2013; Lackenby et al., 2018; Shin and Seong, 2019)]. These challenges can only partly be addressed by existing technologies, since the development of new vaccines, the adaptation of existing manufacturing processes, and the identification of new antiviral targets are time consuming and costly processes. They involve complex decisions regarding the selection of efficient production systems, potency and safety aspects, and comprehensive clinical trials. Moreover, conventional antiviral measures may be too slow to save lives in case of a rapidly spreading virus.

An unconventional option to prevent virus spreading and cure infectious diseases is the use of viruses themselves. This concerns especially defective interfering particles (DIPs)—defective viruses, which suppress the spread of their intact, replication competent counterparts, reducing infectious virus yields by up to five orders of magnitude (e.g., Akkina et al., 1984; Frensing et al., 2014). DIPs were already identified in the early fifties by studies of von Magnus (von Magnus, 1951), who performed undiluted serial passages of IAV. DIPs are characterized by deletions in the viral genome preventing the synthesis of a protein essential for viral spread (Nayak et al., 1985; Dimmock and Easton, 2015; Frensing, 2015). For replication, DIPs rely on the presence of homologous helper virus, further referred to as standard virus (STV), that supplies the missing viral protein(s) *in trans*. Interestingly, the presence of DIPs has been demonstrated for almost every virus studied (Huang and Baltimore, 1977) making DIPs a viable option to prevent and/or treat a larger number of viral diseases.

While initial studies suggested that DIPs suppress STV replication and may thus have the potential to protect against viral disease, it was not until the late eighties that researchers started to systematically exploit this approach (Dimmock et al., 1986). It was Dimmock and colleagues (Dimmock et al., 2008) who demonstrated that the use of molecular cloning technologies enables the generation of DIPs that have the potential to protect animals from IAV infection. They also showed that the DIP isolate named DI244, from Influenza A/Puerto Rico/8/34 (PR8; H1N1), which contains a single deletion in segment 1 (S1; coding for PB2), is suitable to both therapeutically and prophylactically protect animals from a lethal challenge by the 2009 pandemic IAV and, potentially, other respiratory viruses (Duhaut and Dimmock, 2003; Easton et al., 2011; Scott et al., 2011; Dimmock et al., 2012; Dimmock and Easton, 2014). They showed that production of the DI244 antiviral candidate can be realized in eggs followed by an ultraviolet (UV) irradiation process to destroy STV infectivity (Dimmock et al., 2008). More recently, an *in vitro* and *in vivo* antiviral effect was demonstrated for a combination of three defective interfering genes of IAV for avian and seasonal influenza using a dual-functional peptide vector (Zhao et al., 2018).

Despite the increasing interest in the potential use of DIPs as antiviral agents, relatively little is known regarding their spread and accumulation in cell populations. This also applies to large scale manufacturing of DIPs in biopharmaceutical industry where fertilized chicken eggs or animal cell culture technologies could be considered for efficient large scale DIP production. While eggs have been successfully used for the production of DIPs in relatively small amounts (Dimmock and Marriott, 2006; Dimmock et al., 2008), cell culture-based technologies have been less explored and have several additional advantages for large scale DIP manufacturing. Firstly, animal cells are ideal for in-depth investigation of intracellular DIP replication, their release and cell-to-cell spreading under controlled and well-defined cultivation conditions in bioreactors over an extended time period. Secondly, cells could be specifically designed for DIP generation (Ozawa et al., 2011; Bdeir et al., 2019; Yamagata et al., 2019) using plasmids for reverse genetics (Hoffmann et al., 2000), which would allow to overcome the need of any infectious helper virus for DIP replication. Such DIP preparations, in contrast to egg-based production systems, would not be contaminated with STV and would not need UV inactivation for use as antivirals (Dimmock et al., 2008). Finally, there are various quantitative assays available for detailed characterization of the dynamics of virus titers and DIP copy numbers. Together with the use of specific staining methods and flow cytometry for monitoring the progress of infection in cells (Frensing et al., 2014, 2016; Swick et al., 2014), mathematical models for DIP and STV replication can be established to describe their basic dynamics in cell culture (Frensing et al., 2013; Akpinar et al., 2016a,b; Laske et al., 2016; Liao et al., 2016).

In this study, following the general ideas described by Frensing et al. (2013), we investigated DIP production in a continuous cultivation system. Frensing et al. demonstrated that continuous influenza virus production in a cascade of two stirred tank bioreactors showed oscillations in virus and cell concentrations due to the presence of DIPs. In contrast to their approach using only two vessels, we used one bioreactor for continuous cell production (cell bioreactor or CB) feeding two bioreactors for virus propagation (virus bioreactor 1 or VB1; virus bioreactor 2 or VB2) operated in parallel to allow for head-to-head comparisons of virus seeds, media, cell lines, or changes in cultivation parameters under conditions as close to each other as possible. As a starting point, the impact of residence time (RT, 22 and 36 h) on DIP and STV dynamics was investigated. With regard to the establishment of manufacturing processes for DIP production, a MDCK suspension cell line growing in a

fully defined medium was used (Lohr et al., 2010). Virus seeds containing known amounts of DIPs and STV were generated using a reverse genetics approach (Hoffmann et al., 2000). Cultivations were performed over a period of 20 days at two RTs to allow for at least two oscillations in STV and DIP replication dynamics (Frensing et al., 2013). For process monitoring and model development, cell concentrations, infectious and non-infectious virus titers, as well as extracellular copy numbers of S1 for both STV, i.e., full-length (FL) S1, and a known form of DIP, delS1(1), were determined. Based on the newly available quantitative data obtained for DIP and STV concentrations, the mathematical model developed by Frensing et al. (2013) was extended. After fitting, the basic process dynamics for both RTs were described well by the simulations. In particular, these simulations capture the oscillations in process variables, e.g., virus titers. In addition, the model predicts the dynamics of cell subpopulations (uninfected, DIP-only infected, STV-only infected, and co-infected cells).

MATERIALS AND METHODS

Cells and Virus

The canine cell line MDCK.SUS2 (through contact with Prof. Klaus Scharfenberg, University of Applied Sciences Emden-Leer, Germany) was cultivated in chemically defined Smif8 medium (Gibco, Thermo Fischer Scientific, USA), supplemented with glutamine, and pyruvate (both 4 mM final concentration, Sigma, USA). MDCK.SUS2 cells were grown in shake flasks and passaged as described before (Lohr et al., 2010).

Influenza A/Puerto Rico/8/34 virus seed containing DIPs with a deletion in S1, i.e., delS1(1), was generated by reverse genetics using an 8+1 plasmid-system (Hoffmann et al., 2000; Duhaut and Dimmock, 2003). This virus seed will be referred to as A/PR/8/34-delS1(1). Therefore, S1 RNA was isolated from influenza A/Puerto Rico/8/34 (National Institute for Biological Standards and Control (NIBSC), No. 06/114) and the respective cDNA was cloned into the pHW2000 vector provided by Erich Hoffmann and Robert G. Webster from St. Jude Children's Research Hospital (Memphis, TN, USA) (Hoffmann et al., 2000), resulting in the plasmid pHW-S1. The plasmid carrying the defective S1 sequence pHW-A/PR/8/34-delS1(1), previously described by Dimmock et al. (2008), was obtained by cloning the respective sequence into the pHW2000 vector. In addition, pHW plasmids carrying FL segments 2–8 were used (also provided by Erich Hoffmann and Robert G. Webster).

One day before transfection, $5{\cdot}10^5$ HEK-293T cells were seeded into 35 mm dishes. Prior to infection, cells were washed with PBS and 3 mL Opti-MEM (Gibco) were added. Transfection was performed simultaneously with all nine plasmids, 280 ng each, using Lipofectamine LTX & PLUS Reagent (Life Technologies) according to the manufacturer's instructions (5 µL Lipofectamine LTX per dish). To increase the amount of virus particles, $5{\cdot}10^5$ adherent MDCK cells were added 7 h post-transfection. After 24 h at 37°C and 5% CO_2, cells were washed with PBS and medium was replaced with DMEM (Gibco) containing 5 Units/mL trypsin (Gibco, #27250-018, sterile-filtered stock solution prepared in PBS with 500 U/mL and stored at −20°C). Subsequently, the cells were incubated at 37°C for additional 72 h. As a result, a virus seed containing A/PR/8/34-delS1(1) and STV, with a $TCID_{50}$ titer of $5.6{\cdot}10^5$ virions/mL and an HA titer of 1.91 $\log_{10}$(HA Units/100 µL) was obtained. Note, that segment-specific reverse transcription-quantitative PCR (qPCR) to determine A/PR/8/34-delS1(1) copy numbers in virus seeds is biased since it is contaminated with the plasmid carrying the DI S1 sequence, pHW-A/PR/8/34-delS1(1). For low multiplicity of infection (MOI) cultivations in continuous cultures, this is not relevant as plasmids are out-diluted (see below).

In a next step, the virus seed for infection of suspension MDCK cells in bioreactors was generated. Therefore, the A/PR/8/34-delS1(1) virus seed was passaged once in suspension MDCK.SUS2 cells with an MOI of 0.1. The virus was harvested 40 h post infection (p.i.), clarified by centrifugation (1,000 g) and the supernatant was aliquoted. The resulting virus bank had an HA titer of 2.36 $\log_{10}$(HA Units/100 µL), a $TCID_{50}$ titer of $6.76{\cdot}10^7$ virions/mL, a FL S1 content of $9.7{\cdot}10^9$ copies/mL, and a DI S1 (A/PR/8/34-delS1(1)) content of $2.9{\cdot}10^8$ copies/mL. Additionally, virus seeds were probed for remaining plasmids after reverse genetic preparation by qPCR, which could bias reverse transcription-qPCR data of the FL and DI S1 measurements. Quantitative PCR data showed, that initial plasmid contamination was 17.6% for A/PR/8/34-delS1(1) and 0.8% for FL S1. However, from zero h p.i. on the plasmid contamination was not detectable any longer, since the virus preparation was diluted due to the low MOI applied for infection (MOI 0.1). All experiments were performed in laboratories with a biological safety level 2 (BSL 2) certification following the respective safety regulations.

Parallel Bioreactor Setup for Continuous Influenza Virus Propagation

A continuous bioreactor system consisting of three stirred tank bioreactors (STR, Dasgip) was used (**Figure 1**). The first 1.5 L STR (with head space capacity for 1700 mL working volume) was used for cell propagation (CB), and the other two 0.5 L STR were run in parallel and used for virus propagation (VB1 and VB2). After inoculation with MDCK.SUS2 cells at $1.4{\cdot}10^6$ viable cells/mL, the CB was operated in batch mode the first 73 h in 1700 mL working volume (wv). Simultaneously, VB1 and VB2 were inoculated with $1.2{\cdot}10^6$ viable cells/mL and grown in batch mode in 320 mL wv and 520 mL wv, respectively. Working volumes were chosen to achieve RTs of 22 and 36 h in VB1 and VB2, respectively, using the flow rates (F) described in **Figure 1** (RT = wv/F). The choice of 22 h RT was motivated by similar experiments performed previously by our group (Frensing et al., 2013). The 36 h RT was selected based on scouting experiments performed in shake flasks and preliminary mathematical simulations (not shown). The CB was maintained at 1700 mL wv. Cultivations parameters were 37 °C, pH 7.1, and a stirring speed of 130 rpm. Aeration was controlled to 30% dissolved oxygen partial pressure by pulsed addition with a mixture of air, oxygen and nitrogen through a dip tube. For infection, the DIP-containing virus seed (A/PR/8/34-delS1(1))

was added to the VB1 and VB2 at an MOI of 0.1 based on the viable cell count and the $TCID_{50}$ titer of the virus seed at 50 h of culture. Additionally, the virus inoculum was supplemented with 1:100 ratio of trypsin (volume to culture volume). To avoid a fast wash-out of the virus seed, continuous mode was initiated at 23.4 h p.i. with the flow rates depicted in **Figure 1**. During the run, trypsin (0.5 Units/L) was present in the feed medium of the virus bioreactors. Feed media of all three reactors were provided in 5 L bottles chilled at 0-4°C; only the feed medium of the cell bioreactor had to be refilled during the run-time. Samples were taken twice a day from VB1 and VB2 and once a day from CB. About every 12 h, virus harvests reservoirs were stored at−20°C until further analysis. The experiment was terminated 20 days p.i. The average cell concentration input for VB1 and VB2 was $1.13{\cdot}10^6$ cells/mL as determined from the average viable cell count in CB with respect to STR working volumes and feeding rates. RTs were determined from the average volume and the average flow rate at the outlet of both STR over the infection phase.

Cell Counts and Virus Titers

Viable cell concentrations were determined using a ViCellXR (Beckman Coulter) and virus production was monitored by a hemagglutination (HA) assay (Kalbfuss et al., 2008) and a $TCID_{50}$ assay (Genzel and Reichl, 2007). The maximum standard deviation of the HA assay was ± 0.15 $\log_{10}$(HA Units/100 μL) and the dilution error of the $TCID_{50}$ assay was ± 0.3 $\log_{10}$ (Genzel et al., 2014).

Furthermore, we determined the concentration of total virus particles C_V in the supernatant based on the HA values using the following equation,

$$C_V = C_{Ery} \cdot 10^{(log_{10} HAU/100\ \mu L)}, \quad (1)$$

where C_{Ery} denotes the concentration of chicken erythrocyte solution added to the assay (2×10^7 cells/mL).

Segment-Specific Reverse Transcription-PCR for Detection of Defective Genomes

To analyze viral genomes, bioreactor samples were centrifuged for 5 min at 300 g and viral RNA was isolated from supernatants using the NucleoSpin RNA Virus kit (Macherey-Nagel) according to the manufacturer's instructions. Reverse transcription of isolated RNA to cDNA and segment-specific amplification of IAV genomes was performed as described previously (Frensing et al., 2014). Reverse transcription-PCR products were directly analyzed on a 1% agarose gel using electrophoresis (see **Data Sheet 1**; **Figure S4**).

Segment-Specific Reverse Transcription-qPCR for A/PR/8/34-delS1(1) and FL S1 Quantification

Absolute viral RNA (vRNA) copy numbers were determined as described previously (Wasik et al., 2018). In brief, 10-fold series dilutions of the corresponding vRNA reference standards and RNA samples were reverse transcribed with the tagged primer Seg-1-tagRT-for (ATTTAGGTGACACTATAGAAGCGAGC-GAAAGCAGGTCAATTATATTC). Subsequently, a qPCR was performed using the Rotor-Gene SYBR Green PCR Kit (Qiagen) following the manufacturer's recommendations and the primer pairs realtime-rev (GGAATCCCCTCAGTCTTC) and vRNA-tagRealtime-for (ATTTAGGTGACACTATAGAAGCG) for quantification of A/PR/8/34-delS1(1) and the primer pairs FL1-realtime-rev (CATTTCATCCTAAGTGCTGG) and vRNA-tagRealtime-for for quantification of FL S1. Viral RNA copy numbers were calculated based on the vRNA reference standards with linear regression. The lowest concentrations, which allowed quantification, were $2.2{\cdot}10^6$ copies/mL for A/PR/8/34-delS1(1) and $3.8{\cdot}10^6$ copies/mL for FL S1, respectively (Wasik et al., 2018). The relative standard deviation for determining copy numbers by qPCR was 23 and 27% for A/PR/8/34-delS1(1) and FL S1, respectively. Quantification of contaminating plasmids was performed by dilution series of the corresponding plasmid as described above, but without the reverse transcription step. The plasmid pHW-S1 was quantified with the primer pair FL1-realtime-rev and pHW-f (CTCACTATAGGGAGACCC). The plasmid pHW-A/PR/8/34-delS1(1) was quantified with the primer pair realtime-rev and pHW-f.

Since number of genome copies do not directly translate into numbers of virus particles, we adjusted the qPCR measurements of A/PR/8/34-delS1(1) and FL S1. For this, we assumed that the sum of A/PR/8/34-delS1(1)-containing virions and the FL S1-containing virions denotes the maximum number of virions present in a sample, which should equal the concentration of total virus particles C_V. Based on C_V, we calculated the concentration of virions that contain either A/PR/8/34-delS1(1) or FL S1 using Equations (2) and (3), respectively.

$$V_{ddi} = \frac{delS1\ (1)\ (copies/mL)}{delS1\ (1) + FL\ S1\ (copies/mL)} \cdot C_V(virions/mL) \quad (2)$$

$$V_S + V_d = \frac{FL\ S1\ (copies/mL)}{delS1\ (1) + FL\ S1\ (copies/mL)} \cdot C_V(virions/mL) \quad (3)$$

Furthermore, a differentiation between infectious FL S1-containing virions (V_S) and non-infectious FL S1-containing virions (V_d) is made. Since we know the number of V_S, i.e., the $TCID_{50}$ titer, we can easily determine the number of non-infectious FL S1-containing virions by solving Equation (3) for V_d.

Mathematical Modeling

Based on quantitative data available from reverse transcription-qPCR for S1 encoding PB2 of IAV that was established recently by our group, the segregated mathematical model describing this continuous virus production system established by Frensing et al. (2013) was modified. The extended model version describes explicitly the dynamics of replication-incompetent virions (DIPs) containing a deletion in S1 (V_{ddi}) as described above (A/PR/8/34-delS1(1), see Materials and Methods) in addition to non-infectious virions (V_d) and infectious virions (V_s) containing the FL S1.

As another modification, the infection of uninfected target cells (T) is considered separately for V_s and V_{ddi} to account

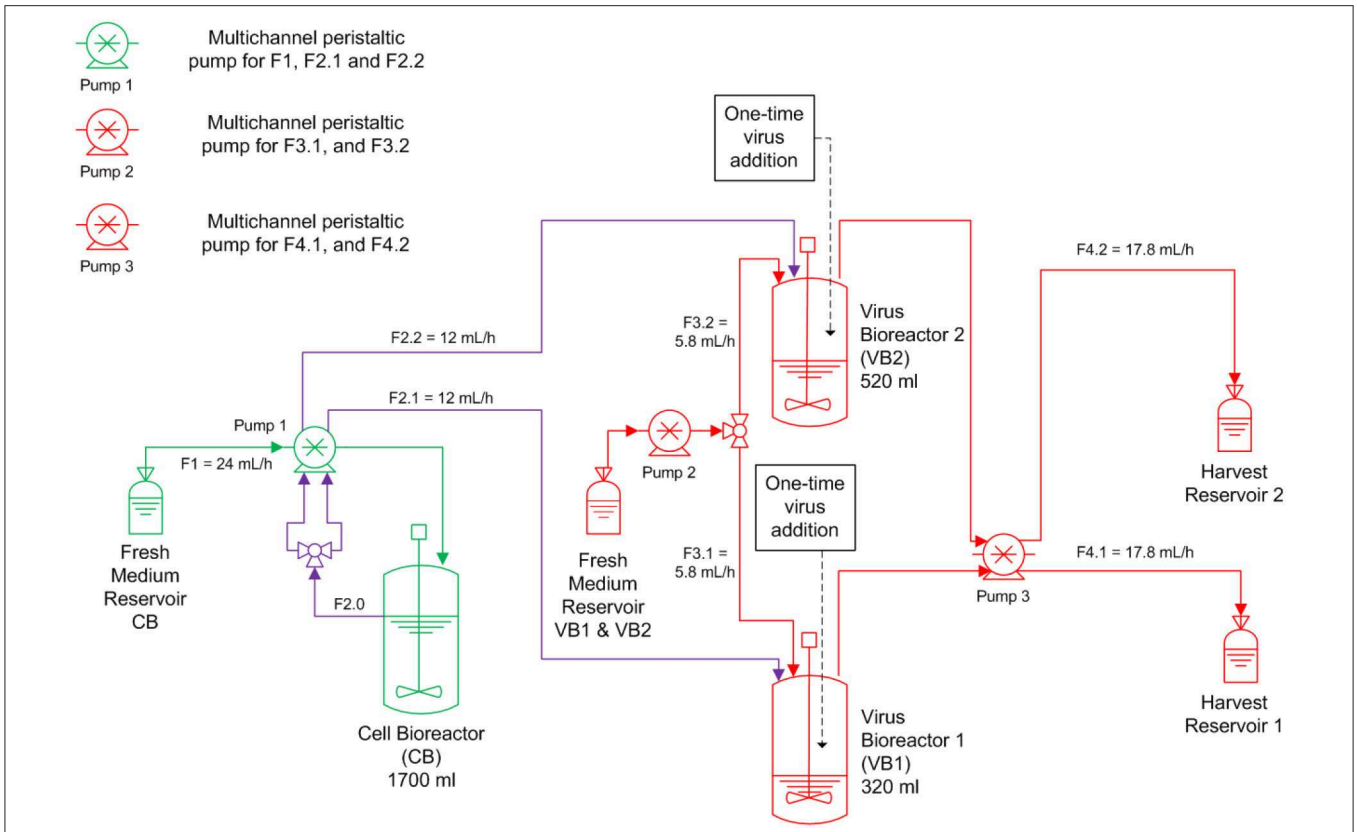

FIGURE 1 | Overview of the bioreactor setup for parallel continuous influenza A virus propagation in two vessels. MDCK suspension cells were grown in a cell bioreactor (CB) feeding two virus production vessels (VB1 and VB2) operated at a residence time of 22 and 36 h, respectively. At time of infection, the suspension MDCK cell-adapted virus seed containing A/PR/8/34-delS1(1) and FL standard virus (STV) was added to VB1 and VB2 at a multiplicity of infection of 0.1. Subsequently, cells were constantly fed into both virus bioreactors (F, feeding rate). Trypsin was added to the fresh medium reservoir of VB1 and VB2. All green components refer to CB, all red components to the VBs; CB and VBs are connected via the purple tubing.

for DIP entry with subsequent DIP replication in case of a co-infection.

$$\frac{d\,T}{d\,t} = \mu \cdot T - kvi \cdot T \cdot V_s - kvidi \cdot T \cdot V_{ddi} + D \cdot (T_{in} - T) \quad (4)$$

Where μ denotes the specific cell growth rate, and *kvi* and *kvidi* are the specific virus infection rates for infectious STVs and DIPs, respectively. The last term in Equation (4) accounts for the continuous feed of cells with concentration T_{in} at dilution rate D, which was set to adjust the two different RTs for both virus reactors (see **Table 1**). With respect to the average concentration of cells observed in CB, we choose T_{in} to be independent of time (data not shown). Ideal mixing is assumed for all vessels.

The population of infected cells is subdivided into cells infected with infectious STVs (I_s), DIPs (I_d), and both (I_c).

$$\frac{d\,I_s}{d\,t} = kvi \cdot T \cdot V_s - kvidi \cdot I_s \cdot V_{ddi} - \ kcdv \ \cdot I_s - D \cdot I_s \quad (5)$$

$$\frac{d\,I_d}{d\,t} = kvidi \cdot T \cdot V_{ddi} - kvi \cdot I_d \cdot V_s - kcdv \cdot I_d - D \cdot I_d \quad (6)$$

$$\frac{d\,I_c}{d\,t} = kvidi \cdot I_s \cdot V_{ddi} + kvi \cdot I_d \cdot V_s - \ kcdv \ \cdot I_c - D \cdot I_c \quad (7)$$

The first term in Equations (5) and (6) accounts for the infection of target cells by infectious STVs or DIPs, respectively. Furthermore, the co-infection of I_s and I_d by DIPs and infectious STVs, respectively, yields co-infected cells I_c in Equation (7). Antiviral mechanisms, such as the interferon-mediated innate immune response, and virus-induced cell death can be triggered by the presence of intracellular viral RNAs. In our experiments, the uptake of a high number of DIPs (10^3-10^4 DIPs per cell) results in a high number of intracellular viral RNAs, comparable to levels reached during a conventional infection (e.g., Frensing et al., 2014). Therefore, and in contrast to Frensing et al. (2013) we assume that DIP-only infected cells (I_d) do not continue to grow, but shut-off essential pathways for cell division, similar to the other infected cell populations I_s and I_c and, thus, die due to virus-induced apoptosis with the specific rate *kcdv*. Note, that Cane and colleagues have shown that DIP-only infected MDCK cells can continue to grow and give rise to DIP-infected daughter cells (Cane et al., 1987). However, the experimental conditions applied in their study, i.e., the use of UV-irradiated virus seed, passaging of cells in a virus-free culture and a culture time of 5-10 days between passages, cannot be compared to the cultivation conditions of our system.

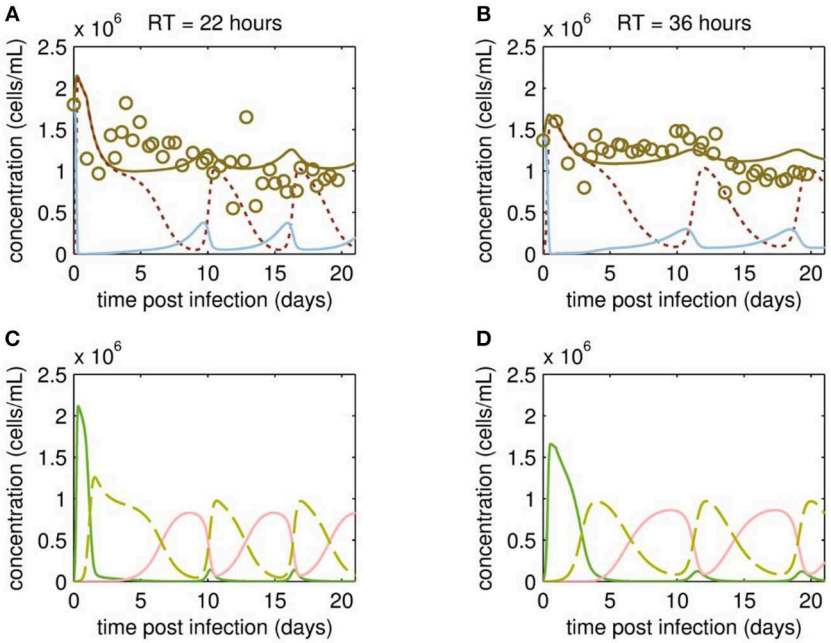

FIGURE 2 | Cell population dynamics of MDCK.SUS2 cells infected by A/PR/8/34-delS1(1) in a parallel continuous bioreactor system at residence times (RTs) of 22 and 36 h. Measurements (open circles) and model fit (brown solid lines) of the total cell concentration, and the simulated number of all productively infected cells, i.e., the sum of STV-only infected and co-infected cells, as (dotted dark red line), and uninfected target cells (blue solid line) in the virus vessels for RTs of 22 h **(A)** and 36 h **(B)**, respectively. Model predictions for the different infected cell populations, cells infected by infectious STV only (green solid line), cells infected by DIP only (red solid line), co-infected cells (dashed yellow line) in the virus vessels are shown for RTs of 22 h **(C)** and 36 h **(D)**, respectively. For both, experiment and model simulations, the continuous culture was started 23.4 h p.i.

The dynamics of infectious STVs (V_s), DIPs (V_{ddi}), and non-infectious virions containing a FL S1 (V_d) are described as

$$\frac{d\,V_s}{d\,t} = \mu vi \cdot I_s - kvi \cdot T \cdot V_s - kvi \cdot I_d \cdot V_s - kdvit \cdot V_s - D \cdot V_s \quad (8)$$

$$\frac{dV_{ddi}}{d\,t} = \mu vddi_C \cdot I_c + \mu vddi_S \cdot I_s - kvidi \cdot T \cdot V_{ddi} - kvidi \cdot I_s \cdot V_{ddi} - kvdt \cdot V_{ddi} - D \cdot V_{ddi} \quad (9)$$

$$\frac{dV_d}{d\,t} = \mu vd_S \cdot I_s + \mu vd_C \cdot I_c + kdvit \cdot V_s - kvdt \cdot V_d - D \cdot V_d \quad (10)$$

Similar to Frensing et al. (2013), we assume that STV-infected cells (I_s) produce infectious STVs (V_s) with the specific rate μvi and also have the potential to release DIPs (V_{ddi}) with the specific rate $\mu vddi_S$. Although in our analysis $\mu vddi_S$ is close to zero (see **Table 1**), the latter should not be ignored to allow for *de novo* generation of DIPs in case a DIP-free virus seed would be used for the infection of bioreactors. Co-infected cells release mainly DIPs containing the deletion in S1 (V_{ddi}) with the specific rate $\mu vddi_C$. In addition, both STV-infected and co-infected cells release non-infectious virus particles (V_d) with rates μvd_S and μvd_C, respectively. Furthermore, we assume that STVs are taken up by uninfected cells and DIP-only infected cells, while DIPs are either infecting uninfected cells or cells already infected by infectious STVs. Finally, we assume that STVs can lose their infectivity with the specific inactivation rate *kdvit* contributing to the population of non-infectious virions (V_d), while both V_{ddi} and V_d deteriorate with the specific lysis rate *kdvt*. In contrast to the previous model (Frensing et al., 2013), we neglected superinfection of I_s and I_c by STVs as well as superinfection of I_d and I_c by DIPs.

To investigate the time course of DIP formation based on reverse transcription-qPCR measurements, the following DIP to STV ratio was determined from experimental data:

$$ratio = \frac{V_{ddi}}{V_s}, \quad (11)$$

where V_{ddi} represent the reverse transcription-qPCR measurement of delS1(1) and V_s the infectious virions with FL S1, respectively. In addition, to describe overall cell growth dynamics, the concentration of all cells ($Cells_{total}$) in the virus bioreactor was estimated.

$$Cells_{total} = \mathrm{T} + I_s + I_d + I_c \quad (12)$$

Taken together, the model comprises seven ordinary differential equations. The set of ten parameters (**Table 1**) was determined by minimizing the least-squares prediction error of the state variables V_s, V_{ddi}, V_d and $Cells_{total}$, for which the error of each variable was weighted with its maximum measurement value.

TABLE 1 | Non-zero initial conditions and parameters including coefficients of variation used for simulations.

Symbol	Description	Value	CoV*	Unit
Continuous cultivation RT 22 h				
μ^{**}	Maximum spec. cell growth rate	0.0454	*Fixed*	$1/h$
D^{**}	Dilution rate of virus reactor	0.0454	*Fixed*	$1/h$
kvi	Spec. virus infection rate, infectious STV	$1.59 \cdot 10^{-7}$	33	$mL/(virion \cdot h)$
kvidi	Spec. virus infection rate, DIP	$2.32 \cdot 10^{-10}$	59	$mL/(virion \cdot h)$
kcdv	Spec. apoptosis rate	0.008	35	$1/h$
μvi	Spec. V_s production rate	2.51	9	$virions/(cell \cdot h)$
$\mu vddi_C$	Spec. V_{ddi} production rate of co-infected cells	203	10	$virions/(cell \cdot h)$
$\mu vddi_S$	*De novo* generation of DIPs	$1.00 \cdot 10^{-5}$	$1.40 \cdot 10^{6}$	$virions/(cell \cdot h)$
μvd_C	Spec. V_d production rate of co-infected cells	$4.91 \cdot 10^{-16}$	$4.07 \cdot 10^{15}$	$virions/(cell \cdot h)$
μvd_S	Spec. V_d production rate of STV-infected cells	120	13	$virions/(cell \cdot h)$
kdvit	Spec. V_s inactivation rate	$1.58 \cdot 10^{-7}$	$1.20 \cdot 10^{4}$	$1/h$
kvdt	Spec. V_{ddi}, V_d lysis rate	$3.82 \cdot 10^{-27}$	$1.15 \cdot 10^{26}$	$1/h$
T_0	Initial target cell concentration	$1.80 \cdot 10^{6}$	–	$cells/mL$
T_{in}	Cell concentration in feed	$1.13 \cdot 10^{6}$	–	$cells/mL$
V_{s0}	Initial infectious STV concentration	$3.16 \cdot 10^{5}$	–	$virions/mL$
V_{ddi0}	Initial DIP concentration	$6.41 \cdot 10^{5}$	–	$virions/mL$
V_{d0}	Initial non-infectious STV concentration	$2.05 \cdot 10^{7}$	–	$virions/mL$
Continuous cultivation RT 36 h				
μ^{**}	Maximum spec. cell growth rate	0.0278	*Fixed*	$1/h$
D^{**}	Dilution rate of virus reactor	0.0278	*Fixed*	$1/h$
kvi	Spec. virus infection rate, infectious STV	$5.38 \cdot 10^{-8}$	15	$mL/(virion \cdot h)$
kvidi	Spec. virus infection rate, DIP	$7.96 \cdot 10^{-11}$	96	$mL/(virion \cdot h)$
kcdv	Spec. apoptosis rate	0.003	80	$1/h$
μvi	Spec. V_s production rate	4.12	25	$virions/(cell \cdot h)$
$\mu vddi_C$	Spec. V_{ddi} production rate	177	7	$virions/(cell \cdot h)$
$\mu vddi_S$	*De novo* generation of DIPs	$1.13 \cdot 10^{-9}$	$1.12 \cdot 10^{4}$	$virions/(cell \cdot h)$
μvd_C	Spec. V_d production rate of co-infected cells	$1.41 \cdot 10^{-8}$	$3.30 \cdot 10^{10}$	$virions/(cell \cdot h)$
μvd_S	Spec. V_d production rate of STV-infected cells	173	9	$virions/(cell \cdot h)$
kdvit	Spec. V_s inactivation rate	0.070	47	$1/h$
kvdt	spec. V_{ddi}, V_d lysis rate	$2.02 \cdot 10^{-9}$	$1.01 \cdot 10^{6}$	$1/h$
T_0	Initial target cell concentration	$1.37 \cdot 10^{6}$	–	$cells/mL$
T_{in}	Cell concentration in feed	$1.13 \cdot 10^{6}$	–	$cells/mL$
V_{s0}	Initial infectious STV concentration	$3.16 \cdot 10^{5}$	–	$virions/mL$
V_{ddi0}	Initial DIP concentration	$8.06 \cdot 10^{5}$	–	$virions/mL$
V_{d0}	Initial non-infectious STV concentration	$2.03 \cdot 10^{7}$	–	$virions/mL$

*Coefficient of variation (%) (Copasi)

**Mean from experimental data of the virus bioreactors with $\mu = D$, not fitted.

Model equations were solved numerically using the CVODE routine from SUNDIALS (Cohen and Hindmarsh, 1996) on a Linux-based system. Model files and experimental data were handled within the Systems Biology Toolbox 2 (Schmidt and Jirstrand, 2006) for MATLAB (version 8.0.0.783 R2012b). Parameter values were estimated using the global stochastic optimization algorithm fSSm (Egea et al., 2007). Initial values were selected based on previous parameters determined for IAV replication in animal cells (e.g., Frensing et al., 2013). The coefficient of variation of parameters was determined using COPASI (Hoops et al., 2006).

RESULTS AND DISCUSSION

In order to reduce the risk of batch-to-batch variations for controlled experiments under different cultivation regimes, we established a parallel continuous production process for IAV propagated in MDCK suspension cells. In the set-up implemented, one cell bioreactor was used to feed two virus vessels (**Figure 1**). As a starting point, we investigated the impact of RT (22 and 36 h) on the accumulation of DIPs and their impact on viral titers over a period of 20 days. Based on quantitative information available from qPCR and the mathematical model established, it is possible to describe the dynamics of the various

cell populations as well as virus populations, i.e., infectious STVs, non-infectious STVs and replication-incompetent DIPs, and the DIP to STV ratio for both cultivation conditions.

Mathematical Model for Continuous Cultivation of Influenza A Virus

The mathematical model used in the present study is loosely based on a previously published model (Frensing et al., 2013) with modifications as explained in section Materials and Methods. We fitted the parameters of the model to the two sets of experimental data and determined their coefficient of variation (CoV) using Copasi (**Table 1**). For RT 22 h, low CoV ($\leq$ 13%) were reached for parameter estimates of the specific growth rates for the different viral subpopulations V_{ddi} and V_S, V_d, which are released by either co-infected cells I_c ($\mu vddi_C$) or by STV-infected cells I_S (μvi, μvd_S), respectively. Similarly, the CoV of estimates for $\mu vddi_C$, μvi and μvd_S for RT 36 h were $\leq$25%.

The specific STV infection rate *kvi* for RT 22 h as well as the specific DIP infection rate *kvidi*, and the specific apoptosis rate *kcdv* for both RT 22 and 36 h were estimated with higher CoV values (25% < CoV < 100%). Interestingly, the specific infection rate of STVs *kvi* for RT 36 h was estimated with a CoV of 15%.

The remaining parameters were estimated with CoV > 100%. In particular, the specific *de novo* generation rate of DIPs $\mu vddi_S$ had a very high CoV in both experimental scenarios. Since DIPs are present in the seed virus, *de novo* generation could also be excluded from modeling assumptions and viral dynamics would still show oscillations due to the amplification of DIPs introduced at infection. In contrast, if a DIP-free virus seed would be used to start infection, the oscillating viral dynamics could only be reproduced if *de novo* generation is accounted for. Thus, we decided to keep this parameter to propose a model that covers more general cases.

The specific production rate of non-infectious FL S1-containing virions μvd_C could also be neglected, since these particles are most likely released only from STV-infected cells, which is supported by the reasonable CoV values for the specific V_d production rate (μvd_S) in both RT 22 and 36 h experiments. In addition, the high CoV values for estimates of the specific virus inactivation and lysis rates (*kdvit*, *kvdt*) indicated that these mechanisms can probably be neglected, which we also analyzed in more detail with respect to the different RTs (see section Model reduction).

Overall, key parameter values estimated in this study, such as specific STV infection rate *kvi*, virus release rates, apoptosis rate *kcdv* and virus degradation rates, were in the same order of magnitude as determined previously for IAV replication models proposed for adherent MDCK cells (Möhler et al., 2005; Schulze-Horsel et al., 2009; Heldt et al., 2013).

Cellular Dynamics

At first, MDCK suspension cells were seeded and grown in batch mode simultaneously in all three bioreactors CB, VB1 and VB2 (**Figure 1**). CB was set to a working volume of 1700 mL and cells were grown in batch mode until a cell concentration of $2.97 \cdot 10^6$ cells/mL (viability 96.7 %) was reached. The infected vessels VB1 and VB2 had a working volume of 320 mL and 520 mL, respectively. VB1 and VB2 were seeded at a similar concentration, however, they reached $1.8 \cdot 10^6$ cells/mL and $1.4 \cdot 10^6$ cells/mL at time of infection, respectively. The infection of VB1 and VB2 took place at 50 h of culture at MOI of 0.1 and left in batch mode for another 23.4 h before initiating the continuous mode (to avoid virus washout). The VB1 and VB2 vessels were operated at an RT of 22 and 36 h, respectively. Those RTs were adjusted using a constant feed of 12 mL/h of cell broth from the CB and of 5.8 mL/h fresh medium into the virus bioreactors. Furthermore (to maintain wv), 17.8 mL/h were harvested from each VBs. The average concentration of target cells transferred from the CB to both VBs T_{in} was $1.13 \cdot 10^6$ cells/mL. Upon parameter estimation, we simulated the cell population dynamics in the virus vessels, which showed oscillations for uninfected target cells and the various infected cell populations for both RT 22 and RT 36 h (**Figure 2**).

Although the total cell concentration in VBs remained stable with an average of $1.12 \cdot 10^6$ cells/mL (standard deviation $\pm$ $0.30 \cdot 10^6$ cells/mL) for RT 22 and $1.17 \cdot 10^6$ cells/mL (standard deviation $\pm$ $0.22 \cdot 10^6$ cells/mL) for RT 36 h, a tendency toward cyclic behavior was observed (**Figures 2A,B**). This is linked to the simulated dynamics of the various cell populations caused by virus propagation. As expected, addition of the virus seed causes a fast increase of STV-only infected cells, followed by a strong drop in their concentration and a simultaneous increase of the co-infected cell population through superinfection by DIPs (**Figures 2C,D**). The co-infected cell population reaches its maxima at ~2 days p.i. and 4 days p.i., for RT 22 and 36 h, respectively. Since co-infected cells release mainly DIPs, uninfected target cells fed into the VBs will be infected by DIP only. While the DIP-only infected cell population reaches a peak concentration at ~8 days p.i. (RT 22 h) and 10 days p.i. (RT 36 h), the population of co-infected cells undergoes virus-induced apoptosis and ceases to a minimum (**Figures 2C,D**). However, the number of co-infected cells rises again quickly, since previously DIP-only infected cells are now superinfected by STVs produced by the small sub-population of STV-only infected cells. This behavior is repeated for another 1 to 1.5 cycles within the cultivation time. Thereby, all subpopulations of infected cells reach their peak concentrations repeatedly, which are similar in both VBs and, thus, seem independent of the RT.

Overall, the variation in the measured cell concentrations in the VBs did not follow the oscillating trend described for similar experiments by Frensing et al. (2013) using the avian AGE1.CR cell line infected with IAV (A/Puerto Rico/8/34, MOI 0.025) for a RT of 25 h. Indeed, there are qualitative and quantitative discrepancies between model simulation and measurement of the total cell concentrations. On the one hand, counting of MDCK suspension cells required the addition of trypsin for dissociation of cell aggregates, which occurred occasionally and increased the risk of outliers in cell concentration measurements. On the other hand, our model is not as well-informed on the dynamics of the various infected cell subpopulations since measurements focused on viral dynamics (see following section Viral Dynamics). To better resolve this issue, follow-up studies are planned to investigate in detail the dynamics of the various cell populations using flow cytometry. Ideally, this would not only involve the

conventional monitoring of infected cells using IAV-specific antibodies (Frensing et al., 2016), but the use of fluorescence markers for specific intracellular labeling of DI RNAs, which are currently not available, but under development and will allow to distinguish co-infected from STV-only infected cells.

Viral Dynamics

The reverse transcription-qPCR measurements that enabled monitoring of both the FL S1 and DI S1 (A/PR/8/34-delS1(1)) copy numbers together with the concentrations of the total number of virus particles (HA titer) and $TCID_{50}$ titer (**Figures 3**, **4**), allowed discrimination of the various virus subpopulations. Using these values, we calculated the concentration of virions containing either FL or DI S1 based on the qPCR measurement given in "copies/mL" to "virions/mL" (see Equations 2 and 3).

Overall, viral titers of FL and DI S1-containing virions showed the same trend for the two RTs tested over the first 10 days of culture (**Figure 3**). Maximum concentrations of FL S1-containing virions with $4.0{\cdot}10^9$ virions/mL and $5.6{\cdot}10^9$ virions/mL were reached at ∼1 day p.i. for RT of 22 and 36 h, respectively (**Figures 3A,B**). For RT 22 h, titers slowly decreased to about 10^7 virions/mL at ∼10 days p.i. For the higher RT, the decrease in titers of FL S1 virions was delayed compared to RT 22 and reached its minimum of about 10^8 virions/mL at ∼11 days p.i. At that time, the VB with RT 22 h already reached its second peak, followed by a decrease in titers leading to a second minimum at about 16 days p.i. The second minimum for RT 36 h was reached once more about 2 days later. The concentrations of DI S1-containing virions showed an initial delay in cycles of about 4 days compared to their corresponding FL counterparts and reached their first maxima with $7.0{\cdot}10^9$ virions/mL (5 days p.i.) and $8.4{\cdot}10^9$ virions/mL (5 days p.i.) for RT 22 and 36 h, respectively (**Figures 3C,D**). The cyclic trend observed in both data sets is described clearly by the model fits. Note, that some quantitative discrepancies between data and model simulation remain, such as underestimation of the FL S1-containing virus titers for various time points (**Figures 3A,B**). Although, measured and simulated virus titers show some discrepancies for these individual runs, simulations are mainly within the error range of the assays for HA (about ± 0.15 log) and $TCID_{50}$ (about ± 0.3 log). Regarding the error for the number of virions containing either FL or DI S1, it has to be considered that those are derived from both qPCR measurements (relative standard deviation of about 25%) and from HA titers (Equations 2 and 3). Nevertheless, further investigations (e.g., next-generation deep sequencing) should be performed to elucidate those discrepancies in more detail.

Time courses for infectious virions V_s measured by the $TCID_{50}$ assay and for the sum of all viral subpopulations determined by the HA assay ($V_s + V_d + V_{ddi}$) also showed pronounced oscillations (**Figure 4**). Furthermore, the HA data indicate a trend for an overall decrease in the amplitude of titers toward later cultivation time points for both RTs (**Figures 4C,D**). The $TCID_{50}$ titers reached their maxima with the initial peaks, while the following peak titers were lower. However, no overall decrease in peak infectious titers was observed (**Figures 4A,B**).

Maximum $TCID_{50}$ titers were achieved around 3 days p.i. with $5.6{\cdot}10^7$ virions/mL and $2.4{\cdot}10^8$ virions/mL for RT 22 and 36 h, respectively. Most likely, the higher infectious titer for the longer RT of 36 h was related to the reduced wash-out (lower dilution rate) compared to RT 22 h. In total, three cycles were observed for the short RT with a second and a third peak of $\sim 3{\cdot}10^6$ virions/mL at 12 and 18 days p.i., respectively (**Figure 4A**). A similar behavior was observed for RT 36 h, however, only about 2.5 cycles were achieved during the cultivation time (**Figure 4B**). While the $TCID_{50}$ dynamics are captured well both quantitatively and qualitatively, simulated and measured HA values deviate to a certain extent (but within the assay error range) for data points after about 10 days p.i. (**Figures 4C,D**). In particular, the decreasing trend of peak HA titers is not reproduced by the model (also in case the system is simulated for 90 days p.i., **Data Sheet 1**; **Figure S1**). Whether the decreasing trend of peak HA titers is an individual characteristic of these particular runs or if the model simulations still lie within the biological variation of these experiments needs to be addressed when more experiments become available. Since the overall goal of this study was to establish and fit a basic model with a minimum number of parameters and simple kinetics, we decided to keep the model structure for now. Likely, also more detailed studies regarding the dynamics of the individual cell populations will allow further improvement of the model (see discussion on *Cellular dynamics*).

Simulation of DIP to STV Ratios

As expected, oscillations were also observed in the dynamics of the DIP to STV ratios (**Figure 5**). In both cultivations, the ratio reached a maximum of about 10^5 at ∼7 days p.i. These maxima are similar for both RTs and correlate with the lowest $TCID_{50}$ titer. We may hypothesize that one infectious STV per 10^5 DIPs is a critical ratio at which DIPs cause self-interference and start to hamper overall virus replication significantly. The impact of too high DIP to STV ratios and related self-interference is supported by a modeling study of our group (Laske et al., 2016). As a consequence of self-interference, DIP concentrations decrease, reaching a minimum around 11 days p.i., and numbers of infectious STVs are rising again, initiating a new cycle (see also **Figures 3**, **4**). It would be interesting to test whether this critical ratio can be reproduced in other experiments of continuous two-stage cultivations.

Model (In)Validation

After fitting the present model ("Model 1") to both data sets, we tested if it could still describe the data if certain parameters were removed. First, we set the parameter for inactivation of V_s (*kdvit*) and the lysis rate of virions (*kvdt*) to zero and re-fitted the model ("Model 2"). For the data set of RT 22 h, the goodness of fit was similar to the full model (Model 1), both visually (**Figure 6**) and quantitatively as based on the objective function values (**Table 2**). This was expected, since both parameters, *kdvit* and *kvdt*, were already close to zero in Model 1. For the second data set with RT 36 h, the re-fitting with Model 2 resulted in a noticeable increase of the objective function value (**Table 3**). In addition, Model 2 was unable to describe the data qualitatively. In particular, the number of cycles in the viral dynamics could not be reproduced

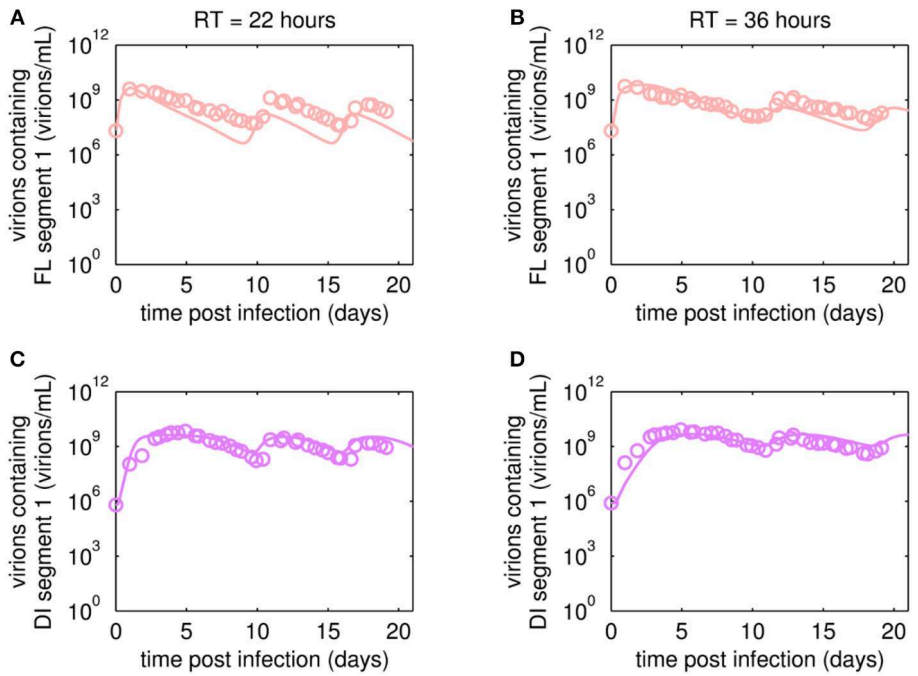

FIGURE 3 | Dynamics of FL or DI segment 1 (S1)-containing virions of A/PR/8/34-delS1(1) produced in MDCK.SUS2 cells in a parallel continuous bioreactor system with residence times (RT) of 22 and 36 h, respectively. Experimental data based on reverse transcription-qPCR (open circles) and model fit (solid lines) are shown for **(A,B)** all virions containing FL S1 and **(C,D)** virions containing DI S1 (A/PR/8/34-delS1(1)). For both, experiment and model simulations, the continuous culture was started 23.4 h p.i.

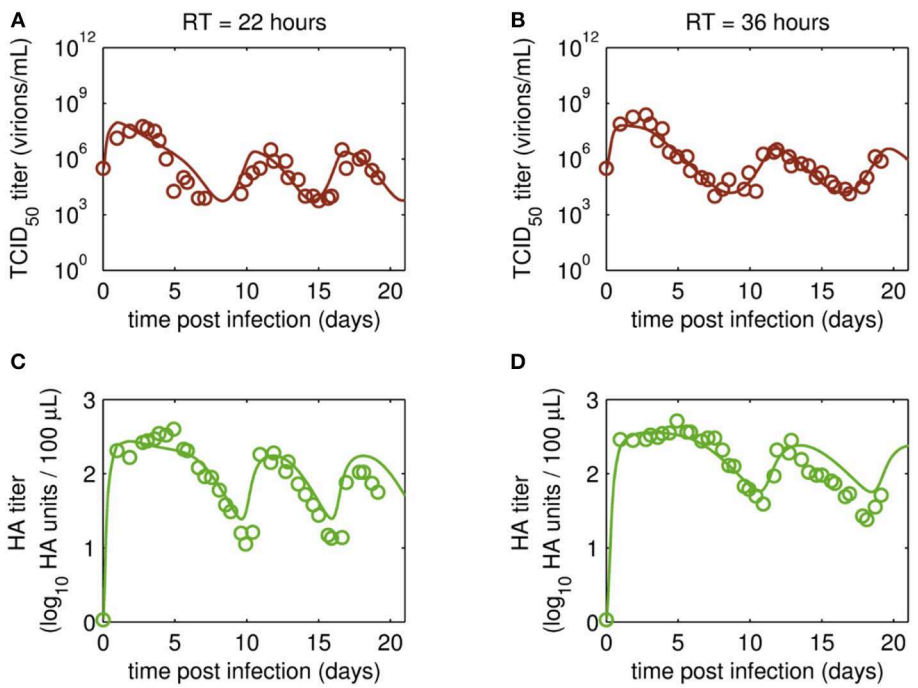

FIGURE 4 | Dynamics of infectious virions and total number of virions produced in MDCK.SUS2 cells infected by A/PR/8/34-delS1(1) in a parallel continuous bioreactor system with residence times (RT) of 22 and 36 h, respectively. Experimental data (open circles) and model fit (solid lines) are shown for **(A,B)** $TCID_{50}$ titer (infectious virion subpopulation of the FL S1-containing virions) and **(C,D)** HA titer which represents the sum of all viral subpopulations containing FL and DI S1. For both, experiment and model simulations, the continuous culture was started 23.4 h p.i.

any more (**Figure 7**). Most likely this points to an important feature of cultivations with long RTs, for which degradation and inactivation processes have to be taken explicitly into account to adequately describe the data. In contrast, in cultivations with short RTs (higher dilution rates), the overall impact of the wash-out of virions on viral dynamics was probably higher than that of inactivation and degradation processes.

Next, we tested whether it is essential to account for separate specific rates of infection, for either STV (*kvi*) or DIP infection (*kvidi*). For this, we used Model 1 and defined one joint infection rate (*kvi* in "Model 3"). Upon fitting Model 3 to the data of RT 22 h, the overall dynamics were still described well. However, the model overestimated the $TCID_{50}$ titer while underestimating the number of FL and DI S1-containing virions as well as the overall number of virions produced (**Figure 6**). We observed a similar effect for the RT 36 h data set, combined with a lower number of cycles compared to the fit with Model 1 (**Figure 7**). This suggests that two separate infection rates are needed to achieve good agreement with experimental data. Although, visually, goodness of fit with Model 1 in both data sets seems better than that of Model 3, the objective function value has decreased only by 6% or by 19% compared to that of Model 1, for the RT 22 h (**Table 2**) and RT 36 h (**Table 3**), respectively. At a first glance, this decrease in the objective function value seems counter-intuitive, however, since Model 3 still has a very good agreement with a majority of measurements for some of the state variables, e.g., DIP concentration (**Figure 7D**), the objective function value might be comparable to that of Model 1. While fitting oscillating data sets, we experienced that the objective function value can be misleading for some parameter regimes and that, for instance, optimizers may also yield "a good quantitative fit" by a straight line through the mean of the experimental data.

Finally, we also tested a fourth version of the model, which consisted of a combination of Model 2 and Model 3, i.e.,

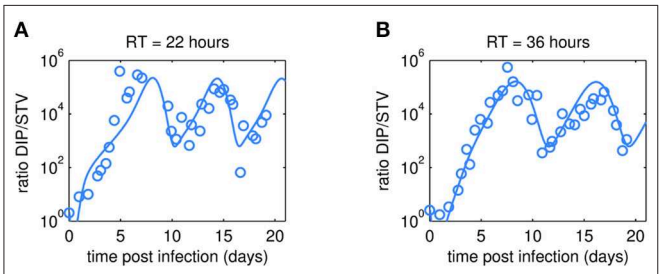

FIGURE 5 | Dynamics of DIP to STV ratios observed in MDCK.SUS2 cells infected by A/PR/8/34-delS1(1) in a parallel continuous bioreactor system at residence times (RT) of 22 h **(A)** and 36 h **(B)**. The experimental DIP to STV ratio determined by dividing the DI S1 containing number of virions by the corresponding $TCID_{50}$ titer (circles) is shown together with the simulated ratio according to Equation (11).

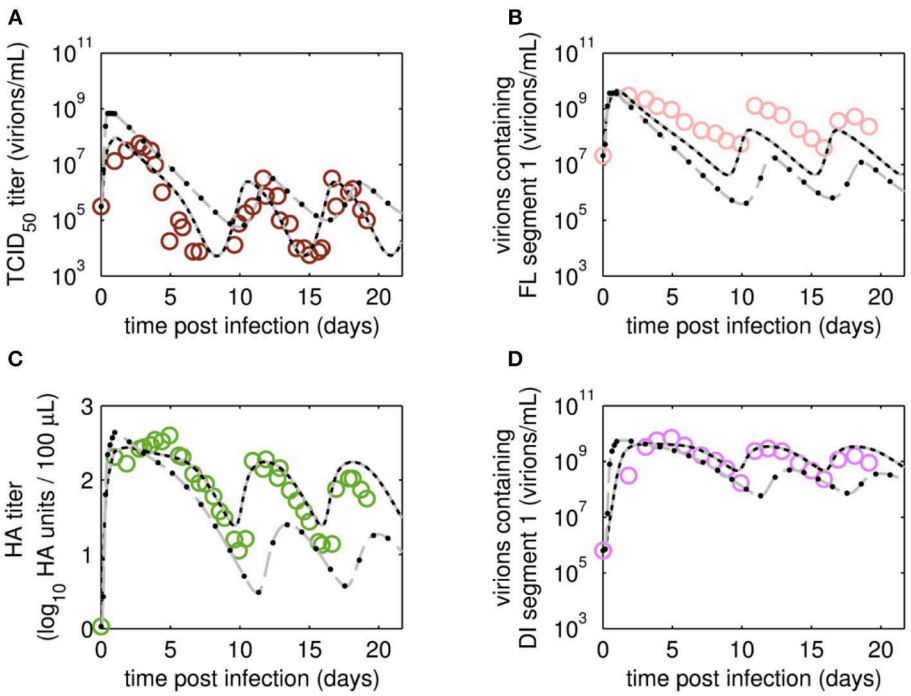

FIGURE 6 | Dynamics of viral subpopulations, produced by MDCK.SUS2 cells infected by A/PR/8/34-delS1(1) in a parallel continuous bioreactor system at RT 22 h, were fitted using different models. Experimental data (open circles) and four model fits (various lines) are shown for **(A)** $TCID_{50}$ titer representing infectious virions of **(B)** the FL S1-containing virions as well as the sum of all viral subpopulations as log HA units **(C)** and DI S1-containing virions **(D)**. Every subfigure shows the four model fits, using Model 1 containing all parameters (gray solid line), Model 2 with $kdvit = kvdt = 0$ (black dotted line), Model 3 with $kvi = kvidi$ (gray dashed line) or Model 4 with $kvi = kvidi$ and $kdvit = kvdt = 0$ (line of black circles). For the sake of simplicity only every 2nd data point is shown for the qPCR-based data **(B,D)**. For both experiment and model simulations, the continuous culture was started 23.4 h p.i.

TABLE 2 | Parameterization and objective function value obtained by fitting different models for the production of A/PR/8/34-delS1(1) by MDCK.SUS2 cells in a parallel continuous bioreactor system at residence time 22 h.

Parameters	Model 1, all parameters	Model 2, *kdvit* = *kvdt* = 0	Model 3, *kvi* = *kvidi*	Model 4, *kdvit* = *kvdt* = 0 and *kvi* = *kvidi*
kvi	$1.59 \cdot 10^{-7}$	$1.59 \cdot 10^{-7}$	$4.58 \cdot 10^{-9}$	$4.58 \cdot 10^{-9}$
kvidi	$2.32 \cdot 10^{-10}$	$2.33 \cdot 10^{-10}$	*kvi*	*kvi*
kcdv	0.008	0.008	0.009	0.009
μvi	2.51	2.50	105	104
$\mu vddi_C$	203	203	168	168
$\mu vddi_S$	$1.00 \cdot 10^{-5}$	$1.15 \cdot 10^{-5}$	0.01	0.01
μvd_C	$4.91 \cdot 10^{-16}$	$3.13 \cdot 10^{-16}$	$2.11 \cdot 10^{-13}$	$2.82 \cdot 10^{-13}$
μvd_S	120	120	439	441
kdvit	$1.58 \cdot 10^{-7}$	0	$1.58 \cdot 10^{-4}$	0
kvdt	$3.82 \cdot 10^{-27}$	0	$6.30 \cdot 10^{-26}$	0
Objective function value[#]	8.50	8.49	7.99	8.00

[#]*Objective function values are the normalized least squared prediction errors of the state variables of all cells* $Cells_{total}$*, fully infectious STVs* V_S*, replication-incompetent DIPs* V_{ddi}*, and non-infectious FL S1-containing virions* V_d*.*

TABLE 3 | Parameterization and objective function value obtained by fitting different models for the production of A/PR/8/34-delS1(1) by MDCK.SUS2 cells in a parallel continuous bioreactor system at residence time 36 h.

Parameters	Model 1, all parameters	Model 2, *kdvit* = *kvdt* = 0	Model 3, *kvi* = *kvidi*	Model 4, *kdvit* = *kvdt* = 0 and *kvi* = *kvidi*
kvi	$5.38 \cdot 10^{-8}$	$1.38 \cdot 10^{-7}$	$2.89 \cdot 10^{-9}$	$2.60 \cdot 10^{-9}$
kvidi	$7.96 \cdot 10^{-11}$	$1.16 \cdot 10^{-10}$	*kvi*	*kvi*
kcdv	0.003	0.002	0.001	0.001
μvi	4.12	1.42	142	80
$\mu vddi_C$	177	93	152	153
$\mu vddi_S$	$1.13 \cdot 10^{-9}$	$2.57 \cdot 10^{-7}$	$1.04 \cdot 10^{-10}$	$1.62 \cdot 10^{-7}$
μvd_C	$1.41 \cdot 10^{-8}$	$1.42 \cdot 10^{-9}$	$1.01 \cdot 10^{-5}$	$2.01 \cdot 10^{-6}$
μvd_S	173	193	613	725
kdvit	0.07	0	$4.35 \cdot 10^{-3}$	0
kvdt	$2.02 \cdot 10^{-9}$	0	$2.15 \cdot 10^{-8}$	0
Objective funciton value[#]	6.19	13.36	4.99	5.06

[#]*Objective function values are the normalized least squared prediction errors of the state variables of all cells* $Cells_{total}$*, fully infectious STVs* V_S*, replication-incompetent DIPs* V_{ddi}*, and non-infectious FL S1-containing virions* V_d*.*

neglecting virus degradation processes and using a joint infection rate, simultaneously. In case of RT 22 h, the Model 4 followed the same dynamics as Model 3 (**Figure 6**). This was expected, since the analysis of Model 2 already showed that degradation processes are not highly relevant for RT 22 h. Thus, Model 3 and Model 4 are mechanistically identical, which also leads to similar parametrizations of these two models (**Table 2**). For RT 36 h, the dynamics of Model 4 were similar to Model 2, showing fewer cycles due to exclusion of virus inactivation and degradation processes (**Figure 7**). In addition, Model 4 showed quantitative deviations similar to those of Model 3. Together, this underlines the importance of virus inactivation and degradation processes as well as the separation of DIP and STV infection rates for RT 36 h, which have to be taken into account to capture the experimental data. Most likely the difference in *kvi* and *kvidi* is related to the underlying mass action kinetics of the model. Since the DIP concentration is, on average, about two orders of magnitude higher than the STV concentration, the model estimates a lower specific DIP infection rate to yield an adequate amount of DIP-only and co-infected cells, and a high DIP titer in the supernatant. Whether this has any biological background still needs to be addressed experimentally.

Ideally, models including parametrization should allow the prediction of viral dynamics for different RT, e.g., to perform model-based process optimization. However, due to some mechanisms that seem dependent on the RT (explained above) none of the current model-parameter-combinations was able to predict viral dynamics for the other RT and *vice versa*

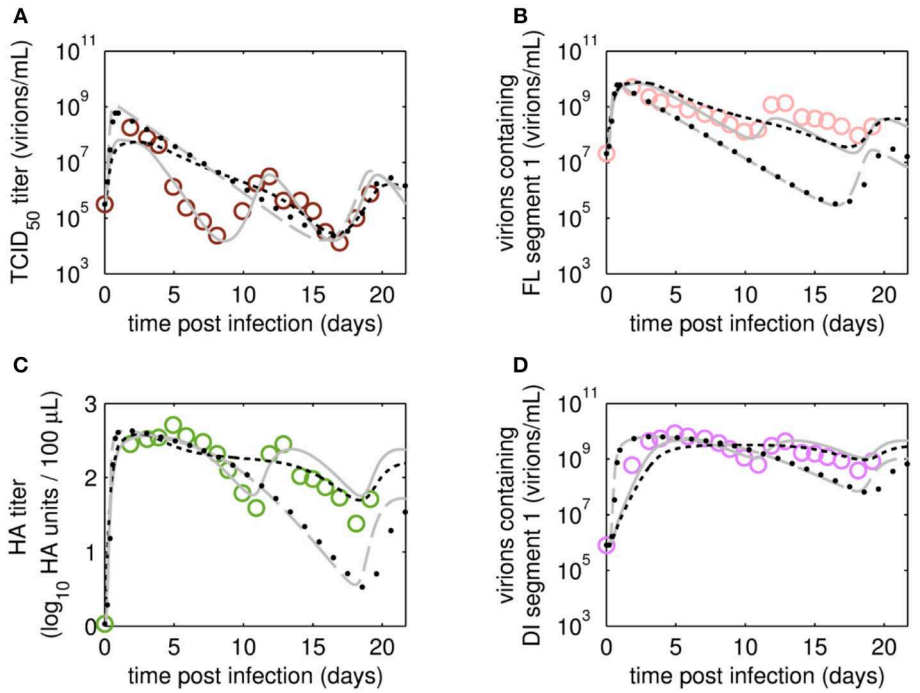

FIGURE 7 | Dynamics of viral subpopulation, produced by MDCK.SUS2 cells infected by A/PR/8/34-delS1(1) in a parallel continuous bioreactor system at RT 36 h, were fitted using different models. Experimental data (open circles) and four model fits (various lines) are shown for **(A)** $TCID_{50}$ titer representing the infectious virions of **(B)** the FL S1-containing virions as well as the sum of all viral subpopulations as log HA units **(C)** and DI S1-containing virions **(D)**. Every subfigure shows the four model fits, using Model 1 containing all parameters (gray solid line), Model 2 with $kdvit = kvdt = 0$ (black dotted line), Model 3 with $kvi = kvidi$ (gray dashed line) or Model 4 with $kvi = kvidi$ and $kdvit = kvdt = 0$ (line of black circles). For the sake of simplicity, only every 2nd data point is shown **(A–D)**. For both, experiment and model simulations, the continuous culture was started 23.4 h p.i.

(see also **Data Sheet 1**; **Figures S2, S3**). Accordingly, we think that the model might still lack certain aspects or kinetics and therefore has room for further model extensions. For instance, including the eclipse phase, i.e., the time delay between virus infection and release of viral progeny, or taking into account the accumulation of other DI RNAs, except for A/PR/8/34-delS1(1), might help to further improve model fits and enable predictions (see **Data Sheet 1**; **Figure S4**).

SUMMARY

In the present study, we introduce a two-stage continuous bioreactor setup for head-to-head comparison of IAV DIP production under different culture conditions. For infection, we used a virus seed generated by reverse genetics, which contained a known DIP, A/PR/8/34-delS1(1), which enabled the monitoring of DI and FL virus replication based on qPCR measurements. We observed oscillations in viral titers, where the frequency was depending on the RT. I.e., an increase in the RT from 22 to 36 h caused a shift in cycles of about 2 days. PCR analysis of IAV segments 1-3 revealed that changes in the RT might also result in the accumulation of different DIP subpopulations in long-term cultures. The mathematical model established allowed to describe the time courses of the various viral and cellular subpopulations. Comparison of model fits to the two data sets obtained suggests that for the longer RT of 36 h, inactivation of infectious STVs and degradation of virions has to be taken into account. Interestingly, the goodness of fit was also affected by the additional assumption that DIPs and STVs infect cells at different rates. Still, we observed some discrepancies between model and experimental data and found that the predictive power of the model needs improvement. This may be related to the fact that the model is still not fully informed, e.g., regarding the dynamics on the different infected cell subpopulations and the *de novo* synthesis and impact of other DIPs except for A/PR/8/34-delS1(1). In addition, the model might be extended further by accounting for the eclipse phase of virus release. The use of reporter viruses and specific probes for DI RNA staining may help to elucidate those mechanisms in more detail. For parameter estimation, we have used the data set of only one parallel run and are, therefore, unable to evaluate goodness of fit with respect to the biological variation of these cultivations. This will be addressed in the future, when more cultivations performed at similar experimental conditions become available.

In summary, the continuous cultivation system established is an excellent tool for detailed studies regarding DIP replication in animal cells. Based on the high DIP concentrations obtained it

also qualifies as a system for production of DIPs for animal trials and influenza antiviral therapy.

DATA AVAILABILITY STATEMENT

All datasets generated for this study are included in the manuscript/**Supplementary Files**.

AUTHOR CONTRIBUTIONS

FT, TL, MW, MR, YG, and UR contributed conception and design of the study. FT performed the experiments. TL, MR, and UR performed the mathematical analysis. UR wrote the first drafts of the manuscript. FT, TL, MW, YG, and UR wrote sections of the manuscript. All authors contributed to manuscript revision, read, and approved the submitted version.

FUNDING

This work was supported by the Defense Advanced Research Projects Agency (https://www.darpa.mil/program/intercept), INTERCEPT program (FT, TL) under Cooperative Agreement W911NF-17-2-0012.

ACKNOWLEDGMENTS

The authors would like to thank Nancy Wynserski for excellent technical assistance.

SUPPLEMENTARY MATERIAL

The Supplementary Material for this article can be found online at: https://www.frontiersin.org/articles/10.3389/fbioe.2019.00275/full#supplementary-material

REFERENCES

Ahmed, S. S., Ellis, R. W., and Rappuoli, R. (2017). "Technologies for Making New Vaccines," in *Plotkin's Vaccines*, eds S. A. Plotkin, W. Orenstein, P. A. Offit, and K. M. Edwards (Philadelphia, PA: Elsevier), 1283–1304. doi: 10.1016/B978-0-323-35761-6.00066-3

Akkina, R. K., Chambers, T. M., and Nayak, D. P. (1984). Mechanism of interference by defective-interfering particles of influenza virus: differential reduction of intracellular synthesis of specific polymerase proteins. *Virus Res.* 1, 687–702. doi: 10.1016/0168-1702(84)90059-5

Akpinar, F., Inankur, B., and Yin, J. (2016a). Spatial-temporal patterns of viral amplification and interference initiated by a single infected cell. *J. Virol.* 90, 7552–7566. doi: 10.1128/JVI.00807-16

Akpinar, F., Timm, A., and Yin, J. (2016b). High-throughput single-cell kinetics of virus infections in the presence of defective interfering particles. *J. Virol.* 90, 1599–1612. doi: 10.1128/JVI.02190-15

Aubrit, F., Perugi, F., Léon, A., Guéhenneux, F., Champion-Arnaud, P., Lahmar, M., et al. (2015). Cell substrates for the production of viral vaccines. *Vaccine* 33, 5905–5912. doi: 10.1016/j.vaccine.2015.06.110

Barrett, P. N., Terpening, S. J., Snow, D., Cobb, R. R., and Kistner, O. (2017). Vero cell technology for rapid development of inactivated whole virus vaccines for emerging viral diseases. *Expert Rev. Vaccines* 16, 883–894. doi: 10.1080/14760584.2017.1357471

Bdeir, N., Arora, P., Gärtner, S., Hoffmann, M., Reichl, U., Pöhlmann, S., et al. (2019). A system for production of defective interfering particles in the absence of infectious influenza A virus. *PLoS ONE* 14:e0212757. doi: 10.1371/journal.pone.0212757

Cane, C., McLain, L., and Dimmock, N. J. (1987). Intracellular stability of the interfering activity of a defective interfering influenza virus in the absence of virus multiplication. *Virology* 159, 259–264. doi: 10.1016/0042-6822(87)90463-6

Cohen, S. D., and Hindmarsh, A. C. (1996). CVODE, a stiff/nonstiff ODE solver in C. *Comput. Phys.* 10, 138–143. doi: 10.1063/1.4822377

De Gregorio, E., and Rappuoli, R. (2014). From empiricism to rational design: a personal perspective of the evolution of vaccine development. *Nat. Rev. Immunol.* 14:505. doi: 10.1038/nri3694

Dimmock, J. N., and Easton, J. A. (2015). Cloned defective interfering influenza RNA and a possible pan-specific treatment of respiratory virus diseases. *Viruses* 7, 3768–3788. doi: 10.3390/v7072796

Dimmock, N. J., Beck, S., and McLain, L. (1986). Protection of mice from lethal influenza: evidence that defective interfering virus modulates the immune response and not virus multiplication. *J. Gen. Virol.* 67, 839–850. doi: 10.1099/0022-1317-67-5-839

Dimmock, N. J., Dove, B. K., Scott, P. D., Meng, B., Taylor, I., Cheung, L., et al. (2012). Cloned defective interfering influenza virus protects ferrets from pandemic 2009 influenza a virus and allows protective immunity to be established. *PLoS ONE* 7:e49394. doi: 10.1371/journal.pone.0049394

Dimmock, N. J., and Easton, A. J. (2014). Defective interfering influenza virus RNAs: time to reevaluate their clinical potential as broad-spectrum antivirals? *J. Virol.* 88, 5217–5227. doi: 10.1128/JVI.03193-13

Dimmock, N. J., and Marriott, A. C. (2006). *In vivo* antiviral activity: defective interfering virus protects better against virulent Influenza A virus than avirulent virus. *J. Gen. Virol.* 87, 1259–1265. doi: 10.1099/vir.0.81678-0

Dimmock, N. J., Rainsford, E. W., Scott, P. D., and Marriott, A. C. (2008). Influenza virus protecting RNA: an effective prophylactic and therapeutic antiviral. *J. Virol.* 82, 8570–8578. doi: 10.1128/JVI.00743-08

Duhaut, S. D., and Dimmock, N. J. (2003). Defective influenza A virus generated entirely from plasmids: its RNA is expressed in infected mouse lung and modulates disease. *J. Virol. Methods* 108, 75–82. doi: 10.1016/S0166-0934(02)00260-4

Easton, A. J., Scott, P. D., Edworthy, N. L., Meng, B., Marriott, A. C., and Dimmock, N. J. (2011). A novel broad-spectrum treatment for respiratory virus infections: influenza-based defective interfering virus provides protection against pneumovirus infection *in vivo*. *Vaccine* 29, 2777–2784. doi: 10.1016/j.vaccine.2011.01.102

Egea, J. A., Rodríguez-Fernández, M., Banga, J. R., and Mart,í, R. (2007). Scatter search for chemical and bio-process optimization. *J. Glob. Optim.* 37, 481–503. doi: 10.1007/s10898-006-9075-3

Frensing, T. (2015). Defective interfering viruses and their impact on vaccines and viral vectors. *Biotechnol. J.* 10, 681–689. doi: 10.1002/biot.201400429

Frensing, T., Heldt, F. S., Pflugmacher, A., Behrendt, I., Jordan, I., Flockerzi, D., et al. (2013). Continuous influenza virus production in cell culture shows a periodic accumulation of defective interfering particles. *PLoS ONE*. 8:e72288. doi: 10.1371/journal.pone.0072288

Frensing, T., Kupke, S. Y., Bachmann, M., Fritzsche, S., Gallo-Ramirez, L. E., and Reichl, U. (2016). Influenza virus intracellular replication dynamics, release kinetics, and particle morphology during propagation in MDCK cells. *Appl. Microbiol. Biotechnol.* 100, 7181–7192. doi: 10.1007/s00253-016-7542-4

Frensing, T., Pflugmacher, A., Bachmann, M., Peschel, B., and Reichl, U. (2014). Impact of defective interfering particles on virus replication and antiviral host response in cell culture-based influenza vaccine production. *Appl. Microbiol. Biotechnol.* 98, 8999–9008. doi: 10.1007/s00253-014-5933-y

Genzel, Y. (2015). Designing cell lines for viral vaccine production: where do we stand? *Biotechnol. J.* 10, 728–740. doi: 10.1002/biot.201400388

Genzel, Y., and Reichl, U. (2007). "Vaccine production - state of the art and future needs in upstream processing," in *Animal Cell Biotechnology: Methods*

and Protocols, ed R. Pörtner (Totowa, NJ: Humana Press Inc.), 457–473. doi: 10.1007/978-1-59745-399-8_21

Genzel, Y., Rödig, J., Rapp, E., and Reichl, U. (2014). "Vaccine production: upstream processing with adherent or suspension cell lines," in *Animal Cell Biotechnology: Methods and Protocols*, ed R. Pörtner (Totowa, NJ: Humana Press Inc.), 371–393. doi: 10.1007/978-1-62703-733-4_23

Heldt, F. S., Frensing, T., Pflugmacher, A., Gröpler, R., Peschel, B., and Reichl, U. (2013). Multiscale modeling of influenza A virus infection supports the development of direct-acting antivirals. *PLoS Comput. Biol.* 9:e1003372. doi: 10.1371/journal.pcbi.1003372

Hoffmann, E., Neumann, G., Kawaoka, Y., Hobom, G., and Webster, R. G. (2000). A DNA transfection system for generation of influenza A virus from eight plasmids. *Proc. Natl. Acad. Sci. U.S.A.* 97, 6108–6113. doi: 10.1073/pnas.100133697

Hoops, S., Sahle, S., Gauges, R., Lee, C., Pahle, J., Simus, N., et al. (2006). COPASI—a COmplex PAthway SImulator. *Bioinformatics* 22, 3067–3074. doi: 10.1093/bioinformatics/btl485

Huang, A. S., and Baltimore, D. (1977). "Defective Interfering Animal Viruses," in *Comprehensive Virology 10*, eds H. Fraenkel-Conrat and R. R. Wagner (New York, NY: Plenum Press), 73–116. doi: 10.1007/978-1-4684-0832-4_2

Kalbfuss, B., Knöchlein, A., Kröber, T., and Reichl, U. (2008). Monitoring influenza virus content in vaccine production: precise assays for the quantitation of hemagglutination and neuraminidase activity. *Biologicals* 36, 145–161. doi: 10.1016/j.biologicals.2007.10.002

Kutzler, M. A., and Weiner, D. B. (2008). DNA vaccines: ready for prime time? *Nat. Rev. Genet.* 9:776. doi: 10.1038/nrg2432

Lackenby, A., Besselaar, T. G., Daniels, R. S., Fry, A., Gregory, V., Gubareva, L. V., et al. (2018). Global update on the susceptibility of human influenza viruses to neuraminidase inhibitors and status of novel antivirals, 2016–2017. *Antiviral Res.* 157, 38–46. doi: 10.1016/j.antiviral.2018.07.001

Laske, T., Heldt, F. S., Hoffmann, H., Frensing, T., and Reichl, U. (2016). Modeling the intracellular replication of influenza A virus in the presence of defective interfering RNAs. *Virus Res.* 213, 90–99. doi: 10.1016/j.virusres.2015.11.016

Liao, L. E., Iwami, S., and Beauchemin, C. A. A. (2016). (In)validating experimentally derived knowledge about influenza A defective interfering particles. *J. R. Soc. Interface* 13:20160412. doi: 10.1098/rsif.2016.0412

Lohr, V., Genzel, Y., Behrendt, I., Scharfenberg, K., and Reichl, U. (2010). A new MDCK suspension line cultivated in a fully defined medium in stirred-tank and wave bioreactor. *Vaccine* 28, 6256–6264. doi: 10.1016/j.vaccine.2010.07.004

Möhler, L., Flockerzi, D., Sann, H., and Reichl, U. (2005). Mathematical model of influenza a virus production in large-scale microcarrier culture. *Biotechnol. Bioeng.* 90, 46–58. doi: 10.1002/bit.20363

Nayak, D. P., Chambers, T. M., and Akkina, R. K. (1985). Defective-interfering (DI) RNAs of influenza viruses: origin, structure, expression, and interference. *Curr. Top. Microbiol. Immunol.* 114, 103–151. doi: 10.1007/978-3-642-70227-3_3

Ozawa, M., Victor, S. T., Taft, A. S., Yamada, S., Li, C., Hatta, M., et al. (2011). Replication-incompetent influenza A viruses that stably express a foreign gene. *J. Gen. Virol.* 92, 2879–2888. doi: 10.1099/vir.0.037648-0

Samson, M., Pizzorno, A., Abed, Y., and Boivin, G. (2013). Influenza virus resistance to neuraminidase inhibitors. *Antiviral Res.* 98, 174–185. doi: 10.1016/j.antiviral.2013.03.014

Schmidt, H., and Jirstrand, M. (2006). Systems Biology Toolbox for MATLAB: a computational platform for research in systems biology. *Bioinformatics* 22, 514–515. doi: 10.1093/bioinformatics/bti799

Schulze-Horsel, J., Schulze, M., Agalaridis, G., Genzel, Y., and Reichl, U. (2009). Infection dynamics and virus-induced apoptosis in cell culture-based influenza vaccine production-Flow cytometry and mathematical modeling. *Vaccine* 27, 2712–2722. doi: 10.1016/j.vaccine.2009.02.027

Scott, P. D., Meng, B., Marriott, A. C., Easton, A. J., and Dimmock, N. J. (2011). Defective interfering influenza A virus protects *in vivo* against disease caused by a heterologous influenza B virus. *J. Gen. Virol.* 92, 2122–2132. doi: 10.1099/vir.0.034132-0

Shin, W.-J., and Seong, B. L. (2019). Novel antiviral drug discovery strategies to tackle drug-resistant mutants of influenza virus strains. *Expert Opin. Drug Discov.* 14, 153–168. doi: 10.1080/17460441.2019.1560261

Simonsen, L., Chowell, G., Andreasen, V., Gaffey, R., Barry, J., Olson, D., et al. (2018). A review of the 1918 herald pandemic wave: importance for contemporary pandemic response strategies. *Ann. Epidemiol.* 28, 281–288. doi: 10.1016/j.annepidem.2018.02.013

Swick, A., Baltes, A., and Yin, J. (2014). Visualizing infection spread: dual-color fluorescent reporting of virus–host interactions. *Biotechnol. Bioeng.* 111, 1200–1209. doi: 10.1002/bit.25170

Volz, A., and Sutter, G. (2017). "Chapter five - modified vaccinia virus ankara: history, value in basic research, and current perspectives for vaccine development," in *Advances in Virus Research,* eds M. Kielian, T. C. Mettenleiter, and V. R. Roossinck (San Diego, CA: Elsevier Academic Press Inc.), 187–243. doi: 10.1016/bs.aivir.2016.07.001

von Magnus, P. (1951). Propagation of the PR8 strain of influenza A virus in chick embryos. III. Properties of the incomplete virus produced in serial passages of undiluted virus. *Acta Pathol. Microbiol. Scand.* 29, 157–181. doi: 10.1111/j.1699-0463.1951.tb00114.x

Wasik, M. A., Eichwald, L., Genzel, Y., and Reichl, U. (2018). Cell culture-based production of defective interfering particles for influenza antiviral therapy. *Appl. Microbiol. Biotechnol.* 102, 1167–1177. doi: 10.1007/s00253-017-8660-3

Yamagata, Y., Muramoto, Y., Miyamoto, S., Shindo, K., Nakano, M., and Noda, T. (2019). Generation of a purely clonal defective interfering influenza virus. *Microbiol. Immunol.* 63, 164–171. doi: 10.1111/1348-0421.12681

Zhao, H., To, K. K. W., Chu, H., Ding, Q., Zhao, X., Li, C., et al. (2018). Dual-functional peptide with defective interfering genes effectively protects mice against avian and seasonal influenza. *Nat. Commun.* 9:2358. doi: 10.1038/s41467-018-04792-7

Conflict of Interest: The authors declare that the research was conducted in the absence of any commercial or financial relationships that could be construed as a potential conflict of interest.

frontiers in Bioengineering and Biotechnology

ORIGINAL RESEARCH
published: 31 October 2019
doi: 10.3389/fbioe.2019.00297

Boosting Recombinant Inclusion Body Production—From Classical Fed-Batch Approach to Continuous Cultivation

Julian Kopp[1], *Anna-Maria Kolkmann*[1], *Patrick Gwen Veleenturf*[1], *Oliver Spadiut*[2], *Christoph Herwig*[1,2] *and Christoph Slouka*[1]*

[1] Christian Doppler Laboratory for Mechanistic and Physiological Methods for Improved Bioprocesses, Institute of Chemical, Environmental and Bioscience Engineering, Vienna University of Technology, Vienna, Austria, [2] Research Division Biochemical Engineering, Institute of Chemical, Environmental and Bioscience Engineering, Vienna University of Technology, Vienna, Austria

State of the art microbial recombinant protein production is regularly performed in fed-batch based cultivations. However, these cultivations suffer from highly time-dependent changes in productivity and product quality, leading to high variations in the downstream process. Continuous biomanufacturing offers the possibility of a time independent process, boosting the time-space-yield of the recombinantly produced protein and further reducing costs for production, also as downstream gets more predictive. In the current work, the continuous production of a pharmaceutically relevant protein in form of an inclusion body in *E. coli* BL21(DE3) was investigated in single vessel cultivations by varying dilution rates using glycerol as carbon source, inducer (lactose or IPTG) and respective inducer concentrations. Attempts to increase low specific productivities observed in single vessel continuous cultivations, led to the establishment of a continuously operated cascade of two stirred tank reactors to spatially separate biomass formation from recombinant protein production. Process performance was substantially improved compared to a single vessel chemostat culture, as specific productivity and space-time yield were boosted using an optimized cascaded process by about a factor of 100. This study shows the potential of a two-stage continuous process as promising alternative to benchmark fed-batch processes achieving constant inclusion body production at a time-independent level.

Keywords: ***Escherichia coli*, fed-batch, continuous biomanufacturing, stirred-tank reactor cascade, inclusion bodies**

OPEN ACCESS

Edited by:
Eduardo Jacob-Lopes, Universidade Federal de Santa Maria, Brazil

Reviewed by:
Peter Neubauer, Technische Universität Berlin, Germany
Claucia Fernanda Volken De Souza, Universidade do Vale do Taquari - Univates, Brazil

***Correspondence:**
Christoph Slouka
christoph.slouka@tuwien.ac.at

Specialty section:
This article was submitted to Bioprocess Engineering, a section of the journal Frontiers in Bioengineering and Biotechnology

Received: *29 August 2019*
Accepted: *15 October 2019*
Published: *31 October 2019*

Citation:
Kopp J, Kolkmann A-M, Veleenturf PG, Spadiut O, Herwig C and Slouka C (2019) Boosting Recombinant Inclusion Body Production—From Classical Fed-Batch Approach to Continuous Cultivation. Front. Bioeng. Biotechnol. 7:297. doi: 10.3389/fbioe.2019.00297

INTRODUCTION

About one third of all recombinant pharmaceuticals in industry is expressed in the Gram-negative bacterium *E. coli* (Walsh, 2010; Gupta and Shukla, 2016). Usage of *E. coli* as host can be advantageous over other organisms due to its well-known genetics, high growth rates as well as relatively inexpensive culture media and process operation (Huang et al., 2012). Recombinant proteins in *E. coli* are often produced in insoluble aggregated form, known as so called inclusion bodies (IBs). Even though IBs have originally been believed to be waste products produced by bacteria (Garcia-Fruitos et al., 2012) the formation of IBs provides unique opportunities in cultivation strategies as IBs show higher densities compared to cellular impurities (Schein, 1989).

Reports show that purity up to 95% of the target proteins were found in IBs (Georgiou and Valax, 1999). Even though long and cost intensive downstream applications cause the bottle neck in IB-based processes the overall time-space-yield tends to be favorable for IB-production when being compared to periplasmic or soluble protein production (Jagschies et al., 2018). *E. coli* BL21(DE3), is often used in industry due to low acetate formation and high production rates as an effect of the integrated T7-polymerase (Steen et al., 1986; Studier and Moffatt, 1986; Studier et al., 1990; Dubendorff and Studier, 1991; Neubauer and Hofmann, 1994; Lyakhov et al., 1998), which is transcribed from the lac-operon and allows expression from pET plasmids using the T7-promoter (Dubendorff and Studier, 1991; Marbach and Bettenbrock, 2011; Wurm et al., 2016). Here induction can be performed either with lactose (converted to allolactose) or the well-known structural analog isopropyl β-d-1 thiogalactopyranoside (IPTG) (Neubauer and Hofmann, 1994; Wurm et al., 2016). However, induction with IPTG stresses the host cells, and IPTG in higher concentrations (higher than 1 mmol/L) is even referred of being toxic at elevated induction times (Neubauer and Hofmann, 1994; Donovan et al., 1996; Viitanen et al., 2003; Marbach and Bettenbrock, 2011). Using either IPTG (Marisch et al., 2013) or lactose (Neubauer et al., 1992; Neubauer and Hofmann, 1994; Ukkonen et al., 2013) as inducer resulted in higher product yields when compared to other inducer supplies (Marschall et al., 2016). "Soft induction" performed with lactose showed especially promising results (Neubauer et al., 1992; Neubauer and Hofmann, 1994; Blommel et al., 2007; Kopp et al., 2017). As lactose can be partly metabolized in *E. coli* BL21(DE3), it does not stress the cells as much as IPTG (Dvorak et al., 2015). For the production of soluble proteins and products located in the periplasm, induction with lactose is referred to be a sufficient method (Wurm et al., 2016), but it has also been shown that lactose provided promising results for IB-production (Wurm et al., 2016, 2017a). As fed-batch cultivations suffer from highly different metabolic loads, which often occur when IPTG is used as inducer (Neubauer et al., 2003), the constant feeding of a soft inducer could help to eliminate time-dependent variations and achieve stable productivity instead.

In general, glucose is used as main carbon source for growth of *E. coli*. However, as glucose in pure form is quite expensive, industry aims for cheap complex media or inexpensive carbon sources for defined media. Glycerol, first noticed in biotechnology as a waste product in the biodiesel production (Martínez-Gómez et al., 2012), has shown beneficial effects in *E. coli* cultivations regarding biomass-substrate yields (Blommel et al., 2007; Ukkonen et al., 2013) and specific productivities (Kopp et al., 2017). As excess glycerol generated cannot be disposed of in the environment, the application of glycerol as a carbon and energy source for microbial growth in industrial microbiology may help to solve environmental problems (da Silva et al., 2009). Unlike glucose, glycerol is an "energy-poor" carbon source (Deutscher et al., 2006) and should not imply catabolite repression when organism are cultivated concomitantly with lactose (Lin, 1976). However, in a previous study we found out, that the inducer uptake rate is rather a function of product formation and phenomena of existing or non-existing catabolite repression are only seen when no product formation occurred (Kopp et al., 2017).

Batch/Fed-batch bioprocessing is today's state of the art in industrial microbial production of biopharmaceuticals (Croughan et al., 2015). The application of chemostat reactors was first described by Monod (1950), Novick and Szilard (1950), Rinas and Bailey (1992). However, establishing continuous biomanufacturing seems to be getting more interesting again, because of optimum use of installed assets and highest achievable time space yields (Hoskisson and Hobbs, 2005). Chemostat systems provide conditions, where cells are maintained in a steady-state growth environment ($dx/dt = 0$) (Hoskisson and Hobbs, 2005). Supplying the cells with a constant flow of nutrients combined with simultaneous removal of spent culture medium at a defined rate enables carbon-limited definition of cell growth (Rinas and Bailey, 1992). Establishing long steady-state conditions is believed to provide stable volumetric productivities and high space-time yields (STY), achieved by lower set-up and running costs such as a straightforward process scalability due to a practicably reduced equipment size compared to fed-batch processes (Walther et al., 2015; Peebo and Neubauer, 2018). Smaller production volumes can support process development, due to rather uncomplicated upscale processing (Croughan et al., 2015) and less complicated plant manufacturing. As a consequence this reduced risk of technology transfer could ease clinical production and commercial manufacturing (Daszkowski, 2013). Although various highly efficient microbial continuous processes for the production of recombinant proteins are described in literature (Domingues et al., 2005; Paulova et al., 2012; Schmideder and Weuster-Botz, 2017), the only known example of a continuous industrial recombinant process dates back to the 1990s, when insulin was produced using the host *S. cerevisiae* (Diers et al., 1991), however process stability was problematic. In particular, continuous recombinant expression of intracellular proteins is challenging because a separation of the retention times of the product and the biocatalyst is impossible, causing a strong metabolic/product burden if strong promotors are applied (Studier and Moffatt, 1986; Striedner et al., 2003; Tripathi, 2009). In batch cultivations, the separation of cell growth and recombinant protein production is done on a time-dependent manner, as biomass growth can be performed in batch and fed-batch mode without additional production stress and induced once the desired biomass concentration is achieved. As continuous cultivation is time-independent, the growth of cells is inhibited and genetic instabilities, such as plasmid loss, occur due to strong selection pressure (Rhee and Schügerl, 1998; Croughan et al., 2015). Moreover, continuous bioprocesses suffer from comparatively low product concentrations (Schmideder and Weuster-Botz, 2017). Nowadays, novel selection marker strategies (Selvamani et al., 2014), tunable protein expression (Marschall et al., 2016) and bioprocess strategies (Gupta et al., 2001) have been developed to face the challenges being associated with long-term cultivations such as stable systems, sterility and genetic instabilities. One possibility to reduce the metabolic burden in continuous cultivations is the decoupling of growth and recombinant protein production by applying a cascade of

two sequentially operated continuous bioreactors (Schmideder and Weuster-Botz, 2017). During biomass formation in the first reactor, cells should be growing burden-free. The non-induced biomass from the first reactor is transferred to a second reactor where the recombinant protein production is induced at much higher cell densities, when compared to a one-compartment system. Using this system, a highly concentrated feed can be used for the induction in the second reactor, giving the chance of applying similar feeding systems used in fed-batch systems. Additionally, each reactor can be operated at optimal conditions (such as pH and temperature) for growth and protein production plus the whole system can be varied in residence times. However, cascaded continuous cultivation is restricted to academic studies so far (Brown et al., 1985; Park et al., 1989, 1990; Park and Ryu, 1990; Hortacsu and Ryu, 1991; Kim and Ryu, 1991; Akhnoukh et al., 1996; Baheri et al., 1996).

In this study, we present the development of an industrial based continuous inclusion body process to produce a pharmaceutically relevant product in *E. coli* BL21(DE3). The glycerol-lactose system being established for fed-batch cultivations is applied in continuous cultivation for the first first-time, providing a suitable alternative to optimized fed-batch processes. By varying cultivation strategies in the cascaded system, recombinant protein formation could be efficiently boosted.

We also want to highlight that the cascaded system, using the cultivation strategies above, is superior to previous cascaded cultivations in terms of volumetric productivity (Schmideder and Weuster-Botz, 2017) and could be a promising alternative to common batch systems as reduced plant dimensions in combination with the usage of relatively cheap carbon sources could significantly reduce the costs for industrial applications.

MATERIALS AND METHODS

Bioreactor Cultivations

All cultivations were carried out with the strain *E. coli* BL21(DE3) consisting of a pet30a plasmid system. The target protein was linked to a N-pro fusion tag (Achmüller et al., 2007). As the given protein is currently under patenting procedure at the industrial partner no further information can be given on the used protein.

All bioreactor and preculture cultivations were carried out using a defined minimal medium referred to DeLisa et al. (1999). Batch media and the preculture media contained of the same ingredients with different amounts of glycerol, respectively, 20 and 8 g/L.

As the used pET30a-system consisted of a Kanamycin resistance gene, antibiotic was added throughout all fermentations, trying to prevent plasmid loss, resulting in a final concentration of 0.02 g L^{-1}. All precultures were performed using 500 mL high yield flasks. They were inoculated with 1.5 mL of bacteria solution stored in cryos at −80°C and subsequently cultivated for 20 h at 230 rpm in an Infors HR Multitron shaker (Infors, Bottmingen Switzerland) at 37°C.

All cultivations were either performed in a DASBox Mini bioreactor 4-parallel fermenter system (max. working volume [=wV].: 250 mL; Eppendorf, Hamburg, Germany) or in a Labfors 4 bioreactor (max. wV: 1 or 5 L; Infors HT, Bottmingen, Switzerland). For the two-stage cultivations, two continuously operated stirred-tank reactors were connected by a transfer tube coupled to a pump (Ismatec, Wertheim, Germany) (**Figure 2**). For measuring the CO_2 and O_2 flows, either a DASGIP-GA gas analyzer (Eppendorf, Hamburg, Germany) or BlueSens Gas sensors (BlueSens Gas analytics, Herten, Germany) were used.

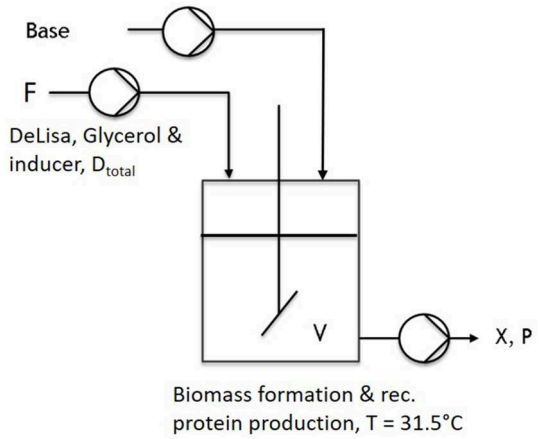

FIGURE 1 | Schematic setup of a common chemostat used throughout first cultivations.

Distributed process control was established using either the PIMS Lucullus (Securecell, Swiss) or DASware-control, respectively. pH was kept constant at 6.7 throughout all cultivations and controlled using a base only control (12.5% NH_4OH), while acid (5% H_3PO_4) was added manually, when necessary. The pH was monitored using an EasyFerm Plus pH-sensor (Hamilton, Reno, NV, USA). The reactors were continuously stirred at 1,000 or 1,400 rpm, respectively. Aeration was absolved using a mixture of pressurized air and pure oxygen at 1 to 3 vvm. As the cultivation volume of the reactor was adjusted via an immersion tube connected to a bleed-pump, no stirrer cascade was implied as volumes and residence times would alter at higher rotation levels. Addition of pure oxygen purged the need for a stirrer cascade, as the ratios of the airflow were mixed together so that the dissolved oxygen (dO_2) was always higher than 30%. The dissolved oxygen was monitored using a fluorescence dissolved oxygen electrode Visiferm DO (Hamilton, Reno, NV, USA).

Cultivation Scheme

During one-stage continuous cultivations (**Figure 1**), a batch phase was applied to gain biomass in a first stage, keeping (20 g L^{-1} glycerol) the temperature constant at 37°C. The chemostat system was applied with the start of the induction phase. Therefore, the feed was changed for continuous application, ensuring continuous supply of a mixed-feed (with specific glycerol uptake rate of $q_{s,gly} = 0.2$ g/g/h and a specific inducer uptake rate of $q_{s,lac} = 0.1$ g/g/h), as well as the start of the bleed pump. Volume was adjusted via an immersion tube adjusted to right height to the liquid surface, ensuring that the

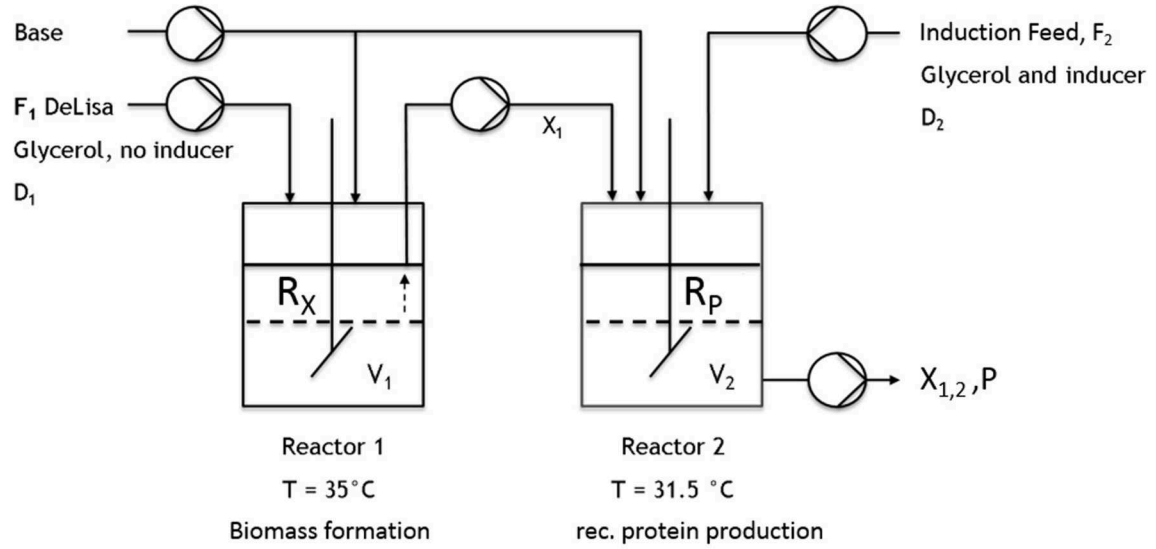

FIGURE 2 | Schematic setup of the implemented cascade using two continuously operated stirred-tank reactors. The first reactor was used for biomass formation (no inducer). The culture broth was then transferred to the second reactor, where recombinant protein production was induced.

bleed pump was working at higher rate than the feed pump. As the bleed pump ensured a complete deduction of the fed media, D was calculated as a flow in, monitored via multiple scales, and the process system Lucullus (Securecell, Schlieren, Switzerland). During cascaded continuous cultivation (250 mL wV in DAS-Box system)—sketch given in **Figure 2**—a batch phase for biomass formation was performed in both reactors. This was followed by a non-induced continuous phase, lasting over night for approximately 2 residence times (depending on the dilution rate) trying to achieve a steady state. Once the equilibrium state was reached, visible by monitoring the off-gas values, a feed containing glycerol (50 g/l) for the first feed and the respective glycerol/inducer feed (500 g/L glycerol 93 g/L lactose monohydrate) was continuously supplied to the second reactor. For biomass formation during continuous cultivation the temperature was set to 35°C. For protein production the temperature of the second vessel, was lowered to 31.5°C as optimized results were obtained at this temperature (Slouka et al., 2018). The inducer concentration in the mixed feed was calculated in order to ensure a maximum specific uptake rate of lactose of $q_{s,lac} = 0.23\,g\,g^{-1}\,h^{-1}$ (Kopp et al., 2017).

Process Analytics

Samples were always taken upon the end of the batch-phase and after the non-induced fed-batch and regularly during continuous process mode. In the induction period, samples were taken every 3 h during the first day of induction, to monitor the first protein production stages, followed by daily sampling, which was increased to two times per day if necessary, for the whole duration of the cultivation. Biomass was measured using optical density (OD_{600}) and gravimetrically by weighing the dry cell weight (DCW), while flow cytometry analysis (FCM) was used for the determination of cell-death. OD_{600} was measured in duplicates using a Genesys 20 photometer (Thermo Scientific, Waltham, MA, USA). Since the linear range of the used photometer was between 0.2 and 0.8 [AU], samples were diluted with dH_2O to stay within the given range. The DCW was determined by centrifuging 1 mL of homogenous sample solution in a pre-tared 2 mL Eppendorf-Safe-Lock Tube (Eppendorf, Hamburg, Germany). Centrifugation conditions were at 10,000 rpm for 10 min at 4°C. After centrifugation, the supernatant was split into two different fractions. One fraction was immediately used for automated at-line measurement of glycerol, phosphate nitrogen and acetate using a Cubian XC (Optocell, Bielefeld, Germany). The second fraction was frozen at −20°C and later used to determine, e.g., sugar accumulation. For washing purpose, the pellet was re-suspended with 1 mL of 0.9% NaCl solution and centrifuged at the same conditions. Afterwards, the pellet was dried for at least 48 h at 105°C and evaluated gravimetrically. DCW measurements were performed in at least three replicates. Samples for FCM were diluted 1:100 with 0.9% NaCl solution, stored at 4°C and measured every day. The measurement was performed using the software Cube 8 (Sysmex, Partec, Grlitz, Germany) according to Langemann et al. (2016) using DiBAC4(3) (bis-(1,3-dibutylbarbituricacid-trimethineoxonol) and Rh414 dye. Rh414 binds to the plasma membrane and visualizes all cells by reducing the background signal, while DiBAC4(3) is sensitive to the plasma membrane potential and thus enables the distinction between viable and non-viable cells.

Sugar concentrations of feed and fermentation broth were measured via HPLC (Thermo Scientific, Waltham, MA, USA) using a Supelcogel-column (Eluent: 0.1% H_3PO_4; Flow: 0.5 mL/min). Glycerol accumulation, lactose decrease, and galactose accumulation were monitored using this method. Standards had a concentration of 1, 5, 10, 20, 30, 40, and 50 g L^{-1} of the respective used carbon sources throughout fermentation. The HPLC run lasted always for 25 min and chromatograms

were analyzed using a Chromeleon Software (Thermo Scientific, Waltham, MA, USA).

Product Analytics

Product samples were taken after the start of the induction phase. Therefore, 5 mL broth was pipetted in a 50 mL falcon tube and centrifuged for 10 min at 4,800 rpm at 4°C. The supernatant was discarded while the pellet was frozen at −20°C. Afterwards the samples were disrupted for homogenization as follows: The pellets were re-suspended in a lysis buffer (0.1 M TRIS, 10 mM EDTA, pH = 7.4) according to the dry cell weight. After suspending the cells with a disperser (T 10 basic ULTRA-TURRAX®, Staufen, Germany) they were treated with an EmusiflexC3 Homogenizer (Avestin, Ottowa, ON, USA) at 1,300 bar. Homogenization always lasted for at least ten passages, ensuring complete cell disruption. After washing the pellets twice with ultrapure water, they were aliquoted and then centrifuged (14,000 rpm, 10 min 4°C). The supernatant was discarded, and the pellets were stored at −20°C until further processing.

For titer measurements of the N-pro-fused protein, the pellets were dissolved using a solubilization buffer (7.5 M Guanidine Hydrochloride, 62 mM Tris at pH = 8). The filtered samples were quantified via RP-HPLC (Thermo Scientific, Waltham, MA, USA) using a Nucleosil-column. The eluent was a gradient mixture of water with 0.1% TFA (tri-fluoric-acid) and acetonitrile mixed with 0.1% TFA with a flow of 3 mL min^{-1}. Standard concentrations were 50, 140, 225, 320, 500, and 1,000 mg mL^{-1} of an industrial supplied reference standard.

RESULTS

From Fed-Batch to Continuous Cultivation

Production of recombinant proteins in *E. coli* is usually carried out as a fed-batch process, which generally consists of a biomass production phase followed by an induction phase for producing the desired recombinant product. Since this approach leads to highly time dependent changes in critical quality attributes (CQAs), such as product titer, purity and size (Garcia-Fruitos et al., 2012; Slouka et al., 2018), the aim of this study was to create a process, providing time-independent product formation. Critical process parameters (CPP), like optimal temperature for growth and recombinant protein expression as well as carbon source and inducer concentrations, were identified in recent fed-batch studies (Kopp et al., 2017). This knowledge paved the way for the first continuous cultivations. First chemostats were operated at dilution rates of approximately D = 0.1 [h^{-1}], as recombinant protein production showed highest specific inducer uptake rates ($=_{qs,lac}$) in previously established fed batch cultivations (Wurm et al., 2016). As shown in **Figure 3**, recombinant protein production reached higher specific productivity using IPTG as an inducer, though after 55 h of induction, product formation dropped down completely. For fed-batch cultivations, q_p and space-time yield do increase within short time spans, however productivity declines within the timespan of induction phase. This effect can be explained by cell lysis and reduced capacity being caused by the high metabolic burden exerted onto host cells (Ceroni et al., 2015; Slouka et al., 2019).

Calculations were performed establishing rates between the corresponding sampling intervals. q_p was calculated using titer measurements from HPLC and the active measured biomass or viable cell concentration (=VCC) in between the sampling interval given in Equations (1–3):

$$Qp = \frac{Titer\ HPLC\ \left[\frac{g}{L}\right] * Reactor\ Volume\ [L]}{\frac{Average(DCW_{1,2})\ [g]}{Sampling\ time\ 2\ [h] - sampling\ time\ 1\ [h]}} \quad (1)$$

$$DCW_1 = [g] = \left(DCW\left[\frac{g}{L}\right] - \left(\%dead\ cells * DCW\left[\frac{g}{L}\right]\right)\right) * Reactor\ Volume[L] \quad (2)$$

$$STY = \left[\frac{\frac{g}{L}}{h}\right] = Titer\ HPLC\left[\frac{g}{L}\right]/t\ [h] \quad (3)$$

With q_p being the specific productivity in g/g/h and STY the time space yield (in g/L/h), which was calculated with product titer measurements derived from HPLC and then calculated for the corresponding time phase. IPTG induction reaches a short time induction maximum after 40 h, hence production stops completely at ongoing induction times. This would correlate to the well-known knowledge, that IPTG cannot be metabolized, eventually creating toxic effects onto *E. coli*, therefore decreasing recombinant product formation at evaluated cultivation times (Dvorak et al., 2015). Performing induction with lactose nearly reached same maximum productivity as performed with IPTG induction, however product formation never dropped down to zero, when comparing to the zoom in **Figure 3C**. Additionally, no lactose accumulation was measured throughout the induction phase of the chemostat (not shown), leaving room for optimization by adaption of the inducer concentration in order to achieve full induction. Still, space time-yield as well as ongoing product formation were favorable for lactose induction, but an optimized fed-batch run was superior in term of productivity to the results derived in chemostats.

In a previous study the growth rate seems to correlate with productivity in fed-batch cultivations for the T7-expression system (Hausjell et al., 2018). Previously performed fed-batch cultivations also revealed that short-term productivity can be boosted by an increase of growth rate, leading to optimized induction times of 6–8 h, depending on the growth rate, respectively (Kopp et al., 2018; Slouka et al., 2019). As a growth rate or a dilution rate of D = 0.16 h^{-1} would implement a residence time of 6.25 h^{-1} the average induction time for host cells would be in the same optimum found out in fed-batch cultivations. Supplying more energy by applying higher dilution rates, therefore should boost product formation (Sandén et al., 2003; Boström et al., 2005). Still, higher dilution rates might be critical, as wash out might occur (Paalme et al., 1995). IPTG induction was not tested at higher dilution rates as induction with lactose showed beneficial results in terms of space-time yield. To compensate for the eventually occurring inducer limitation,

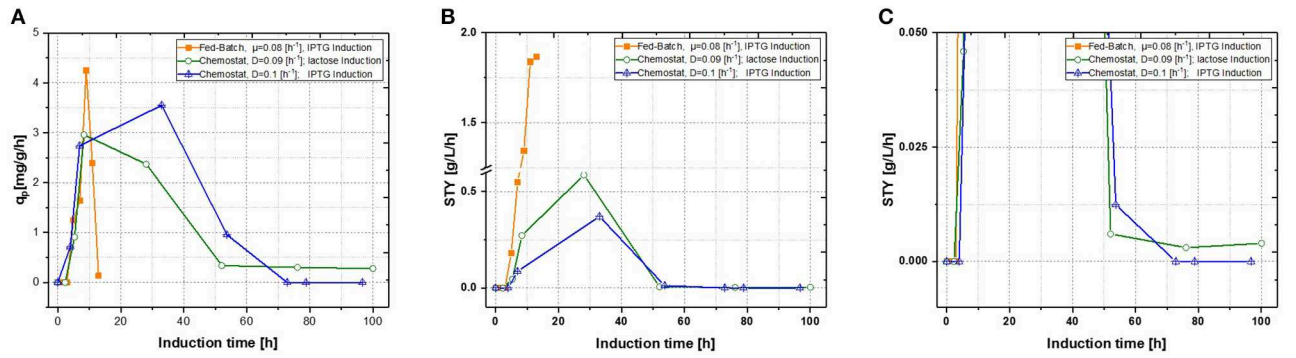

FIGURE 3 | Comparison of two single-stage chemostat systems induced with lactose or IPTG with a state-of-the-art fed-batch **(A)** specific productivity as function of induction time; **(B)** space-time yield as function of induction time. **(C)** Zoom of the space time yield comparing the effects of different inducers within the chemostat cultivations.

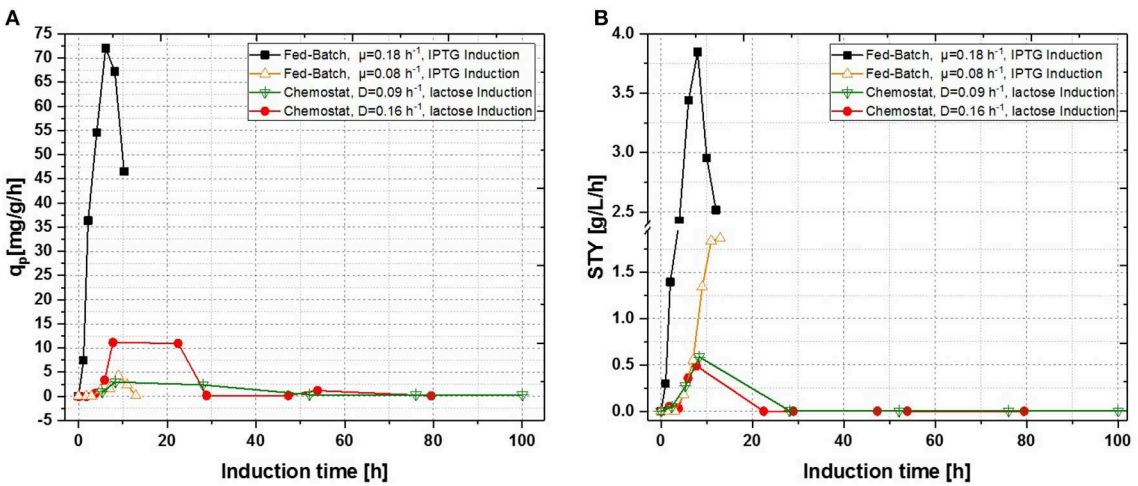

FIGURE 4 | Comparison of a single-stage continuous cultivation of *E. coli* BL21 (DE3) for recombinant inclusion body production ($D = 0.16 \pm 0.021\ h^{-1}$, pH = 6.7, V = 650 mL, T = 31.5°C, induction with lactose) with fed-batch cultivations ($\mu = 0.08 \pm 0.023\ h^{-1}$ and $\mu = 0.18 \pm 0.01\ h^{-1}$, pH = 6.7, $V_{end} = 7.5$ L, T = 31.5°C; induction with IPTG). **(A)** Specific productivity as function of induction time; **(B)** space-time-yield as function of induction time.

lactose concentration in the feed was increased according to the previous established results (**Figures 4A,B**).

Fed-Batch cultivation performed at growth rates of $\mu = 0.15\ h^{-1}$ during induction phase did also provide far higher production levels compared to a fed-batch operated at $\mu = 0.1\ h^{-1}$ during induction phase, which is in accordance with literature (Hausjell et al., 2018; Kopp et al., 2018; Slouka et al., 2019) Short-time specific productivity could be also increased in chemostat cultivation, by applying higher dilution rates when compared to previous chemostat cultivations at $D = 0.1\ [h^{-1}]$, however a constant productivity was not accomplished (compare to **Figures 4A,B**). Low levels of acetate formation were also detected with at-line measurements (data not shown) once q_p decreased, which is in accordance with literature [33]. A comparison of product formation and biomass measurements indicated that simultaneous product formation and biomass production are not capable of being constant over induction time (compare to **Figure 5**). This was confirmed by the increase in biomass production after 29 h again, hence almost no product formation was detectable at the same time of the process (compare to **Figures 4A,B** and **Figure 5**).

Required resources for recombinant protein production such as raw material and energy for the amplification of the foreign DNA and the followed expression of the recombinant protein bear a metabolic burden onto host cells (Hoffmann and Rinas, 2004). As the T7-RNA polymerase system is a very strong expression system, it exerts a high metabolic burden onto the host cells (Heyland et al., 2011). The decrease of DCW during the induction period of the continuous cultivation could therefore be explained due to strong overexpression of the recombinant protein in the beginning of the induction phase, leading to decreased cell growth rates (Scott et al., 2010) and genetic instabilities (Croughan et al., 2015) and consequently to a decrease in productivity.

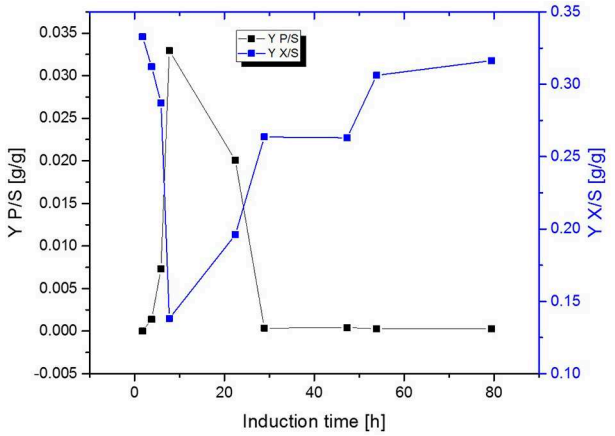

FIGURE 5 | Comparison of the biomass- and product yield throughout induction phase of chemostat operated at D = 0.16 h^{-1} induced with lactose.

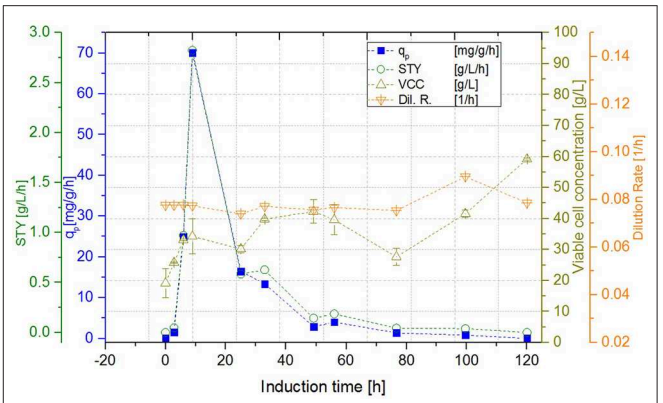

FIGURE 6 | Cascade 2 operated at a dilution rate of $D_{ges} = 0.08 \pm 0.004$ h^{-1} (pH = 6.7, $T_{R1} = 35°C$, $T_{R2} = 31.5°C$).

Cascaded Continuous Cultivation

All previous results obtained in chemostat cultivations (compare to **Figures 3A,B**, **4A,B**, **5**) indicated that biomass production and high protein production cannot be coped within one cultivation step. Therefore, the next approach was to spatially separate biomass production from induction. In order to reduce the metabolic burden, non-induced cell growth and recombinant protein expression were decoupled from each other within this study in subsequent cultivation steps by applying a cascade of two sequentially operated continuous bioreactors as described in **Figure 2**. A batch phase, similar to single-stage continuous cultivation, in all reactors was followed by a non-induced continuous phase in order to achieve steady state conditions, ensuring the constant transfer of exponentially growing cells from the first reactor to the second before the induction of the recombinant protein expression started. The dilution rate of the first reactor was set to $D_1 = 0.08$ h^{-1}, while the highly concentrated feed is added at a dilution rate of $D_{R2} = 0.02$ h^{-1}. The flow out of the second reactor therefore was calculated $D_2 = D_1 + D_{R2}$, resulting in a final dilution rate for the cascade of 0.1 h^{-1} and 10 h of residence time for cells in the second reactor. As the previous chemostat and fed-batch cultivations showed the trend that a higher growth rate/higher dilution rate correlates to higher product formation this was also considered here. By varying the reaction volume of both reactors implemented in the cascade, the residence time could also be varied, optimizing the generation process for inclusion bodies. Presetting optimal dilution rate was thought to be beneficial for biomass formation in the first reactor and recombinant protein production in the second reactor. The following hypothesis are related to these cultivations:

A higher dilution rate D_2 implementing a higher growth rate of expressing cells in the second reactor leads to higher space-time yields and specific productivities (Kopp et al., 2017; Hausjell et al., 2018). Variation of the residence time τ, might lead to different effects onto IB-formation as cells might be washed out before metabolic burden decreases levels of specific productivity (Wurm et al., 2017b). Higher inducer concentrations favor higher specific uptake rates and therefore higher product concentrations and space-time yields can be achieved.

Biomass of Cascaded Continuous Cultivation

While the DCW of the cascade 1 (induction with IPTG) reached a steady state concentration of 29.99 ± 0.71 g L^{-1}, DCW in the second reactor of the cascade 2 (induction with lactose) continued to increase to a maximum of 59.99 ± 0.21 g L^{-1}. Cascade 3 showed slightly lower maximum levels of DCW, reaching amounts of 53.31 ± 1.20 g L^{-1}. However, DCW measured in the lactose induced cascades (cascade 2, 3) fluctuated during the induction phase, as lactose—unlike IPTG—still was metabolized, which can be seen exemplarily in **Figure 6**. During these cultivations, the percentage of living cells, determined via flow cytometry (Langemann et al., 2016), was always above 99% (comparison to DCW therefore not shown). Therefore, the decline in productivity is probably not a result of cell death, which was partially monitored in chemostat cultivations, but could have been caused by the high metabolic burden that the product formation implements onto the cells.

Productivity of Cascaded Continuous Cultivation

In a recent publication, constant productivity in a cascade cultivation system was observed, when performing induction with IPTG (Schmideder and Weuster-Botz, 2017). In order to test the feasibility of this study to produce an industrial relevant protein, we also performed a cascade cultivation testing IPTG as an inducer. However, results were in accordance with the single-stage cultivations described in the previous section and the specific productivity could not be kept constant over a longer period for IPTG induced cascade cultivations. A maximum q_p value of 6.44 mg g^{-1} h^{-1} was reached for the IPTG induced cultivation after 44 h of induction. In case of cascade 1, a later rise of product formation and a later drop of productivity was observed. During induction with IPTG in the cascaded system, the highest STY of was reached after 44 h of induction, shown in **Figure 7A**. Lactose induction (cascade 2) resulted in a maximum value at the very beginning of the induction phase, comparable to the achieved productivity throughout fed-batches induced

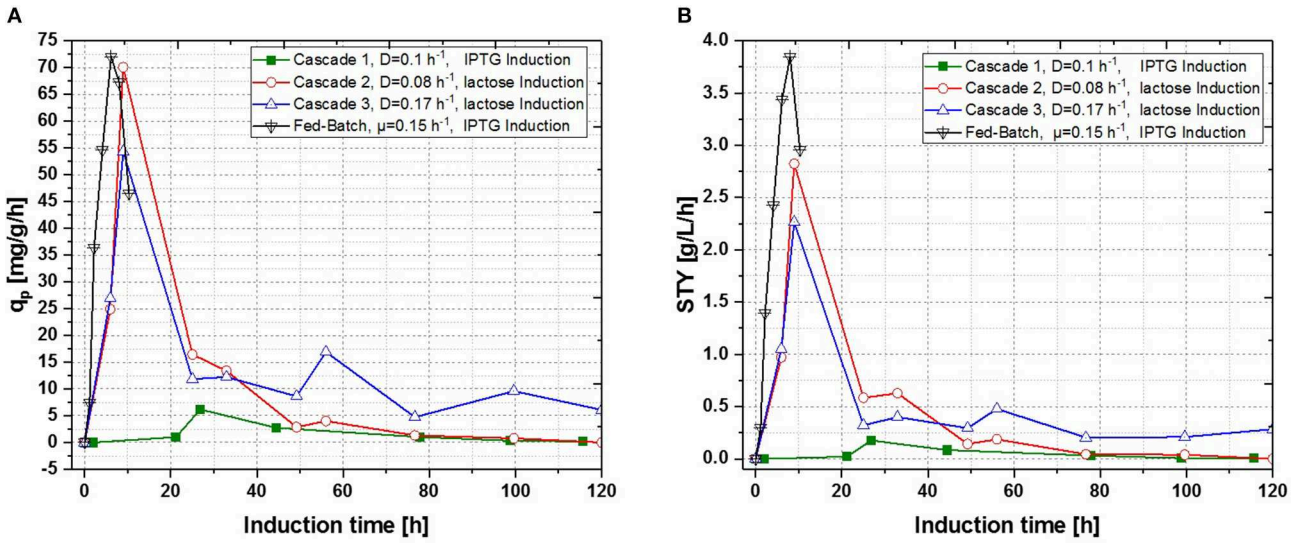

FIGURE 7 | Operated cascades of two reactors compared to an optimized fed-batch for recombinant inclusion body production in *E. coli* BL21 (DE3) with variation of dilution rate and Inducer (pH = 6.7, T_{R1} = 35°C, T_{R2} = 31.5°C). **(A)** Specific productivity as function of induction time; **(B)** STY as function of induction time.

with IPTG, reaching q_p values of approximately 70 mg g^{-1} h^{-1}. Although cascade 2 produced higher amounts than the cascade 1 induced with IPTG, it still follows the same trend, as productivity declines significantly over time and a steady state in terms of productivity was never accomplished. As lactose showed again beneficial results in terms of productivity in cascaded chemostat cultivations, a further alteration of the dilution rate was not considered for IPTG induced cascaded cultivation. During cascade 2 low lactose accumulation was measured with at-line HPLC in the cultivation broth throughout the whole process (data not shown), therefore the lactose concentration was maintained for the mixed feed used for induction of cascade 3. Increasing dilution rate in cascade 3 (induced with lactose) eventually led to a stable productivity after approximately 25 h of induction and showed stable productivity for the ongoing process time. Even though cascade 2, operated at a dilution rate of 0.1 h^{-1}, exceeds higher short-term specific productivity, overall productivity and space time yield of cascade 3 are superior to cascade 2.

Results for the different performed chemostat cultivations are presented in **Figure 7** (a for specific productivity, b for time space yield) compared to an optimized state-of-the-art fed-batch process. Comparing cascade 1 and cascade 3 with each other after 5 residence times, a significant increase in specific productivity and space-time yield is observed. This might be due to a constant washout of producing cells during continuous operation (Schmideder et al., 2016). The first improved cascaded process could not outperform an optimized fed-batch process (compare to **Figure 7** and **Table 1**) regarding product concentration and product yield coefficient yet. As product formation throughout fed-batches is very much dependent on induction time, high standard deviations can be seen for productivity, as values were calculated as an average over the time of induction. Chemostat processes and cascade 1 and 2 did not show constant productivity over time, explaining high standard deviations seen there. Cascade 3 was the only process to feature constant productivity, therefore lower standard deviations compared to the other processes can be seen. Still we would like to highlight that even though a constant productivity could be reached metabolic fluxes (such as shifts in CDW, dO_2, and CER shown in **Supplementary Figures**) occur throughout production. As fed-batch results indicated, that specific productivity declines during an induction time of 12 h, it might be necessary to wash out cells before maximum productivity can be achieved, in order to keep them in a stable production mode. However, when taking sterilization and cleaning times into account, the cascaded process could be a well-used alternative to fed-batch processes in combination with the possibility of creating a fully integrated process.

DISCUSSION

In order to achieve constant productivity of the IB based product, different cultivation modes were tested. Trying to establish a continuous cultivation mode specific productivity and space time yield of chemostat- and the cascaded cultivation were compared to state-of-the-art fed-batch processes. First optimized process parameters such as dilution rate, residence time and inducer concentration led to the optimized cultivation process seen in **Figures 7A,B** tested by IB titer during the cultivation. Results indicate, that lactose is the inducer of choice for induction in all continuous operated systems, when compared to IPTG. In previous studies, it has been shown that cultivations of *E. coli* BL21(DE3) carried out on glycerol tend to produce more recombinant protein with a product optimum at a $q_{s,glycerol}$-level seen around 0.3–0.35 g $g^{-1}h^{-1}$ (Kopp et al., 2017). Space-time yield and product yield of cascade 3 operated at a

TABLE 1 | Comparison of bioprocesses for inclusion body production with *E. coli* BL21(DE3) in chemostat cultivation, an optimized fed-batch process and continuously operated cascades with different dilution rates and $q_{s,lac}$-values regarding cell dry weight (DCW), residence time in the induction reactor (τ), specific glycerol uptake rate ($q_{s,Glycerol}$), product selectivity ($Y_{P/S}$), product yield coefficient ($Y_{P/X}$), space-time yield (STY), and product concentration (C_P).

Parameters	Fed-batch 1 ($\mu = 0.08 \pm 0.024\ h^{-1}$)	Fed-batch 2 ($\mu = 0.18 \pm 0.012\ h^{-1}$)	Chemostat ($D = 0.16 \pm 0.021\ h^{-1}$)	Cascade 1 ($D_2 = 0.1 \pm 0.001\ h^{-1}$)	Cascade 2 ($D_2 = 0.08 \pm 0.004\ h^{-1}$)	Cascade 3 ($D_2 = 0.16 \pm 0.010\ h^{-1}$)
Induction as IPTG or q_{slac} [g g^{-1} h^{-1}]	IPTG, 0.5 mM	IPTG, 0.5 mM	$q_{slac,max}$*0.5	IPTG, 0.5 mM	$q_{slac,max}$	$q_{slac,max}$
CDW [g L^{-1}]	31.6 ± 4.8	34.9 ± 4.1	13.9 ± 5.4	27.5 ± 4.6	39.6 ± 9.8	37.8 ± 8.9
τ [h]	-	-	5.9 ± 0.2	10 ± 0.1	12.55 ± 0.83	6.0 ± 0.4
$q_{s,glycerol}$ [g g^{-1} h^{-1}]	0.19 ± 0.06	0.54 ± 0.1	0.48 ± 0.10	0.22 ± 0.07	0.292 ± 0.05	0.48 ± 0.06
$Y_{P/S}$ [mg g^{-1}]	62 ± 78.4	158.9 ± 189.5	9.5 ± 17.4	8.5 ± 9.0	7.3 ± 7.79	12.7 ± 4.3
$Y_{P/X}$ [mg g^{-1}]	106 ± 29.3	121.6 ± 67.2	27.2 ± 54.9	22.8 ± 23.2	23.7 ± 23.8	147.2 ± 55.9
STY [mg L^{-1} h^{-1}]	825.6 ± 281.1	2411.1 ± 1129.2	89.7 ± 148.6	60.8 ± 64.63	118.5 ± 132.2	311.8 ± 98.6
C_P [mg L^{-1}]	1448.9 ± 1.065	3969 ± 2854.9	236.07 ± 355.368	736.8 ± 720.3	1607.0 ± 925.3	6139.0 ± 2359.1

Values are calculated as an average after 5 residence times for continuous applications, while fed-batch-values are calculated at as an average throughout induction phase; cultivations shown in ***Figures 4A,B*** *are not taken into account of this table, as productivities were very little. Values are calculated as an average after 5 residence times, for the fed-batch they are calculated as an average over induction time. High standard deviation result from time dependent production.*

dilution rate of $D_2 = 0.16\ h^{-1}$ induced at $q_{s,lac,max}$ showed best results up to date compared to the other continuously operated processes performed within this study. As glycerol needs increased cAMP levels, which are also needed for lactose uptake (Bettenbrock et al., 2006), this might be a key function in regulating higher lactose uptake and subsequently increasing productivity and product titer. Higher dilution rates, such as operated in cascade 3, implemented lower residence times of producing cells, which might help to reduce the metabolic burden onto host cells. Hence high dilution rates will consequently decrease DCW values and ongoing lead to a washout of cells (Paalme et al., 1995; Schmideder et al., 2016). Schmideder and Weuster-Botz (2017) improved the overall process performance producing soluble PAmCherry with *E. coli* in a continuously operated cascade by reducing the overall dilution from 0.2 to 0.13 h^{-1}. Dilution rates of 0.2 h^{-1} were not considered within this study but could be investigated in subsequent cultivations in order to further increase the overall process performance. Simulations of plasmid stability in a continuously operated cascade performed by Hortacsu and Ryu (1991) showed that there is an improved plasmid stability at higher dilution rates for long-term cultivations (Park et al., 1990; Hortacsu and Ryu, 1991; Rhee and Schügerl, 1998). Hortacsu and Ryu (1991) also proved that a linear, time-dependent growth rate control, using a slow increase of dilution rate resulted in an increased average productivity when compared to a process operated at a constant growth rate. As a part of this study we show that single vessel chemostat cultivation does not provide stable long-term product formation, when keeping process parameters constant. The cultivation mode proposed by Hortacsu and Ryu (1991), similar to an accelerostat cultivation mode, could therefore be seen as a potential cultivation mode for achieving stable productivity within a single-vessel cultivation mode (Paalme et al., 1995). We were able to show, that cascade system implemented by Schmideder and Weuster-Botz (2017), is very well-suitable to increase continuous microbial processes regarding the space-time-yield. Spatial separation from biomass growth and recombinant protein production clearly seems to be beneficial for process performance. Application of higher dilution rates throughout cascade processes resulted in higher product titers, we hypothesize that shorter residence times in the producing reactors seems to be highly favorable for recombinant protein production. On the other hand, too high dilution rates (lager than 0.25 h^{-1}) might lead to a "washout-effect" of the host cells, so a tradeoff must be found between optimal feeding and optimal residence time. As highest productivity of a fed-batch is generally found after 6–8 h, residence times in this range may be optimal for cascaded cultivations. Therefore, using higher dilution rates smaller than 6 h may result in lower productivity as not enough time for induction is given in the reactor. As biological evolution throughout continuous cultivations might always lead to certain gene up- or downregulations (Wick et al., 2001; Peebo et al., 2015) the results indicate that cells tend to stay in a rather stable system when they are exhibiting lower residence times in a cascaded system. Taking the different amounts of recombinant protein produced as an indicator for changes in metabolome or transcriptome, the cascaded system seems to keep cells in rather stable conditions, when compared to common chemostat cultivation.

During a previous work conducted in fed-batch experiments, we were able to show that cell lysis is occurring at elongated induction times, when induced with IPTG (Kopp et al., 2018; Slouka et al., 2019). As lactose is a rather "soft" inducer and is used in combination with a relatively short average residence time of 6.25 h throughout cascade 3, this is possibly the quintessence for stable protein production within this process. As a continuous process for recombinant protein production can either be improved by increased titer concentrations in the bleed or by increasing $\frac{dV_{Bleed}}{dt}$, cascade 3 operated at $q_{s,lac,max}$ with $D_2 = 0.16\ h^{-1}$ combines both features of a possible improvement and could therefore be a well-suited cultivation system, when implementing a fully integrated continuous process.

In this work, the economical and practical feasibility of a continuous cultivation process to produce a recombinant protein as IB with the genetically modified strain *E. coli* BL21(DE3) was investigated. The overall goal was to provide a promising alternative to optimized fed-batch processes, trying to eliminate time-dependent changes of productivity. It was shown that a spatial separation of biomass formation and recombinant protein expression by setting up a cascade of two stirred tank reactors significantly improves the overall process performance of a continuous cultivation. It was further confirmed that the application of lactose as an inducer instead of IPTG resulted in higher productivities over time in chemostat and in cascaded cultivation. Usage of lactose as an inducer instead of IPTG in combination with a cascaded cultivation mode at optimized dilution rates leads to an increase in specific productivity and space-time yield of the cascaded system when compared to chemostat processing. As higher dilution rates also seem to boost titer formation, the overall mass flow of product out of the cascade was significantly increased. Furthermore, continuous processing is referred to boost the time-space-yield, when taking set-up- and cleaning times into account. As a continuous cultivation mode also provides the possibility of achieving time-independent critical quality attributes, downstream processing should be eased and more robust, consequently. Therefore, we want to highlight, that the optimized cascaded run could potentially fulfill the criteria of an industrial continuous cultivation system. We are currently optimizing the given system in order to achieve a stable long-lasting process, which can outperform the fed-batch as golden standard.

DATA AVAILABILITY STATEMENT

The datasets generated for this study are available on request to the corresponding author.

AUTHOR CONTRIBUTIONS

JK, A-MK, and PV performed the cultivations. CS and CH supervised the work and gave the valuable input. JK, CS, OS, and CH drafted the manuscript.

FUNDING

The authors thank the Christian Doppler Society for funding of this project.

SUPPLEMENTARY MATERIAL

The Supplementary Material for this article can be found online at: https://www.frontiersin.org/articles/10.3389/fbioe.2019.00297/full#supplementary-material

REFERENCES

Achmüller, C., Kaar, W., Ahrer, K., Wechner, P., Hahn, R., Werther, F., et al. (2007). N(pro) fusion technology to produce proteins with authentic N termini in *E. coli*. *Nat. Methods* 4, 1037–1043. doi: 10.1038/nmeth1116

Akhnoukh, R., Kretzmer, G., and Schügerl, K. (1996). On-line monitoring and control of the cultivation of *Spodoptera frugiperda* Sf9 insect cells and β-galactosidase production by *Autographa californica* virus vector. *Enzyme Microb. Technol.* 18, 220–228. doi: 10.1016/0141-0229(95)00093-3

Baheri, H.R., Hill, G.A., and Roesler, W.J. (1996). Optimum design for production of tryptophan synthetase subunit from recombinant *Escherichia coli* in a two-stage continuous flow stirred tank reactor (growth and production stage). *Chem. Eng. J. Biochem. Eng. J.* 62, 143–148. doi: 10.1016/0923-0467(95)03065-4

Bettenbrock, K., Fischer, S., Kremling, A., Jahreis, K., Sauter, T., and Gilles, E.D. (2006). A quantitative approach to catabolite repression in *Escherichia coli*. *J. Biol. Chem.* 281, 2578–2584. doi: 10.1074/jbc.M508090200

Blommel, P.G., Becker, K.J., Duvnjak, P., and Fox, B.G. (2007). Enhanced bacterial protein expression during auto-induction obtained by alteration of lac repressor dosage and medium composition. *Biotechnol. Prog.* 23, 585–598. doi: 10.1021/bp070011x

Boström, M., Markland, K., Sandén, A.M., Hedhammar, M., Hober, S., and Larsson, G. (2005). Effect of substrate feed rate on recombinant protein secretion, degradation and inclusion body formation in *Escherichia coli*. *Appl. Microb. Biotechnol.* 68, 82–90. doi: 10.1007/s00253-004-1855-4

Brown, S.W., Meyer, H.-P., and Fiechter, A. (1985). Continuous production of human leukocyte interferon with*Escherichia coli* and continuous cell lysis in a two stage chemostat. *Appl. Microbiol. Biotechnol.* 23, 5–9. doi: 10.1007/BF02660110

Ceroni, F., Algar, R., Stan, G.-B., and Ellis, T. (2015). Quantifying cellular capacity identifies gene expression designs with reduced burden. *Nat. Methods* 12, 415. doi: 10.1038/nmeth.3339

Croughan, M.S., Konstantinov, K.B., and Cooney, C. (2015). The future of industrial bioprocessing: batch or continuous? *Biotechnol. Bioeng.* 112, 648–651. doi: 10.1002/bit.25529

da Silva, G.P., Mack, M., and Contiero, J. (2009). Glycerol: a promising and abundant carbon source for industrial microbiology. *Biotechnol. Adv.* 27, 30–39. doi: 10.1016/j.biotechadv.2008.07.006

Daszkowski, T. (2013). "Continuous processing in biotech production: an alternative to a modern single use, batch, facility," in *Integrated Continuous Biomanufacturing Conference* (Barcelona).

DeLisa, M.P., Li, J., Rao, G., Weigand, W.A., and Bentley, W.E. (1999). Monitoring GFP-operon fusion protein expression during high cell density cultivation of *Escherichia coli* using an on-line optical sensor. *Biotechnol. Bioeng.* 65, 54–64. doi: 10.1002/(SICI)1097-0290(19991005)65:1<54::AID-BIT7>3.0.CO;2-R

Deutscher, J., Francke, C., and Postma, P.W. (2006). How phosphotransferase system-related protein phosphorylation regulates carbohydrate metabolism in bacteria. *Microbiol. Mol. Biol. Rev.* 70, 939–1031. doi: 10.1128/MMBR.00024-06

Diers, I., Rasmussen, E., Larsen, P., and Kjaersig, I. (1991). Yeast fermentation processes for insulin production. *Bioprocess Technol.* 13, 166.

Domingues, L., Lima, N., and Teixeira, J.A. (2005). Aspergillus niger β-galactosidase production by yeast in a continuous high cell density reactor. *Process Biochem.* 40, 1151–1154. doi: 10.1016/j.procbio.2004.04.016

Donovan, R.S., Robinson, C.W., and Glick, B. (1996). Optimizing inducer and culture conditions for expression of foreign proteins under the control of thelac promoter. *J. Ind. Microbiol.* 16, 145–154. doi: 10.1007/BF01569997

Dubendorff, J.W., and Studier, F.W. (1991). Controlling basal expression in an inducible T7 expression system by blocking the target T7 promoter with lac repressor. *J. Mol. Biol.* 219, 45–59. doi: 10.1016/0022-2836(91)90856-2

Dvorak, P., Chrast, L., Nikel, P.I., Fedr, R., Soucek, K., Sedlackova, M., et al. (2015). Exacerbation of substrate toxicity by IPTG in *Escherichia coli* BL21(DE3) carrying a synthetic metabolic pathway. *Microb. Cell Fact.* 14, 201. doi: 10.1186/s12934-015-0393-3

Garcia-Fruitos, E., Vazquez, E., Diez-Gil, C., Corchero, J.L., Seras-Franzoso, J., Ratera, I., et al. (2012). Bacterial inclusion bodies: making gold from waste. *Trends Biotechnol.* 30, 65–70. doi: 10.1016/j.tibtech.2011.09.003

Georgiou, G., and Valax, P. (1999). Isolating inclusion bodies from bacteria. *Methods Enzymol.* 309. doi: 10.1016/S0076-6879(99)09005-9

Gupta, J.C., Pandey, G., and Mukherjee, K.J. (2001). Two-stage cultivation of recombinant Saccharomyces cerevisiae to enhance plasmid stability under non-selective conditions: experimental study and modeling. *Enzyme Microb. Technol.* 28, 89–99. doi: 10.1016/S0141-0229(00)00285-4

Gupta, S.K., and Shukla, P. (2016). Microbial platform technology for recombinant antibody fragment production: a review. *Crit. Rev. Microbiol.* 43, 31–42. doi: 10.3109/1040841X.2016.1150959

Hausjell, J., Weissensteiner, J., Molitor, C., Halbwirth, H., and Spadiut, O. (2018). *E. coli* HMS174 (DE3) is a sustainable alternative to BL21 (DE3). *Microb Cell Fact.* 17, 169. doi: 10.1186/s12934-018-1016-6

Heyland, J., Blank, L.M., and Schmid, A. (2011). Quantification of metabolic limitations during recombinant protein production in *Escherichia coli*. *J. Biotechnol.* 155, 178–184. doi: 10.1016/j.jbiotec.2011.06.016

Hoffmann, F., and Rinas, U. (2004). "Stress induced by recombinant protein production in *Escherichia coli*," in *Physiological Stress Responses in Bioprocesses* (Oxford: Springer), 73–92. doi: 10.1007/b93994

Hortacsu, A., and Ryu, D.D. (1991). Optimization of a two-stage recombinant fermentation process: the dilution rate effect. *Biotechnol. Bioeng.* 38, 831–837. doi: 10.1002/bit.260380805

Hoskisson, P.A., and Hobbs, G. (2005). Continuous culture-making a comeback? *Microbiology* 151 (Pt 10), 3153–3159. doi: 10.1099/mic.0.27924-0

Huang, C.J., Lin, H., and Yang, X. (2012). Industrial production of recombinant therapeutics in *Escherichia coli* and its recent advancements. *J. Ind. Microbiol. Biotechnol.* 39, 383–399. doi: 10.1007/s10295-011-1082-9

Jagschies, G., Lindskog, E., Lacki, K., and Galliher, P.M. (2018). *Biopharmaceutical Processing: Development, Design, and Implementation of Manufacturing Processes*. Oxford: Elsevier.

Kim, J.Y., and Ryu, D.D. (1991). The effects of plasmid content, transcription efficiency, and translation efficiency on the productivity of a cloned gene protein in *Escherichia coli*. *Biotechnol. Bioeng.* 38, 1271–1279. doi: 10.1002/bit.260381103

Kopp, J., Slouka, C., Strohmer, D., Kager, J., Spadiut, O., and Herwig, C. (2018). Inclusion body bead size in *E. coli* controlled by physiological feeding. *Microorganisms* 6, 116. doi: 10.3390/microorganisms6040116

Kopp, J., Slouka, C., Ulonska, S., Kager, J., Fricke, J., Spadiut, O., et al. (2017). Impact of glycerol as carbon source onto specific sugar and inducer uptake rates and inclusion body productivity in *E. coli* BL21 (DE3). *Bioengineering* 5:1. doi: 10.3390/bioengineering5010001

Langemann, T., Mayr, U.B., Meitz, A., Lubitz, W., and Herwig, C. (2016). Multi-parameter flow cytometry as a process analytical technology (PAT) approach for the assessment of bacterial ghost production. *Appl. Microbiol. Biotechnol.* 100, 409–418. doi: 10.1007/s00253-015-7089-9

Lin, E.C. (1976). Glycerol dissimilation and its regulation in bacteria. *Annu. Rev. Microbiol.* 30, 535–578. doi: 10.1146/annurev.mi.30.100176.002535

Lyakhov, D.L., He, B., Zhang, X., Studier, F.W., Dunn, J.J., and McAllister, W.T. (1998). Pausing and termination by bacteriophage T7 RNA polymerase. *J. Mol. Biol.* 280, 201–213. doi: 10.1006/jmbi.1998.1854

Marbach, A., and Bettenbrock, K. (2011). lac operon induction in *Escherichia coli*: systematic comparison of IPTG and TMG induction and influence of the transacetylase LacA. *J. Biotechnol.* 157, 82–88. doi: 10.1016/j.jbiotec.2011.10.009

Marisch, K., Bayer, K., Cserjan-Puschmann, M., Luchner, M., and Striedner, G. (2013). Evaluation of three industrial *Escherichia coli* strains in fed-batch cultivations during high-level SOD protein production. *Microb. Cell Fact.* 12, 58. doi: 10.1186/1475-2859-12-58

Marschall, L., Sagmeister, P., and Herwig, C. (2016). Tunable recombinant protein expression in E. coli: enabler for continuous processing? *Appl. Microbiol. Biotechnol.* 100, 5719–5728. doi: 10.1007/s00253-016-7550-4

Martínez-Gómez, K., Flores, N., Castañeda, H.M., Martínez-Batallar, G., Hernández-Chávez, G., Ramírez, O.T., et al. (2012). New insights into *Escherichia coli* metabolism: carbon scavenging, acetate metabolism and carbon recycling responses during growth on glycerol. *Microb. Cell Fact.* 11, 46. doi: 10.1186/1475-2859-11-46

Monod, J. (1950). La technique de culture continue, théorie et applications. *Ann. Inst. Pasteur.* 79, 390–410.

Neubauer, P., and Hofmann, K. (1994). Efficient use of lactose for the lac promoter-controlled overexpression of the main antigenic protein of the foot and mouth disease virus in *Escherichia coli* under fed-batch fermentation conditions. *FEMS Microbiol. Rev.* 14, 99–102. doi: 10.1111/j.1574-6976.1994.tb00080.x

Neubauer, P., Hofmann, K., Holst, O., Mattiasson, B., and Kruschke, P. (1992). Maximizing the expression of a recombinant gene in *Escherichia coli* by manipulation of induction time using lactose as inducer. *Appl. Microbiol. Biotechnol.* 36, 739–744. doi: 10.1007/BF00172185

Neubauer, P., Lin, H., Mathiszik, B. (2003). Metabolic load of recombinant protein production: inhibition of cellular capacities for glucose uptake and respiration after induction of a heterologous gene in *Escherichia coli*. *Biotechnol. Bioeng.* 83, 53–64. doi: 10.1002/bit.10645

Novick, A., and Szilard, L. (1950). Experiments with the Chemostat on spontaneous mutations of bacteria. *Proc. Natl. Acad. Sci. U.S.A.* 36, 708–719. doi: 10.1073/pnas.36.12.708

Paalme, T., Kahru, A., Elken, R., Vanatalu, K., Tiisma, K., and Raivo, V. (1995). The computer-controlled continuous culture of *Escherichia coli* with smooth change of dilution rate (A-stat). *J. Microbiol. Methods* 24, 145–153. doi: 10.1016/0167-7012(95)00064-X

Park, S., and Ryu, D.D. (1990). Effect of operating parameters on specific production rate of a cloned-gene product and performance of recombinant fermentation process. *Biotechnol. Bioeng.* 35, 287–295. doi: 10.1002/bit.260350310

Park, S., Ryu, D.D., and Kim, J.Y. (1990). Effect of cell growth rate on the performance of a two-stage continuous culture system in a recombinant *Escherichia coli* fermentation. *Biotechnol. Bioeng.* 36, 493–505. doi: 10.1002/bit.260360509

Park, T.H., Seo, J.H., and Lim, H.C. (1989). Optimization of fermentation processes using recombinant *Escherichia coli* with the cloned trp operon. *Biotechnol. Bioeng.* 34, 1167–1177. doi: 10.1002/bit.260340907

Paulova, L., Hyka, P., Branska, B., Melzoch, K., and Kovar, K. (2012). Use of a mixture of glucose and methanol as substrates for the production of recombinant trypsinogen in continuous cultures with *Pichia pastoris* Mut$^+$. *J. Biotechnol.* 157, 180–188. doi: 10.1016/j.jbiotec.2011.10.010

Peebo, K., and Neubauer, P. (2018). Application of continuous culture methods to recombinant protein production in microorganisms. *Microorganisms* 6:E56. doi: 10.3390/microorganisms6030056

Peebo, K., Valgepea, K., Maser, A., Nahku, R., Adamberg, K., and Vilu, R. (2015). Proteome reallocation in *Escherichia coli* with increasing specific growth rate. *Mol. Biosyst.* 11, 1184–1193. doi: 10.1039/C4MB00721B

Rhee, J.I., and Schügerl, K. (1998). Continuous cultivation of recombinant *Escherichia coli* JM109 in a two-stage cascade reactor and production of the fusion protein EcoRI:: SPA. *Process Biochem.* 33, 213–224. doi: 10.1016/S0032-9592(97)00097-6

Rinas, U., and Bailey, J.E. (1992). Protein compositional analysis of inclusion bodies produced in recombinant *Escherichia coli*. *Appl. Microbiol. Biotechnol.* 37, 609–614. doi: 10.1007/BF00240735

Sandén, A.M., Prytz, I., Tubulekas, I., Förberg, C., Le, H., Hektor, A., et al. (2003). Limiting factors in *Escherichia coli* fed-batch production of recombinant proteins. *Biotechnol. Bioeng.* 81, 158–166. doi: 10.1002/bit.10457

Schein, C.H. (1989). Production of soluble recombinant proteins in bacteria. *Nat. Biotechnol.* 7, 1141. doi: 10.1038/nbt1189-1141

Schmideder, A., Cremer, J.H., and Weuster-Botz, D. (2016). Parallel steady state studies on a milliliter scale accelerate fed-batch bioprocess design for recombinant protein production with *Escherichia coli*. *Biotechnol. Progr.* 32, 1426–1435. doi: 10.1002/btpr.2360

Schmideder, A., and Weuster-Botz, D. (2017). High-performance recombinant protein production with *Escherichia coli* in continuously operated cascades of stirred-tank reactors. *J. Ind. Microbiol. Biotechnol.* 44, 1021–1029. doi: 10.1007/s10295-017-1927-y

Scott, M., Gunderson, C.W., Mateescu, E.M., Zhang, Z., and Hwa, T. (2010). Interdependence of cell growth and gene expression: origins and consequences. *Science* 330, 1099–1102. doi: 10.1126/science.1192588

Selvamani, R.S.V., Friehs, K., and Flaschel, E. (2014). Extracellular recombinant protein production under continuous culture conditions with *Escherichia coli* using an alternative plasmid selection mechanism. *Bioprocess Biosyst. Eng.* 37, 401–413. doi: 10.1007/s00449-013-1005-4

Slouka, C., Kopp, J., Hutwimmer, S., Strahammer, M., Strohmer, D., Eitenberger, E., et al. (2018). Custom Made Inclusion Bodies: impact of classical process parameters and physiological parameters on Inclusion Body quality attributes. *Microb. Cell Fact.* 17, 148. doi: 10.1186/s12934-018-0997-5

Slouka, C., Kopp, J., Strohmer, D., Kager, J., Spadiut, O., and Herwig, C. (2019). Monitoring and control strategies for inclusion body production in *E. coli* based on glycerol consumption. *J. Biotechnol.* 296, 75–82. doi: 10.1016/j.jbiotec.2019.03.014

Steen, R., Dahlberg, A.E., Lade, B.N., Studier, F.W., and Dunn, J.J. (1986). T7 RNA polymerase directed expression of the *Escherichia coli* rrnB operon. *EMBO J.* 5, 1099–1103. doi: 10.1002/j.1460-2075.1986.tb04328.x

Striedner, G., Cserjan-Puschmann, M., Pötschacher, F., and Bayer, K. (2003). Tuning the transcription rate of recombinant protein in strong *Escherichia coli* expression systems through repressor titration. *Biotechnol. Progress* 19, 1427–1432. doi: 10.1021/bp034050u

Studier, F.W., and Moffatt, B.A. (1986). Use of bacteriophage T7 RNA polymerase to direct selective high-level expression of cloned genes. *J. Mol. Biol.* 189, 113–130. doi: 10.1016/0022-2836(86)90385-2

Studier, F.W., Rosenberg, A.H., Dunn, J.J., and Dubendorff, J.W. (1990). Use of T7 RNA polymerase to direct expression of cloned genes. *Methods Enzymol.* 185, 60–89. doi: 10.1016/0076-6879(90)85008-C

Tripathi, N. (2009). High yield production of heterologous proteins with *Escherichia coli*. *Defence Sci. J.* 59, 137. doi: 10.14429/dsj.59.1501

Ukkonen, K., Mayer, S., Vasala, A., and Neubauer, P. (2013). Use of slow glucose feeding as supporting carbon source in lactose autoinduction medium improves the robustness of protein expression at different aeration conditions. *Protein Expr. Purif.* 91, 147–154. doi: 10.1016/j.pep.2013.07.016

Viitanen, M.I., Vasala, A., Neubauer, P., and Alatossava, T. (2003). Cheese whey-induced high-cell-density production of recombinant proteins in *Escherichia coli*. *Microb. Cell Fact.* 2, 2. doi: 10.1186/1475-2859-2-2

Walsh, G. (2010). Biopharmaceutical benchmarks 2010. *Nat. Biotechnol.* 28, 917–924. doi: 10.1038/nbt0910-917

Walther, J., Godawat, R., Hwang, C., Abe, Y., Sinclair, A., and Konstantinov, K. (2015). The business impact of an integrated continuous biomanufacturing platform for recombinant protein production. *J. Biotechnol.* 213, 3–12. doi: 10.1016/j.jbiotec.2015.05.010

Wick, L.M., Quadroni, M., and Egli, T. (2001). Short-and long-term changes in proteome composition and kinetic properties in a culture of *Escherichia coli* during transition from glucose-excess to glucose-limited growth conditions in continuous culture and vice versa. *Environ. Microbiol.* 3, 588–599. doi: 10.1046/j.1462-2920.2001.00231.x

Wurm, D.J., Herwig, C., and Spadiut, O. (2017a). How to determine interdependencies of glucose and lactose uptake rates for heterologous protein production with *E. coli*. *Methods Mol. Biol.* 1586, 397–408. doi: 10.1007/978-1-4939-6887-9_26

Wurm, D.J., Quehenberger, J., Mildner, J., Eggenreich, B., Slouka, C., Schwaighofer, A., et al. (2017b). Teaching an old pET new tricks: tuning of inclusion body formation and properties by a mixed feed system in *E. coli*. *Appl. Microbiol. Biotechnol.* 102, 667–676. doi: 10.1007/s00253-017-8641-6

Wurm, D.J., Veiter, L., Ulonska, S., Eggenreich, B., Herwig, C., and Spadiut, O. (2016). The *E. coli* pET expression system revisited-mechanistic correlation between glucose and lactose uptake. *Appl. Microbiol. Biotechnol.* 100, 8721–8729. doi: 10.1007/s00253-016-7620-7

Conflict of Interest: The authors declare that the research was conducted in the absence of any commercial or financial relationships that could be construed as a potential conflict of interest.

frontiers in Bioengineering and Biotechnology

ORIGINAL RESEARCH
published: 05 November 2019
doi: 10.3389/fbioe.2019.00301

Influence of Unusual Co-substrates on the Biosynthesis of Medium-Chain-Length Polyhydroxyalkanoates Produced in Multistage Chemostat

*Nils Hanik[1], Camila Utsunomia[1], Shuzo Arai[2], Ken'ichiro Matsumoto[3] and Manfred Zinn[1]**

[1] Institute of Life Technologies, University of Applied Sciences and Arts Western Switzerland (HES-SO Valais-Wallis), Sion, Switzerland, [2] Graduate School of Chemical Sciences and Engineering, Hokkaido University, Sapporo, Japan, [3] Division of Applied Chemistry, Faculty of Engineering, Hokkaido University, Sapporo, Japan

A two-stage chemostat cultivation was used to investigate the biosynthesis of functionalized medium-chain-length polyhydroxyalkanoate (mcl-PHA) in the β-oxidation weakened strain of *Pseudomonas putida* KTQQ20. Chemostats were linked in sequence and allowed separation of biomass production in the first stage from the PHA synthesis in the second stage. Four parallel reactors in the second stage provided identical growth conditions and ensured that the only variable was the ratio of decanoic acid (C10) to an unusual PHA monomer precursor, such as 10-undecenoic acid (C11:1) or phenylvaleric acid (PhVA). Obtained PHA content was in the range of 10 to 25 wt%. When different ratios of C10 and C11:1 were fed to *P. putida*, the produced PHA had a slightly higher molar ratio in favor of C11:1-based 3-hydroxy-10-undecenoate. However, in case of PhVA a significantly lower incorporation of 3-hydroxy-5-phenylvalerate over 3-hydroxydecanoate took place when compared to the ratio of their precursors in the feed medium. A result that is explained by a less efficient uptake of PhVA compared to C10 and a 24% lower yield of polymer from the aromatic fatty acid ($y_{\frac{PHA-M}{PhVA}} = 0.25$). In addition, PHA isolated from cultivations with PhVA resulted in the number average molecular weight $\overline{M_n}$ two times lower than the PHA produced from C10 alone. Detection of products from PhVA metabolism in the culture supernatant showed that uptaken PhVA was not entirely converted into PHA, thus explaining the difference in the yield polymer from substrate. It was concluded that PhVA or its related metabolites increased the chain transfer rate during PHA biosynthesis in *P. putida* KTQQ20, resulting in a reduction of the polymer molecular weight.

Keywords: medium-chain-length poly(3-hydroxyalkanoate), functional polymer, aromatic polymer, unsaturated polymer, multistage chemostat, steady-state cultivation, carbon flux, chain transfer

OPEN ACCESS

Edited by:
Thomas Bartholomäus Brück, Technical University of Munich, Germany

Reviewed by:
Christopher John Brigham, Wentworth Institute of Technology, United States
Ignacio Poblete-Castro, Universidad Andrés Bello, Chile

***Correspondence:**
Manfred Zinn
manfred.zinn@hevs.ch

Specialty section:
This article was submitted to Bioprocess Engineering, a section of the journal Frontiers in Bioengineering and Biotechnology

Received: *01 September 2019*
Accepted: *16 October 2019*
Published: *05 November 2019*

Citation:
Hanik N, Utsunomia C, Arai S, Matsumoto K and Zinn M (2019) Influence of Unusual Co-substrates on the Biosynthesis of Medium-Chain-Length Polyhydroxyalkanoates Produced in Multistage Chemostat. Front. Bioeng. Biotechnol. 7:301. doi: 10.3389/fbioe.2019.00301

INTRODUCTION

Tailor-made production of polyhydroxyalkanoates (PHA) bearing unconventional functional groups in the side chain is of high interest since their presence enables the control of the mechanical and physical properties already during biosynthesis (Hany et al., 2005; Tortajada et al., 2013). In addition, these integrated groups enable a further fine-tuning of the PHA using mild,

chemical conditions (Levine et al., 2016). ω-Unsaturated and aromatic substrates are examples of unusual PHA precursors (Hartmann et al., 2004). Most of the functionalized biopolyesters are medium-chain-length PHA (mcl-PHA) consisting of C_6-C_{12} hydroxyalkanoate monomers which have been biosynthesized mainly by *Pseudomonas oleovorans* and *P. putida* (Prieto et al., 2016). Among them, *P. putida* has been shown to be more efficient in the utilization of aromatic carbon substrates for PHA production (Kim et al., 1999).

The wild-type strain *P. putida* KT2440 and its spontaneous rifampicin resistant mutant *P. putida* KT2442 are some of best and most studied producers of mcl-PHA (Follonier et al., 2011; Poblete-Castro et al., 2012). Biosynthesis of mcl-PHA from fatty acids is linked to the fatty acid β-oxidation cycle. Growth substrates that went through β-oxidation build up a pool of different 3-hydroxyalkanoates that can serve for the synthesis of PHA. They differ in their number of C2 units removed during the β-oxidation process and result typically in copolymeric PHAs (Huisman et al., 1989; Ouyang et al., 2007).

In 2011, Liu et al. developed a fatty acid β-oxidation weakened mutant of *P. putida* KT2442, designated as *P. putida* KTQQ20 (Liu et al., 2011). Six key genes of the β-oxidation pathway (*PP2136, PP2137, PP2214, PP2215, PP2047,* and *PP2048*) as well as the 3-hydroxyacyl-CoA-acyl carrier protein transferase (*PP1408*) have been knocked out. This strain still expresses the natural polymerases PhaC1 and PhaC2. The carbon flux is mainly utilized for PHA accumulation. However, the oxidation of fatty acids used as PHA monomer precursors is strongly reduced, rendering *P. putida* KTQQ20 a very suitable strain to study the relationship between substrate and the resulting monomeric unit composition of PHA in detail. Several authors have demonstrated that monomer composition can be tailored to some extent by choosing a specific substrate composition (Hartmann et al., 2006; Liu et al., 2011; Tripathi et al., 2013) using batch, fed-batch or continuous cultivation.

In particular, the continuous cultivation has been identified as a very suitable method to study PHA biosynthesis in a reproducible way (Atlic et al., 2011) once steady-state conditions are achieved. Hartmann et al. found that in contrast to batch cultivation, the chemostat production of PHA in *P. putida* GPo1 results in a time-independent monomeric unit composition when multiple nutrient limited growth was established (Hartmann et al., 2006). The same authors analyzed also in *P. putida* GPo1 the PHA composition when a binary substrate mixture containing *n*-octanoate (C8) and 10-undecenoate (C11:1) was supplied under simultaneous carbon and nitrogen limited growth conditions. Interestingly, they found a non-linear correlation between the fatty acid substrate composition and the 3-hydroxyalkanoates in PHA. In equimolar substrate mixtures, C8 was mainly used as carbon source for biomass formation, thus an increased 3-hydroxy-10-undecenoate content in PHA could be detected.

In this study, we investigated in a two-stage chemostat the accumulation of mcl-PHA in *P. putida* KTQQ20 from unusual substrates as carbon sources in a co-feed experiment. In contrast to the work of Hartmann et al., this experimental set-up allowed the separation of cell growth from accumulation of mcl-PHA precursors. In the first stage, citrate was used as sole carbon source, which was not leading to PHA formation. In the second stage, the transferred cells accumulated PHA because fatty acids were supplied in ample amounts. The weakened β-oxidation leads to PHA monomers structurally related to the supplied fatty acids (i.e., same carbon number) while the co-feed of citric acid in this stage covered maintenance energy requirements of the cells.

Next to composition, the molecular weight of PHAs was shown to play another important role to the mechanical properties of the polymeric materials (Boesel et al., 2014; Arikawa et al., 2016; Huong et al., 2017). Endogenous substrates can influence the molecular weight of the produced polymers by changing the chain transfer rate in the polymerization process (Tomizawa et al., 2010; Tsuge et al., 2013; Hyakutake et al., 2014).

The aim of this work was to study and better understand the substrate kinetics of unusual fatty acids, which are known to strongly influence PHA composition and eventually material properties. Together with the investigation of the effect of unusual substrates on the average molecular weight of the produced polymers, the work aims at influencing the resulting material properties on a molecular level. While the influence of the carbon substrate on the molecular weight was reported elsewhere (Kim et al., 1999; Ward et al., 2006), we propose here for the first time a mechanistic explanation for the observed results based on the kinetic model of the polymerization (Kawaguchi and Doi, 1992).

MATERIALS AND METHODS

All chemicals were purchased from Sigma-Aldrich, Switzerland, and used as received if not stated otherwise.

Cultivation Conditions

The two-stage continuous culture system consisted of one 2.5 L (IMCS-2000, newMBR AG, Switzerland) and in sequence a multifermenter with four parallel units of 0.5 L (Sixfors, Infors AG, Switzerland). The reactors had a working volume of 1.25 L and 0.4 L and were designated as the first (R1) and second stage (R2.1, R2.2, R2.3, and R2.4) bioreactors, respectively (**Figure 1**).

All cultures were performed at 30°C and the pH maintained at 7.0. In R1, cells were grown on the same medium as the preculture. At the end of the batch cultivation in R1, i.e., when the carbon source was fully consumed, the continuous culture system was started. The dilution rates (D) of R1 and R2 were 0.1 h^{-1} and 0.2 h^{-1}, respectively. The culture volume in R1 was kept constant by continuously transferring the broth to R2 from a tube completely immersed in the culture broth of R1 and by using an overflow tube in R1 both connected to peristaltic pumps. The overflow medium from R1 was collected in a 50 L harvest tank. Cells from R2 were also collected using an overflow tube connected to a continuous running peristaltic pump and the cells were finally kept in a 10 L harvest tank. Usually the steady-states were reached after 5 volume changes (50 and 25 h for $D = 0.1$ h^{-1} and for $D = 0.2$ h^{-1}, respectively) and typically PHA production was continued for another 12 h before taking samples. For the different co-substrate feeds, two samples were taken for analyses after steady-state was reached.

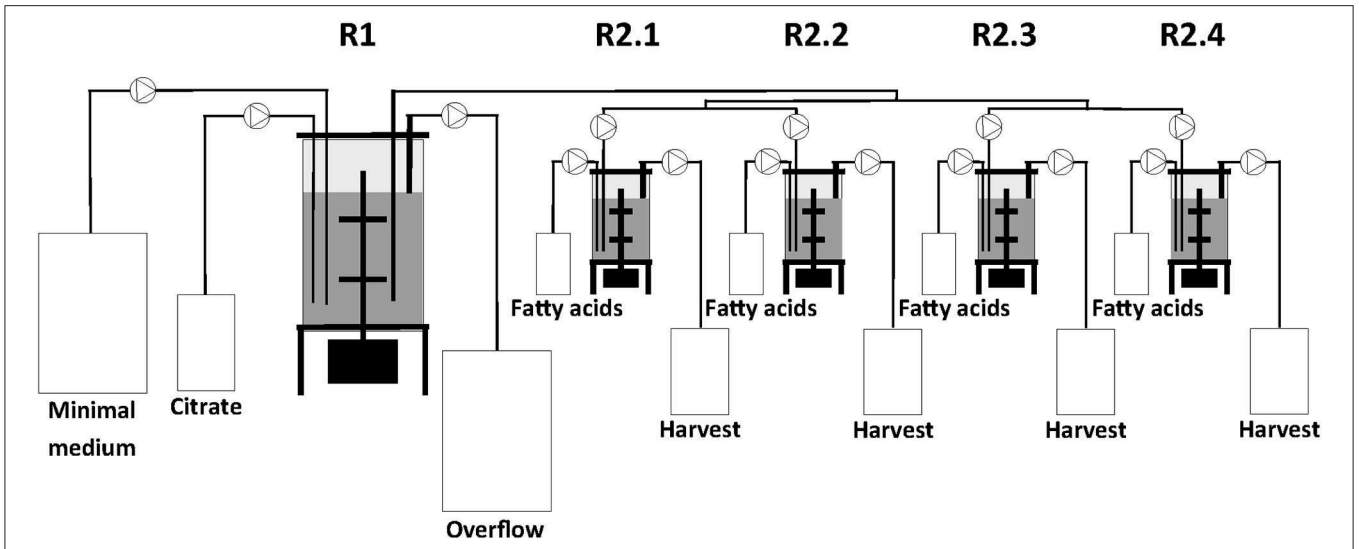

FIGURE 1 | Scheme of the bioreactor set-up showing the combination of serial and parallel reactors.

Strain and Media

Pseudomonas putida KTQQ20 was kindly provided by Prof. G. Q. Chen (Tsinghua University, China) and used for all experiments (Liu et al., 2011). For inoculum preparation, cells from a frozen stock culture were spread onto LB agar plates and incubated at 30°C for 24 h. The cells were recovered from the plates with a 0.9% NaCl solution and inoculated in 100 mL medium E in 500 mL shake flasks with an initial OD of 0.1. Cells were grown overnight at 30°C and 180 rpm. Medium E contained per liter: 3.5 g $NaNH_4HPO_4{\cdot}4H_2O$, 3.7 g KH_2PO_4, 7.5 g K_2HPO_4, and 2.9 g tri-Na-citrate$\cdot 2H_2O$. The pH was adjusted to 7.1 with 5 M NaOH. The medium was autoclaved and subsequently supplemented with 1 mL L^{-1} of filter-sterilized 1 M $MgSO_4{\cdot}7H_2O$ and 1 mL L^{-1} of mineral trace element stock solution which contained per liter 1 M HCl: 2.78 g $FeSO_4{\cdot}7H_2O$, 1.47 g $CaCl_2{\cdot}2H_2O$, 1.98 g $MnCl_2{\cdot}4H_2O$, 2.38 g $CoCl_2{\cdot}6H_2O$, 0.17 g $CuCl_2{\cdot}2H_2O$, 0.29 g $ZnSO_4{\cdot}7H_2O$.

For continuous cultivation, the following medium was used (per liter): 2.7 g $NaNH_4HPO_4{\cdot}4H_2O$, 3.7 g KH_2PO_4, and 7.5 g K_2HPO_4, supplemented with 1 mL L^{-1} of 1 M $MgSO_4{\cdot}7H_2O$ and of mineral trace element stock solution. A total of 40 L of this medium were then filter-sterilized into gamma-sterilized 50 L medium bags (STD FLEXBOY 50 L, Sartorius, Germany). For establishing the dual nutrient (C,N) limited growth regime (DNLGR) with carbon and nitrogen substrates, the amount of $NaNH_4HPO_4{\cdot}4H_2O$ was reduced to 1.9 g L^{-1} (Egli and Zinn, 2003). The carbon to nitrogen ratio (C_0/N_0) of the feed medium was set by the pump flow rates of minimal medium containing ammonium and of a separate feed containing 300 g L^{-1} tri-Na-citrate$\cdot 2H_2O$ as carbon source (**Figure 1**). Feed solutions containing citrate and different ratios of decanoic acid (C10) and a second fatty acid, such as 5-phenylvaleric acid (PhVA) or 10-undecenoic acid (C11:1) (**Tables 1**, **2**) were pumped directly in R2 using peristaltic pumps (LAMBDA Preciflow, Lambda Instruments, Switzerland). The ratio of citrate to total fatty acids was 2:1 mol mol^{-1}.

Cell Dry Weight (CDW)

Polypropylene tubes (1.7 mL, Axygen, Corning Inc., Mexico) were dried overnight at 100°C, cooled down in a desiccator over silicagel, and weighed. One mL of culture broth was then added to the tubes and spun down at 21,913 × g at 4°C for 5 min. The culture supernatant was kept at 4°C for further analyses and the cell pellet was washed with 0.9% NaCl solution. The cell suspension was spun down again and the supernatant discarded. The tubes were dried overnight at 100°C and the weight difference was used to calculate the concentration of biomass in the culture.

Quantification of Substrate Concentrations in the Culture Supernatant

Supernatant resulting from culture centrifugation was filtered through 0.45 μm polyamide filter for all the analyses. Ammonium concentration was measured by using a photometric ammonium test (Spectroquant, Merck, Germany). The detection limit of this method is 0.01 up to 3.00 mg L^{-1} NH_4-N. If necessary the samples were diluted with demineralized water. Citrate was measured by HPLC-UV equipped with an ion exclusion HPX-87H Aminex column (Bio-Rad, U.S.A.). The analysis was performed in an isocratic mode with 5 mM H_2SO_4 as the mobile phase with a flow rate of 0.6 mL min^{-1} for 30 min per sample. C10, C11:1, and PhVa were measured by reversed-phase chromatography equipped with a C18 column (Eclipse XDB-C18, 5 μm, 4.6 × 150 mm, Agilent Technologies) and an UV detector. A gradient of 70% of 0.1% (v v^{-1} formic acid in water to 100% 0.1% (v v^{-1}) formic acid in acetonitrile

TABLE 1 | Composition of aromatic carbon feed to the second stage bioreactors (R2.1–R2.4).

	Fatty acid composition in the feed[a]			
	100 mol% C10	**76 mol% C10**	**53 mol% C10**	**0 mol% C10**
Decanoic acid (C10) (mM)	19.1 ± 0.8	14.5 ± 0.6	10.1 ± 0.4	–
5-Phenylvaleric acid (PhVA) (mM)	–	4.6 ± 0.2	9.0 ± 0.4	19.1 ± 0.8

[a] *The feed of fatty acids was supplemented with a 2-fold molar excess of citric acid to ensure sufficient maintenance energy for the cells, the indicated error is based on an intrinsic error of the analytical method (4%).*

TABLE 2 | Composition of olefinic carbon feed to the second stage bioreactors (R2.1–R2.4).

	Fatty acid composition in the feed[a]			
	100 mol% C10	**74 mol% C10**	**44 mol% C10**	**0 mol% C10**
Decanoic acid (C10) (mM)	19.1 ± 0.8	14.1 ± 0.6	8.4 ± 0.3	–
10-Undecenoic acid (C11:1) (mM)	–	5.0 ± 0.2	10.7 ± 0.4	19.1 ± 0.8

[a] *The feed of fatty acids was supplemented with a 2-fold molar excess of citric acid to ensure sufficient maintenance energy for the cells, the indicated error is based on an intrinsic error of the analytical method (4%).*

was applied as the mobile phase. The flow rate was 1 mL min^{-1} and the gradient was completed after 15 min.

PHA Content and Composition

The composition of the polymer and its amount in relation to the biomass was determined as published elsewhere with minor modifications (Furrer et al., 2007). Pyrex vials were weighed to determine the exact transferred biomass (around 30 mg) then 2 mL of methylene chloride containing 2-ethyl-2-hydroxybutyrate (2 g L^{-1}) were added as internal standard. Furthermore, 2.5 mL of 1.3 M boron trifluoride-methanol solution were added. The suspension was incubated at 80°C for 20 h. After cooling the samples on ice, 2.5 mL of saturated NaCl solution were added and mixed by vortexing. The water phase was discarded (upper phase), including droplets hanging on the tube wall and including the interface to the methylene chloride phase. The addition of NaCl solution and removal of the water phase was repeated twice. Na_2SO_4 and Na_2CO_3 were added to dry the methylene chloride phase. The methylene chloride phase was filtered using solvent resistant filters (PTFE, 0.45 µm) and transferred to a GC sample tube. PHA content and monomer composition were subsequently analyzed on a GC (Agilent Technologies, U.S.A.) equipped with a polar fused silica capillary column (DB-WAX: length 30 m; inside diameter 0.25 mm; film thickness 0.25 µm; Agilent Technologies, U.S.A.). Helium was used as carrier gas (3 mL min^{-1}) and detection was performed with a flame ionization detector (FID) at 240°C. The temperature was increased from 70 to 240°C at a rate of 10°C min^{-1}.

Determination of PHA Molecular Weight Distribution

mcl-PHA was extracted directly from lyophilized cells. The dried biomass was transferred into pure methylene chloride (40 mg CDW in 10 mL methylene chloride). After stirring the suspension at room temperature for 3 h, the solution was filtered through a filter paper (ashless grade 589/2, white ribbon, pore Size: 4–12 µm, Schleicher&Schüll, Germany). The extracted PHA was subjected to gel permeation chromatography (GPC) for determining the molecular weight distribution. The analysis was performed using a chromatographic system consisting of Waters 171 plus autosampling unit and Waters 515 HPLC pump equipped with an Agilent PLgel MiniMIX-C column and an Agilent 1260 Infinity refractive index detector for the detection of the separated polymers. The system was maintained at 40°C and calibrated with polystyrene standards.

Calculations

The conversion yield of PHA-monomer from fatty acid ($y_{\frac{PHA-M}{FA}}$) was calculated according to Equation (1) based on the polymer concentration (c_{PHA}), the molecular weight of the fatty acid (M_{FA}) and the one of the monomer ($M_{monomer}$) which was derived from M_{FA} by taking oxidation and condensation into account (Equation 2). Equation (1) becomes valid for a high degree of polymerization (DP) considering the fact that the small error introduced by the very first monomer is negligible. The analyzed polymers had a DP between 250 and 600 making this expression for $y_{\frac{PHA-M}{FA}}$ suitable.

The taken up amount of fatty acid ($c_{FA,uptaken}$) was calculated from the difference of the fatty acid concentration in the feed ($c_{FA,feed}$) and the residual concentration of the fatty acid found in the supernatant ($c_{FA,supernatant}$) (Equation 3).

$$y_{\frac{PHA-M}{FA}} = \frac{c_{PHA} \times M_{FA}}{c_{FA,\ uptaken} \times (M_{monomer})} = \frac{c_{PHA} \times \frac{M_{monomer}}{M_{FA}}}{c_{FA,uptaken}} = \frac{n_{PHA-M}}{n_{FA,uptaken}} \quad (1)$$

$$M_{monomer} = M_{FA} + M_{oxygen} - M_{H_2O} = M_{FA} - 2 \quad (2)$$

$$c_{FA,uptaken} = c_{FA,feed} - c_{FA,\ supernatant} \quad (3)$$

TABLE 3 | Polymer accumulation on the fatty acids C10 and C11:1 in R2.

Polymer composition	Dry cell weight (g L^{-1})[a]	PHA content (wt%)[a]	Residual ammonium (mg L^{-1})	Residual citrate (mg L^{-1})[a]
100% Decanoate	1.1 ± 0.1	15 ± 0.7	nd	14 ± 1
50% Decanoate + 50% 10-undecenoate	1.2 ± 0.1	18 ± 0.4	nd	14 ± 2
75% Decanoate + 25% 10-undecenoate	1.2 ± 0.2	21 ± 0.7	nd	14 ± 1
100% Undecenoate	1.2 ± 0.1	25 ± 0.9	nd	12 ± 6[b]

[a] *The indicated standard deviation is based on multiple measurements (n = 3).*
[b] *n = 2.*

TABLE 4 | Polymer accumulation on the fatty acids C10 and PhVA in R2.

Polymer composition	Dry cell weight (g L^{-1})[a]	PHA content (wt%)[a]	Residual ammonium (mg L^{-1})[a]	Residual citrate (mg L^{-1})[a]
100% Decanoate	1.1 ± 0.1	10 ± 0.1	25 ± 7	12 ± 2
50% Decanoate + 50% PhVA	0.8 ± 0.1	13 ± 0.0	51 ± 2	11 ± 1
75% Decanoate + 25% PhVA	1.2 ± 0.4	12 ± 0.3	41 ± 7	12 ± 2
100% PhVA	0.8 ± 0.1	8 ± 0.3	53 ± 2	12 ± 2

[a] *The indicated standard deviation is based on multiple measurements (n = 3).*

TABLE 5 | Calculated conversion yield of PHA-monomer from fatty acid for the homopolymer production based on Equation (1).

Substrates	Polymer	$y_{PHA-M/FA}$ [mol mol^{-1}]
5-Phenylvalerate	Poly(3-hydroxy-5-phenylvalerate)	0.25
Decanoate	Poly(3-hydroxydecanoate)	0.33

TABLE 6 | Calculated conversion yield of PHA-monomer from fatty acid for the homopolymer production based on Equation (1).

Substrates	Polymer	$y_{PHA-M/FA}$ [mol mol^{-1}]
10-Undecenoate	Poly(3-hydroxy-10-undecenoate)	0.72
Decanoate	Poly(3-hydroxydecanoate)	0.69

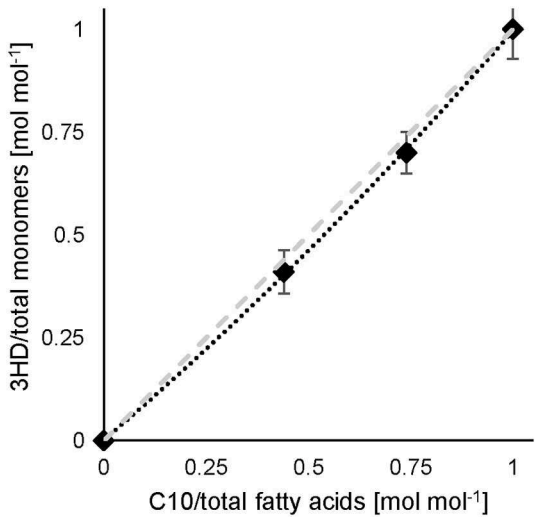

FIGURE 2 | C10 and 10-undecenoate feed and resulting monomer composition. Experimental results (♦) (data see **Table S1**), dashed line illustrates a linear correlation. Error bars indicate the standard deviation from separate composition analyses by GC ($n = 3$).

To calculate the theoretical polymer composition (Equation 5), the intracellular fatty acid ratio was calculated from Equation (4) and multiplied with the polymer from fatty acid yield.

$$\%FA_{1,uptaken} = 100 \times \frac{c_{FA1,\,feed} - c_{FA1,supernatant}}{(c_{FA1,\,feed} - c_{FA1,supernatant} + c_{FA2,\,feed} - c_{FA2,supernatant})} \quad (4)$$

$$Theoretical\ polymer\ composition = \%FA_{1,\,uptaken} \times y_{\frac{PHA-M_1}{FA_1}} \quad (5)$$

The percentile reduction of the number average molecular weight of PHA ($\overline{M_n} - reduction$) in the presence of PhVA is described by Equation (6), using the number average molecular weight obtained from GPC analysis for polymers produced either in absence or presence of PhVA ($\overline{M_n^{-PhVA}}$ and $\overline{M_n^{+PhVA}}$ respectively).

$$\overline{M_n} - reduction = 100 \times \frac{\left(\overline{M_n^{-PhVA}} - \overline{M_n^{+PhVA}}\right)}{\overline{M_n^{-PhVA}}} \quad (6)$$

The number of polymer chains per biomass produced ($N_{\|X\|}$) was calculated from Equation (7), using the total weight of polymer produced and the corresponding number average molecular weight obtained from GPC analysis. In contrast to the expression derived by Tomizawa et al. (2010), this expression for the chain number takes the different

TABLE 7 | Comparison of the theoretical polymer composition calculated from the according conversion yield of PHA-monomer from fatty acid and the experimental results.

Substrate	FA in feed (mol%)	FA, uptaken (mol%)	$y_{PHA-M/FA}$ [mol mol^{-1}]	Theoretical polymer composition (mol%)	Experimental polymer composition (mol%)[a]
10-Undecenoate	56	56	0.72	57	58 ± 7
Decanoate	44	44	0.69	43	42 ± 6
10-Undecenoate	26	26	0.72	27	29 ± 2
Decanoate	74	74	0.69	73	71 ± 5

[a] *The indicated standard deviation is based on multiple measurements (n = 3).*

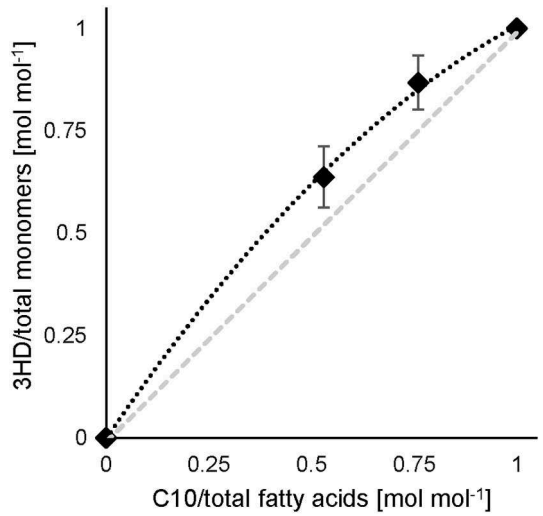

FIGURE 3 | C10 and PhVA feed and resulting monomer composition. Experimental results (♦) (data see **Table S2**), gray dashed line illustrates a linear correlation. Error bars indicate the standard deviation from separate composition analyses by GC ($n = 3$).

amounts of biomass in the cultivations into account, thus correcting changes in cell densities found in different chemostat cultivations.

$$N_{\|x\|} = \frac{c_{biomass} \times \%PHA}{\overline{M_n} \times (100 - \%PHA) \times c_{biomass}} = \frac{\%PHA}{\overline{M_n} \times (100 - \%PHA)} \quad (7)$$

The relative number of PHA chains was defined as the number of chains synthesized in the presence of PhVA divided by the number of chains generated in the absence of PhVA (Equation 8).

$$Relative\ number\ of\ PHA\ chains = \frac{N_{\|x\|}^{+PhVA}}{N_{\|x\|}^{-PhVA}} \quad (8)$$

RESULTS AND DISCUSSION

Effect of Medium Composition on Polymer Accumulation

The experimental set-up used in this study (**Figure 1**) allows screening of a multitude of parameters and conditions in a time efficient manner. The parallel set-up of the second stage is provided with identical and stable biomass feeds from the first stage, thus eliminating uncertainties introduced by batch-to-batch changes. Our experiments were designed to study two different growth conditions on the basis of N-limitation in the first (biomass accumulating) stage (R1) while providing comparable series of four different conditions for polymer accumulation in parallel bioreactors of the second stage (R2.1–R2.4) (PHA production stage). The two sets of experiments performed in this study represent one chemostat cultivation under nitrogen-limiting growth conditions during PHA accumulation from the combination of fatty acids C11:1 and C10, and another set with an increased amount of residual nitrogen in the second stage due to higher initial concentration of ammonium when the fatty acids PhVA and C10 were used. As both sets of experiments included the production of poly(3-hydroxydecanoate) (P3HD), the effect of residual nitrogen was reflected by the different polymer contents (wt%) (**Tables 3**, **4**) and different yields of polymer from fatty acid (**Tables 5**, **6**). The increased polymer yield under nitrogen limitation is in good agreement with results reported earlier (Egli, 1991; Zinn and Hany, 2005).

10-Undecenoate as Co-substrate

In the experiment of co-feeding different mixtures of C11:1 and C10, polymers were obtained representing a slightly higher molar fraction of 3-hydroxy-10-undecenoate monomer (3HUu) than the molar composition of the feed (**Figure 2**).

This correlation was described earlier for a dual nutrient (C,N) limited growth regime (DNLGR) found for chemostat cultures of *P. putida* GPo1 utilizing different feed compositions of mixtures of C8 and C11:1 (Hartmann et al., 2006). In contrast to the culture on PhVA as co-substrate, no fatty acids were detected in the supernatant during chemostat conditions with C11:1 as co-substrate (data not shown). However, the corresponding $y_{\frac{PHA-M}{FA}}$ for the two fatty acids accounts for the composition of the resulting co-polymers. The higher value for $y_{\frac{PHA-M}{FA}}$ in homopolymer accumulation from C11:1 indicates that even in this β-oxidation weakened mutant of *P. putida* the carbon flux from C10 as the fatty acid is not restricted to polymer accumulation (**Table 6**). These results are also in alignment with the calculated $y_{\frac{PHA-M}{FA}}$ and the subsequent determination of the theoretical polymer composition (**Table 7**).

TABLE 8 | Comparison of the theoretical polymer composition calculated according to Equation (5) and the experimentally determined composition from GC analysis.

Substrate	c_{FA} in feed (mol%)	c_{FA} uptaken (mol%)	$y_{PHA-M/FA}$ [mol mol^{-1}]	Theoretical polymer composition (mol%)	Experimental polymer composition (mol%)[a]
5-Phenylvalerate	47	43	0.25	36	37 ± 4
Decanoate	53	57	0.33	64	63 ± 8
5-Phenylvalerate	24	23	0.25	18	13 ± 1
Decanoate	76	77	0.33	82	87 ± 7

[a] *The indicated standard deviation is based on multiple measurements (n = 3).*

TABLE 9 | Overview of the mathematical analysis of the molecular weight reduction and the relative chain number of polymer products.

Substrate composition	Dry cell weight (g L^{-1})[a]	PHA content (wt%)[a]	PHA composition (mol%)		Molecular weight		$\overline{M_n}$ reduction (%)	Relative chain number $\frac{N_{\|x\|}^{+PhVA}}{N_{\|x\|}^{PhVA}}$
			3HPhV	3HD	$\overline{M_n}$ (g mol^{-1})	PDI		
100% Decanoate	1.1 ± 0.1	10 ± 0.1	0	100	102100	2.0	0	nA
100% 5-Phenylvalerate	0.8 ± 0.1	8 ± 0.3	100	0	50700	4.8	50	1.6
76% Decanoate + 24% 5-phenylvalerate	1.2 ± 0.4	12 ± 0.3	20	80	50000	2.7	51	2.5

[a] *The indicated standard deviation is based on multiple measurements (n = 3).*

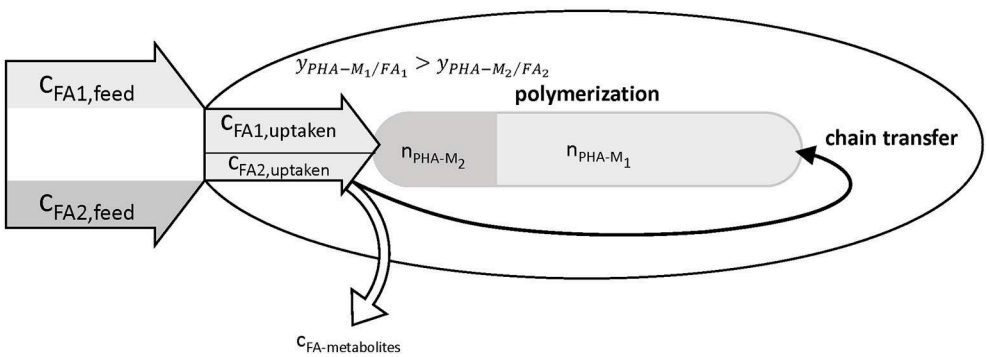

FIGURE 4 | Illustration of the observed effects of PhVA as co-substrate for the accumulation of mcl-polyhydroxyalkanoates. Reduced uptake and lower polymer from fatty acid yields lead to a reduced molar fraction of the corresponding monomer. The metabolites from the non-productive conversion of substrates are suggested to be the reason for the observed increase in chain transfer rate.

These findings fit very well to the observed production of poly(3-hydroxydecanoate-*co*-3-hydroxy-dodecanoate) co-polymers by *P. putida* KTQQ20 on dodecanoate (C12) as the sole source of fatty acids described by Liu et al. (2011), indicating residual β-oxidation activity.

5-Phenylvalerate as Co-Substrate

When co-feeding PhVA and C10 in different ratios to the second stage chemostat for PHA accumulation, the resulting polymer composition showed a non-linear correlation between their molar composition of the PHA monomers (**Figure 3**) and the molar ratio of the substrates fed to the culture. In fact, PhVA is accumulated to a lesser extent than C10. A phenomenon that has been observed as well for simultaneous accumulation of PhVA and *n*-nonanoate (C9) in batch experiments with *Pseudomonas oleovorans* by Kim et al. (1991).

In our experiment, PhVA substrate was detected in the supernatant while C10 was completely consumed. This can be directly correlated to the observed mismatch of fatty acid feed composition and monomer composition in the resulting polymer. However, the extent of differences between these two ratios is still bigger than one would expect considering only the different uptake ratios (**Table 8**). We therefore performed a flux analysis on the fatty acids in homopolymer production of P3HD and poly(3-hydroxy-5-phenylvalerate) (P3HPhV) to calculate $y_{\frac{PHA-M}{FA}}$. To eliminate the influence of the molecular weight of the monomer as well as the average molecular weight of the copolymer on the yield calculations, we expressed the conversion yield as a molar ratio (Equation 1).

The determined yields of polymer on single fatty acid show a lower value for PhVA than for C10 indicating that in addition to a lower intracellular availability of this fatty acid substrate, its utilization for polymer production is lower than the one from C10 (**Table 5**). These two major differences in substrate kinetics account for the overrepresentation of 3-hydroxydecanoate (3HD) monomers in the obtained co-polymers. For the mixture with 53 mol% of C10 the theoretical composition fits very well to the experimental results, under consideration of the different uptake as well as the different conversion yield of PHA-monomer from fatty acid (Equation 5).

For the mixture with 76 mol% of C10 the proposed model underestimates the effect observed from the experimental results (**Table 8**). The differences might be explained by a change in the polymer from fatty acid yield in the presence of a co-substrate.

Effect of 5-Phenylvalerate on the Polymerization Kinetics

Results of the analyzed $\overline{M_n}$ obtained for polymers accumulated in the chemostat cultures were 2-fold reduced for polymers containing 3-hydroxy-5-phenylvalerate (3HPhV) monomers. The molecular weight distribution (PDI) increased with an increasing amount of PhVA in the substrate feed. The obtained $\overline{M_n}$ are in good agreement with the results of Kim et al. (1991). Furthermore, in our experiments the amount of polymer accumulated per biomass was independent from the composition of fatty acid substrates (**Table 9**). While a change in propagation rate would lead to different amounts of polymer per gram of biomass, a higher chain transfer rate of the growing polymer chains for cultures accumulating on PhVA would explain this observation. A mathematical analysis of changes in PHA molecular weight and chain number was performed in analogy to the method proposed by Tomizawa et al. (2010) based on Equations (7) and (8).

The results summarized in **Table 9** show values for the relative chain number bigger than one, hence indicating an increased chain transfer rate. In fact, the supernatant of cultures with PhVA contained increased amounts of byproducts linked to PhVA metabolism, which could explain the lower polymer yield from PhVA (**Table S3**). We consider these metabolites to play an important role on the chain transfer in PHA polymerization (**Figure 4**) resulting in a polymer with reduced molecular weight. Chain transfer reactions in PHA biosynthesis have been extensively studied for short-chain-length PHA. Addition of exogenous chain transfer agents, mostly alcoholic compounds, in bacterial cultures causes large reduction in PHA molecular weight (Tsuge et al., 2013). Ethanol, on the other hand, has been addressed as a natural chain transfer agent in PHA producing bacteria (Hyakutake et al., 2014).

CONCLUSION

Our results show that the presence of PhVA leads to an increased chain transfer rate during polymerization of mcl-PHA by *P. putida* KTQQ20. We have found that the two-stage chemostat is a versatile platform with a high degree of control over important process parameters giving new insights into the mechanism of PHA biosynthesis with reduced molecular weights. Our future work will be dedicated to investigate the role of PhVA in the increased chain transfer rate together with its lower conversion yield by identifying its metabolic fate.

DATA AVAILABILITY STATEMENT

The raw data supporting the conclusions of this manuscript will be made available by the authors, without undue reservation, to any qualified researcher.

AUTHOR CONTRIBUTIONS

NH, CU, and MZ contributed conception and design of the study. NH, CU, and SA organized the database. NH wrote the first draft of the manuscript. NH, CU, and MZ wrote sections of the manuscript. All authors contributed to manuscript revision, read and approved the submitted version.

FUNDING

This work was supported by the program Innovation in Biocatalysis: A toolbox for sustainable bio-based production in the frame of the project based contributions (State Secretariat for Education, Research and Innovation SERI, Switzerland), and by HES-SO Valais-Wallis (Program MOVE).

ACKNOWLEDGMENTS

We thank Julien Pott for the technical support at the Biotech Pilot Plant (HES-SO Valais-Wallis). Pascal Jaqcquemettaz for the assistance on HPLC and GC analyses (Analytical Chemistry Laboratory, HES-SO Valais-Wallis). Moreover, Thierry Udrisard (HES-SO Valais-Wallis) for the support on GPC analysis. Special thanks to Professor G.Q. Chen (Tsinghua University, China) for kindly providing *P. putida* KTQQ20.

SUPPLEMENTARY MATERIAL

The Supplementary Material for this article can be found online at: https://www.frontiersin.org/articles/10.3389/fbioe.2019.00301/full#supplementary-material

REFERENCES

Arikawa, H., Sato, S., Fujiki, T., and Matsumoto, K. (2016). A study on the relation between poly(3-hydroxybutyrate) depolymerases or oligomer hydrolases and molecular weight of polyhydroxyalkanoates accumulating in *Cupriavidus necator* H16. *J. Biotechnol.* 227, 94–102. doi: 10.1016/j.jbiotec.2016.04.004

Atlic, A., Koller, M., Scherzer, D., Kutschera, C., Grillo-Fernandes, E., Horvat, P., et al. (2011). Continuous production of poly([R]-3-hydroxybutyrate) by *Cupriavidus necator* in a multistage bioreactor cascade. *Appl. Microbiol. Biotechnol.* 91, 295–304. doi: 10.1007/s00253-011-3260-0

Boesel, L. F., Le Meur, S., Thöny-Meyer, L., and Ren, Q. (2014). The effect of molecular weight on the material properties of biosynthesized

poly(4-hydroxybutyrate). *Int. J. Biol. Macromol.* 71, 124–130. doi: 10.1016/j.ijbiomac.2014.04.015

Egli, T. (1991). On multiple-nutrient-limited growth of microorganisms, with special reference to dual limitation by carbon and nitrogen substrates. *Antonie Van Leeuwenhoek* 60, 225–234. doi: 10.1007/BF00430367

Egli, T., and Zinn, M. (2003). The concept of multiple-nutrient-limited growth of microorganisms and its application in biotechnological processes. *Biotechnol. Adv.* 22, 35–43. doi: 10.1016/j.biotechadv.2003.08.006

Follonier, S., Panke, S., and Zinn, M. (2011). A reduction in growth rate of *Pseudomonas putida* KT2442 counteracts productivity advances in medium-chain-length polyhydroxyalkanoate production from gluconate. *Microb. Cell Fact.* 10:25. doi: 10.1186/1475-2859-10-25

Furrer, P., Hany, R., Rentsch, D., Grubelnik, A., Ruth, K., Panke, S., et al. (2007). Quantitative analysis of bacterial medium-chain-length poly([*R*]-3-hydroxyalkanoates) by gas chromatography. *J. Chromatogr. A* 1143, 199–206. doi: 10.1016/j.chroma.2007.01.002

Hany, R., Hartmann, R., Bohlen, C., Brandenberger, S., Kawada, J., Lowe, C., et al. (2005). Chemical synthesis and characterization of POSS-functionalized poly [3-hydroxyalkanoates]. *Polymer* 46, 5025–5031. doi: 10.1016/j.polymer.2005.04.020

Hartmann, R., Hany, R., Geiger, T., Egli, T., Witholt, B., and Zinn, M. (2004). Tailored biosynthesis of olefinic medium-chain-length poly [(*R*)-3-hydroxyalkanoates] in *Pseudomonas putida* GPo1 with improved thermal properties. *Macromolecules* 37, 6780–6785. doi: 10.1021/ma040035+

Hartmann, R., Hany, R., Pletscher, E., Ritter, A., Witholt, B., and Zinn, M. (2006). Tailor-made olefinic medium-chain-length poly[(*R*)-3-hydroxyalkanoates] by P*seudomonas putida* GPo1: batch versus chemostat production. *Biotechnol. Bioeng.* 93, 737–746. doi: 10.1002/bit.20756

Huisman, G. W., Deleeuw, O., Eggink, G., and Witholt, B. (1989). Synthesis of poly-3-hydroxyalkanoates is a common feature of fluorescent Pseudomonads. *Appl. Environ. Microbiol.* 55, 1949–1954.

Huong, K. H., Azuraini, M. J., Aziz, N. A., and Amirul, A. A. (2017). Pilot scale production of poly(3-hydroxybutyrate-co-4-hydroxybutyrate) biopolymers with high molecular weight and elastomeric properties. *J. Biosci. Bioeng.* 124, 76–83. doi: 10.1016/j.jbiosc.2017.02.003

Hyakutake, M., Tomizawa, S., Mizuno, K., Abe, H., and Tsuge, T. (2014). Alcoholytic cleavage of polyhydroxyalkanoate chains by class IV synthases induced by endogenous and exogenous ethanol. *Appl. Environ. Microbiol.* 80, 1421–1429. doi: 10.1128/AEM.03576-13

Kawaguchi, Y., and Doi, Y. (1992). Kinetics and mechanism of synthesis and degradation of poly(3-hydroxybutyrate) in *Alcaligenes eutrophus*. *Macromolecules* 25, 2324–2329. doi: 10.1021/ma00035a007

Kim, Y. B., Kim, D. Y., and Rhee, Y. H. (1999). PHAs produced by *Pseudomonas putida* and *Pseudomonas oleovorans* grown with n-alkanoic acids containing aromatic groups. *Macromolecules* 32, 6058–6064. doi: 10.1021/ma982033t

Kim, Y. B., Lenz, R. W., and Fuller, R. C. (1991). Preparation and characterization of poly(β-hydroxyalkanoates) obtained from *Pseudomonas oleovorans* grown with mixtures of 5-phenylvaleric acid and *n*-alkanoic acids. *Macromolecules* 24, 5256–5260. doi: 10.1021/ma00019a004

Levine, A. C., Heberlig, G. W., and Nomura, C. T. (2016). Use of thiol-ene click chemistry to modify mechanical and thermal properties of polyhydroxyalkanoates (PHAs). *Int. J. Biol. Macromol.* 83, 358–365. doi: 10.1016/j.ijbiomac.2015.11.048

Liu, Q., Luo, G., Zhou, X. R., and Chen, G. Q. (2011). Biosynthesis of poly(3-hydroxydecanoate) and 3-hydroxydodecanoate dominating polyhydroxyalkanoates by β-oxidation pathway inhibited *Pseudomonas putida*. *Metab. Eng.* 13, 11–17. doi: 10.1016/j.ymben.2010.10.004

Ouyang, S. P., Liu, Q., Fang, L., and Chen, G. Q. (2007). Construction of pha-operon-defined knockout mutants of *Pseudomonas putida* KT2442 and their applications in poly(hydroxyalkanoate) production. *Macromol. Biosci.* 7, 227–233. doi: 10.1002/mabi.200600187

Poblete-Castro, I., Escapa, I. F., Jager, C., Puchalka, J., Lam, C. M., Schomburg, D., et al. (2012). The metabolic response of *P. putida* KT2442 producing high levels of polyhydroxyalkanoate under single- and multiple-nutrient-limited growth: highlights from a multi-level omics approach. *Microb. Cell Fact.* 11:34. doi: 10.1186/1475-2859-11-34

Prieto, A., Escapa, I. F., Martinez, V., Dinjaski, N., Herencias, C., de la Pena, F., et al. (2016). A holistic view of polyhydroxyalkanoate metabolism in *Pseudomonas putida*. *Environ. Microbiol.* 18, 341–357. doi: 10.1111/1462-2920.12760

Tomizawa, S., Saito, Y., Hyakutake, M., Nakamura, Y., Abe, H., and Tsuge, T. (2010). Chain transfer reaction catalyzed by various polyhydroxyalkanoate synthases with poly(ethylene glycol) as an exogenous chain transfer agent. *Appl. Microbiol. Biotechnol.* 87, 1427–1435. doi: 10.1007/s00253-010-2601-8

Tortajada, M., da Silva, L. F., and Prieto, M. A. (2013). Second-generation functionalized medium-chain-length polyhydroxyalkanoates: the gateway to high-value bioplastic applications. *Int. Microbiol.* 16, 1–15. doi: 10.2436/20.1501.01.175

Tripathi, L., Wu, L. P., Dechuan, M., Chen, J., Wu, Q., and Chen, G. Q. (2013). *Pseudomonas putida* KT2442 as a platform for the biosynthesis of polyhydroxyalkanoates with adjustable monomer contents and compositions. *Bioresour. Technol.* 142, 225–231. doi: 10.1016/j.biortech.2013.05.027

Tsuge, T., Ko, T., Tago, M., and Abe, H. (2013). Effect of glycerol and its analogs on polyhydroxyalkanoate biosynthesis by recombinant *Ralstonia eutropha*: a quantitative structure-activity relationship study of chain transfer agents. *Polymer Degrad. Stab.* 98, 1586–1590. doi: 10.1016/j.polymdegradstab.2013.06.026

Ward, P. G., Goff, M., Donner, M., Kaminsky, W., and O'Connor, K. E. (2006). A two step chemo-biotechnological conversion of polystyreneto a biodegradable thermoplastic. *Environ. Sci. Technol.* 40, 2433–2437. doi: 10.1021/es05 17668

Zinn, M., and Hany, R. (2005). Tailored material properties of polyhydroxyalkanoates through biosynthesis and chemical modification. *Adv. Eng. Mater.* 7, 408–411. doi: 10.1002/adem.200500053

Conflict of Interest: The authors declare that the research was conducted in the absence of any commercial or financial relationships that could be construed as a potential conflict of interest.

frontiers in Bioengineering and Biotechnology

REVIEW
published: 20 November 2019
doi: 10.3389/fbioe.2019.00328

The Rocky Road From Fed-Batch to Continuous Processing With *E. coli*

Julian Kopp[1], *Christoph Slouka*[2], *Oliver Spadiut*[2] *and Christoph Herwig*[1,2]*

[1] Christian Doppler Laboratory for Mechanistic and Physiological Methods for Improved Bioprocesses, Vienna, Austria,
[2] Research Area Biochemical Engineering, Institute of Chemical Engineering, Vienna, Austria

Escherichia coli still serves as a beloved workhorse for the production of many biopharmaceuticals as it fulfills essential criteria, such as having fast doubling times, exhibiting a low risk of contamination, and being easy to upscale. Most industrial processes in *E. coli* are carried out in fed-batch mode. However, recent trends show that the biotech industry is moving toward time-independent processing, trying to improve the space–time yield, and especially targeting constant quality attributes. In the 1950s, the term "chemostat" was introduced for the first time by Novick and Szilard, who followed up on the previous work performed by Monod. Chemostat processing resulted in a major hype 10 years after its official introduction. However, enthusiasm decreased as experiments suffered from genetic instabilities and physiology issues. Major improvements in strain engineering and the usage of tunable promotor systems facilitated chemostat processes. In addition, critical process parameters have been identified, and the effects they have on diverse quality attributes are understood in much more depth, thereby easing process control. By pooling the knowledge gained throughout the recent years, new applications, such as parallelization, cascade processing, and population controls, are applied nowadays. However, to control the highly heterogeneous cultivation broth to achieve stable productivity throughout long-term cultivations is still tricky. Within this review, we discuss the current state of *E. coli* fed-batch process understanding and its tech transfer potential within continuous processing. Furthermore, the achievements in the continuous upstream applications of *E. coli* and the continuous downstream processing of intracellular proteins will be discussed.

Keywords: *E. coli*, continuous processing, process understanding, burden reduction, from batch to continuous manufacturing

OPEN ACCESS

Edited by:
Pau Ferrer, Autonomous University of Barcelona, Spain

Reviewed by:
Frank Delvigne, University of Liège, Belgium
Peter Neubauer, Technische Universität Berlin, Germany

***Correspondence:**
Christoph Herwig
christoph.herwig@tuwien.ac.at

Specialty section:
This article was submitted to Bioprocess Engineering, a section of the journal Frontiers in Bioengineering and Biotechnology

Received: *29 August 2019*
Accepted: *28 October 2019*
Published: *20 November 2019*

Citation:
Kopp J, Slouka C, Spadiut O and Herwig C (2019) The Rocky Road From Fed-Batch to Continuous Processing With E. coli. Front. Bioeng. Biotechnol. 7:328. doi: 10.3389/fbioe.2019.00328

INTRODUCTION

Using equipment at maximum capacity in long-term, quasi-perpetual processes is the dream of any industrial application in biotechnology (Plumb, 2005; Burcham et al., 2018). Many parts of the chemical industry (especially the petrochemical one) are already producing at a continuous level (Glaser, 2015). Continuous production in white biotechnology is also already implemented (Scholten et al., 2009; Kralisch et al., 2010; Luttmann et al., 2015); it is no huge surprise, therefore, that the red biopharmaceutical industry is trying to move toward "continuous processing" (Plumb, 2005; Gutmann et al., 2015; Burcham et al., 2018). Even though biopharmaceutical production is generally still carried out batch-wise, new technology has emerged (Walsh, 2014, 2018), and many drugs can currently be sold at the cheapest prices ever (Berlec and Strukelj, 2013; Jungbauer, 2013; Walsh, 2018). Continuous systems are already partially implemented in red biotechnology. Until

now, however, these processes have only been carried out with mammalian cells (Vogel et al., 2012; Karst et al., 2017; Steinebach et al., 2017; Burgstaller et al., 2018). By switching from a batch-wise to a continuous production system, cultivations can be improved, which affects the duration of the run and thereby reduces the frequency of required setup and cleaning times. Furthermore, by switching to continuous processing, small footprint facilities can be implemented, leading to an increase in the overall space–time yield (Seifert et al., 2012; Bieringer et al., 2013; Lee et al., 2015; Adamo et al., 2016).

Looking at the technical realization of a continuous process, the upstream is regarded as rather simple. Chemostat processing, developed back in the 1950s (Novick and Szilard, 1950a), is well-known. Stable process parameters can be adjusted, and the bleed containing the desired amount of product can be subtracted from the culture vessels and further processed. However, the implementation of the downstream is highly dependent on the location of the product (Jungbauer, 2013; Slouka et al., 2018b). Fusing purification steps into an overall non-stop process seemed unlikely to be achieved a couple of years ago (Rathore, 2015; Vemula et al., 2015; Kante et al., 2018, 2019; VKR et al., 2019). Continuous chromatography in particular created a bottleneck; however, simulated moving bed chromatography (SMBC) improved significantly in terms of performance (Ötes et al., 2017, 2018). With state of the art technology, we are able to process proteins independent of location and at a continuous level (Jungbauer, 2013; Saraswat et al., 2013; Wellhoefer et al., 2013, 2014), and we are able to unite all process unit operations into one overall process (Lee et al., 2015; Zydney, 2015; Burcham et al., 2018).

With emerging process technology, the regulatory authorities evolved as well, and Food and Drug Administration (= FDA) regulations for the release of a product are clearly set (Gassman et al., 2017). Batch-wise production made it rather easy to break down product streams into certain product pools as upstream and downstream applications could be clearly separated and approved by the quality control (Lee et al., 2015). To enable continuous processing from a regulatory point of view, the process has to be separated into different lot numbers, creating a batch-wise system in itself (Jungbauer, 2013) to fulfill acceptance criteria by regulatory authorities (Gassman et al., 2017). As an integrated continuous process can achieve time-independent constant critical quality attributes (=CQAs) (Herwig et al., 2015; Zydney, 2015), the realization of such a process might even shorten the time-to-market. The first product derived from continuous production after its approval was produced in 2015, namely Orkambi (Matsunami et al., 2018). Prezista, being produced at a continuous level by Jansen, was accepted by the FDA in 2016 (Nasr et al., 2017). Ever since first approvals for continuously produced products emerged (Yang et al., 2017; Balogh et al., 2018), companies have tended to invest more into production lines so as to be capable of producing at a continuous level.

Still, the use of bacteria and yeast in continuous production modes is not common and has only been implemented once on an industrial scale for insulin production in *Saccharomyces cerevisiae* back in the 90s (Diers et al., 1991). State of the art recombinant protein production (RPP) in *E. coli* is still carried out in a fed-batch mode, and, with ongoing technology development, very high product titers can be achieved (Kopp et al., 2017; Wurm et al., 2017a; Hausjell et al., 2018; Slouka et al., 2018a). Still, "low-cost" biopharmaceuticals produced in bacteria are expensive to produce (Jia and Jeon, 2016); one gram of IPTG (Isopropyl-β-D-thiogalactopyranosid, currently purchased from Sigma-Aldrich for 76.8 €), is more expensive than one gram of 900 carat gold (currently worth 37.13 €). Therefore, a continuous production model for *E. coli* would be highly beneficial, increasing the overall space–time yield (Seifert et al., 2012; Bieringer et al., 2013). Counter-intuitively, the upstream section, which is technically easy to realize, thwarts industry plans as chemostat cultivations producing recombinant proteins within microbial hosts lack major instabilities (Diers et al., 1991); shifts in the transcriptome and proteome leads to enhanced acetate production, which seems to disturb RPP and decrease the overall specific productivity (q_p) as a consequence (Peebo et al., 2015; Peebo and Neubauer, 2018). As *E. coli* still is a beloved workhorse for industry as well as for research (Rosano et al., 2019), we, within this review, highlight recent achievements in fed-batch processing and the first steps that have been implemented for the ongoing transition toward a continuous recombinant production system.

Additionally, the first achievements in the continuous upstream applications of *E. coli*; and the continuous downstream processing of intracellular proteins are discussed.

THE CURRENT STATE OF *E. COLI* FED-BATCH PROCESS UNDERSTANDING AND ITS TECH TRANSFER POTENTIAL WITHIN CONTINUOUS PROCESSING

Process parameters and their effects on critical quality attributes are well-understood in *E. coli* fed-batch cultivations (Ferrer-Miralles et al., 2009; Babaeipour et al., 2015; Gupta and Shukla, 2017; Hausjell et al., 2018; Kante et al., 2018); they lead to high titers and predictable manufacturing (Slouka et al., 2018a,b). Still, RPP causes stress phenomena in the host cells, leading to decreased host capacity and, consequently, decreased growth rates (Rozkov et al., 2004; Silva et al., 2012; Ceroni et al., 2015; Kopp et al., 2017). Many recent publications revealed that RPP in *E. coli* suffers from a metabolic burden. Therefore, within this section we discuss the effects of metabolic burden on RPP and the determination thereof; intracellular vs. extracellular RPP; and enablers for continuous processing.

Recombinant Protein Production in *E. coli* and Its Effect on Metabolic Burden

Metabolic Burden and Its Effects on Growth Rate

Recombinant protein production (RPP) has always been referred to as exhibiting a high metabolic burden onto the host cells (Heyland et al., 2011; Silva et al., 2012; Ceroni et al., 2015; Dvorak et al., 2015). Effects such as a decrease in the specific growth rate (= μ) and the specific substrate uptake rate (= q_s) over cultivation time have been observed (Scott

et al., 2010; Shachrai et al., 2010; Reichelt et al., 2017a,b). As higher amounts of intracellular proteins can be produced by applying higher feeding rates (Boström et al., 2005; Ukkonen et al., 2013; Peebo et al., 2015), the proteome might change throughout the cultivation and show decreased sugar uptake rates (Borirak et al., 2015; Peebo et al., 2015). Intracellular stress might therefore lead to decreased enzyme activity, such as a reduced activity in the phosphotransferase system, which is primarily responsible for sugar uptake (Deutscher et al., 2006). Neubauer et al. established a model where cellular capacities are limited as an effect of heterologous gene expression (Neubauer et al., 2003). As intracellular proteins are measured also within dry cell weight quantification it is important to separate the cell into a "functional cell part" (showing metabolic activity) and a "recombinant part" (being unable to show metabolic activity). Decreased enzyme availability might lead to high sugar accumulation in the fermentation broth, especially when exponential feeding is applied (Slouka et al., 2018a), as already stressed cells might additionally suffer from osmotic stress, triggering cell death (Slouka et al., 2019). It is shown that high sugar uptake rates tend to shift toward acetate formation, finally leading to decreased levels of production (Fragoso-Jiménez et al., 2019). Therefore, appropriate feeding rates beneath μ_{max} should be set to avoid overflow metabolism; however, acetate production can also be significantly reduced using engineered strains, as shown by Lara et al. (2008), Valgepea et al. (2010), Peebo et al. (2015), and Anane et al. (2017). Higher overall titers within *Pichia pastoris* are achieved when switching from static q_s-based controls to a dynamic feeding strategy (Spadiut et al., 2014c). Feeding strategies using a static q_s control within *E. coli* might therefore need to be adapted.

Metabolic Burden and Its Correlation With IPTG

Declines in growth rates can be linearly correlated to the amount of recombinant protein produced (Scott et al., 2010). However, studies using IPTG as inducer have to take into account that this μ-decrease might result from the inducer itself, as IPTG is known to exhibit toxicity in host cells at long cultivation times (Dvorak et al., 2015). Malakar et al. showed that the growth rate declines in relation to higher amounts of IPTG used, which leads to higher recombinant protein translation rates (Malakar and Venkatesh, 2012). Transcriptomic results derived from fed-batch metabolism hint that essential genes needed for RPP are sequentially turned down when host cells are induced with IPTG, indicating that the metabolism switches toward a stationary phase (Haddadin and Harcum, 2005). As IPTG seems to be causing a high metabolic burden, it might not be a feasible inducer for long-term production.

How to Determine the Metabolic Burden

Operating at high specific feeding rates, such as q_s of 0.4–0.5 g/g/h, during the induction phase shows a trend of decreasing uptake "capacity," which results in high extracellular sugar accumulation and increased cell death (Kopp et al., 2018; Slouka et al., 2019). Ceroni et al. aim to determine the metabolic load using a GFP (green fluorescent protein) cassette as an integrated marker protein to determine the "capacity" of cells (Ceroni et al., 2015). The capacity measurements of the cells match the theory established by Scott et al. even though the overlapping emission of GFP and m-cherry, used within this study, has to be taken into account more thoroughly (Scott et al., 2010; Ceroni et al., 2015). As metabolic burden is known to cause limitations in RPP (Heyland et al., 2011), the burden control system, also established by Ceroni et al. in a follow-up study, could soon be implemented in industry. The results thus indicate that *in-vivo* controlled cells exhibited higher capacity and showed better process performance than common, unregulated cells (Ceroni et al., 2018). As heat-shock promoters were significantly upregulated during recombinant protein expression, RPP is controlled *in vivo* using these promoters for capacity measurement. A dcas9 feedback control is used to adapt the protein expression due to the measured capacity. Application of burden–control systems in continuous cultivations, as demonstrated in **Figure 1**, would be an interesting approach to maintaining cells in a "stable capacity." Furthermore, as GFP is used as a capacity marker within this system, at-line, and even online process controls using plate readers or flow cytometry could be established for this regulated strain.

Intracellular vs. Extracellular Expression for *E. coli*

High metabolic burden is also often associated with the accumulation of intracellular proteins as the chaperones become overloaded and inclusion body formation can be observed (Fahnert et al., 2004; Ramón et al., 2014). As misfolded intracellular proteins are also known to suffer from long purification times and occasionally low refolding yields (Jungbauer and Kaar, 2007; Singh et al., 2015; Slouka et al., 2018b), the production of soluble extracellular proteins might be a feasible approach. Protein secretion, commonly performed in eukaryotic cells, might also be a key solution to reducing the metabolic burden; however, recombinant protein secretion is not easy to establish in bacteria (Berlec and Strukelj, 2013; Rosano and Ceccarelli, 2014). Still, RPP in the periplasm of *E. coli* has shown to yield promising results, especially when producing antibody fragments, making use of the oxidizing environment (Spadiut et al., 2014a; Kasli et al., 2019). To enable protein secretion in *E. coli*, engineering of the Sec-Pathway is commonly performed, leading to unfolded protein secretion (Mergulhão et al., 2005; Burdette et al., 2018). Alternatively, the SRP pathway can be used to secrete unfolded hydrophobic amino acid sequences while the twin-arginine pathway can be used to secrete folded proteins to the outer membrane (Berlec and Strukelj, 2013). As the amount of recombinant protein can be as high as 50% of the complete protein content of the cell, the RPP therefore sometimes might be limited by the secretion system itself (Rosano and Ceccarelli, 2014). Even though it is challenging to achieve extracellular RPP in *E. coli*, the company WACKER engineered a secretion system, called ESETEC, which has been upgraded to ESETEC 2 and is able to achieve high extracellular titers (Richter and Koebsch, 2017). Morra et al. investigated the phenomena of "non-classical protein secretion," where cytoplasmic proteins can be secreted

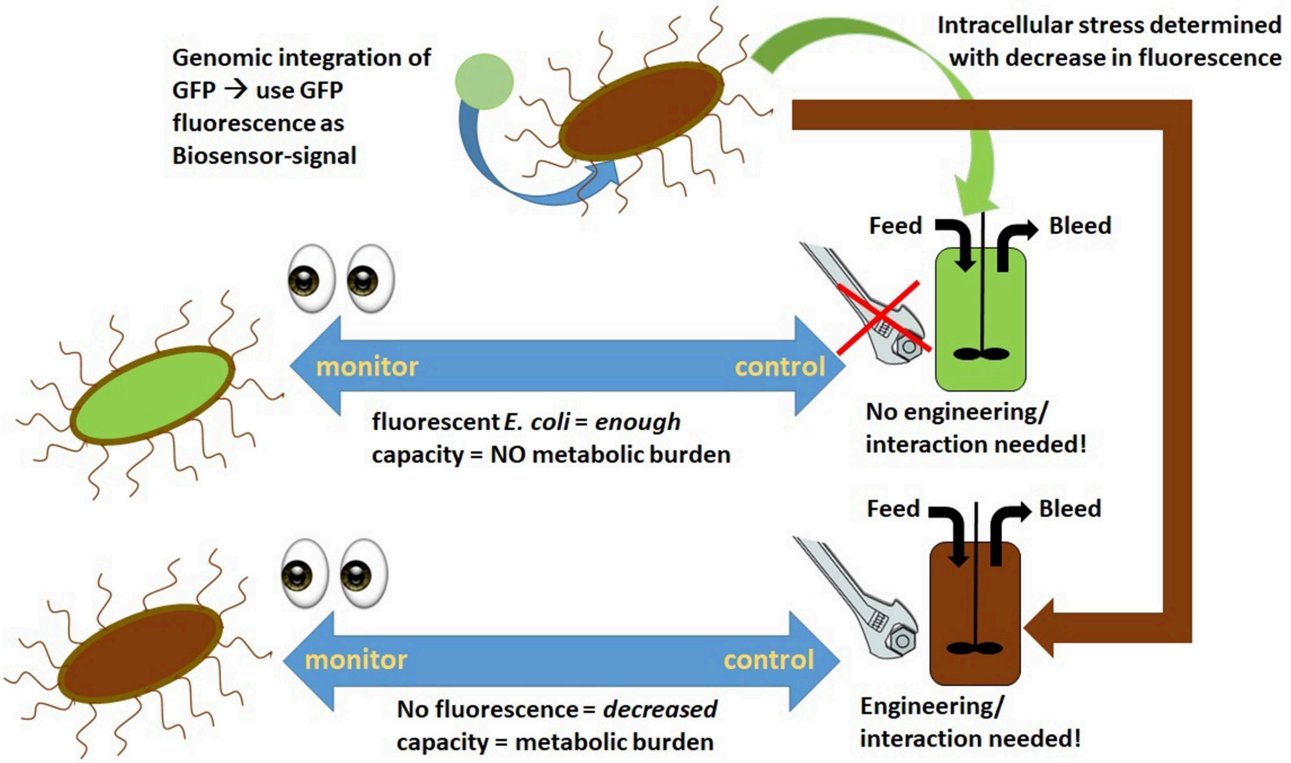

FIGURE 1 | Stress determined via fluorescence measurement application as an on-line tool during chemostat cultivation to determine metabolic burden and, if necessary, intervene.

into the supernatant via mechanosensitive channels, triggering secretion via stress (Morra et al., 2018). Other studies, using triton, sucrose or glycine to secrete product into the supernatant, indicate a promising process strategy for fed-batch cultivations, releasing product into the fermentation broth before harvest and thereby reducing the purification time (Bao et al., 2016; Na et al., 2019). To implement a long-term process, constant, stress-free protein secretion is desired. Previous tests of recombinant protein secretion in chemostat experiments (operated at D=0.1 h^{-1}) show the feasibility of the study; however, the extracellular protein concentration dropped significantly over the period of cultivation (Selvamani, 2014). Although soluble protein production would be promising, it was shown that achieved titers were so far still within non-feasible ranges (mg/L to low g/L range), independent of the cultivation system (Mergulhão et al., 2005; Kleiner-Grote et al., 2018). Still we would like to hypothesize, with ongoing host engineering, that extracellular protein production within *E. coli* might be an interesting approach for the future.

Enablers for Continuous Processing With *E. coli*

Process Controls in Fed Batch With Tech Transfer Possibility to Continuous Processing

Even though intracellular shifts might be noticeable (due to high metabolic burden put on the cells by RPP) the CQAs of the recombinant product have to be maintained constantly throughout the process (Rathore, 2009). We defined CQAs for an *E. coli* inclusion body fed-batch process, investigating IB (inclusion body) size, purity, and titer (Slouka et al., 2018a). Lower temperatures throughout the induction phase seemed to be favorable for RPP throughout this and other studies (Wurm et al., 2017a; Slouka et al., 2018a). This might be due to the high amount of energy needed to produce recombinant proteins. Host cells might shift intracellular fluxes toward toxic pathways in order to regenerate reducing equivalents and further cope with the energy demand needed. A reduction of cell densities, temperature, or separation of biomass growth and RPP might facilitate stability in continuous processes (Rugbjerg and Sommer, 2019). Enabling higher sugar uptake with engineered strains shows that specific productivity and specific sugar uptake rates were correlated in a bell-shaped curve; extreme sugar uptake rates lead to fermentative growth (Basan et al., 2015; Peebo et al., 2015; Basan, 2018; Fragoso-Jiménez et al., 2019). The metabolic load therefore has to be considered, and feeding strategies and model-based approaches that consider the shifts in the growth rate have to be established (Kopp et al., 2018). Schaepe et al. implemented a feeding strategy where the fed carbon is adapted to the control of the online monitored oxygen consumption rate (OUR) in order to avoid overfeeding (Schaepe et al., 2014). As cells exhibiting a high burden tend to shift toward acetate formation (Martínez-Gómez et al., 2012; Schaepe et al., 2014), it might be interesting to control onto pre-established online capacity measurements throughout long-term cultivations (Ceroni et al., 2015).

Promotor Systems Applied in Fed-Batch and Its Tech Transfer Potential Within Continuous Processing

The most frequently used system for RPP used in *E. coli* is still the Bl21(DE3) strain in combination with pET plasmids, which make use of the strong T7 promotor under the control of the lac promotor and its repressor (Studier et al., 1990; Rosano et al., 2019). Even though BL21 (DE3) is considered the state-of-the-art strain for RPP in *E. coli*, homologous recombination rates might occur, especially throughout long-running fermentations (Rugbjerg and Sommer, 2019). Therefore, other strains that experience a *recA* deletion, such as HMS-174, might be a good alternative to promote long-term stability, especially as high product titers have been considered to use this strain (Hausjell et al., 2018). Using the T7-induction system, induction can be performed with a simple inducer pulse as IPTG binds to the lactose repressor (Malakar and Venkatesh, 2012; Marbach and Bettenbrock, 2012). For standard fed-batch approaches this system works fine as high titers can be achieved within short time (Slouka et al., 2019); however, full induction of the T7-polymerase using IPTG puts a high metabolic burden on the host cells (Dvorak et al., 2015). The ptac promotor in combination with IPTG and lactose as an inducer allows the interesting approach of tunable protein expression, resulting in a lower metabolic burden put onto host cells (Marschall et al., 2016). A rather new approach, also making use of the T7-polymerase, is a double induction system, which shuts down the *E. coli* RNA-polymerase, inhibiting host mRNA production (Lemmerer et al., 2019). Therefore, the total energy flux derived from fed carbon could be used for RPP. Regulating this system in a tunable way, with a switch-on/switch-off strategy might be an interesting approach for chemostat experiments. A further method to separate rapid growth from RPP might be the utilization of stress-regulated promoters. Making use of phosphate limitation (phoA-promoter), cAMP/CRP-system regulations (cap promoter with MglD-Repressor), and other promotor systems could enhance a more resistant subpopulation in chemostat cultivations, producing at a low but steady level (Neubauer and Winter, 2001). Further positive regulation systems, also being referred to as tunable, are the araBAD and the rhamBAD induction systems, which are induced by arabinose and rhamnose, respectively (Khlebnikov et al., 2002; Wegerer et al., 2008). Tunable protein expression systems, discussed in detail by Marschall et al. (2016), allow for the control of expression rates and should therefore ease control strategies for continuous processes. However, the major advantage of *E. coli* is still its relatively cheap production, and the utilization of highly expensive inducers in a continuous production scale might not be feasible as media costs would rise drastically. When comparing costs of "tunable" inducers in *E. coli* with the methanol inducible AOX system of *P. pastoris*, it is obvious that a less expensive induction system needs to be found (Mattanovich et al., 2012; Spadiut et al., 2014b). Lactose, also referred to as being be a tunable inducer (Neubauer et al., 1992; Neubauer and Hofmann, 1994), has been shown to boost soluble intracellular protein concentrations in *E. coli* fed-batches so far (Wurm et al., 2016, 2017c). For white biotechnology approaches, lactose could be purchased cheaply as side products of the milk and cheese industry (Viitanen et al., 2003). The implementation of lactose as an inducer in continuous cultivations could therefore lead to interesting and affordable approaches.

Engineering on a Genomic Level and Its Tech Transfer Potential Within Continuous Processing

Plasmid technology is still state of the art for RPP in *E. coli* (Rosano et al., 2019). Selection is commonly employed using antibiotics, though a drug substance (=DS) produced in *E. coli* needs to be free from antibiotics (Silva et al., 2012). As high copy number plasmids, frequently used in industry, put a high metabolic burden onto the host, the regime of plasmid-based systems might slowly fade out (Fink et al., 2019). The production load here is usually used to trigger an escape rate, leading to diverse subpopulations within the cultivation system (Rugbjerg et al., 2018). Non-productive subpopulations might arise from diverse point mutations or reallocations, emerging at an escape rate as high as 10^{-5}-10^{-8} per generation in plasmid-based *E. coli* systems (Rugbjerg and Sommer, 2019). As high burden might also lead to high amounts of recombineering, the genomic integration of the gene of interest (GOI) would reduce host stress as copy numbers can easily be controlled, and no antibiotic selection is required (Mairhofer et al., 2013). Introducing the GOI into the host can be performed by CRISPR-Cas9 strategies or via a recombineering method (Reisch and Prather, 2015). While CRISPR-Cas9 selection functions via a double-strand cleavage, recombineering needs antibiotics resistance to select the GOI. This antibiotic selection, however, can be cured in an ongoing step (Biswas et al., 2012; Chung et al., 2017; Reisch and Prather, 2017). Striedner et al. performed chemostat cultivations with *E. coli* cells, producing GFP, where the gene was integrated into the genome (using the recombineering method). However, production was not stable for 10 generation times (Striedner et al., 2010). Within a recent study it was shown that the location is highly dependent on the expression of the GOI (Englaender et al., 2017), which probably explains the difficulties in stability. In a different study, the integration of large DNA-fragments, like complete pathways, was performed. This is sometimes difficult to reproduce within different strains (Chung et al., 2017; Englaender et al., 2017). On the other hand, Wang et al. showed that genomic engineering of the complete mevalonate pathway exceeded plasmid-based mevalonate production (Wang et al., 2016).

An interesting approach was performed by Rovner et al. who engineered a codon-optimized *E. coli*, creating auxothrophy for phenylalanine-derived amino acids (Rovner et al., 2015). Coupling the expression of essential genes to synthetic amino acids, no escape rate could be monitored within 20 days of cultivation. Even though the selection criteria of synthetic amino acids might be much more effective than common selection systems, the amount of synthetic amino acids needed for feeding at an industrial scale might not be feasible (Stokstad, 2015). This results in the need for a selection mechanism being "cheap enough" to boost selection criteria also at large volumes. Strategies such as connecting cell growth with product formation would increase the fitness of the subpopulation needed for RPP and further enhance overall yields (Buerger et al., 2019). Furthermore, the idea of a two-way selection was shown to improve the host, as exemplarily shown for an *E. coli* naringenin

producer, which was increased by a factor of 36 (Raman et al., 2014). As negative selection does delete escaped subpopulations, positive selection can help to find high-productive mutations. The toggling selection mechanism, which regulates between positive and negative selection, could be the way to go to create strains needed for long-term stable production systems.

Trying to reduce the host's metabolic burden, the usage of protein secretion or the integration of the target sequence into the genome seem to be promising tools. Further host engineering might enable the continuous production of recombinant proteins in *E. coli* by eliminating the needs of antibiotics. However, it seems like neither industry nor academia is there yet, as a complete understanding of the interactions between the GOI and integration site is still missing and needs to be tested (Englaender et al., 2017). Strains commonly employed in continuous cultivations are screened for maximum production within short cultivation times (Jia and Jeon, 2016). Even though it is rather time consuming, it might be necessary to screen for long-term stable strains in order to find appropriate candidates for the implementation of continuous cultivations.

ACHIEVEMENTS IN CONTINUOUS UPSTREAM APPLICATIONS WITH *E. COLI*

Basing their description of bacterial growth on that which was established by Monod (Monod, 1949b), the term "chemostat" was defined by Novick and Szilard in the 1950s (Novick and Szilard, 1950a). Many physiological characterization studies have been carried out in *E. coli* chemostat processing since then, and the behavior of cells is understood in more depth nowadays (Wick et al., 2001; Peebo et al., 2015; Kurata and Sugimoto, 2018). As RPP in continuous cultivation systems in *E. coli* leads to uncharacteristic intracellular fluxes (Peebo and Neubauer, 2018), there is a high demand in process analytical tools to monitor and control cultivation systems (Esmonde-White et al., 2017; Vargas et al., 2018; Zobel-Roos et al., 2019). Within this section we therefore discuss the physiological characterizations of *E. coli* chemostat cultures; process analytical tools (PAT) implemented in *E. coli* processes and their applicability within continuous systems; and engineering screws to optimize long-term *E. coli* cultivations.

Physiological Characterization of *E. coli* Chemostat Cultures

The introduction of steady-state cultivation systems back in that 1950s was applied to ease research approaches, such as estimating mutation rates (Monod, 1949a; Novick and Szilard, 1950a,b, 1951). The "competitive ability" of *E. coli* was investigated already back in the 1980s, using a molecular clock principle, and showed that most changes in population fitness occur within the first 200 h of a cultivation (Dykhuizen and Hartl, 1981). Proteome changes in *E. coli* chemostat cultivations were monitored when switching from glucose-limiting conditions to glucose excess after 500 h of cultivation (Wick et al., 2001). This study shows that the proteome can be distinguished in a short and in a long-term response (Wick et al., 2001), indicating that changes in the transcriptome could be monitored in long-term cultivations even without the production of recombinant proteins (Peebo and Neubauer, 2018). Chemostat cultivations, performed with different dilution rates, revealed that RPP is fairly constant within an induction time of 6 h (Vaiphei et al., 2009). Q_p can be correlated to the growth rate, which is in accordance with other studies and independent from the cultivation mode (Peebo and Neubauer, 2018; Slouka et al., 2019). The phenomenon of growth-dependent production shows a need for investigating intracellular pathways in more detail (Valgepea et al., 2013). A kinetic model, developed by Kurata et al. describes intracellular carbon pathways down to the TCA-cycle and can be verified for non-induced cultivations (Kurata and Sugimoto, 2018). Still, it has to be taken into account that intracellular fluxes tend to shift, once RPP is induced, as the maximum growth rate decreases due to limited host cell capacity (Scott et al., 2010; Heyland et al., 2011; Ceroni et al., 2015). As seven volume changes in a steady-state recombinant protein production in single-vessel *E. coli* cultivations are regarded as a steady-state (Vemuri et al., 2006), studies in this field are tricky to implement, as cultivations might suffer from unexpected metabolic shifts before reaching a "steady-state" mode. Characterizing intracellular fluxes via a metabolome analysis indicates a high diversity occurring between different strains (Basan, 2018; McCloskey et al., 2018). The metabolome analysis state, which we use to deal with a highly complex system as different intracellular pathways are up- or downregulated, is very dependent on the host and the target protein (McCloskey et al., 2018). As shifts already occur without RPP, showing that cells try to adapt to the environment in chemostat cultivation, we hypothesize that the production of recombinant proteins will increase these shifts to a maximum.

Process Analytical Tools (PAT) in *E. coli* Cultivations

Defining a certain time span of a continuous production as a lot number has opened up the possibility of releasing products of long-term processes, providing constant CQAs of each lot number independently from process time (Allison et al., 2015). In process realization, analytical methods often create a bottleneck as they are highly time consuming [taking sample preparation and data treatment into account (Pais et al., 2014; Gomes et al., 2015; Sommeregger et al., 2017)]. At-line analytics might provide useful information (Lee et al., 2015); however, process control in continuous manufacturing should be implemented using online signals (Rathore et al., 2010), if possible, making use of PAT (process analytic tools) (Rathore, 2015; Vargas et al., 2018). Process controls using a "digital twin" are the way to move toward Biopharma 4.0 (Nargund et al., 2019), but they still need to be established for long-term *E. coli* cultivations. Within this monitoring strategy, first brought to public by NASA (Rosen et al., 2015), real processes are represented by virtual simulations and are continuously fed with all process parameters and sensor results monitored throughout the process (Zobel-Roos et al., 2019). Using model-based controls in combination with online data transmission, process variances can be predicted, and operators can intervene to keep processes going (Zahel et al., 2017a; Steinwandter et al., 2019).

Some online process controls implementing PAT are nowadays carried out with Raman spectroscopy measurements in cell culture cultivations (Abu-Absi et al., 2011; Lewis et al., 2018; Nagy et al., 2018). Esmonde-White et al. found that Raman spectroscopy is already applied in GMP facilities (good manufacturing practice) for monoclonal antibody (mAB) production (Esmonde-White et al., 2017). Raman spectroscopy can be found in diverse fields, ranging from bacterial impurity measurement of water (Li et al., 2017) to surface-enhanced Raman spectroscopy (SERS), which can be used to determine bacterial contaminations in cell cultures (Esmonde-White et al., 2017). Teng et al. monitored stress reactions using Raman spectroscopy on a single-cell bacterial level (Teng et al., 2016), and overflow metabolites in an *E. coli* fermentation were monitored by Lee et al. using online Raman spectroscopy (Lee et al., 2004). Nevertheless, process controls for RPP in *E. coli* have not been established until now.

As biomass provides important information about *E. coli* process characteristics (Slouka et al., 2016), online dry cell weight estimations have been performed with online microscopy and back-scattered light (Marquard et al., 2017; Mühlmann et al., 2018). Since scattered light analysis is difficult to implement on a large scale, and microscopy might suffer from the use of complex media, process control implementation is tricky. At-line flow cytometry measuring viable cell concentration can provide useful information to determine states throughout a cultivation (Langemann et al., 2016). Using GFP reporter strains, it has been shown that the adaption of glucose pulses in chemostat cultivation could be monitored using flow cytometry analysis (Heins et al., 2019). Baert et al. also used flow cytometry as a tool to determine variations in phenotypes (Baert et al., 2015). Cell filamentation and its correlation with high productive subpopulations are also monitored with flow cytometry in fed-batch cultivations (Fragoso-Jiménez et al., 2019). Measuring filamented populations via PI-staining showed that the filamented subpopulation had enhanced PI uptake, forming the so-called red but not dead phenotype (Shi et al., 2007; Davey and Hexley, 2011). Sassi et al. presented an interesting follow-up approach, which showed the possibility of monitoring and controlling subpopulations with online PI staining being detected with online flow cytometry in chemostat cultivations (Sassi et al., 2019). The red but not dead phenotype population can be regulated at a constant level of 10% using a cultivation system called the "segregostat," which applies starvation or glucose pulses. Still, the feasibility of this cultivation mode needs to be tested for continuous recombinant protein formation, and proper online dilution systems need to be established in order to dilute high cell density cultivations (Langemann et al., 2016). Nevertheless, the applicability of an online flow cytometer as a PAT for continuous microbial fermentations is clearly needed in order to characterize heterogeneous differences throughout cultivation (Delvigne et al., 2017). The determination of viable biomass with rheological measurements (Newton et al., 2016) could also be implemented in an at-line application. Soft-sensor cultivation for recombinant GFP production was also established using NIR-signals and at-line HPLC to control metabolite accumulation by Gustavsson and Mandenius (2013). Applications like this could be of particularly high interest for continuous cultivations. High throughput metabolite quantification such as the RP-LC-MS/MS method by McCloskey et al. may help to get an at-line "host response" (McCloskey et al., 2018). Understanding intracellular dynamics on a single-cell level might additionally help to characterize different phenotypes occurring throughout the cultivation (Leygeber et al., 2019). Nevertheless, further understanding on a transcriptome and proteome level will be needed to shed more light on intracellular fluxes. Therefore, characterizing the intracellular fluxes throughout the production of recombinant molecules, with metabolites being measured at-line, is the way to develop adequate process control strategies. **Table 1** gives a short overview of monitoring tools developed for *E. coli* cultivations up until now, and these can be implemented in an online control mode for continuous cultivations.

Mammalian cell cultivations for RPP already make use of RAMAN- and NIR-signals (Iversen et al., 2014; Berry et al., 2015; Esmonde-White et al., 2017; Li et al., 2017), and even have implemented signal-derived feedback controls (Li et al., 2013; Craven et al., 2014). As the major advantage of microbial processes compared to mammalian cell line cultivations is the cheap manufacturing, the devices and detectors needed for Raman and NIR spectroscopy are possibly too high in price to establish microbial process controls until now (Rathore, 2014). With cheaper analytical devices being developed, the future might show a new trend in process controls within *E. coli*.

Engineering Screws to Optimize Long-Term *E. coli* Cultivations

As different continuous cultivation modes for microbial systems have been discussed by Adamberg et al. (2015), we will focus on continuous cultivation systems, which are feasible for RPP. Fermentations with *E. coli* need high gas flows and high stirrer velocities to accomplish the respiratory demand of the host cells (Schaepe et al., 2014). Scale-up via k_{LA} is well-understood and can be performed without observing a large-scale yield decrease (Junker, 2004; Islam et al., 2008). The development of continuous cultivation systems using mini-reactor systems is therefore a feasible approach (Lis et al., 2019), especially as continuous culture development is highly time and media consuming (Schmideder et al., 2016). Multiple small-scale reactors can be operated in parallel, increasing the number of experiments (Schmideder et al., 2015). Furthermore, it opens up the possibility to screen multiple candidates in a high throughput manner (Bergenholm et al., 2019), which might be necessary to develop suitable strains for continuous manufacturing.

To overcome stability issues in long-term RPP within *E. coli*, Schmideder et al. implement a cascaded system, pictured in **Figure 2**, where two stirred tank reactors were operated in parallel at different conditions (Schmideder and Weuster-Botz, 2017). Steady-state production within an *E. coli* plasmid-based system could be reached for two residence times within this study. Higher dilution rates seem to be beneficial for RPP in cascade cultivations, which is in accordance with chemostat- and

TABLE 1 | PAT tools established in *Escherichia coli* or with promising prospects for establishment.

Monitoring tool	Scale & cultivation mode	Application	Host & target product	References
Raman-spectroscopy	Fermentation 2.5 L, batch mode	Measuring of glucose, lactate, formate, acetate	*E coli* ATCC31883, for phenylalanine production	Lee et al., 2004
NIR (near infra-red) spectroscopy	Fermentation 2 L, batch mode	Glucose, glycerol, ammonium, and acetate measurement with at line NIR	*E. coli* ML308 & *E. coli* W310	Schenk et al., 2008
In situ microscopy (ISM)	Fermentation 2 L, fed-batch	Cell concentration measurement up to 70 g/L	*E. coli* BL21(DE3)	Marquard et al., 2017
Electrochemical impedance spectroscopy (EIS)	Fermentation, 10 L, fed-batch	increase in the double layer capacitance at low frequency can be correlated to biomass growth; offline and online analysis	*E. coli BL21 DE3, horseradish peroxidase production*	Slouka et al., 2016
Viscosity monitoring for cell lysis	Fermentation 5 L, fed batch	DNA release due to cell lysis increases viscosity up to 25%; cell lysis can be determined with at-line rheological measurement	*E. coli* W3110, for Fab production	Newton et al., 2016
Scattered light for predication of burden	Biolector plate & RAMOS shake-flask	Scattered light is calculated to oxygen transfer rate & biomass prediction on burden	*E. coli* BL21 (DE3) for cellulose and fluorescent protein FbFP production	Mühlmann et al., 2018
Fermentation off-gas analysis to determine metabolic state	Fermentation 15 L, fed batch	Online Oxygen transfer-rate monitoring, Sugar accumulation/Overfeeding can be correlated with decreased signal of OTR	*E. coli BL21 DE3, sfGFP production*	Schaepe et al., 2014
At-line flow cytometry for bacterial cell lysis	Fermentation 20 L, fed batch	Combination of 2 fluorescent stains [$DiBac_4(3)$) & Rh414] showed that viable cell counts from FCM measurements could be correlated with viable CFUs	*E. coli* NM522, no RPP	Langemann et al., 2016
Online flow cytometer control—"segregostat"	Fermentation 2 L, chemostat	Monitoring & control of PI-positive phenotype with online FCM and control via glucose pulses or starvation	*E. coli* JW2203-1 Δ*ompC,* no RPP	Sassi et al., 2019
Soft-sensor-sensor PAT application (NIR + at-line HPLC)	Fermentation 10 L, fed batch	NIR *in situ* probe & at-line HPLC for measuring overflow metabolites to control metabolites at a set level	*E. coli* HMS174, GFP production	Gustavsson and Mandenius, 2013
Full-rip (RP-LC-Ms/Ms) for metabolome characterization	Shake flask cultivation, 25 m L	Offline measurements of metabolomics with RP-LC-MS/MS; determining 100 metabolites within 5 min; differences in the central, amino acid, nucleotide, and energy pathways were found	*E. coli C, E. coli Crooks, E. coli DH5a, E. coli W, E. coli W3110, E. coli BL21 (DE3), E. coli K-12-MG1655*	McCloskey et al., 2018
Online scattered light measurement for IB measuring at 625 nm	Shakeflask cultivation	180° measurement for morphological, opacity & color change	*E. coli*, BL21 (DE3) for GFP & hLIF production	Ude et al., 2016

fed-batch experiments (Vaiphei et al., 2009; Peebo and Neubauer, 2018; Slouka et al., 2019). As product formation within the host cells is a time-dependent process in *E. coli*, there is a trade-off between maximum productivity and steady state production. Maximum q_p in fed-batch usually is usually achieved after ∼10 h of induction when maintaining a growth rate of $\mu = 0.1\ h^{-1}$ (Slouka et al., 2018a). As occurring cell lysis and decreased host capacity towards the end of a fed-batch cultivation possibly lead to "non-productive" subpopulations, continuous cascaded systems operating at higher dilution rates, washing out cells before achieving maximum productivity seems to be beneficial to achieve stable productivity in two-compartment systems.

An interesting approach on the pharmaceutical horizon might be moving away from only RPP and move onto recombinant mRNA production (Pardi et al., 2018; Zhang et al., 2019). As *E. coli* is a well-characterized host, with cheap cultivation possibilities (Gupta and Shukla, 2017; Wurm et al., 2017c; Slouka et al., 2018b; Rosano et al., 2019), recombinant mRNA production might soon be performed within *E. coli*. Establishing continuous cultivation systems for recombinant mRNA is yet to come; however, we would suggest that process technology should be ready for such implementations.

THE CONTINUOUS DOWNSTREAM PROCESSING OF INTRACELLULAR PROTEINS

The continuous downstream processing of extracellular proteins derived from cell culture cultivations (mostly monoclonal antibody production) is already implemented in some branches of the pharmaceutical industry (Vogel et al., 2012; Ötes et al., 2018). Proteins can be separated from impurities at

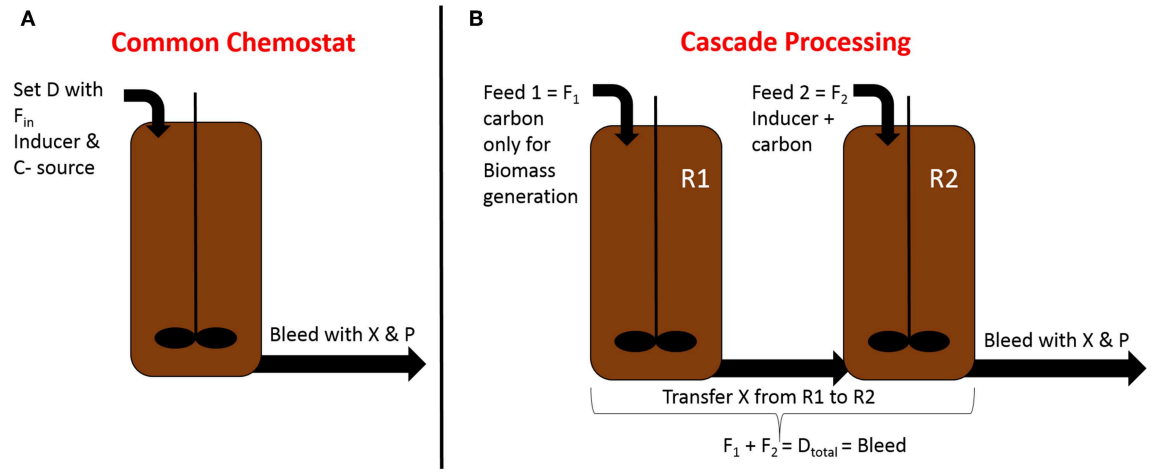

FIGURE 2 | Comparison of common chemostat processing in **(A)** with the established cascaded processing system in **(B)**; different process parameters for biomass growth and RPP can be adjusted in each reactor using the cascaded system, optimizing RPP; X, Biomass; P, Product; D, dilution rate; R1, reactor 1 for biomass production; R2, reactor 2 for recombinant protein production.

high efficiency either with SMB (simulated moving bed)-chromatography or continuous membrane chromatography (Shekhawat and Rathore, 2019). Workflows and the processing of proteins in a continuous mode have recently been discussed by Jungbauer in more depth (Jungbauer, 2013). While extracellular proteins are separated via centrifugation from the host cells, are captured as they go, and then purified and polished, intracellular proteins need more downstream unit operations to achieve the same quality attributes. As stable product formation within *E. coli* in a continuous mode has so far been difficult to realize; the difficulties of continuous purification of intracellular protein have not been discussed in much depth (Peebo and Neubauer, 2018). Therefore, we will give an update on the newest achievements in continuous downstream processing for intracellular proteins derived from *E. coli*.

Purification of intracellular proteins generally starts with a centrifugation step, separating biomass from the supernatant (Jungbauer, 2013). Simulations of a disc stack centrifugation applied in a continuous mode have been done and technical realization is feasible for continuous application (Chatel et al., 2014). Ongoing cell disruption is performed with high-pressure homogenization, as high-pressure homogenization is the only scalable form of cell disruption (Balasundaram et al., 2009; Lin and Cai, 2009). Homogenizers can be operated at high velocities; realizing cell disruption within one passage and the implementation of a continuous cell disruption mode is rather easy (Barazzone et al., 2011). The following centrifugation step, separating cell debris from soluble proteins, is also feasible in a continuous mode with techniques available nowadays (Palmer and Wingfield, 2012; Chatel et al., 2014). Even though IBs suffer occasionally from low yields throughout refolding unit operation, product purity was found to be as high as 80% after differential centrifugation, which would lead to a decreased demand in chromatography (Jungbauer, 2013).

It was shown that IB processing can be boosted when operating the notorious refolding step in a continuous mode (Wellhoefer et al., 2014; Walch and Jungbauer, 2017). Within different studies, the continuously refolded lysozyme exhibited higher refolding yields than commonly performed batch/fed-batch refolding (Farshbaf et al., 2002). As a lysozyme is known to have high refolding yields (Sakamoto et al., 2004; Rathore, 2013) when compared to many other proteins, yield enhancement by continuous refolding still needs to be verified with different proteins (Yamaguchi and Miyazaki, 2014; Pieracci et al., 2018). Still, Schlegl et al. simulated the refolding efficiency in continuous stirred-tank reactors, and the results showed that higher refolding yields could be achieved in continuous applications when compared to batch processing (Schlegl et al., 2005). As dilutions in batch refolding unit operation increase the refolding yield (Vemula et al., 2015), huge volume capacities are needed (Yamaguchi and Miyazaki, 2014). Wellhoefer et al. further mark that continuous refolding could save up to 98% of the refolding buffer applied within a process (Wellhoefer et al., 2014). Mild solubilization techniques were discussed in more detail by Singh et al. and are also known to enhance product yield depending on the target protein (Singh et al., 2015). Applying continuous solubilization in a plug-flow reactor system and passing the solubilized protein on to a continuous refolding unit operation seems to be the holy grail in continuous IB processing, as reactor volumes can be reduced and efficiency can be enhanced.

Endotoxin removal represents a further issue in bacterial processing as purification is dependent on the target protein (Hyun et al., 2009; Lopes et al., 2010). Depending on the target protein size, lipopolysaccharide purification can be performed with an ultrafiltration step (Pieracci et al., 2018). However, establishing a clean cutoff might be tricky as endotoxins usually are in the size-range of 10–20 kDa (Hyun et al., 2009). Two phase applications for endotoxin removals might also be challenging

TABLE 2 | Current problem states and approaches to move on toward continuous processing with *E. coli*.

Chapter	Problem state	Effect	Current approach	Proposed next step	References
The current state in *E. coli* fed-batch process understanding and its tech transfer potential to continuous processing	Metabolic burden & measurement of such	Intracellular stress, decreasing viable cell concentration & decreased levels of RPP	Time of induction is adapted to achieve high RPP; new *in vivo* burden control system tunable promotor systems, extracellular protein formation	Establish online burden control using online PAT applications→ biological system = complex→ get process understanding establish→ robust process	Neubauer et al., 2003; Scott et al., 2010; Ceroni et al., 2018; Fragoso-Jiménez et al., 2019
	Extracellular protein production	Reduce complexity and time of protein purification	Chemostat cultivations with extracellular protein production suffers from q_p decrease over time	Establish better secretion systems, protein→ strain engineering; q_p needs to be comparable to intracellular concentrations	Mergulhão et al., 2005; Selvamani, 2014; Kleiner-Grote et al., 2018
	Tunable promotor systems	Reduce metabolic burden on host cells during RPP	Arabinose & rhamnose can be used as tunable induction systems but are expensive in utilization	Lactose might be used as a tunable inducer; Development of new tunable inducer systems feasible for industrial approaches	Marschall et al., 2016; Wurm et al., 2017a,b,c
	Genomic integration	Stable product formation due to reduced burden	Integration of GOI with Recombineering/ CRISPR-Cas9; integration of complete pathways	Understand effects between GOI and integration site→ need screening approaches for long-term stable production	Reisch and Prather, 2015; Chung et al., 2017; Englaender et al., 2017
The achievements in continuous Upstream applications with *E. coli*	Instable product formation in chemostat	Product formation decreases due to instable metabolome	Parallelization, Cascade processing;	Analysis and characterization of metabolome & transcriptome investigate & understand intracellular shifts; move on toward different feeding approaches; optimization of Cascade-processing;	Schmideder and Weuster-Botz, 2017; Peebo and Neubauer, 2018; Bergenholm et al., 2019; Sassi et al., 2019
	Lack of proper PAT in Upstream processing	Process control via at-line/offline measurements→ time-delay in control→ suffer from process variances	compare to **Table 1** for PAT approaches	Monitoring of subpopulations establish→ population controls with online flow cytometry; establish new process control with different spectroscopies like EIS;	Slouka et al., 2016; Esmonde-White et al., 2017; McCloskey et al., 2018
The continuous downstream processing of intracellular proteins	Lack of proper PAT in Downstream processing	Process control via at-line/offline measurements time-delay in control& quality check longer times to market	Offline sampling, model-based approaches	Monte-Carlo Simulations in order to find out criticality of each step Downstream = cell free, non-biological (ease in prediction) establish digital twin control	Wellhoefer et al., 2014; Kateja et al., 2017; Zahel et al., 2017b; Sauer et al., 2019

to operate in a continuous mode as long residence times are needed to extract endotoxins (Lopes et al., 2010). This leaves chromatography as the most efficient operation mode to continuously purify proteins from lipopolysaccharides (Lin et al., 2005). A case study is shown by Kateja et al. where IBs are purified in a continuous mode using two different chromatography systems, each of them using three stacked columns, operated in a counter current system (Kateja et al., 2017). Defined CQAs can be kept at a constant level within a processing timeframe of 26 h, but analysis is performed after the process as the PAT for each unit operation still needs to be established. Progress in downstream PAT development is carried out by using a model for real-time monitoring, and this was established using standard measurements such as, pH, conductivity, and UV-VIS absorption as a model input (Sauer et al., 2019). Online prediction of host cell proteins, DNA impurities, and an estimation of the protein content throughout the purification step is possible using this model. Methods of establishing more model-based PATs and using process parameters as inputs are yet to be established for each unit operation. By understanding the effects of process parameters onto product quality, a digital process can be simulated, and process control can be implemented, making use of digital twins, also in downstream processing (Zobel-Roos et al., 2019).

DISCUSSION

Up until now, continuous RPP in a one-compartment system (Adamberg et al., 2015); using *E. coli* as a host is still lacking in stability issues (Peebo and Neubauer, 2018). It was always thought that *E. coli* fed-batch processes were already fully characterized, but occurring stress responses by host cells might have never been monitored until now due to the short time span of fed-batch cultivations. Trying to establish a time-independent cultivation system, we have to go back to a black-box model as, so far, unexplainable effects have occurred throughout long-term cultivations. Even though *E. coli* exhibits slightly slower mutation rates than mammalian cells (10-^{10}/base pair per generation for *E. coli*; 10-^{8}/base pair per generation for mammalian cells), the high growth rate of bacteria and therefore the high amount of generation times might explain the potential shifts in continuous systems with *E. coli* (Rugbjerg and Sommer, 2019). We hypothesize that the same shifts in transcriptomes and proteomes would occur through continuous processes with mammalian cells if processes ran long enough to achieve a comparable number of generation times. However, we believe that, once intracellular fluxes can be monitored and are understood in greater depth, we can adapt control strategies to keep subpopulations at a constant level, which has been exhibited for uninduced systems already (Sassi et al., 2019). Even though single-stage cultivation systems might not be ready yet for continuous RPP in *E. coli*, the previously mentioned two-compartment system showed stable RPP with *E. coli* (Schmideder and Weuster-Botz, 2017). The feasibility of a continuous inclusion body downstream process has also been demonstrated (Kateja et al., 2017); therefore, it seems like process technology is ready for implementing RPP in a continuous mode, using *E. coli* as a host. Still, we believe that more work needs to be done in the physiological characterization and implementation of process analytical tools to establish a more robust process control. Current problems in the continuous processing with *E. coli* and solutions are thus summarized and highlighted in **Table 2**. Once online monitoring devices are ready, we only need a change of mind-set and a switch from batch processing toward a fully integrated continuous process, and there are indeed multiple benefits to performing continuous RPP within *E. coli*.

AUTHOR CONTRIBUTIONS

JK, CS, OS, and CH drafted the manuscript. JK and CS performed the literature research while OS and CH gave valuable scientific input.

ACKNOWLEDGMENTS

We thank the Christian Doppler Society for funding this project.

REFERENCES

Abu-Absi, N. R., Kenty, B. M., Cuellar, M. E., Borys, M. C., Sakhamuri, S., Strachan, D. J., et al. (2011). Real time monitoring of multiple parameters in mammalian cell culture bioreactors using an in-line Raman spectroscopy probe. *Biotechnol. Bioeng.* 108, 1215–1221. doi: 10.1002/bit.23023

Adamberg, K., Valgepea, K., and Vilu, R. (2015). Advanced continuous cultivation methods for systems microbiology. *Microbiology* 161, 1707–1719. doi: 10.1099/mic.0.000146

Adamo, A., Beingessner, R. L., Behnam, M., Chen, J., Jamison, T. F., Jensen, K. F., et al. (2016). On-demand continuous-flow production of pharmaceuticals in a compact, reconfigurable system. *Science* 352, 61–67. doi: 10.1126/science.aaf1337

Allison, G., Cain, Y. T., Cooney, C., Garcia, T., Bizjak, T. G., Holte, O., et al. (2015). Regulatory and quality considerations for continuous manufacturing. May 20–21, 2014 continuous manufacturing symposium. *J. Pharmaceut. Sci.* 104, 803–812. doi: 10.1002/jps.24324

Anane, E., López, C., D. C., Neubauer, P., and Cruz Bournazou, M. N. (2017). Modelling overflow metabolism in *Escherichia coli* by acetate cycling. *Biochem. Eng. J.* 125, 23–30. doi: 10.1016/j.bej.2017.05.013

Babaeipour, V., Khanchezar, S., Mofid, M. R., and Pesaran Hagi Abbas, M. (2015). Efficient process development of recombinant human granulocyte colony-stimulating factor (rh-GCSF) production in *Escherichia coli*. *Iran. Biomed. J.* 19, 102–110. doi: 10.6091/ibj.1338.2015

Baert, J., Kinet, R., Brognaux, A., Delepierre, A., Telek, S., Sørensen, S. J., et al. (2015). Phenotypic variability in bioprocessing conditions can be tracked on the basis of on-line flow cytometry and fits to a scaling law. *Biotechnol. J.* 10, 1316–1325. doi: 10.1002/biot.201400537

Balasundaram, B., Harrison, S., and Bracewell, D. G. (2009). Advances in product release strategies and impact on bioprocess design. *Trends Biotechnol.* 27, 477–485. doi: 10.1016/j.tibtech.2009.04.004

Balogh, A., Domokos, A., Farkas, B., Farkas, A., Rapi, Z., Kiss, D., et al. (2018). Continuous end-to-end production of solid drug dosage forms: coupling flow

synthesis and formulation by electrospinning. *Chem. Eng. J.* 350, 290–299. doi: 10.1016/j.cej.2018.05.188

Bao, R.-M., Yang, H.-M., Yu, C.-M., Zhang, W.-F., and Tang, J.-B. (2016). An efficient protocol to enhance the extracellular production of recombinant protein from *Escherichia coli* by the synergistic effects of sucrose, glycine, and Triton X-100. *Protein Expr. Purif.* 126, 9–15. doi: 10.1016/j.pep.2016.05.007

Barazzone, G. C., Carvalho, R., Kraschowetz, S., Horta, A. L., Sargo, C. R., Silva, A. J. (2011). Production and purification of recombinant fragment of pneumococcal surface protein A (PspA) in *Escherichia coli*. *Procedia Vaccinol.* 4, 27–35. doi: 10.1016/j.provac.2011.07.005

Basan, M. (2018). Resource allocation and metabolism: the search for governing principles. *Curr. Opin. Microbiol.* 45, 77–83. doi: 10.1016/j.mib.2018.02.008

Basan, M., Hui, S., Okano, H., Zhang, Z., Shen, Y., Williamson, J. R., et al. (2015). Overflow metabolism in *Escherichia coli* results from efficient proteome allocation. *Nature* 528, 99–104. doi: 10.1038/nature15765

Bergenholm, D., Liu, G., Hansson, D., and Nielsen, J. (2019). Construction of mini-chemostats for high-throughput strain characterization. *Biotechnol. Bioeng.* 116, 1029–1038. doi: 10.1002/bit.26931

Berlec, A., and Strukelj, B. (2013). Current state and recent advances in biopharmaceutical production in *Escherichia coli*, yeasts and mammalian cells. *J. Ind. Microbiol. Biotechnol.* 40, 257–274. doi: 10.1007/s10295-013-1235-0

Berry, B., Moretto, J., Matthews, T., Smelko, J., and Wiltberger, K. (2015). Cross-scale predictive modeling of CHO cell culture growth and metabolites using Raman spectroscopy and multivariate analysis. *Biotechnol. Prog.* 31, 566–577. doi: 10.1002/btpr.2035

Bieringer, T., Buchholz, S., and Kockmann, N. (2013). Future production concepts in the chemical industry: modular – small-scale – continuous. *Chem. Eng. Technol.* 36, 900–910. doi: 10.1002/ceat.201200631

Biswas, K., Stauffer, S., and Sharan, S. K. (2012). Using recombineering to generate point mutations:galK-based positive-negative selection method. *Methods Mol. Biol.* 852, 121–131. doi: 10.1007/978-1-61779-564-0_10

Borirak, O., Rolfe, M. D., de Koning, L. J., Hoefsloot, H. C., Bekker, M., Dekker, H. L., et al. (2015). Time-series analysis of the transcriptome and proteome of *Escherichia coli* upon glucose repression. *Biochim Biophys Acta* 1854(10 Pt A), 1269–1279. doi: 10.1016/j.bbapap.2015.05.017

Boström, M., Markland, K., Sandén, A. M., Hedhammar, M., Hober, S., and Larsson, G. (2005). Effect of substrate feed rate on recombinant protein secretion, degradation and inclusion body formation in *Escherichia coli*. *Appl. Microbiol. Biotechnol.* 68, 82–90. doi: 10.1007/s00253-004-1855-4

Buerger, J., Gronenberg, L. S., Genee, H. J., and Sommer, M. O. A. (2019). Wiring cell growth to product formation. *Curr. Opin. Biotechnol.* 59, 85–92. doi: 10.1016/j.copbio.2019.02.014

Burcham, C. L., Florence, A. J., and Johnson, M. D. (2018). Continuous manufacturing in pharmaceutical process development and manufacturing. *Annu. Rev. Chem. Biomol. Eng.* 9, 253–281. doi: 10.1146/annurev-chembioeng-060817-084355

Burdette, L. A., Leach, S. A., Wong, H. T., and Tullman-Ercek, D. (2018). Developing Gram-negative bacteria for the secretion of heterologous proteins. *Microb. Cell Fact.* 17:196. doi: 10.1186/s12934-018-1041-5

Burgstaller, D., Krepper, W., Haas, J., Maszelin, M., Mohoric, J., Pajnic, K., et al. (2018). Continuous cell flocculation for recombinant antibody harvesting. *J. Chem. Technol. Biotechnol.* 93, 1881–1890. doi: 10.1002/jctb.5500

Ceroni, F., Algar, R., Stan, G. B., and Ellis, T. (2015). Quantifying cellular capacity identifies gene expression designs with reduced burden. *Nat. Methods* 12, 415–418. doi: 10.1038/nmeth.3339

Ceroni, F., Boo, A., Furini, S., Gorochowski, T. E., Borkowski, O., Ladak, Y. N., et al. (2018). Burden-driven feedback control of gene expression. *Nat. Methods* 15, 387–393. doi: 10.1038/nmeth.4635

Chatel, A., Kumpalume, P., and Hoare, M. (2014). Ultra scale-down characterization of the impact of conditioning methods for harvested cell broths on clarification by continuous centrifugation-Recovery of domain antibodies from rec *E. coli*. *Biotechnol. Bioeng.* 111, 913–924. doi: 10.1002/bit.25164

Chung, M. E., Yeh, I. H., Sung, L. Y., Wu, M. Y., Chao, Y. P., Ng, I. S., et al. (2017). Enhanced integration of large DNA into *E. coli* chromosome by CRISPR/Cas9. *Biotechnol Bioeng.* 114, 172–183. doi: 10.1002/bit.26056

Craven, S., Whelan, J., and Glennon, B. (2014). Glucose concentration control of a fed-batch mammalian cell bioprocess using a nonlinear model predictive controller. *J. Process Control* 24, 344–357. doi: 10.1016/j.jprocont.2014.02.007

Davey, H. M., and Hexley, P. (2011). Red but not dead? Membranes of stressed *Saccharomyces cerevisiae* are permeable to propidium iodide. *Environ. Microbiol.* 13, 163–171. doi: 10.1111/j.1462-2920.2010.02317.x

Delvigne, F., Baert, J., Sassi, H., Fickers, P., Grünberger, A., and Dusny, C. (2017). Taking control over microbial populations: current approaches for exploiting biological noise in bioprocesses. *Biotechnol. J.* 12:1600549. doi: 10.1002/biot.201600549

Deutscher, J., Francke, C., and Postma, P. W. (2006). How phosphotransferase system-related protein phosphorylation regulates carbohydrate metabolism in bacteria. *Microbiol. Mol. Biol. Rev.* 70, 939–1031. doi: 10.1128/MMBR.00024-06

Diers, I. V., Rasmussen, E., Larsen, P. H., and Kjaersig, I. L. (1991). Yeast fermentation processes for insulin production. *Bioproc. Technol.* 13, 166–176.

Dvorak, P., Chrast, L., Nikel, P. I., Fedr, R., Soucek, K., Sedlackova, M., et al. (2015). Exacerbation of substrate toxicity by IPTG in *Escherichia coli* BL21(DE3) carrying a synthetic metabolic pathway. *Microb. Cell Fact.* 14:201. doi: 10.1186/s12934-015-0393-3

Dykhuizen, D., and Hartl, D. (1981). Evolution of competitive ability in *Escherichia coli*. *Evolution* 35, 581–594. doi: 10.1111/j.1558-5646.1981.tb04919.x

Englaender, J. A., Jones, J. A., Cress, B. F., Kuhlman, T. E., Linhardt, R. J., and Koffas, M. A. G. (2017). Effect of genomic integration location on heterologous protein expression and metabolic engineering in *E. coli*. *ACS Synth. Biol.* 6, 710–720. doi: 10.1021/acssynbio.6b00350

Esmonde-White, K. A., Cuellar, M., Uerpmann, C., Lenain, B., and Lewis, I. R. (2017). Raman spectroscopy as a process analytical technology for pharmaceutical manufacturing and bioprocessing. *Anal. Bioanal. Chem.* 409, 637–649. doi: 10.1007/s00216-016-9824-1

Fahnert, B., Lilie, H., and Neubauer, P. (2004). Inclusion bodies: formation and utilisation. *Adv. Biochem. Eng. Biotechnol.* 89, 93–142. doi: 10.1007/b93995

Farshbaf, M., Katoh, Y., Udaka, T., Katsuda, T., Noda, H., and Katoh, S. (2002). Characterization of continuous refolding apparatus using different mixing methods. *J. Chem. Eng. Jpn.* 35, 963–968. doi: 10.1252/jcej.35.963

Ferrer-Miralles, N., Domingo-Espin, J., Corchero, J. L., Vazquez, E., and Villaverde, A. (2009). Microbial factories for recombinant pharmaceuticals. *Microb. Cell Fact.* 8:17. doi: 10.1186/1475-2859-8-17

Fink, M., Vazulka, S., Egger, E., Jarmer, J., Grabherr, R., Cserjan-Puschmann, M., et al. (2019). Micro-bioreactor cultivations of Fab producing *Escherichia coli* reveal genome-integrated systems as suitable for prospective studies on direct Fab expression effects. *Biotechnol. J.* 14:e1800637. doi: 10.1002/biot.201800637

Fragoso-Jiménez, J. C., Baert, J., Nguyen, T. M., Liu, W., Sassi, H., Goormaghtigh, F., et al. (2019). Growth-dependent recombinant product formation kinetics can be reproduced through engineering of glucose transport and is prone to phenotypic heterogeneity. *Microb. Cell Fact.* 18:26. doi: 10.1186/s12934-019-1073-5

Gassman, A. L., Nguyen, C. P., and Joffe, H. V. (2017). FDA regulation of prescription drugs. *N. Engl. J. Med.* 376, 674–682. doi: 10.1056/NEJMra1602972

Glaser, J. A. (2015). Continuous chemical production processes. *Clean Tech. Environ. Policy* 17, 309–316. doi: 10.1007/s10098-015-0903-3

Gomes, J., Chopda, V. R., and Rathore, A. S. (2015). Integrating systems analysis and control for implementing process analytical technology in bioprocess development. *J. Chem. Tech. Biotechnol.* 90, 583–589. doi: 10.1002/jctb.4591

Gupta, S. K., and Shukla, P. (2017). Microbial platform technology for recombinant antibody fragment production: a review. *Crit. Rev. Microbiol.* 43, 31–42. doi: 10.3109/1040841X.2016.1150959

Gustavsson, R., and Mandenius, C.-F. (2013). Soft sensor control of metabolic fluxes in a recombinant *Escherichia coli* fed-batch cultivation producing green fluorescence protein. *Bioprocess Biosyst. Eng.* 36, 1375–1384. doi: 10.1007/s00449-012-0840-z

Gutmann, B., Cantillo, D., and Kappe, C. O. (2015). Continuous-flow technology—a tool for the safe manufacturing of active pharmaceutical ingredients. *Angew. Chem. Int. Ed Engl.* 54, 6688–6728. doi: 10.1002/anie.201409318

Haddadin, F. T., and Harcum, S. W. (2005). Transcriptome profiles for high-cell-density recombinant and wild-type *Escherichia coli*. *Biotechnol. Bioeng.* 90, 127–153. doi: 10.1002/bit.20340

Hausjell, J., Weissensteiner, J., Molitor, C., Halbwirth, H., and Spadiut, O. (2018). *E. coli* HMS174(DE3) is a sustainable alternative to BL21(DE3). *Microb. Cell Fact.* 17:169. doi: 10.1186/s12934-018-1016-6

Heins, A.-L., Johanson, T., Han, S., Lundin, L., Carlquist, M., Gernaey, K. V., et al. (2019). Quantitative flow cytometry to understand population heterogeneity in response to changes in substrate availability in *Escherichia coli* and *Saccharomyces cerevisiae* chemostats. *Front. Bioeng. Biotechnol.* 7:187. doi: 10.3389/fbioe.2019.00187

Herwig, C., Garcia-Aponte, O. F., Golabgir, A., and Rathore, A. S. (2015). Knowledge management in the QbD paradigm: manufacturing of biotech therapeutics. *Trends Biotechnol.* 33, 381–387. doi: 10.1016/j.tibtech.2015.04.004

Heyland, J., Blank, L. M., and Schmid, A. (2011). Quantification of metabolic limitations during recombinant protein production in *Escherichia coli*. *J. Biotechnol.* 155, 178–184. doi: 10.1016/j.jbiotec.2011.06.016

Hyun, J., lt, sup, gt, Hyo-Seung, K., Seung-Cheol, M., et al. (2009). Effects of protein concentration and detergent on endotoxin reduction by ultrafiltration. *BMB Rep.* 42, 462–466. doi: 10.5483/BMBRep.2009.42.7.462

Islam, R. S., Tisi, D., Levy, M. S., and Lye, G. J. (2008). Scale-up of *Escherichia coli* growth and recombinant protein expression conditions from microwell to laboratory and pilot scale based on matched kLa. *Biotechnol. Bioeng.* 99, 1128–1139. doi: 10.1002/bit.21697

Iversen, J. A., Berg, R. W., and Ahring, B. K. (2014). Quantitative monitoring of yeast fermentation using Raman spectroscopy. *Anal. Bioanal. Chem.* 406, 4911–4919. doi: 10.1007/s00216-014-7897-2

Jia, B., and Jeon, C. O. (2016). High-throughput recombinant protein expression in *Escherichia coli*: current status and future perspectives. *Open Biol.* 6:160196. doi: 10.1098/rsob.160196

Jungbauer, A. (2013). Continuous downstream processing of biopharmaceuticals. *Trends Biotechnol.* 31, 479–492. doi: 10.1016/j.tibtech.2013.05.011

Jungbauer, A., and Kaar, W. (2007). Current status of technical protein refolding. *J. Biotechnol.* 128, 587–596. doi: 10.1016/j.jbiotec.2006.12.004

Junker, B. H. (2004). Scale-up methodologies for *Escherichia coli* and yeast fermentation processes. *J. Biosci. Bioeng.* 97, 347–364. doi: 10.1016/S1389-1723(04)70218-2

Kante, R. K., Somavarapu, S., Vemula, S., Kethineni, C., Mallu, M. R., and Ronda, S. (2019). Production of recombinant human asparaginase from *Escherichia coli* under optimized fermentation conditions: effect of physicochemical properties on enzyme activity. *Biotechnol. Bioproc.* E 24:824. doi: 10.1007/s12257-019-0147-x

Kante, R. K., Vemula, S., Somavarapu, S., Mallu, M. R., Boje Gowd, B. H., and Ronda, S. R. (2018). Optimized upstream and downstream process conditions for the improved production of recombinant human asparaginase (rhASP) from *Escherichia coli* and its characterization. *Biologicals* 56, 45–53. doi: 10.1016/j.biologicals.2018.10.002

Karst, D. J., Steinebach, F., Soos, M., and Morbidelli, M. (2017). Process performance and product quality in an integrated continuous antibody production process. *Biotechnol. Bioeng.* 114, 298–307. doi: 10.1002/bit.26069

Kasli, I. M., Thomas, O. R. T., and Overton, T. W. (2019). Use of a design of experiments approach to optimise production of a recombinant antibody fragment in the periplasm of *Escherichia coli*: selection of signal peptide and optimal growth conditions. *AMB Exp.* 9:5. doi: 10.1186/s13568-018-0727-8

Kateja, N., Agarwal, H., Hebbi, V., and Rathore, A. S. (2017). Integrated continuous processing of proteins expressed as inclusion bodies: GCSF as a case study. *Biotechnol. Prog.* 33, 998–1009. doi: 10.1002/btpr.2413

Khlebnikov, A., Skaug, T., and Keasling, J. D. (2002). Modulation of gene expression from the arabinose-inducible araBAD promoter. *J. Ind. Microbiol. Biotechnol.* 29, 34–37. doi: 10.1038/sj.jim.7000259

Kleiner-Grote, G. R. M., Risse, J. M., and Friehs, K. (2018). Secretion of recombinant proteins from *E. coli*. *Eng. Life Sci.* 18, 532–550. doi: 10.1002/elsc.201700200

Kopp, J., Slouka, C., Strohmer, D., Kager, J., Spadiut, O., and Herwig, C. (2018). Inclusion body bead size in *E. coli* controlled by physiological feeding. *Microorganisms* 6:116. doi: 10.3390/microorganisms6040116

Kopp, J., Slouka, C., Ulonska, S., Kager, J., Fricke, J., Spadiut, O., et al. (2017). Impact of glycerol as carbon source onto specific sugar and inducer uptake rates and inclusion body productivity in *E. coli* BL21(DE3). *Bioengineering* 5:E1. doi: 10.3390/bioengineering5010001

Kralisch, D., Hessler, N., Klemm, D., Erdmann, R., and Schmidt, W. (2010). White biotechnology for cellulose manufacturing—The HoLiR concept. *Biotechnol. Bioeng.* 105, 740–747. doi: 10.1002/bit.22579

Kurata, H., and Sugimoto, Y. (2018). Improved kinetic model of *Escherichia coli* central carbon metabolism in batch and continuous cultures. *J. Biosci. Bioeng.* 125, 251–257. doi: 10.1016/j.jbiosc.2017.09.005

Langemann, T., Mayr, U. B., Meitz, A., Lubitz, W., and Herwig, C. (2016). Multi-parameter flow cytometry as a process analytical technology (PAT) approach for the assessment of bacterial ghost production. *Appl. Microbiol. Biotechnol.* 100, 409–418. doi: 10.1007/s00253-015-7089-9

Lara, A. R., Caspeta, L., Gosset, G., Bolívar, F., and Ramírez, O. T. (2008). Utility of an Escherichia coli strain engineered in the substrate uptake system for improved culture performance at high glucose and cell concentrations: an alternative to fed-batch cultures. *Biotechnol. Bioeng.* 99, 893–901. doi: 10.1002/bit.21664

Lee, H. L. T., Boccazzi, P., Gorret, N., Ram, R. J., and Sinskey, A. J. (2004). In situ bioprocess monitoring of *Escherichia coli* bioreactions using Raman spectroscopy. *Vib. Spectrosc.* 35, 131–137. doi: 10.1016/j.vibspec.2003.12.015

Lee, S. L., O'Connor, T. F., Yang, X., Cruz, C. N., Chatterjee, S., Madurawe, R. D., et al. (2015). Modernizing pharmaceutical manufacturing: from batch to continuous production. *J. Pharm. Innov.* 10, 191–199. doi: 10.1007/s12247-015-9215-8

Lemmerer, M., Mairhofer, J., Lepak, A., Longus, K., Hahn, R., and Nidetzky, B. (2019). Decoupling of recombinant protein production from *Escherichia coli* cell growth enhances functional expression of plant Leloir glycosyltransferases. *Biotechnol. Bioeng.* 116, 1259–1268. doi: 10.1002/bit.26934

Lewis, A. T., Gaifulina, R., Guppy, N. J., Isabelle, M., Dorney, J., Lloyd, G. R., et al. (2018). Developing raman spectroscopy as a diagnostic tool for label-free antigen detection. *J. Biophotonics* 11:e201700028. doi: 10.1002/jbio.201700028

Leygeber, M., Lindemann, D., Sachs, C. C., Kaganovitch, E., Wiechert, W., Nöh, K., et al. (2019). Analyzing microbial population heterogeneity-expanding the toolbox of microfluidic single-cell cultivations. *J. Mol. Biol.* doi: 10.1016/j.jmb.2019.04.025. [Epub ahead of print].

Li, B., Ray, B. H., Leister, K. J., and Ryder, A. G. (2013). Performance monitoring of a mammalian cell based bioprocess using Raman spectroscopy. *Anal. Chim. Acta* 796, 84–91. doi: 10.1016/j.aca.2013.07.058

Li, H., Li, C., Martin, F. L., and Zhang, D. (2017). Diagnose pathogens in drinking water via magnetic surface-enhanced raman scattering (SERS) assay. *Materials Today* 4, 25–31. doi: 10.1016/j.matpr.2017.01.189

Lin, M.-F., Williams, C., Murray, M. V., and Ropp, P. A. (2005). Removal of lipopolysaccharides from protein–lipopolysaccharide complexes by nonflammable solvents. *J. Chromatogr.* 816, 167–174. doi: 10.1016/j.jchromb.2004.11.029

Lin, Z., and Cai, Z. (2009). Cell lysis methods for high-throughput screening or miniaturized assays. *Biotechnol. J.* 4, 210–215. doi: 10.1002/biot.200800222

Lis, A. V., Schneider, K., Weber, J., Keasling, J. D., Jensen, M. K., and Klein, T. (2019). Exploring small-scale chemostats to scale up microbial processes: 3-hydroxypropionic acid production in *S. cerevisiae*. *Microbial Cell Factor.* 18:50. doi: 10.1186/s12934-019-1101-5

Lopes, A. M., Magalhães, P. O., Mazzola, P. G., Rangel-Yagui, C. O., de Carvalho, J. C. M., Penna, T. C. V., et al. (2010). LPS removal from an *E. coli* fermentation broth using aqueous two-phase micellar system. *Biotechnol. Prog.* 26, 1644–1653. doi: 10.1002/btpr.463

Luttmann, R., Borchert, S.-O., Mueller, C., Loegering, K., Aupert, F., Weyand, S., et al. (2015). Sequential/parallel production of potential Malaria vaccines – a direct way from single batch to quasi-continuous integrated production. *J. Biotechnol.* 213, 83–96. doi: 10.1016/j.jbiotec.2015.02.022

Mairhofer, J., Scharl, T., Marisch, K., Cserjan-Puschmann, M., and Striedner, G. (2013). Comparative transcription profiling and in-depth characterization of plasmid-based and plasmid-free *Escherichia coli* expression systems under production conditions. *Appl. Environ. Microbiol.* 79, 3802–3812. doi: 10.1128/AEM.00365-13

Malakar, P., and Venkatesh, K. V. (2012). Effect of substrate and IPTG concentrations on the burden to growth of *Escherichia coli* on glycerol due to the expression of Lac proteins. *Appl. Microbiol. Biotechnol.* 93, 2543–2549. doi: 10.1007/s00253-011-3642-3

Marbach, A., and Bettenbrock, K. (2012). lac operon induction in *Escherichia coli*: systematic comparison of IPTG and TMG induction and influence of the transacetylase LacA. *J. Biotechnol.* 157, 82–88. doi: 10.1016/j.jbiotec.2011.10.009

Marquard, D., Schneider-Barthold, C., Düsterloh, S., Scheper, T., and Lindner, P. (2017). Online monitoring of cell concentration in high cell density *Escherichia coli* cultivations using *in situ* Microscopy. *J. Biotechnol.* 259, 83–85. doi: 10.1016/j.jbiotec.2017.08.003

Marschall, L., Sagmeister, P., and Herwig, C. (2016). Tunable recombinant protein expression in *E. coli:* enabler for continuous processing? *Appl. Microbiol. Biotechnol.* 100, 5719–5728. doi: 10.1007/s00253-016-7550-4

Martínez-Gómez, K., Flores, N., Castañeda, H. M., Martínez-Batallar, G., Hernández-Chávez, G., Ramírez, O. T., et al. (2012). New insights into *Escherichia coli* metabolism: carbon scavenging, acetate metabolism and carbon recycling responses during growth on glycerol. *Microb. Cell Fact.* 11:46. doi: 10.1186/1475-2859-11-46

Matsunami, K., Miyano, T., Arai, H., Nakagawa, H., Hirao, M., and Sugiyama, H. (2018). Decision support method for the choice between batch and continuous technologies in solid drug product manufacturing. *Ind. Eng. Chem. Res.* 57, 9798–9809. doi: 10.1021/acs.iecr.7b05230

Mattanovich, D., Branduardi, P., Dato, L., Gasser, B., Sauer, M., and Porro, D. (2012). Recombinant protein production in yeasts. *Methods Mol. Biol.* 824, 329–358. doi: 10.1007/978-1-61779-433-9_17

McCloskey, D., Xu, J., Schrübbers, L., Christensen, H. B., and Herrgård, M. J. (2018). RapidRIP quantifies the intracellular metabolome of 7 industrial strains of *E. coli*. *Metab. Eng.* 47, 383–392. doi: 10.1016/j.ymben.2018.04.009

Mergulhão, F. J., Summers, D. K., and Monteiro, G. A. (2005). Recombinant protein secretion in *Escherichia coli*. *Biotechnol. Adv.* 23, 177–202. doi: 10.1016/j.biotechadv.2004.11.003

Monod, J. (1949a). Adaptation, mutation and segregation in relation to the synthesis of enzymes by bacteria. *Biochem. J.* 44:xix.

Monod, J. (1949b). The growth of bacterial cultures. *Annu. Rev. Microbiol.* 3, 371–394. doi: 10.1146/annurev.mi.03.100149.002103

Morra, R., Del Carratore, F., Muhamadali, H., Horga, L. G., Halliwell, S., Goodacre, R., et al. (2018). Translation stress positively regulates mscl-dependent excretion of cytoplasmic proteins. *MBio* 9:e02118–17. doi: 10.1128/mBio.02118-17

Mühlmann, M. J., Forsten, E., Noack, S., and Büchs, J. (2018). Prediction of recombinant protein production by *Escherichia coli* derived online from indicators of metabolic burden. *Biotechnol. Prog.* 34, 1543–1552. doi: 10.1002/btpr.2704

Na, K. I., Kim, S. J., Choi, D. S., Min, W. K., Kim, S. G., and Seo, J. H. (2019). Extracellular production of functional single-chain variable fragment against aflatoxin B1 using *Escherichia coli*. *Lett. Appl. Microbiol.* 68, 241–247. doi: 10.1111/lam.13110

Nagy, B., Farkas, A., Borbás, E., Vass, P., Nagy, Z. K., and Marosi, G. (2018). Raman spectroscopy for process analytical technologies of pharmaceutical secondary manufacturing. *AAPS Pharm. Sci. Tech.* 20:1. doi: 10.1208/s12249-018-1201-2

Nargund, S., Guenther, K., and Mauch, K. (2019). The move toward biopharma 4.0. *Genet. Eng. Biotechnol. News* 39, 53–55. doi: 10.1089/gen.39.06.18

Nasr, M. M., Krumme, M., Matsuda, Y., Trout, B. L., Badman, C., Mascia, S., et al. (2017). Regulatory perspectives on continuous pharmaceutical manufacturing: moving from theory to practice: september 26-27, 2016, international symposium on the continuous manufacturing of pharmaceuticals. *J. Pharm. Sci.* 106, 3199–3206. doi: 10.1016/j.xphs.2017.06.015

Neubauer, P., and Hofmann, K. (1994). Efficient use of lactose for the lac promoter-controlled overexpression of the main antigenic protein of the foot and mouth disease virus in *Escherichia coli* under fed-batch fermentation conditions. *FEMS Microbiol. Rev.* 14, 99–102. doi: 10.1111/j.1574-6976.1994.tb00080.x

Neubauer, P., Hofmann, K., Holst, O., Mattiasson, B., and Kruschke, P. (1992). Maximizing the expression of a recombinant gene in *Escherichia coli* by manipulation of induction time using lactose as inducer. *Appl. Microbiol. Biotechnol.* 36, 739–744. doi: 10.1007/BF00172185

Neubauer, P., Lin, H. Y., and Mathiszik, B. (2003). Metabolic load of recombinant protein production: inhibition of cellular capacities for glucose uptake and respiration after induction of a heterologous gene in *Escherichia coli*. *Biotechnol. Bioeng.* 83, 53–64. doi: 10.1002/bit.10645

Neubauer, P., and Winter, J. (2001). "Expression and fermentation strategies for recombinant protein production in *Escherichia coli*," in *Recombinant Protein Production with Prokaryotic and Eukaryotic Cells. A Comparative View on Host Physiology: Selected articles from the Meeting of the EFB Section on Microbial Physiology, Semmering, Austria, 5th—8th October 2000,* eds O. W. Merten, D. Mattanovich, C. Lang, G. Larsson, P. Neubauer, D. Porro, P. Postma, J. T. de Mattos, and J. A. Cole (Dordrecht: Springer Netherlands), 195–258.

Newton, J. M., Schofield, D., Vlahopoulou, J., and Zhou, Y. (2016). Detecting cell lysis using viscosity monitoring in *E. coli* fermentation to prevent product loss. *Biotechnol. Prog.* 32, 1069–1076. doi: 10.1002/btpr.2292

Novick, A., and Szilard, L. (1950a). Description of the chemostat. *Science* 112, 715–716. doi: 10.1126/science.112.2920.715

Novick, A., and Szilard, L. (1950b). Experiments with the chemostat on spontaneous mutations of bacteria. *Proc. Natl. Acad. Sci. U.S.A.* 36, 708–719. doi: 10.1073/pnas.36.12.708

Novick, A., and Szilard, L. (1951). Experiments on spontaneous and chemically induced mutations of bacteria growing in the Chemostat. *Cold Spring Harb. Symp. Quant. Biol.* 16, 337–343. doi: 10.1101/SQB.1951.016.01.025

Ötes, O., Flato, H., Vazquez Ramirez, D., Badertscher, B., Bisschops, M., and Capito, F. (2018). Scale-up of continuous multicolumn chromatography for the protein a capture step: from bench to clinical manufacturing. *J. Biotechnol.* 281, 168–174. doi: 10.1016/j.jbiotec.2018.07.022

Ötes, O., Flato, H., Winderl, J., Hubbuch, J., and Capito, F. (2017). Feasibility of using continuous chromatography in downstream processing: comparison of costs and product quality for a hybrid process vs. a conventional batch process. *J. Biotechnol.* 259, 213–220. doi: 10.1016/j.jbiotec.2017.07.001

Pais, D. A. M., Carrondo, M. J. T., Alves, P. M., and Teixeira, A. P. (2014). Towards real-time monitoring of therapeutic protein quality in mammalian cell processes. *Curr. Opin. Biotechnol.* 30, 161–167. doi: 10.1016/j.copbio.2014.06.019

Palmer, I., and Wingfield, P. T. (2012). Preparation and extraction of insoluble (inclusion-body) proteins from *Escherichia coli*. *Curr. Protoc. Protein Sci. Chapter* 6, Unit6.3. doi: 10.1002/0471140864.ps0603s70

Pardi, N., Hogan, M. J., Porter, F. W., and Weissman, D. (2018). mRNA vaccines — a new era in vaccinology. *Nat. Rev. Drug Discov.* 17, 261–279. doi: 10.1038/nrd.2017.243

Peebo, K., and Neubauer, P. (2018). Application of continuous culture methods to recombinant protein production in microorganisms. *Microorganisms* 6:56. doi: 10.3390/microorganisms6030056

Peebo, K., Valgepea, K., Maser, A., Nahku, R., Adamberg, K., and Vilu, R. (2015). Proteome reallocation in *Escherichia coli* with increasing specific growth rate. *Mol. Biosyst.* 11, 1184–1193. doi: 10.1039/C4MB00721B

Pieracci, J. P., Armando, J. W., Westoby, M., and Thommes, J. (2018). "Chapter 9—Industry review of cell separation and product harvesting methods," in *Biopharmaceutical Processing,* eds G. Jagschies, E. Lindskog, K. Łacki, and P. Galliher (Cambridge, MA: Elsevier), 165–206. doi: 10.1016/B978-0-08-100623-8.00009-8

Plumb, K. (2005). Continuous processing in the pharmaceutical industry: changing the mind set. *Chem. Eng. Res. Design* 83, 730–738. doi: 10.1205/cherd.04359

Raman, S., Rogers, J. K., Taylor, N. D., and Church, G. M. (2014). Evolution-guided optimization of biosynthetic pathways. *Proce. Natl. Acad. Sci. U.S.A.* 111, 17803–71808. doi: 10.1073/pnas.1409523111

Ramón, A., Señorale-Pose, M., and Marín, M. (2014). Inclusion bodies: not that bad. *Front. Microbiol.* 5:56. doi: 10.3389/fmicb.2014.00056

Rathore, A. S. (2009). Roadmap for implementation of quality by design (QbD) for biotechnology products. *Trends Biotechnol.* 27, 546–553. doi: 10.1016/j.tibtech.2009.06.006

Rathore, A. S. (2013). Refolding of biotech therapeutic proteins expressed in bacteria: review. *J. Chem. Technol. Biotechnol.* 84, 279–284. doi: 10.1002/jctb.4152

Rathore, A. S. (2014). QbD/PAT for bioprocessing: moving from theory to implementation. *Curr. Opin. Chem. Eng.* 6, 1–8. doi: 10.1016/j.coche.2014.05.006

Rathore, A. S. (2015). Continuous processing for production of biotech therapeutics. *PDA J. Pharm. Sci. Technol.* 69:333. doi: 10.5731/pdajpst.2015.01072

Rathore, A. S., Bhambure, R., and Ghare, V. (2010). Process analytical technology (PAT) for biopharmaceutical products. *Anal. Bioanal. Chem.* 398, 137–154. doi: 10.1007/s00216-010-3781-x

Reichelt, W. N., Brillmann, M., Thurrold, P., Keil, P., Fricke, J., and Herwig, C. (2017a). Physiological capacities decline during induced bioprocesses leading to substrate accumulation. *Biotechnol. J.* 12:1600547. doi: 10.1002/biot.201600547

Reichelt, W. N., Haas, F., Sagmeister, P., and Herwig, C. (2017b). Bioprocess development workflow: transferable physiological knowledge instead of technological correlations. *Biotechnol. Prog.* 33, 261–270. doi: 10.1002/btpr.2377

Reisch, C. R., and Prather, K. L. (2015). The no-SCAR (Scarless Cas9 Assisted Recombineering) system for genome editing in *Escherichia coli*. *Sci. Rep.* 5:15096. doi: 10.1038/srep15096

Reisch, C. R., and Prather, K. L. J. (2017). Scarless Cas9 assisted recombineering (no-SCAR) in *Escherichia coli*, an easy-to-use system for genome editing. *Curr. Protoc. Mol. Biol.* 117, 31.38.31–31.38.20. doi: 10.1002/cpmb.29

Richter, H., and Koebsch, I. (2017). Microbial secretion via esetec technology. *Genet. Eng. Biotechnol. News* 37, 22–23. doi: 10.1089/gen.37.10.09

Rosano, G. L., and Ceccarelli, E. A. (2014). Recombinant protein expression in *Escherichia coli*: advances and challenges. *Front. Microbiol.* 5:172. doi: 10.3389/fmicb.2014.00172

Rosano, G. L., Morales, E. S., and Ceccarelli, E. A. (2019). New tools for recombinant protein production in *Escherichia coli*: a 5-year update. *Protein Sci.* 28, 1412–1422. doi: 10.1002/pro.3668

Rosen, R., von Wichert, G., Lo, G., and Bettenhausen, K. D. (2015). About the importance of autonomy and digital twins for the future of manufacturing. *IFAC-PapersOnLine* 48, 567–572. doi: 10.1016/j.ifacol.2015.06.141

Rovner, A. J., Haimovich, A. D., Katz, S. R., Li, Z., Grome, M. W., Gassaway, B. M., et al. (2015). Recoded organisms engineered to depend on synthetic amino acids. *Nature* 518, 89–93. doi: 10.1038/nature14095

Rozkov, A., Avignone-Rossa, C. A., Ertl, P. F., Jones, P., O'Kennedy, R. D., Smith, J. J., et al. (2004). Characterization of the metabolic burden on *Escherichia coli* DH1 cells imposed by the presence of a plasmid containing a gene therapy sequence. *Biotechnol. Bioeng.* 88, 909–915. doi: 10.1002/bit.20327

Rugbjerg, P., Myling-Petersen, N., Porse, A., Sarup-Lytzen, K., and Sommer, M. O. A. (2018). Diverse genetic error modes constrain large-scale bio-based production. *Nat. Commun.* 9:787. doi: 10.1038/s41467-018-03232-w

Rugbjerg, P., and Sommer, M. O. A. (2019). Overcoming genetic heterogeneity in industrial fermentations. *Nat. Biotechnol.* 37, 869–876. doi: 10.1038/s41587-019-0171-6

Sakamoto, R., Nishikori, S., and Shiraki, K. (2004). High temperature increases the refolding yield of reduced lysozyme: implication for the productive process for folding. *Biotechnol. Prog.* 20, 1128–1133. doi: 10.1021/bp034385b

Saraswat, M., Musante, L., Ravida, A., Shortt, B., Byrne, B., and Holthofer, H. (2013). Preparative purification of recombinant proteins: current status and future trends. *Biomed Res. Int.* 2013:312709. doi: 10.1155/2013/312709

Sassi, H., Nguyen, T. M., Telek, S., Gosset, G., Grünberger, A., and Delvigne, F. (2019). Segregostat: a novel concept to control phenotypic diversification dynamics on the example of Gram-negative bacteria. *Microb. Biotechnol.* 12, 1064–1075. doi: 10.1111/1751-7915.13442

Sauer, D. G., Melcher, M., Mosor, M., Walch, N., Berkemeyer, M., Scharl-Hirsch, T., et al. (2019). Real-time monitoring and model-based prediction of purity and quantity during a chromatographic capture of fibroblast growth factor 2. *Biotechnol. Bioeng.* 116, 1999–2009. doi: 10.1002/bit.26984

Schaepe, S., Kuprijanov, A., Simutis, R., and Lübbert, A. (2014). Avoiding overfeeding in high cell density fed-batch cultures of *E. coli* during the production of heterologous proteins. *J. Biotechnol.* 192 Pt A, 146–153. doi: 10.1016/j.jbiotec.2014.09.002

Schenk, J., Viscasillas, C., Marison, I. W., and von Stockar, U. (2008). On-line monitoring of nine different batch cultures of *E. coli* by mid-infrared spectroscopy, using a single spectra library for calibration. *J. Biotechnol.* 134, 93–102. doi: 10.1016/j.jbiotec.2007.12.014

Schlegl, R., Tscheliessnig, A., Necina, R., Wandl, R., and Jungbauer, A. (2005). Refolding of proteins in a CSTR. *Chem. Eng. Sci.* 60, 5770–5780. doi: 10.1016/j.ces.2005.04.086

Schmideder, A., Cremer, J. H., and Weuster-Botz, D. (2016). Parallel steady state studies on a milliliter scale accelerate fed-batch bioprocess design for recombinant protein production with *Escherichia coli*. *Biotechnol. Prog.* 32, 1426–1435. doi: 10.1002/btpr.2360

Schmideder, A., Severin, T. S., Cremer, J. H., and Weuster-Botz, D. (2015). A novel milliliter-scale chemostat system for parallel cultivation of microorganisms in stirred-tank bioreactors. *J. Biotechnol.* 210, 19–24. doi: 10.1016/j.jbiotec.2015.06.402

Schmideder, A., and Weuster-Botz, D. (2017). High-performance recombinant protein production with *Escherichia coli* in continuously operated cascades of stirred-tank reactors. *J. Ind. Microbiol. Biotechnol.* 44, 1021–1029. doi: 10.1007/s10295-017-1927-y

Scholten, E., Renz, T., and Thomas, J. (2009). Continuous cultivation approach for fermentative succinic acid production from crude glycerol by Basfia succiniciproducens DD1. *Biotechnol. Lett.* 31, 1947–1951. doi: 10.1007/s10529-009-0104-4

Scott, M., Gunderson, C. W., Mateescu, E. M., Zhang, Z., and Hwa, T. (2010). Interdependence of cell growth and gene expression: origins and consequences. *Science* 330, 1099–1102. doi: 10.1126/science.1192588

Seifert, T., Sievers, S., Bramsiepe, C., and Schembecker, G. (2012). Small scale, modular and continuous: a new approach in plant design. *Chem. Eng. Proc.* 52, 140–150. doi: 10.1016/j.cep.2011.10.007

Selvamani, V. (2014). Extracellular recombinant protein production under continuous culture conditions with *Escherichia coli* using an alternative plasmid selection mechanism. 37, 401–413. doi: 10.1007/s00449-013-1005-4

Shachrai, I., Zaslaver, A., Alon, U., and Dekel, E. (2010). Cost of unneeded proteins in *E. coli* is reduced after several generations in exponential growth. *Mol. Cell* 38, 758–767. doi: 10.1016/j.molcel.2010.04.015

Shekhawat, L. K., and Rathore, A. S. (2019). An overview of mechanistic modeling of liquid chromatography. *Preparat. Biochem. Biotechnol.* 49, 623–638. doi: 10.1080/10826068.2019.1615504

Shi, L., Günther, S., Hübschmann, T., Wick, L. Y., Harms, H., and Müller, S. (2007). Limits of propidium iodide as a cell viability indicator for environmental bacteria. *Cytometry* 71, 592–598. doi: 10.1002/cyto.a.20402

Silva, F., Queiroz, J. A., and Domingues, F. C. (2012). Evaluating metabolic stress and plasmid stability in plasmid DNA production by *Escherichia coli*. *Biotechnol. Adv.* 30, 691–708. doi: 10.1016/j.biotechadv.2011.12.005

Singh, A., Upadhyay, V., Upadhyay, A. K., Singh, S. M., and Panda, A. K. (2015). Protein recovery from inclusion bodies of *Escherichia coli* using mild solubilization process. *Microb. Cell Fact.* 14:41. doi: 10.1186/s12934-015-0222-8

Slouka, C., Kopp, J., Hutwimmer, S., Strahammer, M., Strohmer, D., Eitenberger, E., et al. (2018a). Custom made inclusion bodies: impact of classical process parameters and physiological parameters on inclusion body quality attributes. *Microb. Cell Fact.* 17:148. doi: 10.1186/s12934-018-0997-5

Slouka, C., Kopp, J., Spadiut, O., and Herwig, C. (2018b). Perspectives of inclusion bodies for bio-based products: curse or blessing? *Appl. Microbiol. Biotechnol.* 103, 1143–1153. doi: 10.1007/s00253-018-9569-1

Slouka, C., Kopp, J., Strohmer, D., Kager, J., Spadiut, O., and Herwig, C. (2019). Monitoring and control strategies for inclusion body production in *E. coli* based on glycerol consumption. *J. Biotechnol.* 296, 75–82. doi: 10.1016/j.jbiotec.2019.03.014

Slouka, C., Wurm, D. J., Brunauer, G., Welzl-Wachter, A., Spadiut, O., Fleig, J., et al. (2016). A novel application for low frequency electrochemical impedance spectroscopy as an online process monitoring tool for viable cell concentrations. *Sensors* 16:1900. doi: 10.3390/s16111900

Sommeregger, W., Sissolak, B., Kandra, K., von Stosch, M., Mayer, M., and Striedner, G. (2017). Quality by control: towards model predictive control of mammalian cell culture bioprocesses. *Biotechnol. J.* 12:1600546. doi: 10.1002/biot.201600546

Spadiut, O., Capone, S., Krainer, F., Glieder, A., and Herwig, C. (2014a). Microbials for the production of monoclonal antibodies and antibody fragments. *Trends Biotechnol.* 32, 54–60. doi: 10.1016/j.tibtech.2013.10.002

Spadiut, O., Dietzsch, C., and Herwig, C. (2014b). Determination of a dynamic feeding strategy for recombinant *Pichia pastoris* strains. *Methods Mol. Biol.* 1152, 185–194. doi: 10.1007/978-1-4939-0563-8_11

Spadiut, O., Zalai, D., Dietzsch, C., and Herwig, C. (2014c). Quantitative comparison of dynamic physiological feeding profiles for recombinant protein production with *Pichia pastoris*. *Bioproc. Biosyst. Eng.* 37, 1163–1172. doi: 10.1007/s00449-013-1087-z

Steinebach, F., Ulmer, N., Wolf, M., Decker, L., Schneider, V., Wälchli, R., et al. (2017). Design and operation of a continuous integrated monoclonal antibody

production process. *Biotechnol. Prog.* 33, 1303–1313. doi: 10.1002/btpr.2522

Steinwandter, V., Borchert, D., and Herwig, C. (2019). Data science tools and applications on the way to Pharma 4.0. *Drug Discov. Today*. 24, 1795–1805. doi: 10.1016/j.drudis.2019.06.005

Stokstad, E. (2015). Genetic firewall' holds engineered microbes captive. *Science* 345:558. doi: 10.1126/science.aaa6379

Striedner, G., Pfaffenzeller, I., Markus, L., Nemecek, S., Grabherr, R., and Bayer, K. (2010). Plasmid-free T7-based *Escherichia coli* expression systems. *Biotechnol. Bioeng.* 105, 786–794. doi: 10.1002/bit.22598

Studier, F. W., Rosenberg, A. H., Dunn, J. J., and Dubendorff, J. W. (1990). Use of T7 RNA polymerase to direct expression of cloned genes. *Meth. Enzymol.* 185, 60–89. doi: 10.1016/0076-6879(90)85008-C

Teng, L., Wang, X., Gou, H., Ren, L., Wang, T., Wang, Y., et al. (2016). Label-free, rapid and quantitative phenotyping of stress response in *E. coli* via ramanome. *Sci. Rep.* 6:34359. doi: 10.1038/srep34359

Ude, C., Ben-Dov, N., Jochums, A., Li, Z., Segal, E., Scheper, T., et al. (2016). Online analysis of protein inclusion bodies produced in *E. coli* by monitoring alterations in scattered and reflected light. *Appl. Microbiol. Biotechnol.* 100, 4147–4159. doi: 10.1007/s00253-016-7403-1

Ukkonen, K., Mayer, S., Vasala, A., and Neubauer, P. (2013). Use of slow glucose feeding as supporting carbon source in lactose autoinduction medium improves the robustness of protein expression at different aeration conditions. *Protein Expr. Purif.* 91, 147–154. doi: 10.1016/j.pep.2013.07.016

Vaiphei, S. T., Pandey, G., and Mukherjee, K. J. (2009). Kinetic studies of recombinant human interferon-gamma expression in continuous cultures of *E. coli*. *J. Industr. Microbiol. Biotechnol.* 36, 1453–1458. doi: 10.1007/s10295-009-0632-x

Valgepea, K., Adamberg, K., Nahku, R., Lahtvee, P.-J., Arike, L., and Vilu, R. (2010). Systems biology approach reveals that overflow metabolism of acetate in *Escherichia coli* is triggered by carbon catabolite repression of acetyl-CoA synthetase. *BMC Syst. Biol.* 4:166. doi: 10.1186/1752-0509-4-166

Valgepea, K., Adamberg, K., Seiman, A., and Vilu, R. (2013). *Escherichia coli* achieves faster growth by increasing catalytic and translation rates of proteins. *Mol. Biosyst.* 9, 2344–2358. doi: 10.1039/c3mb70119k

Vargas, J. M., Nielsen, S., Cárdenas, V., Gonzalez, A., Aymat, E. Y., Almodovar, E., et al. (2018). Process analytical technology in continuous manufacturing of a commercial pharmaceutical product. *Int. J. Pharm.* 538, 167–178. doi: 10.1016/j.ijpharm.2018.01.003

Vemula, S., Thunuguntla, R., Dedaniya, A., Kokkiligadda, S., Palle, C., and Ronda, S. R. (2015). Improved production and characterization of recombinant human granulocyte colony stimulating factor from *E. coli* under optimized downstream processes. *Protein Expr. Purif.* 108, 62–72. doi: 10.1016/j.pep.2015.01.010

Vemuri, G. N., Altman, E., Sangurdekar, D. P., Khodursky, A. B., and Eiteman, M. A. (2006). Overflow metabolism in *Escherichia coli* during steady-state growth: transcriptional regulation and effect of the redox ratio. *Appl. Environ. Microbiol.* 72, 3653–3661. doi: 10.1128/AEM.72.5.3653-3661.2006

Viitanen, M. I., Vasala, A., Neubauer, P., and Alatossava, T. (2003). Cheese whey-induced high-cell-density production of recombinant proteins in *Escherichia coli*. *Microb. Cell Fact.* 2:2. doi: 10.1186/1475-2859-2-2

VKR, D., DAVR, J., LN, M., and KSBR, A. (2019). Optimization of the downstream process for high recovery of rhG-CSF from inclusion bodies expressed in *Escherichia coli*. *Proc. Biochem.* 43, 566–575. doi: 10.1016/j.procbio.2008.01.024

Vogel, J. H., Nguyen, H., Giovannini, R., Ignowski, J., Garger, S., Salgotra, A., et al. (2012). A new large-scale manufacturing platform for complex biopharmaceuticals. *Biotechnol. Bioeng.* 109, 3049–3058. doi: 10.1002/bit.24578

Walch, N., and Jungbauer, A. (2017). Continuous desalting of refolded protein solution improves capturing in ion exchange chromatography: a seamless process. *Biotechnol. J.* 12:1700082. doi: 10.1002/biot.201700082

Walsh, G. (2014). Biopharmaceutical benchmarks 2014. *Nat. Biotechnol.* 32, 992–1000. doi: 10.1038/nbt.3040

Walsh, G. (2018). Biopharmaceutical benchmarks 2018. *Nat. Biotechnol.* 36, 1136–1145. doi: 10.1038/nbt.4305

Wang, J., Niyompanich, S., Tai, Y.-S., Wang, J., Bai, W., Mahida, P., et al. (2016). Engineering of a highly efficient *Escherichia coli* strain for mevalonate fermentation through chromosomal integration. *Appl. Environ. Microbiol.* 82, 7176–7184. doi: 10.1128/AEM.02178-16

Wegerer, A., Sun, T., and Altenbuchner, J. (2008). Optimization of an *E. coli* L-rhamnose-inducible expression vector: test of various genetic module combinations. *BMC Biotechnol.* 8:2. doi: 10.1186/1472-6750-8-2

Wellhoefer, M., Sprinzl, W., Hahn, R., and Jungbauer, A. (2013). Continuous processing of recombinant proteins: integration of inclusion body solubilization and refolding using simulated moving bed size exclusion chromatography with buffer recycling. *J. Chromatogr.* 1319, 107–117. doi: 10.1016/j.chroma.2013.10.039

Wellhoefer, M., Sprinzl, W., Hahn, R., and Jungbauer, A. (2014). Continuous processing of recombinant proteins: integration of refolding and purification using simulated moving bed size-exclusion chromatography with buffer recycling. *J. Chromatogr.* 1337, 48–56. doi: 10.1016/j.chroma.2014.02.016

Wick, L. M., Quadroni, M., and Egli, T. (2001). Short- and long-term changes in proteome composition and kinetic properties in a culture of *Escherichia coli* during transition from glucose-excess to glucose-limited growth conditions in continuous culture and vice versa. *Environ. Microbiol.* 3, 588–599. doi: 10.1046/j.1462-2920.2001.00231.x

Wurm, D. J., Hausjell, J., Ulonska, S., Herwig, C., and Spadiut, O. (2017a). Mechanistic platform knowledge of concomitant sugar uptake in *Escherichia coli* BL21(DE3) strains. *Sci. Rep.* 7:45072. doi: 10.1038/srep45072

Wurm, D. J., Herwig, C., and Spadiut, O. (2017b). How to determine interdependencies of glucose and lactose uptake rates for heterologous protein production with *E. coli*. *Methods Mol Biol* 1586, 397–408. doi: 10.1007/978-1-4939-6887-9_26

Wurm, D. J., Quehenberger, J., Mildner, J., Eggenreich, B., Slouka, C., Schwaighofer, A., et al. (2017c). Teaching an old pET new tricks: tuning of inclusion body formation and properties by a mixed feed system in *E. coli*. *Appl Microbiol Biotechnol.* 102, 667–676. doi: 10.1007/s00253-017-8641-6

Wurm, D. J., Veiter, L., Ulonska, S., Eggenreich, B., Herwig, C., and Spadiut, O. (2016). The *E. coli* pET expression system revisited-mechanistic correlation between glucose and lactose uptake. *Appl. Microbiol. Biotechnol.* 100, 8721–8729. doi: 10.1007/s00253-016-7620-7

Yamaguchi, H., and Miyazaki, M. (2014). Refolding techniques for recovering biologically active recombinant proteins from inclusion bodies. *Biomolecules* 4, 235–251. doi: 10.3390/biom4010235

Yang, X., Acevedo, D., Mohammad, A., Pavurala, N., Wu, H., Brayton, A. L., et al. (2017). Risk considerations on developing a continuous crystallization system for carbamazepine. *Org. Process Res. Dev.* 21, 1021–1033. doi: 10.1021/acs.oprd.7b00130

Zahel, T., Hauer, S., Mueller, E. M., Murphy, P., Abad, S., Vasilieva, E., et al. (2017a). Integrated process modeling-a process validation life cycle companion. *Bioengineering* 4:86. doi: 10.3390/bioengineering4040086

Zahel, T., Marschall, L., Abad, S., Vasilieva, E., Maurer, D., Mueller, E. M., et al. (2017b). Workflow for criticality assessment applied in biopharmaceutical process validation stage 1. *Bioengineering* 4:85. doi: 10.3390/bioengineering4040085

Zhang, C., Maruggi, G., Shan, H., and Li, J. (2019). Advances in mRNA vaccines for infectious diseases. *Front. Immunol.* 10:594. doi: 10.3389/fimmu.2019.00594

Zobel-Roos, S., Schmidt, A., Mestmäcker, F., Mouellef, M., Huter, M., Uhlenbrock, L., et al. (2019). Accelerating biologics manufacturing by modeling or: is approval under the QbD and PAT approaches demanded by authorities acceptable without a digital-twin? *Processes* 7:94. doi: 10.3390/pr7020094

Zydney, A. L. (2015). Perspectives on integrated continuous bioprocessing—opportunities and challenges. *Curr. Opin. Chem. Eng.* 10, 8–13. doi: 10.1016/j.coche.2015.07.005

Conflict of Interest: The authors declare that the research was conducted in the absence of any commercial or financial relationships that could be construed as a potential conflict of interest.

frontiers in Bioengineering and Biotechnology

ORIGINAL RESEARCH
published: 07 February 2020
doi: 10.3389/fbioe.2020.00024

Use of Changestat for Growth Rate Studies of Gut Microbiota

Kaarel Adamberg[1,2], Grete Raba[1] and Signe Adamberg[1]*

[1] Department of Chemistry and Biotechnology, Tallinn University of Technology, Tallinn, Estonia, [2] Center of Food and Fermentation Technologies, Tallinn, Estonia

Human colon microbiota, composed of hundreds of different species, is closely associated with several health conditions. Controlled *in vitro* cultivation and up-to-date analytical methods make possible the systematic evaluation of the underlying mechanisms of complex interactions between the members of microbial consortia. Information on reproducing fecal microbial consortia can be used for various clinical and biotechnological applications. In this study, chemostat and changestat cultures were used to elucidate the effects of the physiologically relevant range of dilution rates on the growth and metabolism of adult fecal microbiota. The dilution rate was kept either at D = 0.05 or D = 0.2 1/h in chemostat cultures, while gradually changing from 0.05 to 0.2 1/h in the A-stat and from 0.2 to 0.05 1/h in the De-stat. Apple pectin as a substrate was used in the chemostat experiments and apple pectin or birch xylan in the changestat experiments, in the presence of porcine mucin in all cases. The analyses were comprised of HPLC for organic acids, UPLC for amino acids, GC for gas composition, 16S-rDNA sequencing for microbial composition, and growth parameter calculations. It was shown that the abundance of most bacterial taxa was determined by the dilution rate on both substrates. *Bacteroides ovatus*, *Bacteroides vulgatus*, and *Faecalibacterium* were prevalent within the whole range of dilution rates. *Akkermansia muciniphila* and Ruminococcaceae UCG-013 were significantly enriched at D = 0.05 1/h, while *Bacteroides caccae*, Lachnospiraceae unclassified and *Escherichia coli* clearly preferred D = 0.2 1/h. In the chemostat cultures, the production of organic acids and gases from pectin was related to the dilution rate. The ratio of acetate, propionate and butyrate was 5:2:1 (D = 0.05 1/h) and 14:2:1 (D = 0.2 1/h). It was shown that the growth rate-related characteristics of the fecal microbiota were concise in both directions between D = 0.05 and 0.2 1/h. Reproducible adaptation of the fecal microbiota was shown in the continuous culture with a changing dilution rate: changestat. Consortia cultivation is a promising approach for research purposes and several biotechnological applications, including the production of multi-strain probiotics and fecal transplantation mixtures.

Keywords: continuous cultivation, changestat, fecal microbiota, apple pectin, birch xylan

OPEN ACCESS

Edited by:
Thomas Egli,
ETH Zürich, Switzerland

Reviewed by:
Lars Regestein,
Leibniz Institute for Natural Product Research and Infection Biology, Germany
Sergio Revah,
Autonomous Metropolitan University, Mexico

****Correspondence:***
Kaarel Adamberg
kaarel.adamberg@taltech.ee

Specialty section:
This article was submitted to Bioprocess Engineering, a section of the journal Frontiers in Bioengineering and Biotechnology

Received: *30 August 2019*
Accepted: *13 January 2020*
Published: *07 February 2020*

Citation:
Adamberg K, Raba G and Adamberg S (2020) Use of Changestat for Growth Rate Studies of Gut Microbiota. Front. Bioeng. Biotechnol. 8:24. doi: 10.3389/fbioe.2020.00024

INTRODUCTION

The cultivation of fecal consortia is essential for understanding the mechanisms behind the coexistence of gut microbial species under changing environmental conditions. This information is required in biotechnological and clinical applications, although better defined methods are required for safer procedures. As the desired consortia can be composed of tens or even hundreds of strains,

e.g., next generation probiotics, the cultivation of a balanced consortium saves time and labor compared to the production of single cultures. Moreover, the biomass yields of pure cultures can remain below those of natural bacterial communities, because of a deficiency of several growth factors produced by other consortia members. In this field, the culturomics approach has been developed, where a set of different media are used to cultivate each isolate in a multi-parallel approach (Lagier et al., 2012). This approach has expanded the range of microorganisms that can be cultivated in the lab. The reintroduction of fecal microbiota is a promising method to cure certain gastrointestinal conditions (Petrof et al., 2013). Previously, the most diverse stool substitute containing 33 single fecal isolates was developed by Petrof et al. (2013) to cure antibiotic-resistant *Clostridium difficile*-induced colitis. Also, batch cultures have been used for the production of fecal biomass to treat diarrhea caused by *C. difficile* infection (Jorup-Rönström et al., 2012). Batch cultures are most commonly used for high-throughput small-scale parallel experiments. However, such conditions as substrate concentrations and the accumulation of metabolites are continuously changing. Furthermore, the overgrowth of fast-growing bacteria in mixed cultures is common for batch cultures; for instance, an over 10% increase in *Escherichia coli* from the total population has been reported (Brahma et al., 2017; Adamberg et al., 2018). Thus, it is difficult to analyze the actual selectivity of a tested substrate. Consequently, batch technologies are well suited for high throughput screening or for the industrial production of biomass, but have limited value for studies of specific growth mechanisms and the metabolism of complex microbial consortia.

In a microbial consortium, the steady state composition is defined by complex microbial interactions. These interactions can be supportive (mutual or commensal) or inhibitory (ammensal or competitive), and are driven by residual concentrations of substrates, bacterial metabolites and cross-feeding between different bacteria (Gottschal, 1990). By cultivating 37 mouse gut bacteria in continuous mode, Freter et al. (1983) demonstrated that the population dynamics of indigenous intestinal bacteria are controlled by one or a few substrates. Chung et al. (2019) studied the degradation of five different fibers or fiber mixtures by fecal microbiota in a chemostat and showed that mixed fiber substrates led to the growth of more diverse microbiota than inulin alone. In the cultures of gut microbes, cross-feeding has been supposed to be one of the most important factors for gut microbiota richness. To explain the interactions between different microorganisms in a consortium, in addition to cell modeling, simple culture systems, such as defined mixed cultures and single substrates, should be studied first. This makes it possible to elucidate the primary degraders and substrates (hetero- or autotrophies), auxotrophies and compounds derived from cross-feeding. The dynamic data for predicting bacterial behavior in communities can be best obtained from continuous cultures at low substrate concentrations (Russell and Baldwin, 1979; Tannock, 2017). For example, ecological studies have shown that growth under multiple substrate limitations at very low dilution rates supports species having high growth efficiency (higher yield) but low maximal specific growth rate (Gottschal, 1990). Auxotrophy to a specific compound can be used to promote a species in a mixed culture by supplementing the culture medium with this substrate. Two species containing batch experiments revealed that acetate or lactate produced by *Bacteroides* or *Bifidobacterium* stimulated the growth of butyric acid producing bacteria, while formate and hydrogen enhanced methanogens (Rowland et al., 2018). The dynamics and stability of freshly collected fecal cultures have been studied by several groups, although the use of fresh samples does not allow for direct comparison of the results from different studies (Miller and Wolin, 1981; Macfarlane et al., 1998; Sghir et al., 1998; McDonald et al., 2013; Yen et al., 2015; Chung et al., 2016; von Martels et al., 2017).

The determination of community composition is essential in microbiota research. Next-generation sequencing methods, such as 16S rDNA analysis and whole genome sequencing (WGS), are high throughput approaches that make it possible to identify all of the taxa in whole consortia, but only semi-quantitatively as proportions of the bacteria in a consortium. To obtain quantitative data, bacterial counting through flow cytometry, dry weight analysis or plate counting should be carried out in parallel. Moreover, to determine the taxa of low abundance, the coverage of sequences has to be proportionally higher. Also, species level analysis might require more detailed sequence analysis (WGS) than is available by 16S rDNA sequencing. For the quantitative analysis of bacteria in fecal consortia, species are usually assessed by fluorescent *in situ* hybridization with 16S rRNA probes (Langendijk et al., 1995), although as each species requires a specific probe, this approach is limited by the number of species analyzed or is expensive in an array setup, such as HITChip (Rajilić-Stojanović et al., 2009).

With all cultivation models it should be kept in mind that the specific growth rate of bacteria is not linearly related to the colonic transit rate, since the density of bacteria gradually increases, while the moving rate decreases along the colon. An alternative continuous cultivation technology, changestat, in which all cultivation parameters are computer-controlled, has been developed in our lab. In changestat, the effect of a selected parameter is studied by the gradual change in this parameter within a certain range, while keeping all other conditions constant (Paalme et al., 1995; Kasemets et al., 2003; Adamberg et al., 2015). Our recent study highlighted the importance of dilution rate in determining the composition and diversity of fecal microbiota (Adamberg and Adamberg, 2018). It was also shown that by using de-celerostat (De-stat), the fast- and slow-growing consortia were differentiated from the fecal microbiota during the same experiment (Adamberg and Adamberg, 2018). To analyze whether these results were too biased depending on the starting point, we carried out experiments in both directions: gradually moving dilution rates from slow to fast (accelerostat: A-stat) and from fast to slow (De-stat), between 0.05 and 0.2 1/h.

The main aims of the current study were: (1) to elucidate the reproducibility of the chemostat cultures by using the same adult fecal pool, (2) to study the effects of dilution rate on the dynamics and metabolism of fecal microbiota by using A-stat and De-stat cultures, and (3) to elucidate the metabolism of two common dietary fibers, pectin and xylan, by fecal microbiota. Food is an important factor in modulating colonic microbiota and through

bacterial metabolism promoting health-supporting or disease-activating mechanisms. Pectins are a part of the daily diet, consumed in the form of fruits and vegetables and used as food additives. Xylans are abundant in nature as major constituents of hemicellulose in plant cells.

MATERIALS AND METHODS

Fecal Inoculum

Fecal samples were collected from seven healthy adult volunteers (19–37 years old, Caucasian, both male and female) and homogenized in four volumes of 5% DMSO-containing buffer, as described in Adamberg et al. (2015). The exclusion criteria included the use of supplements of prebiotics and probiotics, laxatives and antibiotics for 4 weeks prior to donation. Equal volumes of the seven fecal slurries were pooled together and aliquots were kept at −80°C for repetitive cultivation experiments. Similar sample preparation (standardization by pooling) has also been used and approved by others for *in vitro* testing in the TIM-2 proximal colon model (Aguirre et al., 2015; Bussolo de Souza et al., 2019).

Defined Base Medium

The defined growth medium was prepared in a 0.05 M potassium phosphate buffer made from 1 M stock solutions (ml/L): K_2HPO_4 (28.9) and KH_2PO_4 (21.1); mineral salts (mg/L): $MgSO_4{*}7H_2O$ (36), $FeSO_4{*}7H_2O$ (0.1), $CaCl_2$ (9), $MnSO_4{*}H_2O$ (3), $ZnSO_4{*}7H_2O$ (1), $CoSO_4{*}7H_2O$ (1), $CuSO_4{*}5H_2O$ (1), $(NH_4)_6Mo_7O_{24}{*}4H_2O$ (1), NaCl (527); hemin (5 mg/L); vitamin K1 (0.5 mg/L); L-amino acids (g/L): Ala (0.044), Arg (0.023), Asn (0.038), Asp (0.038), Glu (0.036), Gln (0.018), Gly (0.032), His (0.027), Ile (0.060), Leu (0.120), Lys-HCl (0.080), Met (0.023), Phe (0.050), Pro (0.041), Ser (0.095), Thr (0.041), Trp (0.009), Val (0.060), Tyr (0.015); vitamins (mg/L): biotin (0.25), Ca-pantothenate (0.25), folic acid (0.25), nicotinamide (0.25), pyridoxine-HCl (0.50), riboflavin (0.25), thiamine-HCl (0.25) and other components (g/L): bile salts (0.5), $NaHCO_3$ (2.0), Tween-80 (0.5), Na-thioglycolate (0.5), and Cys-HCl (0.5, freshly made). The carbohydrate substrates were sterilized separately and mixed with the medium before cultivation. Two substrate combinations, either birch xylan (Sigma-Aldrich, United States) or apple pectin (Sigma-Aldrich, United States) with porcine mucin (Type II, Sigma Aldrich, United States), were added to the base medium in equal amounts (2.5 g/L each). The pH of the growth medium was 7.2 ± 0.1.

Fermentation System

The Biobundle cultivation system consisted of the ADI 1030 bio-controller and cultivation control program "BioXpert" (Applikon, Netherlands). The fermenter was equipped with sensors for pH, pO_2, and temperature. Variable speed pumps for feeding and outflow were controlled by a De-stat or A-stat algorithm: $D = D_0 - d{*}t$ or $D = D_0 + a{*}t$, respectively, where D is the dilution rate (1/h), D_0 is the initial dilution rate, d and a are the deceleration and acceleration rate ($1/h^2$), respectively, and t is the time (h). In accelerostat (A-stat), the dilution rate was gradually increased from 0.05 to 0.2 1/h and in decelerostat (De-stat) the dilution rate was gradually decreased from 0.2 to 0.05 1/h in accordance with the typical transit rate of the human colon (Adamberg and Adamberg, 2018). pH was controlled by a 1M NaOH addition according to the pH set-point. The culture volume was kept constant (300 mL) by monitoring the weight of the fermenter with the PC-linked balance and outflow pump. The pH of the culture was kept at 7.0 and the temperature was kept constant at 36.6°C. The medium in the feeding bottle and the fermenter was flushed with sterile-filtered nitrogen gas (99.9%, AGA) overnight before inoculation and throughout the cultivation to maintain anaerobiosis. Nitrogen flushing was on during the whole experiment. Two mL of the pooled fecal culture was inoculated to start the experiment.

The cultivation algorithm was started 15–17 h after inoculation in the midst of the exponential growth of bacteria. The dilution rate was stabilized at either 0.05 or 0.2 1/h, at pH 7.0, and run for stabilization at these conditions by 6–7 residence times. After achieving a stable titration rate and gas production, the dilution rate was decreased to 0.05 1/h or increased to 0.2 1/h at a rate of 0.05 units per day (the experimental timeline is presented in **Figure 1**). The dilution rate interval was chosen to cover the realistic growth rates of luminal bacteria in the colon. The range of the specific growth rate of the bacteria was calculated based on the colonic transit time of digesta in people consuming Western diets, which varies from 40 to 140 h (median 60–70 h) (Burkitt et al., 1972; Cummings et al., 1976; Fallingborg et al., 1989), and the estimated amount of bacteria, which increases from 10^8 in the proximal colon to 10^{11} cfu/g in feces (Sender et al., 2016). Considering both the period the bacteria have for degradation of dietary fibers and the coinciding increase in the bacterial biomass in the colon, the specific growth rate of the bacteria decreased from 0.3 to 0.02 1/h. Thus, the range of the dilution rates tested in the cultivation experiments, 0.05–0.2 1/h, was chosen.

Analytical Methods

Samples from the outflow were collected on ice, centrifuged (14,000 g, 5 min, 4°C) and stored separately as pellets and supernatants at −20°C until HPLC analyses (sugars and organic acids), UPLC analyses (amino acids), and microbial 16S rDNA sequencing were carried out.

For chromatographic analyses, culture supernatants were filtered using AmiconR Ultra-10K Centrifugal Filter Devices, cut-off 3 kDa according to the manufacturer's instructions (Millipore, United States). The concentrations of organic acids (succinate, lactate, formate, acetate, propionate, isobutyrate, butyrate, isovalerate, and valerate), ethanol and free sugars (mono-, di-, and trisaccharides) were determined by high-performance liquid chromatography (HPLC, Alliance 2795 system, Waters, Milford, MA, United States), using BioRad HPX-87H column (Hercules, CA, United States) with isocratic elution of 0.005 M H_2SO_4 at a flow rate of 0.5 mL/min and at 35°C. Refractive index (RI) (model 2414; Waters, United States) and UV (210 nm; model 2487; Waters, United States) detectors were used for quantification of the substances. The detection limit for the HPLC method was 0.1 mM. Concentrations of

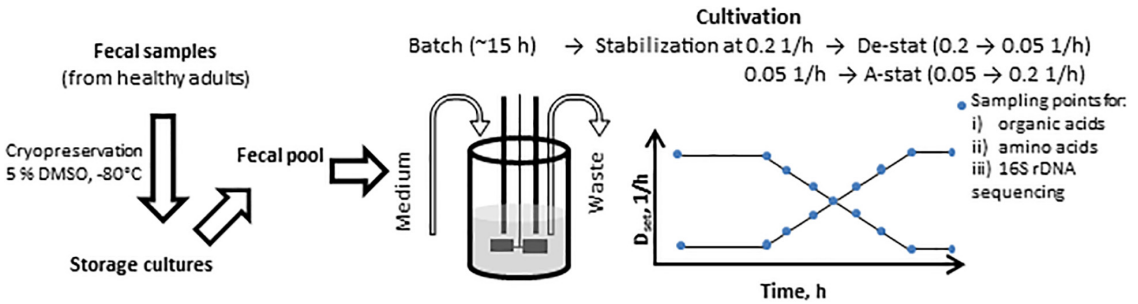

FIGURE 1 | Scheme of the A-stat (accelerostat) and De-stat (decelerostat) experimental set-up. The pooled fecal inoculum was added into 300 ml growth medium at time 0 h followed by batch phase (ca 15 h) until mid- exponential growth phase. Then continuous mode was started and after the stabilization of the fecal culture at D = 0.2 1/h (De-stat) or D = 0.05 1/h (A-stat, 6-7 residential times in total), the dilution rate was gradually decreased down to 0.05 1/h or increased up to 0.2 1/h (deceleration or acceleration rate 0.05 1/h per day), respectively, followed by re-stabilization for approximately 2 residential times. The same procedure was applied for two substrate combinations (birch xylan + mucin and, apple pectin + mucin). D_{set} indicates the controlled change of the dynamics of the pre-set dilution rate.

amino acids and amines were determined with an amino acid analyzer (UPLC; Waters, Milford, United States) according to the manufacturer's instructions. The detection limit of the method was 0.01 mM. All standard substrates were of analytical grade. Empower software (Waters, United States) was used for the processing of HPLC and UPLC data.

The composition of the gas outflow (H_2, CO_2, H_2S, CH_4, and N_2) was analyzed using an Agilent 490 Micro GC Biogas Analyzer (Agilent 269 Technologies Ltd., United States) connected to a thermal conductivity detector. The volume of the gas flow was regularly recorded.

The Redox potential of the growth medium and culture supernatant was measured by a pH/Redox meter using an InLab® Redox electrode (Mettler Toledo).

The biomass dry weight was measured gravimetrically by centrifuging the biomass from a 10 mL culture, washing twice with distilled water and drying in an oven at 105°C for 24 h.

DNA Extraction and Amplification

DNA was extracted from the pellets using a PureLink Microbiome DNA extraction kit (Thermo Fisher Scientific, United Kingdom) according to the manufacturer's instructions. Universal primers:

S-D-Bact-0341-b-S-17 Forward (5′TCGTCGGCAGCGTCAGATGTGTATAAGAGACAGCCTACGGGNGGCWGCAG) and S-D-Bact-0785-a-A-21 Reverse (5′GTCTCGTGGGCTCGGAGATGTGTATAAGAGACAGGACTACHVGGGTATCTAATCC) were used for PCR amplification of the V3-V4 hypervariable regions of the 16S rRNA genes (Klindworth et al., 2013). The amplified region was 390–410 bp long and an average of 67,000 reads per sample were obtained. The mixture of amplicons was sequenced using an Illumina MiSeq 2 × 250 v2 platform (Estonian Genome Centre, University of Tartu, Estonia).

Taxonomic Profiling of Microbiota Samples

The DNA sequence data was analyzed using a BION-meta[1], currently unpublished open source program, according to the author's instructions. Sequences were first cleaned at both ends using a 99.5% minimum quality threshold for at least 18 of 20 bases for 5′-end and 28 of 30 bases for 3′-end, then joined, followed by the removal of contigs shorter than 350 bp. Then sequences were cleaned of chimeras and clustered by 95% oligonucleotide similarity (k-mer length of 8 bp, step size 2 bp). Lastly, consensus reads were aligned to the SILVA reference 16S rDNA database (v123) using a word length of 8 and similarity cut-off of 90%. The bacterial designation was analyzed at different taxonomic levels, down to species if applicable.

[1]www.box.com/bion

Calculations

For quantitative data analysis, the relative data of bacterial abundances from 16S rDNA sequencing analysis were first converted to quantitative values [X_i (g/L), where i illustrates bacterial taxa i] by the formula: $X_i = X_t * A_i$, where X_t is the dry weight of the total biomass of bacteria (g/L) and A_i is the relative abundance of bacterial taxa i in the sample.

The growth characteristics of the bacteria in A-stat and De-stat experiments were calculated based on bacterial mass, total volume of medium pumped out from the fermenter (V_{OUT}, L) and product concentrations in the culture medium (mol/L) as follows:

$$\mu = \frac{d(V_{OUT})}{V \times dt} + \frac{d(X_t)}{dt \times X_t} \quad (1)$$

$$Q_{Si} = \frac{S_i \times d(V_{OUT})}{V \times X_t \times dt} - \frac{d(S_i)}{dt \times X_t} \quad (2)$$

$$Q_{Pi} = \frac{P_i \times d(V_{OUT})}{V \times X_t \times dt} + \frac{d(P_i)}{dt \times X_t} \quad (3)$$

where μ is the specific growth rate (1/h), Q_S is the specific consumption rate of carbohydrate (in carbon equivalents, mol-C/g-X_t/h), S_i is the concentration of consumed carbohydrate i (C-mol/L), Q_{Pi} is the specific production rate of product i (mol-prod/g-X/h), P_i is the concentration of product i (mol/L), V is the current fermenter volume (L), V_{OUT} is the outflow volume and t is the cultivation time (h).

Statistical Analysis

Concentrations of metabolites or abundances of bacteria from three independent experiments were compared by average values and by unpaired and t-test (unadjusted *P*-values < 0.05 were considered significant) for chemostat point comparison. To compare differences in bacterial abundances and metabolite productions during A-stat and De-stat experiments, samples were divided into two groups: (1) samples taken at $D < 0.07$ 1/h (slow growth) and (2) samples taken at $D > 0.17$ 1/h (fast growth). Average and standard deviation of bacterial abundances and metabolite productions were calculated in both groups and a single parametric t-test was used to estimate statistical significance.

Ethics Statement

This study was approved by the Tallinn Medical Research Ethics Committee, Estonia (protocol no. 554).

RESULTS

Reproducibility of Chemostat Cultures of Fecal Microbiota

Until now, continuous fecal cultures have mostly been inoculated with fresh fecal inocula and information on reproducibility of this type of experiment is scarce. Hence, the aim of this work was to elucidate the reproducibility of the continuous fecal cultures. To elucidate the reproducibility of the growth of biological replicates of adult pooled fecal microbiota, six chemostat cultures (three at D_{low} = 0.05 1/h and three at D_{high} = 0.2 1/h) in a defined base medium with apple pectin and mucin were carried out.

Formation of Organic Acids and Gases

The production of organic acids and gases from pectin and mucin was related to the specific growth rate (**Figure 2**). The most abundant organic acid in all chemostat cultures was acetate [23.2 ± 3.1 and 25.2 ± 2.0 mM at D_{low} (0.05 1/h) and D_{high} (0.2 1/h), respectively]. Compared to D_{high}, the production of propionate, butyrate and carbon dioxide was more enhanced at D_{low}. At D_{low}, 9.4 ± 0.3 mM propionate and less than 4 mM succinate were produced, while at D_{high}, concentrations of propionate and succinate were practically equal (4.2 ± 0.3 and 3.9 ± 0.8 mM, respectively). The ratio of acetate, propionate and butyrate was 5:2:1 at D_{low} and 14:2:1 at D_{high}. Similar to the product profile at D_{low}, a ratio of 4:2:1 for acetate:propionate:butyrate was reported by Larsen et al. (2019) in TIM-2 experiments. In accordance with the organic acid profiles, about twice as much carbon dioxide was produced at D_{low} than at D_{high} (20.3 ± 2.4 and 10.5 ± 2.8 mmol per L medium, respectively). On average, the relative difference between parallels of the concentrations of propionate, butyrate and lactate in stabilized fecal cultures (after six residential times) remained below 10% and that of acetate below 25% at both dilution rates (D_{low} and D_{high}).

In addition to organic acids and gases, the consumption of amino acids was analyzed. It was determined that amino acids were fully depleted from the culture medium at both dilution rates, except for alanine and branched-chain amino acids (BCAA), which were practically not consumed at D_{high} (**Figure 3**). The increased production of propionate, butyrate and CO_2 at D_{low} was accompanied by the conversion of BCAA to isobutyric (0.27 ± 0.29 mM) and isovaleric acids (0.87 ± 0.82 mM). Another amino acid degradation product significantly higher at D_{low} was H_2S (0.76 ± 0.12 vs. 0.36 ± 0.09 mmol per L medium at D_{low} vs. D_{high}, respectively) derived from the sulfur-containing amino acids Cys and Met. At D_{high}, isoleucine and leucine were consumed in the range required for biomass formation (0.18–0.24 and 0.45–0.58 mmol/gDW, respectively. **Supplementary Table S2** Chemostat), based on the amino acid contents in the biomass of *E. coli* (0.22 and 0.37 mmol/gDW for Ile and Leu, respectively; Valgepea et al., 2011) and *Lactococcus lactis* (0.25 and 0.37 mmol/gDW for Ile and Leu, respectively; Adamberg et al., 2012). As the total amount of biomass produced was 0.5–0.7 g/L (**Supplementary Table S2** Chemostat), the consumption of other amino acids exceeded 1.6–5.5 times the amount required for biomass synthesis, except for serine, which was consumed about 10 times as much. Serine is the major amino acid in mucins and may be converted to acetate. However, serine degradation (2.1 and 2.6 mmol/gDW at D_{low} and D_{high}, respectively) could not have contributed to more than 5% of the total acetate production (39 and 51 mmol/gDW at D_{low} vs. D_{high}, respectively) as 80–86% of the carbon was derived

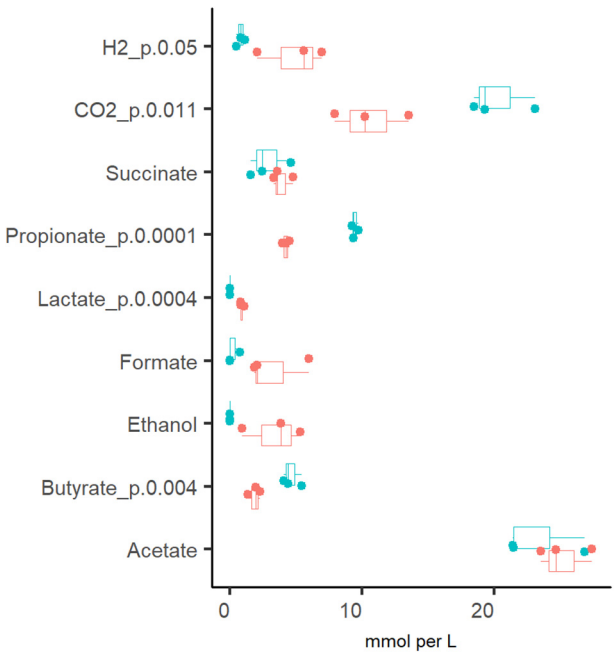

FIGURE 2 | Comparison of the fermentation products from three (independent) chemostat experiments with the same pooled fecal culture at dilution rates 0.05 (blue dots) and 0.2 (red dots) 1/h in apple pectin containing medium. Numbers behind the metabolite name indicate significant difference between D_{low} and D_{high} (D = 0.05 and 0.2 1/h, respectively).

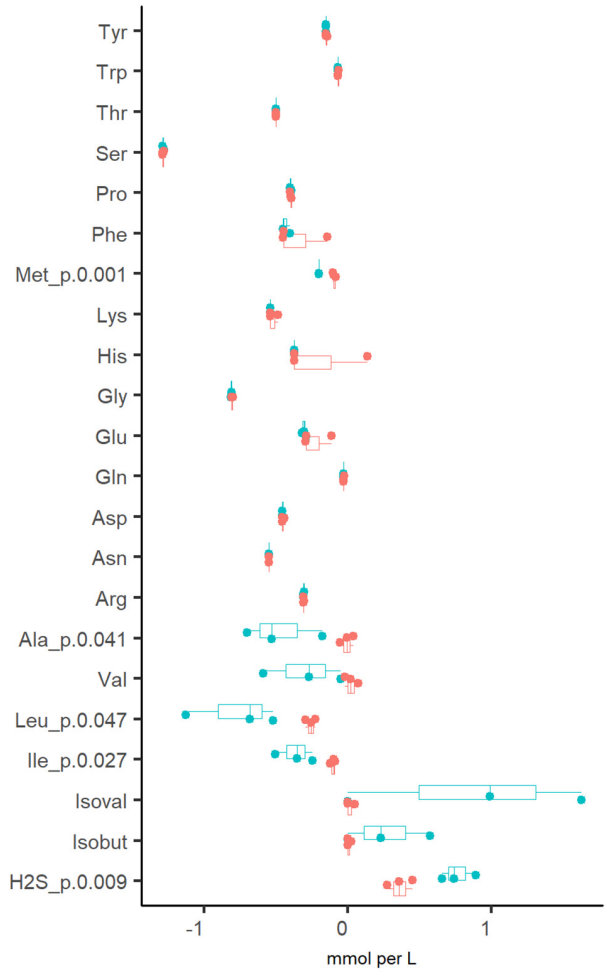

FIGURE 3 | Comparison of amino acid consumptions and related metabolites (branched chain fatty acids and H_2S) from three independent chemostat experiments of fecal culture at dilution rate 0.05 (blue dots) and 0.2 (red dots) 1/h in apple pectin medium. Positive values indicate the production and negative values indicate the consumption of the amino acid. Numbers behind the metabolite name indicate significant difference between D_{low} and D_{high} (D = 0.05 and 0.2 1/h, respectively). isoval, isovalerate; isobut, isobutyrate.

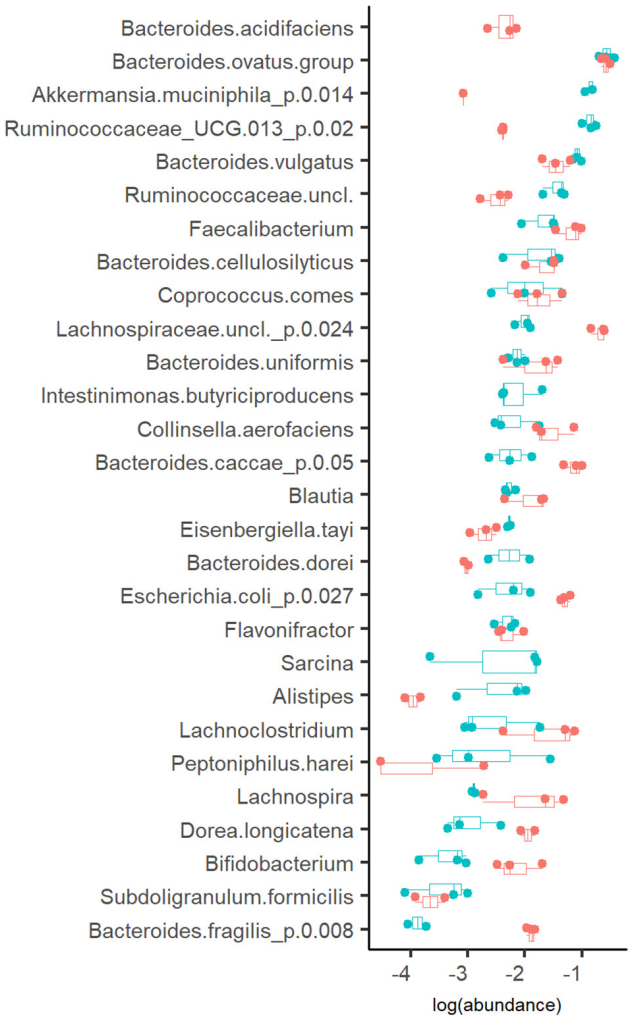

FIGURE 4 | Abundance of bacteria (in log scale) at dilution rate 0.05 (blue dots) and 0.2 (red dots) 1/h in apple pectin medium. Each dot represents an independent chemostat experiment. Numbers behind the metabolite name indicate significant difference between D_{low} and D_{high} (D = 0.05 and 0.2 1/h, respectively).

from carbohydrate fermentation. The overall carbon recovery was 79% and 67% at D_{low} and D_{high}, respectively, showing that some products were under-determined or missing, especially at high dilution rate.

Growth Rate Specific Differences of Fecal Microbiota

The profiles of the metabolic products were in accordance with the bacterial compositions detected (**Figures 2–4**). Three taxa clearly prevalent at both dilution rates were the acetate- and propionate- or succinate-producing species *Bacteroides ovatus* (17 and 14%, at D_{low} and D_{high}, respectively), *Bacteroides vulgatus* (7.9 and 3.6%, at D_{low} and D_{high}, respectively) and butyrate-producing bacterium *Faecalibacterium* (2.4 and 7.2%, at D_{low} and D_{high}, respectively). Also several other bacteria were abundant (1–4% of the total population) at both dilution rates, such as mixed acid (acetate, propionate and butyrate) fermenting *bacteria*, and the acetate- and propionate-producing *Bacteroides uniformis* and *Bacteroides cellulosilyticus* (**Figure 4**). At D_{low} the mucin degrading species *Akkermansia muciniphila* and a group of Ruminococcaceae UCG-013 (from 0.1 to 16% and from 0.5 to 14%, respectively) were significantly enriched. In different, at D_{high}, *Bacteroides caccae*, Lachnospiraceae unclassified and mainly acetate-producing *E. coli* (7.7%, 21% and 6.3% of total reads, respectively) became dominant. The butyrate-producing bacterium *Intestimonas butyriciproducens* and *Sarcina* were detected only at D_{low}, whereas *Bacteroides acidifaciens* was found only at D_{high}. The increased production of ethanol and formate at D_{high} can be linked to higher abundances of *Dorea* and *Blautia*.

A remarkable enrichment of Enterobacteriaceae (up to 60% of total population) was observed in batch phase before starting the

continuous flow. The amount of *E. coli* formed nearly 50% of the microbial population but decreased to about 10% in a chemostat stabilized at D_{high}, and to 1.2% at D_{low}. These data confirm the competitiveness of the fast-growing *E. coli* at high dilution rates.

Comparison of A-Stat and De-Stat Cultures

Changes in the dilution rate in both directions between 0.05 to 0.2 1/h, starting from the stabilized cultures of pooled fecal microbiota in apple pectin and birch xylan media, were analyzed. In A-stat, the dilution rate was gradually increased from 0.05 to 0.2 1/h, and in De-stat the dilution rate was gradually decreased from 0.2 to 0.05 1/h. The stabilization of the chemostat culture was controlled by the titration rate of sodium hydroxide, indicating the rate of acid production rate, and the gas production rate (**Supplementary Figure S1**). Average fluctuations of these parameters below 5% within the last three residential times were considered to be stable cultures to start the changestat algorithm (on average, six or seven residential volumes were needed to achieve the stable cultures).

Formation of Organic Acids and Gases

In total, of one mole of carbohydrates, 1.2–1.3 and 1.7–1.9 mol of acids were produced in xylan and pectin supplemented media, respectively. Acetate formed in nearly two thirds of all fermentation products and its production did not depend on the dilution rate (**Figure 5**). Except for acetate and carbon dioxide, the formation of other metabolites from pectin and xylan was comparable in both directions of the dilution rate change (from 0.05 to 0.2 and from 0.2 to 0.05 1/h). Almost twice as much acetate was produced from xylan than from pectin (0.6–0.7 and 1.1–1.2 mol per mole of carbohydrates consumed, respectively). As xylose is a five-carbon sugar and galacturonic acid is a six-carbon compound, the lower amount of acids produced in the xylan medium can partly be explained by these differences. However, at all dilution rates, the carbon balance ($C_{substrates} - C_{products}$) was still lower in the xylan- than in the pectin-containing medium (average values 74 ± 5% and 82 ± 2%, respectively). The formation of other metabolites, especially carbon dioxide and propionate, was strongly dilution rate-dependent. The synthesis of carbon dioxide was 0.9 and 0.4 mmol per L medium at D_{low} and at D_{high} in the pectin medium in both experimental directions (A-stat and De-stat). A similar trend was observed for xylan, suggesting that the production of carbon dioxide is linked to the growth rate rather than the substrate. To compensate for the change in the carbon flux caused by the decreased production of CO_2, the succinate production increased, especially in the xylan medium. For example, in the A-stat experiment of the xylan medium, the reduction of CO_2 production from 0.42 to 0.22 mol per mole of carbohydrates was compensated for by enhanced formation of succinate (0.26 to 0.42 at D = 0.05 1/h and D = 0.2 1/h, respectively) and formate (0.02 to 0.2 mol per mol carbohydrates at D = 0.05 1/h and D = 0.2 1/h, respectively). Similarly, propionate synthesis was decreased as a response to increasing formate production, keeping the carbon flux consistent (0.27 to 0.09 mol per mol carbohydrates at D = 0.05 1/h and D = 0.2 1/h, respectively). A reverse correlation between concentrations of propionic and succinic acids was observed. In comparing the gas production, notably less carbon dioxide (0.3–0.4 mol per mole of carbohydrates consumed) was formed from xylan, built of xylose, a five-carbon molecule, at all dilution rates. Carbon dioxide may originate from succinate to propionate conversion or butyrate production or demetoxylation of metoxylated galacturonic acid (**Figure 5**).

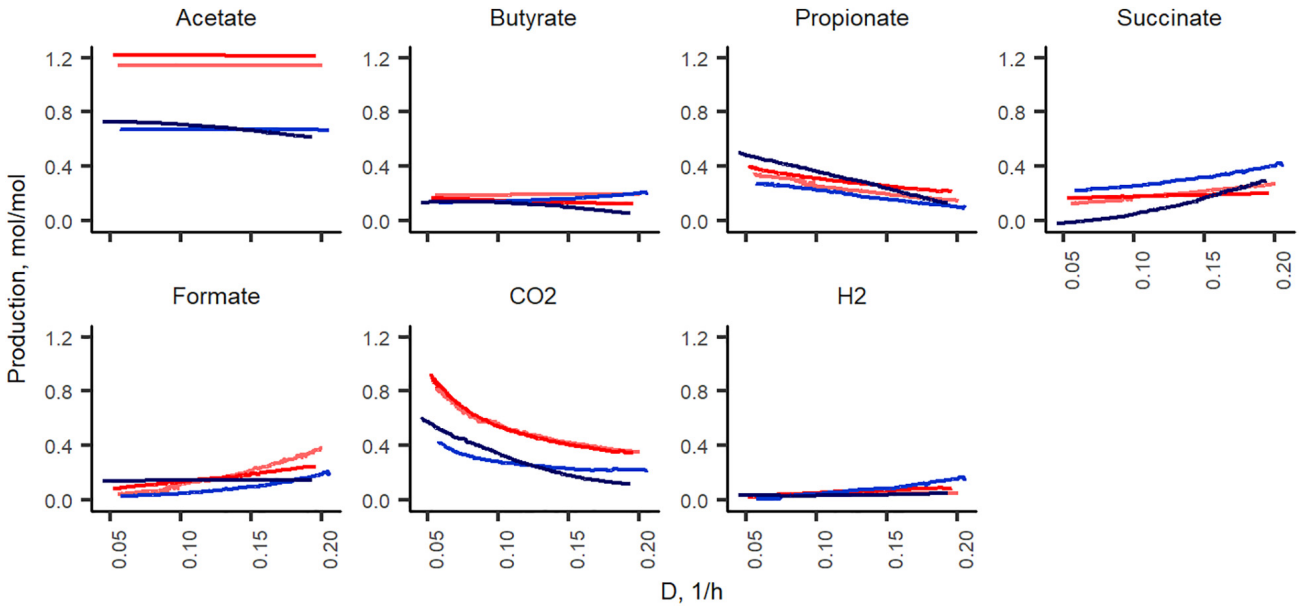

FIGURE 5 | Fermentation product yields per carbohydrates consumed (mol/mol) during the growth in change-stat experiments. The fiber source is indicated by color (red, apple pectin; blue, birch xylan), and the color intensity refers to culture type: A-stat (light color) and De-stat (dark color). D – dilution rate (1/h).

The described changes were characteristic under both directions of the dilution rate (A-stat and De-stat). These data suggest that the acceleration rate applied allowed the culture to adapt to the changing conditions.

Consumption and Formation of Amino Acids

Similarly to the chemostat cultures, most of the amino acids were completely depleted from the medium, except for alanine and BCAA (**Table 1**). The consumption of valine and leucine increased at lower dilution rates. The formation of isobutyrate and isovalerate was practically missing at high dilution rates, but they were produced in concentrations of 2.2–11 and 13–44 mmol/mol-carbohydrates, respectively, at low dilution rates (D < 1/h) (**Table 1**). In both media, the alanine metabolism was more intensive at low dilution rates (up to 14 mmol/mol-carbohydrates). The degradation of the reducing agent cysteine to H_2S up to 41 mmol/mol-carbohydrates was observed at low dilution rates in all experiments (**Table 1**), which corresponds to the degradation of 22% of the total cysteine.

Growth Rate Specific Changes in Fecal Microbiota

The initial fecal slurry contained 88 bacterial species with abundance above 0.1% and, of these, 25 species had abundance higher than 1% (**Supplementary Table S1**). During the chemostat and the following A-stat and De-stat cultivations, the species richness decreased to 27–32 and 10–18 species with abundance of 0.1 and 1% with apple pectin and xylan, respectively. A significant decrease in species richness has been shown by other authors (McDonald et al., 2013; Chung et al., 2016). The abundance of the majority of bacterial taxa was determined by the dilution rate on both substrates. The prevailing genus in the consortia – *Bacteroides* (up to 58% of the total population) – adapted well within the whole range of specific growth rates tested. However, the abundances of some species, such as *B. ovatus* and *Bacteroides cellulosilyticus,* tended to decrease at higher dilution rates (A-stat) in the xylan-supplemented medium (p = 0.02) (**Figure 6**). Pectin selectively enriched the Ruminococcaceae group UCG013, which was never detected in the xylan-containing medium. The abundance of the Ruminococcaceae group UCG-013 was also related to the dilution rate being 17% at lower dilution rates and down to 5% at dilution rates below D < 0.15 in both change directions (**Figure 6**). These data are in accordance with the chemostat results.

Significant increases in abundances of *Collinsella aerofaciens* (p = 0.002), *E. coli* (p = 0.001), *Faecalibacterium prausnitzii* (p = 0.009) and a group of Lachnospiraceae (closest similarity to *Coprococcus*, p = 0.008) (median abundances 1.6, 12, 5.1, and 19%, respectively) were observed at dilution rates above 0.17 1/h on both substrates. Although the abundances of butyrate-producing bacteria (*Faecalibacterium*, *Coprococcus*, and Lachnospiraceae) increased along with the increasing dilution rate, the tested substrates and conditions did not enhance the production of butyrate, resulting in other fermentation products instead.

At higher dilution rates, the increased formate production was accompanied by higher amounts of species from the genus *Lachnoclostridium* that are known to be involved in formate production. The abundance of the prevailing species at dilution rates below 0.07 1/h, *A. muciniphila* (median abundance 22%) decreased significantly at dilution rates above 0.17 1/h (abundance > 1%) in all changestat experiments. This is in accordance with the production of propionic acid, the characteristic metabolite of *Akkermansia* (**Figure 5**). Another taxa inhibited at higher dilution rates was *Intestinimonas* (**Figure 6**).

DISCUSSION

In continuous cultures, the environmental parameters, including substrate concentrations, pH, and flow rate, can be precisely controlled. The *in vivo* situation in the colon probably remains somewhere between chemostat and batch states, i.e., the availability of fermentable substrates decreases, the amounts of metabolites change dynamically and pH moves toward the alkaline region slowly. Our results demonstrate that the changestat techniques, the A-stat and De-stat, can be applied to study the effects of growth rate on the composition and metabolism of fecal microbiota. Using the same fecal inoculum, we showed that continuous cultures are reproducible at dilution rates of D = 0.2 and 0.05 1/h. The dilution rate during the stabilization phase impacts the results of

TABLE 1 | Consumption of amino acids and formation of degradation products from amino acids (mmol per mol carbohydrates consumed) during A-stat and De-stat experiments and significantly different at fast or slow dilution rate.

Experiment*	State**	D, 1/h	Isobutyrate	Isovalerate	H_2S	Ala	Ile	Leu
Xyl_A	SS	0.058	2.2	13.6	22.1	11.0	6.4	12.7
Xyl_D	Q	0.058	ND	ND	29.7	2.3	4.8	12.6
Xyl_D	SS	0.193	ND	23.9	7.4	ND	2.8	6.8
Xyl_A	Q	0.193	ND	1.0	12.4	3.4	4.1	5.5
Pec_A	SS	0.055	11.3	44.1	29.1	6.9	10.6	16.3
Pec_D	Q	0.054	2.7	17.1	41.3	14.3	8.8	15.2
Pec_D	SS	0.196	0.2	1.8	12.2	ND	5.7	8.5
Pec_A	Q	0.197	4.1	12.2	16.0	ND	5.4	2.2

**A and D indicate A-stat and De-stat, respectively. **SS and Q indicate steady state and quasi steady state, respectively. ND, not detected.*

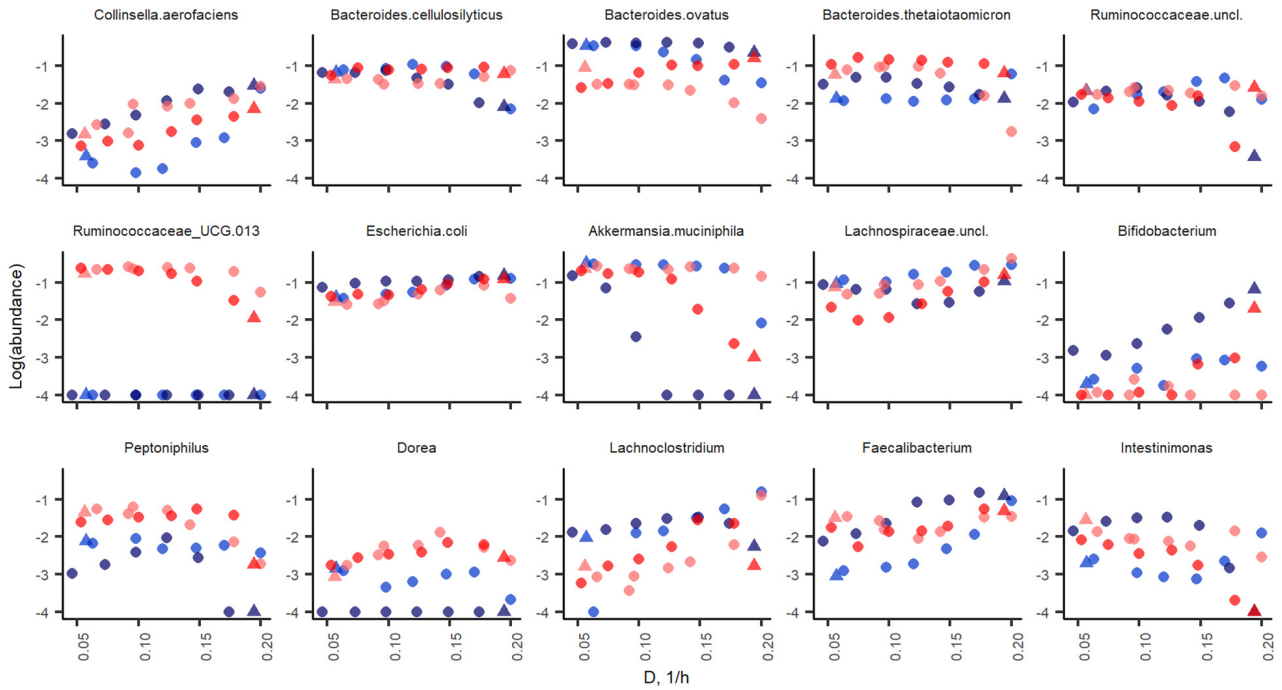

FIGURE 6 | Bacterial taxa enriched in apple pectin (red) and xylan (blue) medium during A-stat (light color) and De-stat (dark color) experiments. Color indicates the fiber source in the medium (red, apple pectin; blue, birch xylan). D-dilution rate (1/h). Only taxa those of which abundance was changed during experiments are shown.

the following culture characteristics. Therefore, the microbiota and metabolite patterns were comparatively analyzed in A-stat and De-stat cultures in a defined base medium containing mucin and either apple pectin or xylan. Similar microbiota and metabolite structures were observed within the scanned range of dilution rates in both directions, from D = 0.05 to 0.2 1/h or vice versa. The data of the steady state point of the chemostat at D = 0.2 1/h and the end point of the A-stat (D = 0.2 1/h) coincided well. Thus, the fecal culture was able to adapt to the change rate applied. This shows that by using suitable acceleration or deceleration rates it is possible to achieve a state of culture comparable to those of classical chemostat cultures. This is new information for consortia cultivation, although it has long been known for pure cultures.

In a previous De-stat study with fecal samples from children (5–15 years old), similar structural changes in the fecal microbiota were seen (Adamberg and Adamberg, 2018). This suggests that for this age group adult-like microbiota are mostly established. Moreover, these data indicate the crucial role of the growth rate in metabolism and the structure of colon microbiota. For example, in both studies, the taxa clearly preferring high dilution rates were *C. aerofaciens*, *Bifidobacterium*, *B. vulgatus*, *E. coli*, *Lachnospira* and *Lachnoclostridium*, whereas *A. muciniphila* and the Ruminococcaceae group UCG-013 were enriched at low dilution rates. Accordingly, *in vivo* studies have shown that *Akkermansia* and ruminococci are more prevalent in people with slow colonic transit, while *Bifidobacterium* and *Lachnospiraceae* correlate with high transit rates (Kim et al., 2015; Roager et al., 2016; Vandeputte et al., 2016). The impact of pectin structure on the dynamics metabolism and fecal microbiota has been shown by Larsen et al. (2019). Highly methoxylated pectins were shown to stimulate *F. prausnitzii*, commonly referred to as a health-promoting species. In both of our studies with apple pectin, the abundance of *Faecalibacterium* was 1-7% of the total population within the whole range of dilution rates, indicating the importance of pectin for the growth of colonic *Faecalibacterium* (the current study, and Adamberg and Adamberg, 2018).

Similarities between child and adult fecal pools were also observed at the metabolic level, but with some minor differences. Although the abundances of *Faecalibacterium* in adult and child cultures were similar (1.9–5.2% and 4.5–7.5%, respectively), about twice as much butyrate and CO_2 were produced by adults' than by children's consortia at slow dilution rates, suggesting higher activity of the butyrate producers in adult microbiota. The dynamics of other metabolites, including BCFA and H_2S, from the degradation of amino acids was comparable in both fecal consortia. The enhanced production of propionate, as well as the extensive use of amino acids and BCFA formation at low specific growth rates, may be related to a shortage of energy, ammonia, or NAD^+ regeneration. These properties are known for pure cultures (Tempest, 1984) but seem to also be common for fecal microbial consortia (Adamberg and Adamberg, 2018). K_s values of carbohydrates and amino acids

for different species should be measured to determine the carbon or nitrogen limitation, but these data are very scarce for gut bacteria.

The application of changestat makes it possible to elucidate the mechanisms of the co-existence of different bacteria by adapting mixed cultures under different environmental conditions. The cultivation of microbial consortia instead of single cultures is a promising approach for several biotechnological applications, including the development of multi-strain probiotics or material for fecal transplantation. As mentioned above, this and previous studies reveal that various consortia can be generated using continuous cultivation strategies. Still, the question remains of how to produce safe consortia with desired properties and/or therapeutic effects. Thus, detailed information is needed about selective pressure on the development of bacterial consortia under various environmental conditions: pH, the availability and concentration of substrate, dilution rate, selective additives, defining the inocula, etc. The changestat approach makes it possible to scan selected environmental conditions in an adaptive manner; providing an opportunity to predict appropriate conditions for the development of a consortium with a desired bacterial pattern.

CONCLUSION

The changestat experiments presented in this paper showed that continuous cultures of complex fecal consortia are reproducible in chemostat. Similar microbiota and metabolite changes were observed within the scanned range of dilution rates in changestat cultures in both directions, from $D = 0.05$ to 0.2 1/h or vice versa. This is new information for consortia cultivation, although it has long been known for pure cultures.

Our work confirmed that dilution rate is a crucial trigger in consortia development. Some species, such as propionate-producing *B. ovatus* and *B. vulgatus* and butyrate-producing *Faecalibacterium,* were prevalent within the whole range of dilution rates, while the mucin-degrading bacterium *A. muciniphila* and some ruminococci were enriched at low dilution rates only.

The production of organic acids and gases from pectin in the presence of mucin was related to the dilution rate in chemostat cultures. The ratio of acetate, propionate and butyrate was 5:2:1 at $D = 0.5$ 1/h and 14:2:1 at $D = 0.2$ 1/h. Most amino acids were completely depleted from the medium except for alanine and BCAA, which were metabolized to isobutyric and isovaleric acids in chemostat as well as changestat cultures.

For further analysis of the interactions in complex consortia, other gut-relevant environmental conditions and substrates available in the colon will be studied. It should be stressed that, in addition to high-throughput sequencing analysis, it is necessary to concentrate on the growth and metabolism of fecal consortia to work out novel methods for bacterial therapies. Changestat cultures make it possible to screen the combined effects of important environmental and feed parameters, such as acidity, temperature, medium composition, dilution rate, and the effects of inocula and multiple substrates.

DATA AVAILABILITY STATEMENT

The datasets analyzed for this study can be found in the European Nucleotide Archive on the site PRJEB33931 (ERP116764, dataset name "Run26_cult2").

ETHICS STATEMENT

The studies involving human participants were reviewed and approved by the Tallinn Medical Research Ethics Committee, Estonia (protocol No. 554). The patients/participants provided their written informed consent to participate in this study.

AUTHOR CONTRIBUTIONS

KA and SA designed the study. KA, GR, and SA carried out the experiments and data analyses. KA drafted the first manuscript. GR and SA contributed by writing and editing the final manuscript. All authors approved the submitted version.

FUNDING

This work was supported by the Estonian Ministry of Science and Education, Project number IUT1927.

ACKNOWLEDGMENTS

We would like to thank the Estonian Ministry of Science and Education for their funding. We are grateful to Betti Nigul for help in performing the growth experiments and Madis Jaagura for carrying out the bioinformatic analyses.

SUPPLEMENTARY MATERIAL

The Supplementary Material for this article can be found online at: https://www.frontiersin.org/articles/10.3389/fbioe.2020.00024/full#supplementary-material

FIGURE S1 | On-line measured data that are used for stability analyses during chemostat before A-stat (left side figures) or De-stat (right side figures) experiments. Upper figures show data in xylan + mucin medium and lower figures in apple pectin medium. Base rate, titration rate of 1M NaOH (ml/min); rGas, gas production rate (ml/min); D, dilution rate (1/h).

TABLE S1 | Abundances of bacteria in the inocula and samples from A-stat and De-stat experiments.

TABLE S2 | Production of metabolites per carbohydrate consumed (mol/mol-carbohydrates and mmol/gDW), carbon recovery, and biomass yield (gDW/g-carbohydrates) during A-stat and De-stat experiments.

REFERENCES

Adamberg, K., and Adamberg, S. (2018). Selection of fast and slow growing bacteria from fecal microbiota using continuous culture with changing dilution rate. *Microb. Ecol. Health Dis.* 29:1549922. doi: 10.1080/16512235.2018.1549922

Adamberg, K., Kolk, K., Jaagura, M., Vilu, R., and Adamberg, S. (2018). The composition and metabolism of faecal microbiota is specifically modulated by different dietary polysaccharides and mucin: an isothermal microcalorimetry study. *Benef. Microbes* 9, 21–34. doi: 10.3920/BM2016.0198

Adamberg, K., Seiman, A., and Vilu, R. (2012). Increased biomass yield of *Lactococcus lactis* by reduced overconsumption of amino acids and increased catalytic activities of enzymes. *PLoS One.* 7:e48223. doi: 10.1371/journal.pone.0048223

Adamberg, K., Valgepea, K., and Vilu, R. (2015). Advanced continuous cultivation methods for systems microbiology. *Microbiolgy* 161, 1707–1719. doi: 10.1099/mic.0.000146

Aguirre, M., Eck, A., Koenen, M. E., Savelkoul, P. H. M., Budding, A. E., and Venema, K. (2015). Evaluation of an optimal preparation of human standardized fecal inocula for in vitro fermentation studies. *J. Microbiol. Methods* 117, 78–84. doi: 10.1016/j.mimet.2015.07.019

Brahma, S., Martínez, I., Walter, J., Clarke, J., Gonzalez, T., Menon, R., et al. (2017). Impact of dietary pattern of the fecal donor on in vitro fermentation properties of whole grains and brans. *J. Funct. Foods* 29, 281–289. doi: 10.1016/j.jff.2016.12.042

Burkitt, D. P., Walker, A. R. P., and Painter, N. S. (1972). Effect of dietary fibre on stools and transit-times, and its role in the causation of disease. *Lancet* 30, 1408–1411. doi: 10.1016/s0140-6736(72)92974-1

Bussolo de Souza, C., Jonathan, M., Saad, S. M. I., Schols, H. A., and Venema, K. (2019). Degradation of fibres from fruit by-products allows selective modulation of the gut bacteria in an in vitro model of the proximal colon. *J. Funct. Foods* 57, 275–285. doi: 10.1016/j.jff.2019.04.026

Chung, W. S. F., Walker, A. W., Louis, P., Parkhill, J., Vermeiren, J., Bosscher, D., et al. (2016). Modulation of the human gut microbiota by dietary fibres occurs at the species level. *BMC Biol.* 14:3. doi: 10.1186/s12915-015-0224-3

Chung, W. S. F., Walker, A. W., Vermeiren, J., Sheridan, P. O., Bosscher, D., Garcia-Campayo, V., et al. (2019). Impact of carbohydrate substrate complexity on the diversity of the human colonic microbiota. *FEMS Microbiol. Ecol.* 95:fiy201. doi: 10.1093/femsec/fiy201

Cummings, J. H., Jenkins, D. J. A., and Wiggins, H. S. (1976). Measurement of the mean transit time of dietary residue through human gut. *Gut* 17, 210–218. doi: 10.1136/gut.17.3.210

Fallingborg, J., Christensen, L. A., Ingeman-Nielsen, M., Jacobsen, B. A., Abildgaard, K., and Rasmussen, H. H. (1989). PH-profile and regional transit times of the normal gut measured by a radiotelemetry device. *Aliment. Pharmacol. Ther.* 3, 605–613.

Freter, R., Stauffer, E., Cleven, D., Holdeman, L., and Moore, W. E. C. (1983). Continuous-flow cultures as in vitro models of the ecology of large intestinal flora. *Infect. Immun.* 39, 666–675. doi: 10.1128/iai.39.2.666-675.1983

Gottschal, J. C. (1990). Different types of continuous culture in -ecological studies. *Methods Microbiol.* 22, 87–124. doi: 10.1016/s0580-9517(08)70240-x

Jorup-Rönström, C., Håkanson, A., Sandell, S., Edvinsson, O., Midtvedt, T., Persson, A. K., et al. (2012). Fecal transplant against relapsing Clostridium difficile-associated diarrhea in 32 patients. *Scand. J. Gastroenterol.* 47, 548–552. doi: 10.3109/00365521.2012.672587

Kasemets, K., Drews, M., Nisamedtinov, I., Adamberg, K., and Paalme, T. (2003). Modification of a-stat for the characterization of microorganisms. *J. Microbiol. Methods* 55, 187–200. doi: 10.1016/S0167-7012(03)00143-X

Kim, S. E., Choi, S. C., Park, K. S., Park, M. I., Shin, J. E., Lee, T. H., et al. (2015). Change of fecal flora and effectiveness of the short-term VSL#3 probiotic treatment in patients with functional constipation. *J. Neurogastroenterol. Motil.* 21, 111–120. doi: 10.5056/jnm14048

Klindworth, A., Pruesse, E., Schweer, T., Peplies, J., Quast, C., Horn, M., et al., (2013). Evaluation of general 16S ribosomal RNA gene PCR primers for classical and next-generation sequencing-based diversity studies. *Nucleic Acids Res.* 41, 1–11. doi: 10.1093/nar/gks808

Lagier, J.-C., Armougom, F., Million, M., Hugon, P., Pagnier, I., Robert, C., et al. (2012). Microbial culturomics: paradigm shift in the human gut microbiome study. *Clin. Microbiol. Infect.* 18, 1185–1193. doi: 10.1111/1469-0691.12023

Langendijk, P., Schut, F., Jansen, G., Raangs, G., Kamphuis, G., Wilkinson, M., et al., (1995). Quantitative fluorescence in situ hybridization of *Bifidobacterium* spp. with genus-specific 16S rRNA-targeted probes and its application in fecal samples. *Appl. Environ. Microbiol.* 61, 3069–3075.

Larsen, N., Bussolo de Souza, C., Krych, L., Cahú, T. B., Wiese, M., Kot, W., et al. (2019). Potential of pectins to beneficially modulate the gut microbiota depends on their structural properties. *Front. Microbiol.* 10:223. doi: 10.3389/fmicb.2019.00223

Macfarlane, S., Quigley, M. E., Hopkins, M. J., Newton, D. F., and Macfarlane, G. T. (1998). Polysaccharide degradation by human intestinal bacteria during growth under multi-substrate limiting conditions in a three-stage continuous culture system. *FEMS Microbiol. Ecol.* 26, 231–243. doi: 10.1016/S0168-6496(98)00039-7

McDonald, J. A. K., Schroeter, K., Fuentes, S., Heikamp-deJong, I., Khursigara, C. M., de Vos, W. M., et al. (2013). Evaluation of microbial community reproducibility, stability and composition in a human distal gut chemostat model. *J. Microbiol. Methods* 95, 167–174. doi: 10.1016/j.mimet.2013.08.008

Miller, T. L., and Wolin, M. J. (1981). Fermentation by the human large intestine microbial community in an in vitro semicontinuous culture system. *Appl. Environ. Microbiol.* 42, 400–407. doi: 10.1128/aem.42.3.400-407.1981

Paalme, T., Kahru, A., Elken, R., Vanatalu, K., Tiisma, K., and Vilu, R. (1995). The computer-controlled continuous culture of *Escherichia Coli* with smooth change of dilution rate (A-Stat). *J. Microbiol. Methods* 24, 145–153. doi: 10.1016/0167-7012(95)00064-x

Petrof, E. O., Gloor, G. B., Vanner, S. J., Weese, S. J., Carter, D., Daigneault, M. C., et al. (2013). Stool substitute transplant therapy for the eradication of clostridium difficile infection: 'RePOOPulating' the gut. *Microbiome* 1:3. doi: 10.1186/2049-2618-1-3

Rajilić-Stojanović, M., Heilig, H. G. H. J., Molenaar, D., Kajander, K., Surakka, A., Smidt, H., et al. (2009). Development and application of the human intestinal tract chip, a phylogenetic microarray: analysis of universally conserved phylotypes in the abundant microbiota of young and elderly adults. *Environ. Microbiol.* 11, 1736–1751. doi: 10.1111/j.1462-2920.2009.01900.x

Roager, H. M., Hansen, L. B. S., Bahl, M. I., Frandsen, H. L., Carvalho, V., Gøbel, R. J., et al. (2016). Colonic transit time is related to bacterial metabolism and mucosal turnover in the gut. *Nat. Microbiol.* 1:16093. doi: 10.1038/nmicrobiol.2016.93

Rowland, I., Gibson, G., Heinken, A., Scott, K., Swann, J., Thiele, I., et al. (2018). Gut microbiota functions: metabolism of nutrients and other food components. *Eur. J. Nutr.* 57, 1–24. doi: 10.1007/s00394-017-1445-8

Russell, J. B., and Baldwin, R. L. (1979). Comparison of substrate affinities among several rumen bacteria: a possible determinant of rumen bacterial competition. *Appl. Environ. Microbiol.* 37, 531–536. doi: 10.1128/aem.37.3.531-536.1979

Sender, R., Fuchs, S., and Milo, R. (2016). Are we really vastly outnumbered? Revisiting the ratio of bacterial to host cells in humans. *Cell* 164, 337–340. doi: 10.1016/j.cell.2016.01.013

Sghir, A., Chow, J. M., and Mackie, R. I. (1998). Continuous culture selection of bifidobacteria and lactobacilli from human faecal samples using fructooligosaccharide as selective substrate. *J. Appl. Microbiol.* 85, 769–777. doi: 10.1111/j.1365-2672.1998.00590.x

Tannock, G. W. (2017). *Understanding Bowel Bacteria*. Hoboken, NJ: John Wiley & Sons, Inc.

Tempest, D. (1984). The status of YATP and maintenance energy as biologically interpretable phenomena. *Annu. Rev. Microbiol.* 38, 459–486. doi: 10.1146/annurev.micro.38.1.459

Valgepea, K., Adamberg, K., and Vilu, R. (2011). Decrease of energy spilling in *Escherichia coli* continuous cultures with rising specific growth rate and carbon wasting. *BMC Syst. Biol.* 5, 106.

Vandeputte, D., Falony, G., Vieira-Silva, S., Tito, R. Y., Joossens, M., and Raes, J. (2016). Stool consistency is strongly associated with gut microbiota richness and composition. Enterotypes and bacterial growth rates. *Gut* 65, 57–62. doi: 10.1136/gutjnl-2015-309618

von Martels, J. Z. H., Sadabad, M. S., Bourgonje, A. R., Blokzijl, T., Dijkstra, G., Faber, K. N., et al. (2017). The role of gut microbiota in health and disease: *in vitro* modeling of host-microbe interactions at the aerobe-anaerobe interphase of the human gut. *Anaerobe* 44, 3–12. doi: 10.1016/j.anaerobe.2017.01.001

Yen, S., McDonald, J. A. K., Schroeter, K., Oliphant, K., Sokolenko, S., Blondeel, E. J. M., et al. (2015). Metabolomic analysis of human fecal microbiota: a comparison of feces-derived communities and defined mixed communities. *J. Proteome Res.* 14, 1472–1482. doi: 10.1021/pr501247

Conflict of Interest: The authors declare that the research was conducted in the absence of any commercial or financial relationships that could be construed as a potential conflict of interest.

frontiers in Bioengineering and Biotechnology

ORIGINAL RESEARCH
published: 11 February 2020
doi: 10.3389/fbioe.2020.00051

Bioproduct Potential of Outdoor Cultures of *Tolypothrix* sp.: Effect of Carbon Dioxide and Metal-Rich Wastewater

*Chinnathambi Velu[1], Samuel Cirés[1,2], Diane L. Brinkman[3] and Kirsten Heimann[1,4]**

[1] North Queensland Algal Identification Facility, Aquaculture, College of Science and Engineering, James Cook University, Townsville, QLD, Australia, [2] Departamento de Biología, Universidad Autónoma de Madrid, Madrid, Spain, [3] Australian Institute of Marine Science (AIMS), Townsville, QLD, Australia, [4] Centre for Marine Bioproducts Development (CMBD), College of Medicine and Public Health, Flinders University, Bedford Park, SA, Australia

Rising CO_2 levels, associated climatic instability, freshwater scarcity and diminishing arable land exacerbate the challenge to maintain food security for the fast growing human population. Although coal-fired power plants generate large amounts of CO_2 emissions and wastewater, containing environmentally unsafe concentrations of metals, they ensure energy security. Nitrogen (N_2)-fixation by cyanobacteria eliminate nitrogen fertilization costs, making them promising candidates for remediation of waste CO_2 and metals from macronutrient-poor ash dam water and the biomass is suitable for phycocyanin and biofertilizer product development. Here, the effects of CO_2 and metal mixtures on growth, bioproduct and metal removal potential were investigated for the self-flocculating, N_2-fixing freshwater cyanobacterium *Tolypothrix* sp. *Tolypothrix* sp. was grown outdoors in simulated ash dam wastewater (SADW) in 500 L vertical bag suspension cultures and as biofilms in modified algal-turf scrubbers. The cultivation systems were aerated with air containing either 15% CO_2 (v/v) or not. CO_2-fertilization resulted in ∼1.25- and 1.45-fold higher biomass productivities and ∼40 and 27% increased phycocyanin and phycoerythrin contents for biofilm and suspension cultures, respectively. CO_2 had no effect on removal of Al, As, Cu, Fe, Sr, and Zn, while Mo removal increased by 37% in both systems. In contrast, Ni removal was reduced in biofilm systems, while Se removal increased by 73% in suspension cultures. Based on biomass yields and biochemical data obtained, net present value (NPV) and sensitivities analyses used four bioproduct scenarios: (1) phycocyanin sole product, (2) biofertilizer sole product, (3) 50% phycocyanin and 50% biofertilizer, and (4) 100% phycocyanin and 100% biofertilizer (residual biomass) for power station co-located and not co-located 10 ha facilities over a 20-year period. Economic feasibility for the production of food-grade phycocyanin either as a sole product or with co-production of biofertilizer was demonstrated for CO_2-enriched vertical and raceway suspension cultures raised without nitrogen-fertilization and co-location with power stations significantly increased profit margins.

Keywords: biofertilizer, bioremediation, metals, biorefinery, coal-fired power, phycobiliproteins, nitrogen-fixing cyanobacteria, economics

OPEN ACCESS

Edited by:
Manfred Zinn,
HES-SO Valais-Wallis, Switzerland

Reviewed by:
Sergio Revah,
Autonomous Metropolitan University, Mexico
Changhong Yao,
Sichuan University, China

***Correspondence:**
Kirsten Heimann
kirsten.heimann@flinders.edu.au

Specialty section:
This article was submitted to Bioprocess Engineering, a section of the journal Frontiers in Bioengineering and Biotechnology

Received: *29 October 2019*
Accepted: *22 January 2020*
Published: *11 February 2020*

Citation:
Velu C, Cirés S, Brinkman DL and Heimann K (2020) Bioproduct Potential of Outdoor Cultures of Tolypothrix sp.: Effect of Carbon Dioxide and Metal-Rich Wastewater. Front. Bioeng. Biotechnol. 8:51. doi: 10.3389/fbioe.2020.00051

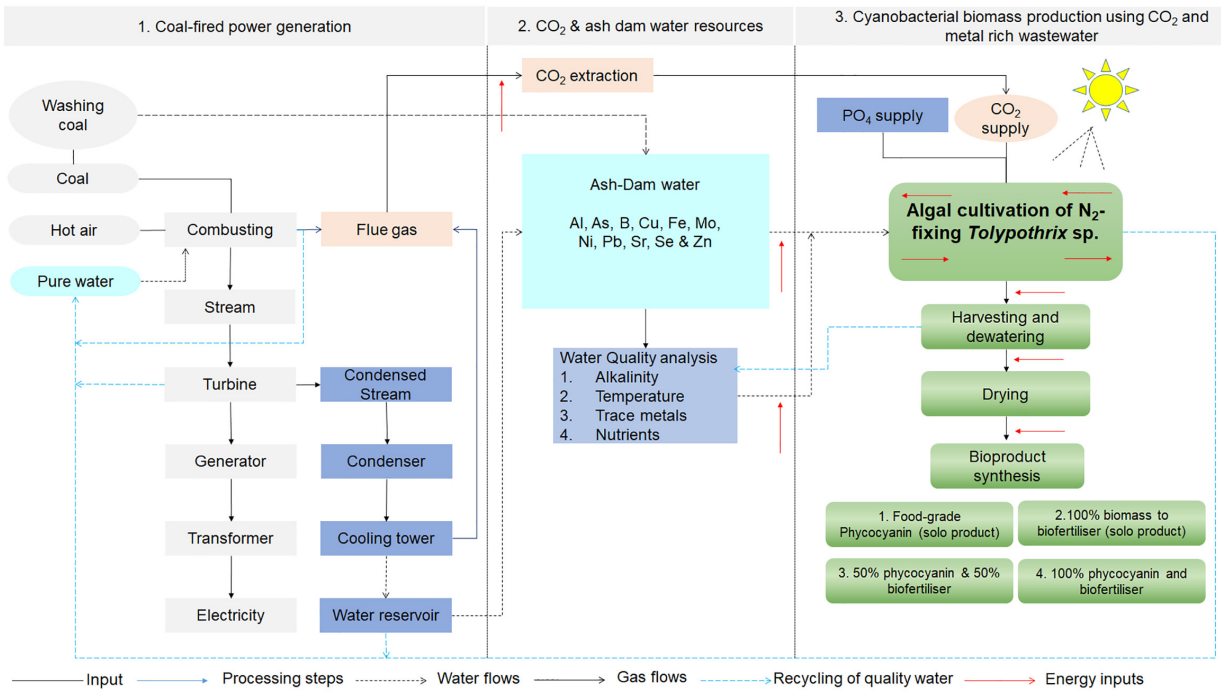

GRAPHICAL ABSTRACT | Framework for an integrated bio-economic model for co-locating cyanobacterial cultivation with coal-fired power station based on a biorefinery approach.

INTRODUCTION

Anthropogenic emissions of carbon dioxide (CO_2) account for 68% of total emissions (Ho et al., 2011), posing a threat to the global climatic equilibrium. At present, coal-powered electricity generation is still required in Australia and globally to meet energy requirements and – security (Stock, 2014). Flue gas from coal-fired power plants contain 10–15% CO_2 (v/v) and generate wastewater enriched with heavy metals (Artanto et al., 2014). Biological fixation of CO_2 and absorption of nutrients/metals from wastewaters by photosynthetic organisms such as microalgae and cyanobacteria is gaining industrial interest, as the biomass produced can yield a variety of high- and low-value renewable products (Wang et al., 2008). Wastewater generated at coal-fired power plants (ash dam water) cannot be discharged due to its potential toxicity and is therefore stored in ash dams (Roberts et al., 2015; Velu et al., 2019). The ash dam water contains metals, many of which serve as micronutrients important for plant growth, but macro-nutrients, such as nitrogen and phosphate, are lacking (Saunders et al., 2012). As the cultivation of eukaryotic photosynthetic organisms requires nitrogen and phosphate for growth, ash dam water needs to be supplemented with these macro-nutrients, increasing the cost of bioremediation and biomass production (Velu et al., 2019). In contrast, the cultivation of diazotrophic cyanobacteria does not require nitrogen fertilization, as these organisms can fix atmospheric nitrogen (N_2), making them an ideal choice for bioremediation of metals from nitrogen-limited wastewaters (Markou and Georgakakis, 2011). This is a clear advantage, as globally 85 million tons of nitrogenous fertilizer were used in 2000 for food production. Synthetic nitrogenous fertilizers are projected to not meet the demands of the ever growing human population in the near future (Singh et al., 2016). In addition, the current exploitation of chemically derived fertilizers have been shown to contribute to environmental problems, such as pollution, reduced soil fertility and adverse impacts on the ozone layer (Benemann, 1979; Singh et al., 2016). In an Australian context, agricultural productivity is declining in regions with marginal/leached soils, as microbial consortia, essential for soil fertility, are negatively affected by declining soil carbon contents. Soil fertility cannot be improved by provision of nitrogen without the addition of large amounts of carbon (QLD, 2016). Despite the realization of adverse impacts of synthetic nitrogenous fertilizers, ~5.3 million tonnes of chemical fertilizers were used on 49.1 million ha agricultural land in Australia between 2014–2015 (ABS, 2015). Thus, there is a pressing need for the sustainable production of innovative fertilizers that are effective, renewable, environmentally friendly, cost-efficient, and improve soil fertility to ensure food security in the future. In this context, fertilizers derived from biological nitrogen fixation and through recycling and re-use of nitrogen contained in various wastewaters offer great potential benefits (Benemann, 1979; Singh et al., 2016).

Nitrogen fixation is carried out by the oxygen-sensitive, iron and molybdenum-containing nitrogenase complex (Abed et al., 2009), resulting in higher iron and molybdenum requirements, elements that are present at elevated concentrations in ash dam wastewater (Saunders et al., 2012). While excessive metal concentrations can retard cyanobacterial growth

(Pereira et al., 2011), species such as *Anabaena subcylindrica*, *Aphanocapsa* sp., *Calothrix* sp., *Microcystis* sp., *Oscillatoria salina*, *Plectonema terebrans*, and *Synechococcus* sp. can be used for the treatment of domestic and industrial wastewater (Dubey et al., 2011). Biomineralisation of metals by cyanobacteria occurs via intracellular bioaccumulation and/or passive biosorption, the latter is mediated by the presence of an exopolysaccharide layer (EPS) on the outside of many cyanobacterial species (Pereira et al., 2011). The EPS consists of complex heteropolysaccharides on a glucosamine backbone, providing an accumulation of negative charges that play an essential role in the chelation of metal ions (De Philippis et al., 2011). On a dry weight basis, *Calothrix scopulorum* and *C. marchica* chelated 0.7 and 6.4% of lead (Weckesser et al., 1988; Ruangsomboon et al., 2007). *Nostoc muscorum* chelated 22.5, 11.8, 26.4, and 32% of copper, cobalt, lead and manganese, while *Anabaena subcylindrica* performed much better (81.8. 33.7, 100, and 100%, respectively) (El-Sheekh et al., 2005). The large differences in the biosorption of metals indicates that the choice of species is an important criterion to consider, especially when the reutilization of large volumes of wastewater is an important aspect of the industrial process. As CO_2-fertilization enhances cyanobacterial growth (Velu et al., 2015, 2019), EPS content will increase simultaneously, which should enhance metal chelation capacity of the cultures and, hence, remediation capacity. The presence of complex metals mixtures in industrial wastewaters may, however, result in competition for the same binding sites, which can result in reduced adsorption efficiencies (Pereira et al., 2011). The diazotrophic filamentous freshwater cyanobacterium, *Tolypothrix* sp. has been used for treatment of domestic and industrial wastewaters and *T. ceytonica* achieved an 86 and 64.4% efficiency for the removal of zinc and total suspended solids (El-Bestawy, 2008).

In addition to the exploitation of environmental services (CO_2 and metal remediation), the prokaryotic cyanobacteria show additional advantages for biotechnological applications, such as strain-dependent wide environmental tolerances, e.g., marine to freshwater, acid and/or alkaline conditions (Gupta et al., 2013), rapid growth and high photosynthetic activities (Hall et al., 1995). Furthermore, the produced biomass has multiple commercial applications through bioproduct development. In general, potential algal bioproducts include medicinal compounds, food and feed supplements (restricted to CO_2 enriched grown species without inclusion of metal- or other potentially toxic compound-containing wastewater treatment), pigments (e.g., β-carotene, astaxanthin, fucoxanthin, lutein, phycocyanin, phycoerythrin, the latter two from cyanobacteria), protein, carbohydrate, biofuel and biohydrogen, and biofertilizers (Setta et al., 2017; von Alvensleben and Heimann, 2019). Specific cyanobacterial bioproducts could be protein, mineral and unsaturated fatty acid supplements and the pigments phycocyanin and phycoerythrin from *Arthrospira platensis* or *Limnospira maxima* (formerly *Spirulina platensis* and *S. maxima*), where the protein content of the biomass can reach 74% (Cohen, 1997), which can be extracted through biorefining (Borowitzka, 2013). It might be argued that cyanobacterial biomass produced using metal-rich wastewater is not suitable for high-value phycocyanin product development. Indeed some binding of iron and mercury, the latter not present in ash dam water of coal-fired power plants used in this study, and less efficient binding of some other metals to phycocyanin has been described (Bermejo et al., 2008; Gelagutashvili and Tsakadze, 2013; Bhayani et al., 2016). It is, however, unclear how much binding would occur and how irreversible the binding would be. In addition, affinity of the metals present in ash dam water can be expected traditional metal chelating proteins, such as metallothioneins, and the highly negatively charged EPS, both present in cyanobacterial including *Tolypothrix* sp. biomass, would be more efficient binding sites. In addition, as proposed in this study, phycocyanin extracted from *Tolypothrix* sp. biomass will be purified to upgrade the product to food-grade phycocyanin to obtain a higher sales price, which would further remove any metals bound to phycocyanin. It will nonetheless be essential to analyze the final product for metal contents for quality assurance.

While light, temperature and CO_2 supplies can be easily controlled at laboratory scale, therefore producing best biomass yields, biomass productivities are typically reduced in large volume suspension-based systems, due to light and carbon limitation, particularly in raceway pond cultivation (Pierobon et al., 2018). Under outdoor large-scale cultivation conditions, improved solar and carbon supplies can be achieved in closed bioreactors, but this adds energy and infrastructure costs, limiting suitability to high-value product development (Pierobon et al., 2018). In contrast, cyanobacterial biofilm reactors are better suited for cost-effective biomass production and are frequently used for wastewater treatment (Hoh et al., 2016). Cyanobacterial biofilm cultivation requires minimal water supplies, gas exchange (CO_2 absorption and O_2 venting) is more efficient and harvesting is energy-efficient (Heimann, 2016). Recently developed porous substrate biofilm reactors show efficient light –, carbon – and water utilization and scale-up of this technology is easily possible, making them a promising technology for economical microalgal/microbial biomass production (Pierobon et al., 2018). For example, cyanobacterial biomass productivity was greater in rotating biofilm reactors without aeration or additional CO_2-supplementation compared to suspension reactors (Gross and Wen, 2014), but the adhesion process for mat establishment is sensitive to shear forces, and species- and substrate-dependent.

Integrated biomass production with wastewater and CO_2 emission-generating industries has many advantages, i.e., use of non-arable land, non-potable water and provision of trace metals, and CO_2 to support biomass and bioproduct productivities (Roberts et al., 2015; Moheimani, 2016; Aslam et al., 2019). Nonetheless, economic feasibility still needs to be demonstrated on a case-by-case basis, as outcomes are dependent on the value of the bioproduct(s) and yields. In addition, in the case of ash dam water generated at coal-fired power plants, metal toxicity may occur, reducing yields and application potential of generated bioproducts (Velu et al., 2019). Previous research established that the diazotrophic *Tolypothrix* sp. (isolated from tropical Australia) efficiently self-flocculates, reducing energy requirements for harvesting/dewatering of biomass by 90% (Heimann et al., 2013; Velu et al., 2015). Furthermore, no metal toxicity was observed for *Tolypothrix* sp. biomass production in simulated ash dam

water (SADW) and growth performance was independent of nitrogen supply, yet costs for phosphate fertilization are incurred (Velu et al., 2019). The graphical abstract illustrates the integrated production of *Tolypothrix* sp. biomass and potential bioproducts when co-located at a coal-fired power plant.

Therefore, this study used the Australian isolate of *Tolypothrix* sp. to contrast biomass productivities, metal removal capacity and bioproduct potential for biomass cultivated in simulated ash dam water (SADW) between a traditional bubble column reactor and a modified algal turf scrubber with and without CO_2 supplementation under outdoor conditions. Additionally, the economic feasibility for bioproduct development was estimated, considering four scenarios: (1) production of food-grade phycocyanin as a sole product, (2) biofertilizer as a sole product, (3) use of half the biomass for biofertilizer and food-grade phycocyanin production and (4) biorefining of the high-value phycocyanin with the residue being used as biofertilizer. This study modeled net present value (NPV) and sensitivity analysis for these four scenarios under conditions of co-location with coal-fired power plants and traditional cultivation (not co-located) for a 10 ha plant using suspension bubble columns and raceways for biomass production.

MATERIALS AND METHODS

Culture Collection and Strain Characterization

The diazotrophic, filamentous, freshwater cyanobacterial strain *Tolypothrix* sp. NQAIF319 was isolated and maintained as described in Velu et al. (2015).

Synthetic Ash Dam Wastewater Preparation

Synthetic ash dam wastewater was prepared as described in Velu et al. (2019) based on concentrations obtained for ash dam water of a Queensland coal-fired power plant, Australia (Saunders et al., 2012).

Outdoor Cultivation Set Up, Growth Estimation and Biochemical Profiling

Outdoor cultivation of *Tolypothrix* sp. NQAIF319 occurred in SADW in four meso-scale open bioreactor prototypes: (1) two algal turf scrubbers (ATS) of 2.2 m^2 each (2.2 m long × 1 m wide) (**Supplementary Figure S1** and **Supplementary Table S1**); (2) two suspension vertical bags of 500 L each with a 0.3 m^2 area footprint, designed and assembled at James Cook University Australia (**Supplementary Figure S2** and **Supplementary Table S2**). The cultivation area was shaded with a UV-shade cloth (Coolaroo, 3.66 m wide, 60% shading) to control photon flux density between 500 and 900 μmol m^{-2} s^{-1} at the Freshwater Compound at James Cook University, Townsville, Australia (19.33 S, 146.76 E). The plastic trays of the ATSs were lined with polystyrene for attachment of *Tolypothrix* sp. and had a slope of 7%. Water flow conditions were continuous at 66 L min^{-1} delivered from a sump with a 500 L fill volume beneath the ATS. The 500 L vertical bubbled suspension culture systems were constructed from PVC bag material contained in a wire cage with a plastic keeled footing of 0.3 m^2. A tap was fitted to the bottom corner of the vertical bag for harvesting, while aeration was provided by a suspended diffuser delivering 0.05 L air L^{-1} min^{-1} from the main compressor.

The two ATS tanks and two suspension vertical bags were filled with 500 L SADW. Outdoor culture inoculi (starter cultures) were grown in 20 L polycarbonate carboys in BG11 medium without nitrogen [BG11(-N)] at 28°C and a photon flux density of 100 μmol m^{-2} s^{-1} until cultures reached stationary phase. For inoculation of the vertical bag system, the starter cultures were centrifuged (8,000 × *g*, 20 min; Beckman Avanti® J-26XP, Australia) and an adequate volume of the cell pellet was resuspended into 500 L of fresh SADW medium to reach an initial biomass concentration of 0.1 g dry weight L^{-1}. The ATS were inoculated by spreading the centrifuged *Tolypothrix* sp. biomass to an initial concentration of 5 g DW m^{-2} without water flow. After an overnight attachment period, water was supplied to the top of the system via a baffle.

A total of 16-day growth experiments were simultaneously performed in both systems in two consecutive runs, during September 2016 (run 1) and October 2016 (run 2). In both runs, one set of each cultivation system was supplemented with CO_2-enriched air (15% v/v), while the other sets were supplied with air at atmospheric CO_2 levels (non-CO_2 controls). CO_2-enriched air and air were baffled in both cultivation systems. Gases were 99.9% pure, ISO certified and supplied by BOC, a member of the Linde Group, Townsville, Australia. Temperature and pH were monitored twice daily (WP-81, TPS Instruments, Australia) and irradiance was measured at the time of sampling with a LI-250A photosynthetic active radiation (PAR) light probe (LiCor, Biosciences, United States). The incident sun light at sample time varied between 500 and 700 μmol m^{-2} s^{-1}. Due to infrastructure and space limitations, replication for each system was carried out sequentially. Thus changes in the outdoor environmental parameters, such as light, temperature, and humidity, the latter especially affecting the biofilm cultivation system, is expected to additionally influence biomass production and metabolic profiles, rendering formal statistical analysis of the data inappropriate.

Samples were collected via a tap for the vertical suspension bag systems and by scraping a 100 cm^{-2} biofilm square (10 × 10 cm) using a silicone rubber cell scraper (IWAKI, Japan) every 4 days. Biomass growth (g DW m^{-2}) was determined gravimetrically. Biomass productivities (g DW m^{-2} day^{-1}) were calculated as per von Alvensleben et al. (2013), while doubling rate (k) and doubling time (T_2) calculations followed Gour et al. (2014). Water samples for nutrient and metal analyses were collected from the ATS sumps and the supernatant of the centrifuged samples of the vertical suspension culture systems. Culture media phosphate and metal concentrations followed procedures described in detail in Velu et al. (2019), and biomass growth (g DW m^{-2}) and productivity (g DW m^{-2} day^{-1}) was determined gravimetrically

(von Alvensleben et al., 2013) on days 0, 4, 8, 12, and 16. Biomass-specific growth rates (μ_{1-3}), doubling rate (k) and doubling time (T2) were calculated as per Gour et al. (2014) and von Alvensleben et al. (2013).

Biomass was harvested on day 16 and biomass pellets were freeze-dried (Dynavac model Fd12, Australia) and stored in the dark at −80°C (Sanyo MDF-U33V, Japan) until analyses. Procedures for analyses of pigments (phycocyanin and phycoerythrin), fatty acids (fatty acid methyl esters (FAME), total lipid, alkane/alkene, protein, carbohydrate and carbon, hydrogen, sulphur, phosphorous, potassium (CHNSPK) contents followed Velu et al. (2019).

All chemicals and solvents were obtained from Sigma-Aldrich, Sydney, Australia.

Net Present Value (NPV) and Sensitivity Analyses

A techno-economic cost assessment was used to evaluate the economic feasibility for production of food-grade phycocyanin and biofertilizer from *Tolypothrix* sp. biomass, assuming either co-location with a coal-fired power plant or traditional cultivation, which is classified here as biomass production solely for bioproduct development without co-location with either an industrial wastewater producer and/or CO_2 emitter. The following boundaries were set: (1) The algae cultivation plant has a 10 ha cultivation area and employs suspension-based open cultivation systems with an annual biomass production period of 300 days year^{-1}. (2) The operating life was set to 20 years. (3) Production data generated in this study in vertical suspension culture systems in SADW and supplied with 15% CO_2 (v/v) and average biomass productivities achieved for *Nannochloropsis oculata* in large-scale outdoor raceways formed the basis of the analyses. (4) All costs were adjusted to increase by 5% annually, while production sale prices were not adjusted. (5) Food-grade phycocyanin production assumed an extraction/purification efficiency of 67% (Chaiklahan et al., 2018) and a sale price for total phycocyanin of US$ 500 kg^{-1} (Querques et al., 2015), while the sale price for biofertilizer was estimated to be US$ 500 t^{-1}.

The NPV was calculated by difference between the present value of cash income and the present value of all cash expenditures following the equation

$$NPV = \sum_{t=1}^{r} \frac{C_t}{(1+r)^2} - C_0$$

where C_t is the net cash flow during the period t, C_0 is the total initial investment cost, t is the number of time periods (years) and r is the discount rate.

The weighted average costs of capital (WACC) was set to 10% and sensitivity analyses were performed for two scenarios: (1) a reduced biofertilizer price of 25% of the current value (US$ 125 t^{-1}) and (2) a reduced sales price for food-grade phycocyanin at 25% of today's price (US$ 125 kg^{-1}).

RESULTS

Effect of Culture System and CO_2-Supplementation on Growth and Phosphate Uptake of SADW-Grown *Tolypothrix* sp.

CO_2-supplementation enhanced growth of *Tolypothrix* sp. in both types of outdoor cultivation systems. A 1.15- and 1.26-times higher final biomass yield of 34 and 42 g DW m^{-2} was obtained for biofilm cultures (**Figure 1A**$_{1,2}$), while a 1.2- and 1.3-times higher yield in vertical suspension-based systems achieved a final biomass yield of 870 and 1310 g DW m^{-2} for runs 1 and 2, respectively (**Figure 1B**$_{1,2}$). Growth over the 16-day time course could be divided into two phases of specific growth rate ($\mu_{1,2}$) (**Table 1**). μ_1 was not affected by CO_2-supplementation for any of the cultivation systems, whereas μ_2 was ∼21 and 30% higher for biofilm cultures and ∼11 and 32% higher for vertical bag suspension cultures for runs 1 and 2, respectively, when CO_2 was supplied. The difference in μ_2 between the two systems is not surprising, as CO_2 requirements of the biofilms are supplemented by direct access to CO_2 from the atmosphere. As such, growth in the bubble column suspension system appears to be light- and CO_2-limited in dense cultures. CO_2-supplementation had no effect on doubling rates (k) in either cultivation system, but doubling time was generally reduced by 15% for suspension-grown *Tolypothrix* sp. Despite positive outcomes of CO_2-fertilization on biomass productivity (**Figures 1A**$_p$, **B**$_p$) and system-dependent differences in growth performance, phosphate removal from the medium were slightly higher when supplemented with CO_2, showing rapid uptake for the first 3 days of cultivation (**Figures 2A,B**). In contrast, phosphate removal rates (mg PO_4^{3-} g^{-1} DW d^{-1}) were higher for CO_2-supplemented suspension cultures, while no trends were discernible for biofilms (**Figures 2A**$_1$**,B**$_1$). Growth of *Tolypothrix* sp. was phosphate-limited from day 8, and systems were devoid of phosphate from days 16 and 12 for CO_2-supplemented cultures and non-CO_2 controls of biofilm and suspension cultures, respectively. Biomass-standardized phosphate uptake rates were 0.2 to 0.3 for biofilms, but only 0.0065 to 0.0074 mg PO_4^{3-} g^{-1} DW d^{-1} for suspension cultures and uptake rates were much lower for both cultivation systems from days 8 to 16, reflecting phosphate depletion from the SADW medium.

Effect of Culture System and CO_2-Supplementation on the Biochemical Profile of SADW-Grown *Tolypothrix* sp.

Carbohydrate, Protein, Lipid, Phycocyanin and Phycoerythrin Contents

CO_2-supplementation increased carbohydrate and lipid contents of *Tolypothrix* sp. by 16 and 25% for biofilms and 26 and 38% for suspension cultures for runs 1 and 2, respectively (**Figures 3A**$_1$**,B**$_1$). In contrast, effects of CO_2-supplementation on protein contents were marginal (**Figures 3A**$_1$**,B**$_1$). Maximal carbohydrate, protein and lipid contents were ∼49.2, 25.1,

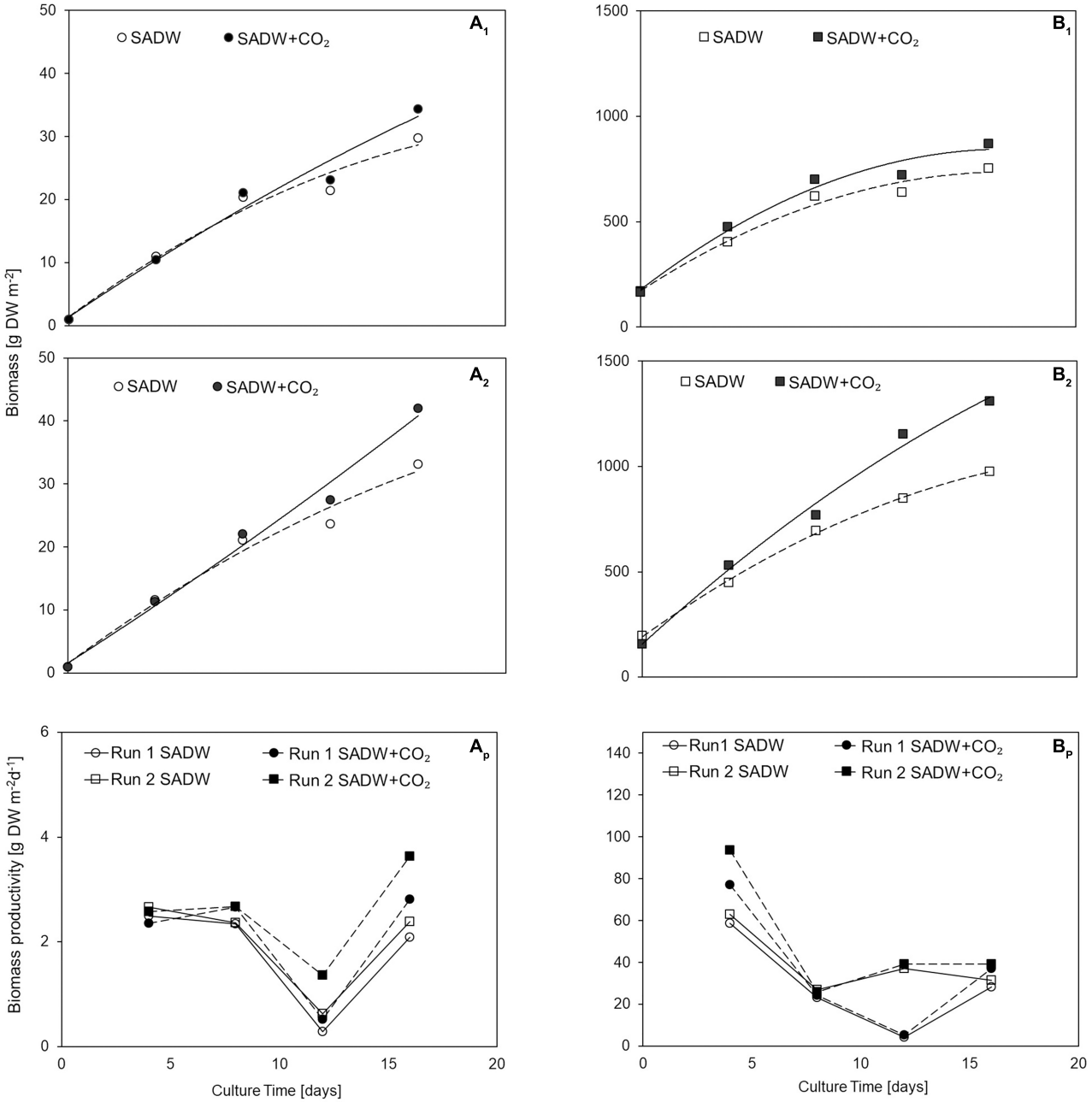

FIGURE 1 | Effect of heavy metal and CO_2 on *Tolypothrix* sp. growth in outdoor cultivation **(A_1)** ATS run 1, **(A_2)** ATS run 2, **(Ap)** ATS biomass productivity, **(B_1)** V. Bag run 1, **(B_2)** V. Bag run 2, **(Bp)** V. Bag biomass productivity.

and 12.4% of cell dry weight (DW) for *Tolypothrix* sp. biofilms and ∼54.7, 26.0, and 14.8% of DW for suspension cultures when fertilized with CO_2 (**Figures 3A**$_1$,**B**$_1$). Similarly, fertilization with 15% CO_2 (v/v) increased phycobiliprotein (phycocyanin, phycoerythrin) contents (% w/w) by ∼40 and 27% for *Tolypothrix* sp. biofilms and suspension cultures, respectively. Maximal phycocyanin and phycoerythrin productivities were 0.3, 0.2, 3.6, and 2.9 g m^{-2} d^{-1} for biofilms and suspension cultures, respectively (**Figures 3A,B**).

Fatty Acid and Elemental Composition

As growth, lipid and phycobiliprotein contents were increased under CO_2-fertilization, potential effects on fatty acid profiles and elemental composition (C, H, N, S, P, and K) and C/N ratios were investigated. Total fatty acid (TFA) contents and TFA productivities were ∼19 and 12% higher under CO_2 supply for *Tolypothrix* sp. biofilms and suspension cultures, respectively. Maximal TFA yields were ∼75 mg g^{-1} DW for biofilms and ∼38 and 47 mg g^{-1} DW for runs 1 and 2, respectively (**Table 2**).

TABLE 1 | Effect of CO_2 and heavy metals on growth of *Tolypothrix* sp. in outdoor cultivation.

	Outdoor cultivation system							
	Algal turf-scrubber				Vertical bag			
	SADW		SADW + CO_2		SADW		SADW + CO_2	
	Run 1	Run 2	Run 1	Run 2	Run 1	Run 2	Run 1	Run 2
Specific growth rate (μ_1) [d^{-1}]	0.377	0.381	0.381	0.386	0.162	0.159	0.180	0.199
(μ_2) [d^{-1}]	0.048	0.057	0.061	0.081	0.024	0.045	0.027	0.066
Doubling rate (k) [d^{-1}]	0.543	0.550	0.549	0.558	0.234	0.229	0.260	0.287
Doubling time (t_2)	1.841	1.818	1.820	1.793	4.268	4.371	3.840	3.482

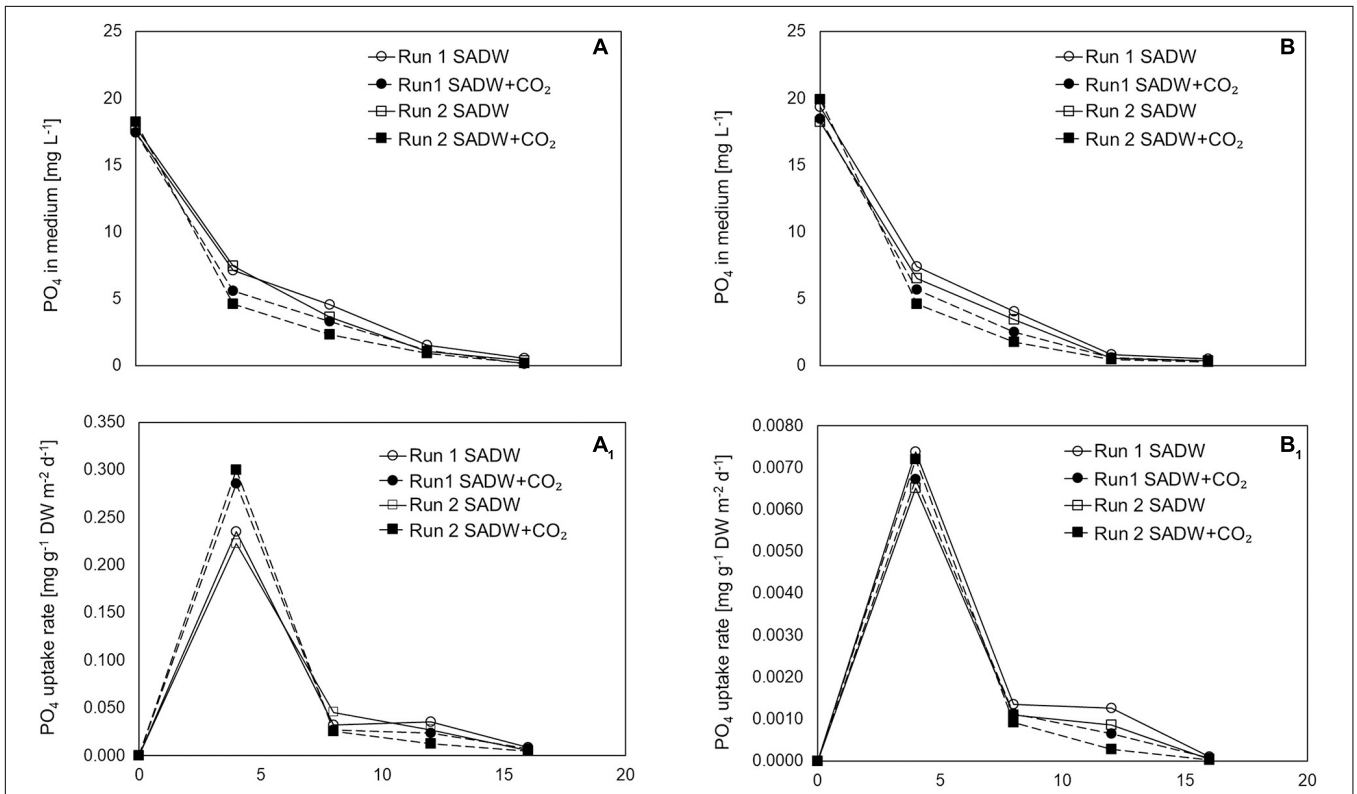

FIGURE 2 | Effect of heavy metal and CO_2 on culture medium phosphate levels and uptake rate of *Tolypothrix* sp. in outdoor cultivation. **(A,A$_1$)** ATS and **(B,B$_1$)** V. Bag.

A positive effect of CO_2-supplementation on saturated – (SFA), mono-unsaturated – (MUFA) and polyunsaturated fatty acid (PUFA) contents was noticeable for suspension-grown *Tolypothrix* sp., where the fatty acid profile was dominated by SFA, followed by PUFA and MUFA (**Table 2**). In contrast, responses to CO_2-fertilization varied between both runs for *Tolypothrix* sp. biofilms, especially for MUFA and PUFA (**Table 2**), possibly due to variations in co-habiting bacterial communities, which are present and required for biofilm establishment and stabilization. The most abundant fatty acids were palmitic (hexadecanoic) acid (C16:0), followed by the ω-3-group of fatty acids α-linolenic acid [C18:3 (*cis* 9. 12. 15)], myristoleic acid (C14:1), the SFA myristic acid (C14:0), linoleic acid [C18:2 (cis/*trans* 9, 12)], the ω-9 oleic acid (C18:1) and the ω-6 γ-linolenic acid [C18:3 (*cis* 6, 9, 12)] (**Table 2**).

CO_2-fertilization increased contents of C14:1, palmitoleic acid (C16:1), α-linolenic acid [C18:3 (*cis* 9. 12. 15)], C18:2 and C18:1 by 33, 31, 45, 72 and 48% in *Tolypothrix* sp. biofilms, respectively, while contents of C16:0 and C18:0 were unaffected. In contrast, CO_2-supplementation increased C16:0, C18:3, C18:2, and C18:1 by 25, 57, 33 and 32% for *Tolypothrix* sp. suspension cultures, respectively (**Table 2**).

Culture system and CO_2-supplementation did not result in large differences in C, H, N, S, P, and K contents. Carbon [∼45 and 47, and ∼47% (w/w)], K [∼0.79, 0.99, 0.68, and 0.79% (w/w)], and S [0.5, 0.7, and 0.7% (w/w)] were higher when supplemented

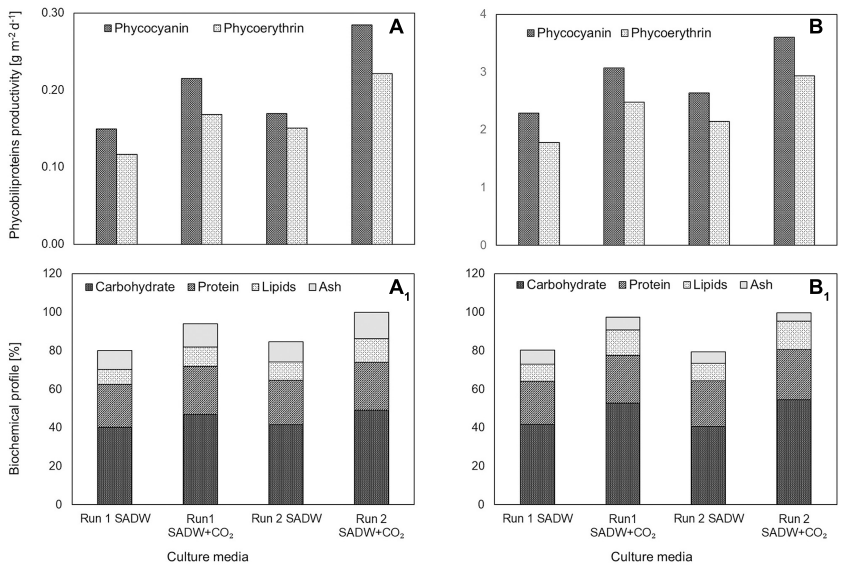

FIGURE 3 | Effect of heavy metal and CO_2 on pigments and biochemical profile of *Tolypothrix* sp. in outdoor cultivation. **(A,A$_1$)** ATS and **(B,B$_1$)** V. Bag.

TABLE 2 | Effect of CO_2 and heavy metals on fatty acid profiles of *Tolypothrix* sp. in outdoor cultivation.

Fatty acids [mg g^{-1} DW]	**Outdoor cultivation system**							
	Algal turf-scrubber – biofilm				**Vertical bag**			
	SADW		**SADW + CO_2**		**SADW**		**SADW + CO_2**	
	Run 1	**Run 2**	**Run 1**	**Run 2**	**Run 1**	**Run 2**	**Run 1**	**Run 2**
14:1 (*cis*-9)	8.6	6.0	9.6	12.2	1.4	1.7	1.0	1.0
14:0	6.0	7.5	0.7	8.6	1.6	1.5	0.9	1.9
16:1	9.8	9.5	7.7	20.1	3.9	3.7	0.9	0.9
16:0	13.0	14.2	11.8	13.1	8.0	11.0	10.9	14.9
18:3 (*cis*-6, 9,12)	2.2	4.9	0.2	0.2	1.2	1.7	1.5	1.5
18:3 (*cis*-9,12,15)	10.1	7.1	18.5	13.0	1.4	4.7	6.1	8.1
18:2 (*cis/trans*-9,12)	1.0	1.6	8.9	0.4	2.6	3.3	4.4	4.5
18:1 (*cis/trans*-9)	3.0	2.7	7.6	3.4	3.0	5.0	4.9	6.9
18:0	0.2	0.2	0.5	0.2	1.2	1.3	1.2	1.8
SFA [mg g^{-1} FA]	20.7	22.9	14.9	23.8	13.5	17.5	15.1	20.0
MUFA [mg g^{-1} FA]	25.8	18.5	23.1	36.6	8.7	10.7	7.4	9.4
PUFA [mg g^{-1} FA]	13.4	14.6	33.7	13.5	8.9	12.8	14.8	17.9
Total Fatty acids [mg g^{-1} DW]	59.9	60.1	74.6	73.9	31.0	41.0	38.3	47.3
FA productivity [g g^{-1} DW m^{-2} d^{-1}]	0.2	0.1	0.2	0.3	1.1	1.3	1.4	1.9

with CO_2 for *Tolypothrix* sp. biofilms and suspension cultures in runs 1 and 2, respectively (**Table 3**). A small positive effect of CO2-fertilization on nitrogen content and C/N ratios was also evident for *Tolypothrix* sp. biofilms, but not for suspension cultures (**Table 3**). In contrast, CO_2 supply had a positive effect on P content of suspension cultures, but not biofilms (**Table 3**).

Metal Removal

A total of 16-day time course experiments investigated the effect of cultivation system and CO_2 on metal removal from SADW, containing metals and concentrations typically found in ash dam water of coal-fired power plants, by *Tolypothrix* sp. (**Table 4**). Cultivation system and CO_2-fertilization had no effect on maximal cumulative metal removal (Al, Sr, and Zn ($\geq$90%), followed by Cu and Fe ($\sim$70–80%), and As [$\sim$65–75%)] for both biofilms and suspension cultures. In contrast, CO_2-supplementation increased Mo removal by 37% in both cultivation systems, but an additional cultivation system effect was evident under CO_2-fertilization, i.e., maximal Mo removal was $\sim$98% for biofilms but only $\sim$60% for suspension cultures. Conversely, a cultivation system effect was evident under CO_2 supply for Se removal, with a 73% increase but a slight

TABLE 3 | Effect of CO_2 and heavy metals on the elemental composition of *Tolypothrix* sp. in outdoor cultivation.

Elements [%]	Outdoor cultivation system							
	Algal turf-scrubber - biofilm				Vertical bag - suspension			
	SADW		SADW + CO_2		SADW		SADW + CO_2	
	Run 1	Run 2	Run 1	Run 2	Run 1	Run 2	Run 1	Run 2
Carbon (C)	41.21	44.38	45.12	47.0	43.17	44.53	47.43	47.47
Hydrogen (H)	6.42	7.18	7.07	7.03	6.99	7.21	7.10	7.13
Nitrogen (N)	6.63	6.88	7.18	7.01	7.18	7.33	7.05	7.06
Sulfur (S)	0.25	0.37	0.46	0.65	0.41	0.47	0.69	0.67
Phosphorous (P)	2.48	2.56	2.41	2.57	0.70	0.98	1.53	1.74
Potassium (K)	0.46	0.71	0.80	0.99	0.44	0.51	0.68	0.79
C/N ratio (C: N)	6.21	6.45	6.28	6.70	6.01	6.08	6.73	6.72

TABLE 4 | Effect of CO_2 on cumulative metal removal from SADW medium by *Tolypothrix* sp. over a 16-day time course.

Metals	Initial concentration [$\mu g\ L^{-1}$]	Metal removal in outdoor cultivation system [%]							
		Algal turf-scrubber - biofilm				Vertical bag - suspension			
		SADW		SADW + CO_2		SADW		SADW + CO_2	
		Run 1	Run 2	Run 1	Run 2	Run 1	Run 2	Run 1	Run 2
Al	200.00	99.8	99.8	99.8	99.8	99.8	99.8	99.8	99.8
As	31.60	70.0	68.4	69.0	69.0	67.4	63.5	75.7	75.7
Cu	38.20	83.2	82.3	79.5	74.3	76.2	72.5	77.2	77.2
Fe	1110.00	81.0	79.5	75.7	65.5	72.4	70.8	79.7	76.9
Mo	1040.00	63.6	58.9	98.9	98.9	38.9	27.5	60.3	60.3
Ni	22.90	80.1	79.1	57.5	57.5	69.6	63.7	68.3	54.6
Se	174.00	82.5	81.7	77.8	77.7	23.2	12.3	84.2	84.2
Sr	830.97	99.2	99.1	98.6	98.4	98.8	98.8	99.3	99.0
Zn	90.70	94.0	93.5	90.8	90.6	100.0	87.00	100.0	98.0

decrease for suspension-cultivated *Tolypothrix* sp. and biofilms, respectively. An even stronger cultivation effect was observed for Ni, where CO_2-supplementation negatively affected removal in biofilm cultures, but not suspension cultures of *Tolypothrix* sp.

Economic Viability Assessment of Bioproduct Commercialization Derived From SADW-Produced *Tolypothrix* sp. Biomass – Effect of Co-location With Coal-Fired Power Plants

Direct and Indirect Capital and Operational Costs

Based on the biomass productivities and biochemical profiles achieved with CO_2 supplementation of SADW-grown *Tolypothrix* sp. in vertical bubble column suspension cultures, NPV analyses assessed the economic viability of four bioproduct scenarios under co-location with coal-fired power stations and traditional cultivation (no co-location) in raceway ponds, commonly used for production at commercial scale. The four bioproduct scenarios modeled were: (1) food-grade phycocyanin as the sole product, (2) biofertilizer as the sole product, (3) 50% of biomass used each for food-grade phycocyanin and biofertilizer production, and (4) biorefining of phycocyanin (100%) and use of the extracted biomass as a biofertilizer (**Table 5**). All capital costs and operating costs for *Tolypothrix* sp. cultivation (**Table 5**) were derived from published data for production of microalgal biomass (Davis et al., 2011; Griffin and Batten, 2013; Heimann et al., 2015; Schenk, 2016; Doshi, 2017; Fornarelli et al., 2017). Direct and indirect capital costs (engineering fees set at 15% of capital and contingency set at 5% of capital) for building a 10 ha production facility and some operational expenses were considered to be unavoidable. The co-location scenario considered savings on capital costs (land acquisition) and operational costs for maintenance and insurance, water (ash dam wastewater) and CO_2 supply (flue gas) (**Table 5**), but did not apply potential income generated through CO_2 emission reduction and wastewater treatment, as these were deemed covered by the savings made. Irrespective of location scenario, the lack of nitrogen-fertilization and the benefits of the self-settling properties of *Tolypothrix* sp. on energy saving for harvesting were considered by applying no costs for

TABLE 5 | Microalgal culturing facility capital and operating costs, product income potential, net profit value and sensitivity analyses.

Size of *Tolypothrix* facility [ha]	**10**		
Microalgal culturing facility costs			
Direct unavoidable capital costs	**Units**	**Cost (USD) ha^{-1}**	**Cost (USD) 10 ha^{-1}**
Open raceway pond construction	\$ ha^{-1}	35,436	354,368
CO_2 feed system	\$ ha^{-1}	6,717	67,170
Water and nutrient system	\$ ha^{-1}	15,832	158,321
Harvesting and dewatering system	\$ ha^{-1}	12,606	126,057
Total unavoidable direct capital cost	**\$**		**705,916**
Direct capital costs avoided by co-location			147,526
Land acquisition Co-located (assumed land owned by partner industry)	\$ ha^{-1}	14,753	
Total avoidable capital cost	**\$**		**147,526**
Grand total of all capital cost	***\$***		***853,442***
Standardized indirect capital costs			
Engineering Fees – unavoidable	15% capital		105,887
Land acquisition fees – avoidable	15% capital		22,129
Engineering fees – total	**15% capital**		**128,016**
Contingency – unavoidable	5% capital		35,296
Contingency – avoidable	5% capital		7,377
Contingency – total	5% capital		**42,673**
Total indirect costs - unavoidable	**\$**		**141,183**
Total indirect costs - avoidable	**\$**		**29,505**
Total indirect costs	***\$***		***170,688***
Working capital - all unavoidable	**5%capital**		**51,206**
Operational costs			
Operational costs not co-located	**Units**		
Labor-plant manager/supervisor	1 person (\$)		81,072
Labor-Engineer	1 person (\$)		60,333
Labor-Lab analyst	2 persons (\$)		90,499
Labor-Administration	1 person (\$)		43,364
Labor-Technician/pond operator	2 persons (\$)		71,645
Maintenance and insurance	10%[B]		84,710
Phosphate input	\$ t^{-1}		35,757
Water requirement-avoidable if co-located with waste water industry	\$	1,217,646	1,217,646
CO_2 purchase - unpaid able if co-located with coal fired power stations	\$	397,127	397,127
Energy demand cultivation, dewatering and drying	\$ y^{-1}	10,980	10,980
Costs for pigment extraction and purification[A]	\$ t^{-1} biomass		347,500
Total annual operating costs when not co-located	\$		**2,440,633**
Operational costs when co-located			
Labor-plant manager/supervisor	1 person (\$)		81,072
Labor-Engineer	1 person (\$)		60,333
Labor-Lab analyst	2 persons (\$)		90,499
Labor-Administration	1 person (\$)		43,364
Labor-Technician/pond operator	2 persons (\$)		71,645
Maintenance and insurance	10%[B]		17,703
Phosphate input	\$ t^{-1}		35,757
Ash dam water	\$		0
Flue gas	\$		0
Energy demand for flue gas supply (at 10% of supply charge to customer)	\$ y^{-1}	9,270	9,270
Energy demand cultivation, dewatering and drying (at 10% of supply charge to customer)	\$ y^{-1}	1,098	1,098
Costs for pigment extraction and purification[A]	\$ t^{-1} biomass		347,500
Total annual operating costs when co-located	**\$**		**758,241**

(Continued)

TABLE 5 | Continued

Size of *Tolypothrix* facility [ha]	**10**		
Bioproduct income			
Biomass derived potential income			
Food-grade phycocyanin 10.8 t ha^{-1} y^{-1} (US$ 500 kg^{-1}) at an extraction/purification efficiency of 67%[A]	\$ ha^{-1} y^{-1}	3,448,155	34,481,550
Biofertilizer/Biochar (US$ 500 t^{-1} DW) (117.5 t biomass dry weight)	\$ ha^{-1} y^{-1}	58,750	587,500
Biofertilizer from 50% biomass (US$ 500 t^{-1} DW) (58.57 t biomass dry weight)	\$ ha^{-1} y^{-1}	29,375	293,750
Weighted average costs of capital (WACC)	**%**		**10**
Net profit value analyses			
Profit value (PV) scenarios over a 20-year period		**Co-located**	**Not co-located**
1) Food-grade phycocyanin (sole product)	\$	538,038,679	491,380,960
2) 100% of biomass converted to biofertilizer (sole product)	\$	−12,294,786	−58,952,5056
3) 50% of biomass converted to biofertilizer +50% food-grade phycocyanin	\$	273,711,820	250,382,961
4) 100% food-grade phycocyanin and biofertilizer yields	\$	547,423,641	500,765,922
Sales tax and distribution costs for PV scenarios 1–4			
1) Assumed tax and distribution costs including transport as % sales value (50%)	\$	269,019,340	245,690,480
2) Assumed tax and distribution costs including transport as % sales value (50%)	\$	0	0
3) Assumed tax and distribution costs including transport as % sales value (50%)	\$	136,855,910	125,191,480
4) Assumed tax and distribution costs including transport as % sales value (50%)	\$	273,711,820	250,382,961
Net profit value for scenarios 1–4			
1) Food-grade phycocyanin (sole product)	\$	269,019,340	245,690,480
2) 100% of biomass converted to biofertilizer (sole product)	\$	−12,294,78	−58,952,50
3) 50% of biomass converted to biofertilizer +50% food-grade phycocyanin	\$	136,855,910	125,191,480
4) 100% food-grade phycocyanin and biofertilizer yields	\$	273,711,820	250,382,961
Sensitivity Analyses for NPV scenarios 1–4			
Biofertilizer price at 25% (125 USD t^{-1})			
1) Food-grade phycocyanin (sole product)	\$	269,019,340	245,690,480
2) 100% of biomass converted to biofertilizer (sole product)	\$	0	0
3) 50% of biomass converted to biofertilizer +50% food-grade phycocyanin	\$	135,244,045	123,431,800
4) 100% food-grade phycocyanin and biofertilizer yields	\$	270,488,090	246,863,600
Food-grade phycocyanin price at 25% (125 USD kg^{-1})			
1) Food-grade phycocyanin (sole product)	\$	59,067,104	35,738,244
2) 100% of biomass converted to biofertilizer (sole product)	\$	0	0
3) 50% of biomass converted to biofertilizer +50% food-grade phycocyanin	\$	32,471,052	20,215,362
4) 100% food-grade phycocyanin and biofertilizer yields	\$	64,942,104	40,430,725
Net Profit Value and Sensitivity Analysis For Raceway Production Scenario for Biomass Production at 6 t DW ha^{-1} y^{-1}			
Net profit value analyses			
Profit Value (PV) scenarios over a 20-year period			
1. Food-grade phycocyanin (sole product)	\$	264,058,457	217,400,737
2. 100% of biomass converted to biofertilizer (sole product)	\$	−16,962,887	−63,620,607
3. 50% of biomass converted to biofertilizer +50% food-grade phycocyanin	\$	136,721,709	113,392,849
4. 100% food-grade phycocyanin and biofertilizer yields	\$	273,443,418	226,785,699
Sales tax and distribution costs for PV scenarios 1–4			
1. Assumed tax and distribution costs including transport as % sales value (50%)	\$	132,029,228	108,700,369
2. Assumed tax and distribution costs including transport as % sales value (50%)	\$	0	0
3. Assumed tax and distribution costs including transport as % sales value (50%)	\$	68,360,855	56,696,425
4. Assumed tax and distribution costs including transport as % sales value (50%)	\$	136,721,709	113,392,849
Net profit value for scenarios 1–4			
1. Food-grade phycocyanin (sole product)	\$	132,029,228	108,700,369
2. 100% of biomass converted to biofertilizer (sole product)	\$	−16,962,887	−63,620,607
3. 50% of biomass converted to biofertilizer +50% food-grade phycocyanin	\$	68,360,855	56,696,425
4. 100% food-grade phycocyanin and biofertilizer yields	\$	136,721,709	113,392,849

(Continued)

TABLE 5 | Continued

Size of *Tolypothrix* facility [ha]	10		
Sensitivity Analyses for NPV scenarios 1–4			
Biofertilizer price at 25% (125 USD t^{-1})			
1. Food-grade phycocyanin (sole product)	$	132,029,228	108,700,369
2. 100% of biomass converted to biofertilizer (sole product)	$	−20,616,184	−67,273,904
3. 50% of biomass converted to biofertilizer + 50% food-grade phycocyanin	$	68,360,855	56,696,425
4. 100% food-grade phycocyanin and biofertilizer yields	$	136,721,709	113,392,849
Food-grade phycocyanin price at \$125 kg^{-1}			
1. Food-rade phycocyanin (sole product)	$	24,819,576	1,490,716
2. 100% f biomass converted to biofertilizer (sole product)	$	−16,962,887	−63,620,607
3. 50% of biomass converted to biofertilizer +50% food-grade phycocyanin	$	14,756,028	3,091,598
4. 100% food-grade phycocyanin and biofertilizer yields	$	29,512,057	6,183,197

[A] *(Chaiklahan et al., 2018);* [B] *Total direct and indirect capital.*

nitrogen fertilization and a 90% saving on dewatering costs (**Table 5**). Accordingly, total capital costs for constructing the 10 ha facility not co-located with a coal-fired power plant were estimated at US$ 853,442 for pond construction, CO_2, nutrient supply, water-recirculation, and harvest/dewatering systems and land acquisition. The only direct capital cost avoided by co-location was for land acquisition (US$ 147,526), reducing the direct capital cost to US$ 705,916 (**Table 5**). Standardized indirect capital costs for engineering fees (including land acquisition), set at 15% and applying a 5% contingency were estimated to be US$ 170,688 for a not co-located facility, of which US$ 29,505 were avoided through free land provided in the co-location scenario, reducing indirect capital costs to US$ 141,183 (**Table 5**). A working capital of 5% of the total costs did not consider any of the benefits derived through co-location. Total annual operating costs for a not co-located facility was estimated to be US$ 2,440,633 for the 10 ha facility and included cost for salaries, maintenance and insurance, phosphate fertilizer and water requirements, CO_2, energy for cultivation, dewatering and drying, and pigment extraction and purification (**Table 5**). Co-location resulted in significant operational savings of ∼70%, particularly through avoiding water and CO_2 supply costs and a 90% saving on maintenance and insurance, and energy expenditure; the latter considered that energy would be purchased from the power station at 10% of the sales price to ordinary customers, and maintenance/insurance costs would also be 10% of ordinary costs. Therefore, annual operational costs were estimated to be US$ 758,241 when co-located (**Table 5**).

Bioproduct-Generated Income, Net Present Value and Sensitivity Analyses

Bioproduct yields were estimated from biomass productivity and bioproduct productivities obtained in this study and for average productivities achieved for *Nannochloropsis* occulata in large-scale outdoor raceway cultivation. Based on this, it is estimated that a 10 ha facility could produce 117.5 and 60 t *Tolypothrix* sp. biomass ha^{-1} y^{-1} for a 300-day production period, respectively. The average phycocyanin content of *Tolypothrix* sp. used in this study is 8.8% (w/w), although as shown here, higher yields are possible. In order to put the NPV on a realistic footing, the average yields were used to calculate the yields of food-grade phycocyanin (A620 nm/A280 nm: 0.7), which can be extracted and purified with an efficiency of 67% (Chaiklahan et al., 2018). This equates to a production of 10.3 t unpurified phycocyanin ha^{-1} y^{-1}, which yields 6.9 t food-grade phycocyanin ha^{-1} y^{-1}, valued at US$ 3,448,155 ha^{-1} y^{-1} based on a sales price at US$ 500 kg^{-1} (**Table 5**). The final purified product will require metal analysis for quality assurance, which has not been considered as a cost, as costs for these analyses are expected to be absorbed by the coal-fired power plant the production would be collocated with. Furthermore, production of the food-grade phycocyanin produced when not collocated would not be subject to such analyses, i.e., in this scenario no metal analyses costs would be incurred. Biofertilizer/biochar can fetch a sales price of US$ 500 t^{-1}, which, based on biomass productivities achieved here, equates to US$ 58,750 ha^{-1} y^{-1} (**Table 5**). Based on this, the predicted values for the modeled bioproduct scenarios are highest for co-located production for phycocyanin extraction in a biorefinery approach and conversion of the extracted biomass to biofertilizer (scenario 4, US$ 547,423,641), closely followed by producing food-grade phycocyanin as the sole product (scenario 1, US$ 538,038,679) (**Table 5**). Net present values were 50% lower based on assumed tax and distribution costs (**Table 5**).

In order to decide whether a project remains commercially viable, sensitivity analyses are essential. Accordingly, the weighted average costs of capital (WACC) is 10% and the sensitivity analyses modeled two scenarios: (1) reduction of the biofertilizer price to 25% of the current value (US$ 125 t^{-1}) and (2) a food-grade phycocyanin price to 25% of the current value due to market saturation (US$ 125 kg^{-1}). This showed that producing biofertilizer as the sole product (scenario 2) is not commercially viable even when the production facility is co-located. It is assumed that income for environmental services provided at the coal-fired power plant would not provide a strong business incentive. In contrast, producing phycocyanin as

the sole product (scenario 1) remains to be of commercial interest (**Table 5**).

DISCUSSION

Effect of CO_2-Supplementation on Biomass Production

Successful cultivation of microalgae and cyanobacteria in wastewaters arising from energy -, mining - and mineral-processing industries would provide for a sustainable platform for production of algal biomass and bioproducts, whilst simultaneously providing for efficient bioremediation of potentially harmful nutrients and metals (Roberts et al., 2013). Significant growth challenges, hampering overall productivities and economics when using wastewater for production, must be addressed first for the realization of the true commercial potential.

This study demonstrated that CO_2 supplementation significantly improved final phycobiliprotein and biomass yields, as well as biomass productivities of the diazotrophic cyanobacterium *Tolypothrix* sp. grown in SADW under outdoor conditions as biofilms of suspension cultures. Similar increases of up to 60% have been reported for biomass productivities using the non-diazotrophic cyanobacterium *Arthrospira platensis* for cultures supplemented with 1% CO_2 (v/v) (Ravelonandro et al., 2011). In contrast, growth of *Tolypothrix* sp. was reduced by 60% under outdoor (this study) compared to indoor suspension cultivation under the same CO_2-supplemented – and wastewater conditions (Velu et al., 2019). Growth of outdoor cultures is often generally lower due to difficulties in controlling cultivation and environmental conditions, such as hydrodynamics, temperature, UV irradiation and irradiance within optimal ranges (Chen et al., 2011). Light intensity is one of the major factors affecting cyanobacterial and microalgal growth. The optimal light intensity for growth of *Tolypothrix* sp. is ∼500 μmol photons m^{-2} s^{-1}, however, observed light intensities at noon varied from 500 to 900 μmol photons m^{-2} s^{-1} (**Supplementary Table S3**). This could suggest that periodic photoinhibition might have occurred, especially in younger cultures with low cell concentrations. It must be emphasized that the reported CO_2-supplemented growth performance was comparable to other microalgae and cyanobacteria grown in various cultivation systems but was achieved without nitrogen-fertilization (**Table 6**). In addition, biomass growth was phosphate-limited after ∼3 to 8 days of cultivation. It is therefore conceivable that phosphate fertilization at appropriate intervals should improve biomass yields and productivities further. High temperature and irradiance experienced in the ATS were the most likely factors impeding growth performance of biofilms of *Tolypothrix* sp. (Del Campo et al., 2007; Chen et al., 2011), a conclusion supported by higher growth performance of indoor-cultivated microalgal biofilms (**Table 6**).

The observed higher growth performance of *Tolypothrix* sp. when supplemented with CO_2 could be attributable to positive effects on nitrogen – and photosynthesis-linked carbon fixation. For example, supplementation of cultures of the marine diazotrophic cyanobacterium *Trichodesmium* sp. with large amounts of CO_2 resulted in a 20% increase in nitrogen fixation rates (Levitan et al., 2007). In addition, CO_2 supplementation could have allowed for the reallocation of energy required for inorganic carbon (C_i) uptake and scavenging of O_2. For instance, CO_2-supplementation reduced the energy requirements for C_i uptake in *Trichodesmium* sp. by suppressing the energy-intensive carbon concentrating mechanism (CCM), which are employed under carbon-limiting conditions, freeing up this energy for the fixation of atmospheric nitrogen, another metabolic pathway with large energy requirements (Levitan et al., 2007). In contrast, despite a large effect of CO_2-supplementation on biomass productivity, no effect was observed for phosphate requirements in biofilm and suspension-grown *Tolypothrix* sp., which was also observed for indoor-cultivated suspension cultures (Velu et al., 2019). This could represent a direct result of phosphate limitation after large uptake over the first 3 days of the growth period for replenishing internal phosphate stores, providing sufficient energy for CO_2 fixation. In the context of deploying industrial cultivation of *Tolypothrix* sp. for the bioremediation of macronutrient-poor ash dam wastewaters at coal-fired power plants, the ability of sustained growth without requirements for nitrogen-fertilization offers a distinctive economical advantage. For example, nitrate provision for large-scale production of the non-diazotrophic *Arthrospira platensis* (synonym *Spirulina platensis*) was estimated to account for 50% of the overall production costs (Vonshak and Richmond, 1988). Energy savings provided by the self-settling ability of *Tolypothrix* sp. is another significant advantage for wastewater-utilizing large-scale cultivation, as costly dewatering infrastructure and energy requirements, that apply to the commonly used microalgal genera *Chlorella* spp. and *Scenedesmus* spp. (Silva and Silva, 2007), is abolished. For example, biofilms and self-flocculated biomass of *Tolypothrix* sp. were 80- and 53-fold more concentrated than the original suspension culture (Velu et al., 2015). Taken together, these properties reduce the need for finite chemical fertilizers and improve the overall economics of cultivation in macronutrient-limited ash dam wastewaters.

Effect of CO_2-Supplementation on Biochemical Profiles, Metal Removal Capacity and Bioproduct Potential

CO_2-fertilization of outdoor-grown biofilms and suspension cultures of *Tolypothrix* sp. resulted in increased total carbohydrate and lipid contents, as has also been reported for indoor cultivated suspension cultures (Velu et al., 2019). Similarly, an increase in CO_2 supply from 5 to 25% (v/v) increased total carbohydrate and lipid contents of *Scenedesmus bajacalifornicus* by up to 20 and 10%, respectively (Patil and Kaliwal, 2017). Elevated CO_2 supplies typically result in increased carbohydrate contents in microalgae, and are likely a result of enhanced photosynthetic efficiencies (Giordano, 2001) or CO_2-induced low pH stress (Dragone et al., 2011). In contrast, 15% CO_2 (v/v) supplementation led to an increase in pH from 6.0 to 9.0 and 7.0 to 9.0 for CO_2-supplemented and non-CO_2 controls under outdoor cultivation of *Tolypothrix* sp.

TABLE 6 | Effect of CO_2 on the performance of cyanobacterial and microalgal cultivation systems.

Culturing mode	System	Species	Culture medium	CO_2 [%]	Location	Cultivation system working volume/area	Biomass productivity [g m^{-2} d^{-1}]	References
Suspension	Vertical flat-plate photobioreactor (PBR)	*Synechocystis aquatilis* SI-2	Modified SOT inorganic medium	10 40	Outdoor[1]	24 L 9 L	31–45 18.3	Zhang et al., 1999, 2001
	Bubble column PBR	*Anabaena* sp. ATCC 33047	Detailed in[a]	NG	Indoor[2]	9 L	81	López et al., 2009
	Acrylic cylindrical tank	*Phormidium valderianum*	TDS effluent[b]	NG	Outdoor[3]	550 L	0.03	Dineshbabu et al., 2017
	PBR	*Anabaena sp.* CH1	Arnen medium	15	Indoor[4]	5 L	∼31	Chiang et al., 2011
	PBR	*Chlorella* sp. MM-2	Modified f/2	5	Indoor[4]	0.8 L	∼51	Kao et al., 2012
	PBR	*Chlorella* sp. MM-2	Swine wastewater	20	Outdoor[4]	50 L	∼36	
	Column PBR	*Spirulina* sp. (*Arthrospira*)	Zarrouk medium	6 and 12	Indoor[5]	1.8 L	27 and 22	De Morais and Costa, 2007
		Scenedesmus obliquus	MC medium			1.8 L	12 and 17	
	Aerated vertical bag	*Tolypothrix* sp.	SADW[c]	15	Outdoor[6]	500 L	25–95	This study
Biofilm	Single layer PBR	*Botryococcus braunii*	Autotrophic nutrient medium	1	Indoor[7]	0.08 m^{-2}	6.5	Cheng et al., 2013
	Multi-layer PBR					0.08 m^{-2}	49.1	
	Twin-Layer PBR	*Halochlorella rubescens*	LSBM[d]	3 and 5	Indoor[8]	3 m^{-2}	∼30 and 24	Schultze et al., 2015
	PBR	*Pseudochlorococcum* sp.	BG11	10	Indoor[7]	0.00025 m^{-2}	∼5.5	Ji et al., 2014
	Algal turf-scrubber	*Tolypothrix* sp.	SADW	15	Outdoor[6]	2.2 m^{-2}	1.36–3.63	This study

[1]Japan; [2]Spain; [3]South India;[4]Taiwan;[5] Brazil; [6]Queensland, Australia; [7]China; [8]Germany. [a]Culture medium detailed in Moreno et al. (1998); [b]Seawater and ossein effluent from gelatin manufacturing industry;. [c]Simulated ash-dam wastewater; [d] Large Scale Brackish Medium prepared based on Bold's Basal medium NG- CO_2 percentage not given but CO_2 was used.

biofilms and suspension cultures (**Table 6**), suggesting strongly that cultures were still carbon-limited (Coleman and Colman, 1981). Accounting for the fact that nitrogen-requirements for growth had to be met solely through nitrogen fixation, it is not surprising that CO_2-supplementation had no effect on protein content for biomass cultivated in either system, which differs from other reported outcomes, where CO_2-supplementation has been shown to correlate with improved nitrate uptake and thus higher protein production (Xia and Gao, 2005). As demonstrated by significant CO_2-induced increases in the nitrogen-containing pigments phycocyanin and phycoerythrin, nitrogen supply through nitrogen fixation must have been sufficient under outdoor cultivation of *Tolypothrix* sp. The increase in the content of these pigments could have been also responsible for improved growth performance under CO_2-supplementation, as they are accessory pigments for the capture of light in the light harvesting complexes of the photosystems and protect the photosynthetic apparatus from excess light and reactive oxygen damage (Chakdar and Pabbi, 2016).

Similar to the increase in phycobiliprotein contents, i.e., phycocyanin and phycoerythrin, CO_2-supplementation resulted in 19 and 12% higher TFA contents in *Tolypothrix* sp. biofilms and suspension-grown biomass, which is similar to results obtained in indoor cultivation (Velu et al., 2019) and with eukaryotic microalgae (Tsuzuki et al., 1990), but no significant effect on MUFA or PUFA content was evident. α- (C18:3 ω-3) and γ-Linolenic acid (C18:3 ω-6) are important dietary supplements with critical health benefits, and the latter is also an ingredient in cosmetics (Ryckebosch et al., 2012). Similar to indoor suspension cultivation (Velu et al., 2019), *Tolypothrix* sp. produced 25% C18:3 ω-6 or 18.5 mg g^{-1} TFA, which is higher than reported for *Arthrospira* (*Spirulina*) sp. (11–16%) (De Oliveira et al., 1999). In contrast to phycocyanin, yields of (C18:3 ω-6), however, remained insufficient for consideration as a main target product in a biorefinery approach, due to low TFA contents characteristic for cyanobacteria.

Irrespective of cultivation system and CO_2-fertilization, metal bioremediation of *Tolypothrix* sp. from macronutrient-poor ash dam wastewater, containing concentrations of Al, As, Cd, Ni, and Zn that exceed the ANZECC guidelines (Roberts et al., 2013), showed that levels were lowered to acceptance thresholds at the end of the cultivation period. This demonstrated that *Tolypothrix* sp. is a suitable organism for the bioremediation of metals from complex mixtures, under macronutrient-limiting conditions. The produced *Tolypothrix* sp. biomass was rich in carbon (45%) and nitrogen (7%), resulting in a C/N ratio of 6.58, similar to results obtained in indoor cultivation (Velu et al., 2019). In addition, the elemental composition and concentrations were comparable to those found in other cyanobacteria, previously reported as suitable for biofertilizer applications (Osman et al., 2010). Importantly, biomass of *Tolypothrix* sp. remained suitable at application rates required for the fertilization of wheat, supplying in addition to nitrogen and carbon also essential trace elements, such as Cu, Fe, Mo, and Zn (Velu et al., 2019). Diazotrophic

cyanobacteria, such as *Tolypothrix* sp., are natural and renewable sources of biological nitrogen, contributing up to 30 kg N ha^{-1} and providing large quantities of organic matter and important plant hormones (i.e., gibberellin, auxin and cytokines) to soils, thereby improving soil fertility (Issa et al., 2014), supporting plant development and protecting against pathogens (Singh et al., 2016). Diazotrophic cyanobacteria, such as *Tolypothrix* sp., are commonly employed as biofertilizers in rice fields (Karthikeyan et al., 2007) and applications of *Tolypothrix* sp. specifically resulted in a 25% increase in crop yields in poorly drained rice fields (Watanabe et al., 1951). Long-term applications improved nitrogenous fertility of soils, attributable to the increase in soil carbon and nitrogen through accumulation of decomposing and live biomass, respectively (Watanabe, 1962). In summary, the above application potential, together with CO_2-enhanced growth responses and phycocyanin yields, makes *Tolypothrix* sp. biomass production for use as a biofertilizer a real potential in regions, where agricultural production is located near freshwater-using coal-fired power plants, as is the case for the Tarong power station in Queensland, Australia.

To test and substantiate the commercial viability of *Tolypothrix* sp.-derived food-grade phycocyanin and biofertilizer, net present value and sensitivity analyses evaluated four bioproduct scenarios for the production of *Tolypothrix* sp. biomass under coal-fired power plant co-location and non-colocation of the production facility. Production in traditional raceway ponds was chosen, as no published data on the construction costs of large-scale production facilities using bubble columns could be found and a comparison of average microalgal and cyanobacterial maximal biomass productivities was not strongly influenced by cultivation system when operated under outdoor conditions (Heimann et al., 2015). In addition, biofilm cultivation was not considered in the modeled scenarios for several reasons. (1) Systems used in the study have a very large areal production footprint. (2) The areal productivity is low. (3) The systems are more prone to contamination by other microalgae when used for extended periods under outdoor conditions (Velu et al., 2015). (4) Establishment costs for large-scale production cannot be applied with any certainty, as biofilm cultivation systems vary significantly in design (Heimann, 2016). (5) As the biofilms were not harvested at regular intervals, it is impossible to determine the true yield potential of the systems at this stage, as regrowth of the remaining turf may have vastly different biomass production characteristics compared to freshly seeded turfs.

The modeled NPV and sensitivity analyses showed that the production of food-grade phycocyanin is advantageous for commercial viability, whether or not the facility would be co-located, whereas biofertilizer production as a sole product was not commercially viable in any of the modeled scenarios. Outcomes for biofertilizer income were similar to the commercial production of *Azospirillum*, a nitrogen-fixing bacterium, simulated for liquid biofertilizer production in Cuba, but the production scale for the plant was 4-fold larger in terms of product volume (Pérez Sánchez et al., 2018) than for the *Tolypothrix* sp. plant in the presented study. In that analysis, salary costs accounted for >50% of the production cost, as the process is labor-intensive, requiring 29 employees to man 24 h shifts (Pérez Sánchez et al., 2018), while production of *Tolypothrix* sp. biomass represented only 10% of the overall production costs. An NPV analysis for the commercial production of dried microalgal biomass (US$625 t^{-1}) using dairy effluent as a nutrient and water supply also concluded that the process is commercially feasible for a plant size treating 1 million liter of dairy effluent over a 20-year period (Kumar et al., 2020). The sensitivity analyses using one quarter of today's food-grade phycocyanin sales price demonstrated that facilities producing phycocyanin as a sole product or phycocyanin and biofertilizer remain commercially viable whether co-located or not. Instead of using product sales prices, reduction of biomass yields are an alternative parameter in sensitivity analyses. Reduction of biomass yields to one quarter of the original tonnage therefore had a comparable effect on NPV outcomes (Kumar et al., 2020). An obvious worst-case scenario for commercial production would be reduced yearly biomass yields (reduced to 33%) and reduced product sales prices (at 25% each of today's sales prices). Applying this situation to the *Tolypothrix* sp. production scenario proposed here over the entire 20-year period determined that production of food-grade phycocyanin as a sole product, 50% of biomass extraction for each food-grade phycocyanin and biofertilizer, and 100% food-grade phycocyanin with the residual biomass converted to biofertilizer (100%) remain commercially feasible irrespective of co-location or not for the bubble column production scenario, but only when co-located for the raceway production simulation. Therefore, with regards to a decision whether co-location offers significant benefits, the profit difference predicted here would be as large as ∼US$ 23 million over 20 years for production of 100% food-grade phycocyanin at a quarter of today's sale price with 100% co-production of biofertilizer. This provides a significant incentive for co-locating production facilities with CO_2-polluting and metal-rich wastewater generating industries, for the simultaneous application of the environmental services of diazotrophic cyanobacteria and bioproduct development.

CONCLUSION

This study demonstrated significantly enhanced biomass and phycocyanin yields and productivities in response to CO_2-fertilization and excellent metal removal capacity of *Tolypothrix* sp. cultivated under outdoor conditions in meso-scale systems without supply of nitrogen fertilization. This makes *Tolypothrix* sp. an outstanding candidate for bioremediation of CO_2 and metals at freshwater-utilizing coal-fired power plants. Obtained growth performance suggests that 10.91 and 117.5 t dry biomass ha^{-1} can be produced in a year set at 300 days of cultivation in biofilms and vertical bag suspension cultures, respectively. The NPV and sensitivity analyses performed with production data obtained in this study and modeled for a simulated raceway production scenario, taking the organism's self-settling

ability into account, demonstrated that co-location with coal-fired power plants was not essential for commercial viability, but significantly increased achievable net present values for all modeled product scenarios, making it an attractive proposition, if freshwater-utilizing plants are in close proximity to agricultural land. The most profitable scenario was production of food-grade phycocyanin (100%) coupled with co-production of biofertilizer (100%), followed by food-grade phycocyanin as the sole product, and 50% of each phycocyanin and biofertilizer production. In contrast, production of biofertilizer as a sole product was not commercially viable under any of the modeled scenarios. Based on the above, cultivation of *Tolypothrix* sp. in vertical suspension cultures with CO_2 supply, but without nitrogen-fertilization is recommended for the production of food-grade phycocyanin either as a sole product or with co-production of biofertilizer.

DATA AVAILABILITY STATEMENT

The raw data supporting the conclusions of this article will be made available by the authors, without undue reservation, to any qualified researcher.

AUTHOR CONTRIBUTIONS

KH, SC, and CV were responsible for the experimental design of this study and analyzed all the data. CV carried out the experimental work of the outdoor growth experiments, protein – and phycobiliprotein contents. DB and CV conducted the analysis and quantification of biomass lipid content and fatty acid profiles. KH and CV performed the NPV and sensitivity analyses. KH, CV, SC, and DB jointly assembled and critically interpreted these data for publication. All authors contributed to writing the manuscript, provide approval for publication, and agreed to be accountable for all aspects of the work.

FUNDING

KH acknowledges grant funding by the Advanced Manufacturing Co-operative Research Centre (AMCRC), Melbourne, Australia, grant number 2.3.4. CV gratefully acknowledges receipt of an AMCRC Ph.D. scholarship and JCU tuition fee waiver, receipt of project funding through the Graduate Research School at James Cook University (JCU) and Essential Aquaculture.

ACKNOWLEDGMENTS

The authors thank the Advanced Analytical Centre at James Cook University for metal analysis, the Australian Institute of Marine Science for fatty acid, and hydrocarbon analyses and OEA Labs Ltd., for elemental analysis.

SUPPLEMENTARY MATERIAL

The Supplementary Material for this article can be found online at: https://www.frontiersin.org/articles/10.3389/fbioe.2020.00051/full#supplementary-material

REFERENCES

Abed, R. M. M., Dobretsov, S., and Sudesh, K. (2009). Applications of cyanobacteria in biotechnology. *J. Appl. Microbiol.* 106, 1–12. doi: 10.1111/j.1365-2672.2008.03918.x

ABS (2015). *Fertiliser use, Australia, Year Ended 30 June 2015*. Kolkata: ABS.

Artanto, Y., Jansen, J., Pearson, P., Puxty, G., Cottrell, A., Meuleman, E., et al. (2014). Pilot-scale evaluation of AMP/PZ to capture CO2 from flue gas of an Australian brown coal–fired power station. *Int. J. Greenhous Gas Convers.* 20, 189–195. doi: 10.1016/j.ijggc.2013.11.002

Aslam, A., Thomas-Hall, S. R., Mughal, T., Zaman, Q.-U., Ehsan, N., Javied, S., et al. (2019). Heavy metal bioremediation of coal-fired flue gas using microalgae under different CO2 concentrations. *J. o Environ. Manag.* 241, 243–250. doi: 10.1016/j.jenvman.2019.03.118

Benemann, J. R. (1979). Production of nitrogen fertilizer with nitrogen-fixing blue-green algae. *Enzyme Microbial Technol.* 1, 83–90. doi: 10.1016/0141-0229107990103-90100

Bermejo, P., Piñero, E., and Villar, ÁM. (2008). Iron-chelating ability and antioxidant properties of phycocyanin isolated from a protean extract of *Spirulina platensis*. *Food Chem.* 110, 436–445. doi: 10.1016/j.foodchem.2008.02.021

Bhayani, K., Mitra, M., Ghosh, T., and Mishra, S. (2016). C-Phycocyanin as a potential biosensor for heavy metals like Hg2+ in aquatic systems. *RSC Adv.* 6, 111599–111605. doi: 10.1039/C6RA22753H

Borowitzka, M. A. (2013). High-value products from microalgae—their development and commercialisation. *J. Appl. Phycol.* 25, 743–756. doi: 10.1007/s10811-013-9983-9

Chaiklahan, R., Chirasuwan, N., Loha, V., Tia, S., and Bunnag, B. (2018). Stepwise extraction of high-value chemicals from *Arthrospira* (*Spirulina*) and an economic feasibility study. *Biotechnol. Rep.* 20:e00280. doi: 10.1016/j.btre.2018.e00280

Chakdar, H., and Pabbi, S. (2016). "Cyanobacterial phycobilins: production, purification, and regulation," in *Frontier Discoveries and Innovations in Interdisciplinary Microbiology*, 1 Edn, ed. P. Shukla, (New York, NY: Springer), 45–69. doi: 10.1007/978-81-322-2610-9_4

Chen, C.-Y., Yeh, K.-L., Aisyah, R., Lee, D.-J., and Chang, J.-S. (2011). Cultivation, photobioreactor design and harvesting of microalgae for biodiesel production: a critical review. *Bioresour. Technol.* 102, 71–81. doi: 10.1016/j.biortech.2010.06.159

Cheng, P., Ji, B., Gao, L., Zhang, W., Wang, J., and Liu, T. (2013). The growth, lipid and hydrocarbon production of *Botryococcus braunii* with attached cultivation. *Bioresour. Technol.* 138, 95–100. doi: 10.1016/j.biortech.2013.03.150

Chiang, C.-L., Lee, C.-M., and Chen, P.-C. (2011). Utilization of the cyanobacteria *Anabaena* sp. CH1 in biological carbon dioxide mitigation processes. *Bioresour. Technolo.* 102, 5400–5405. doi: 10.1016/j.biortech.2010.10.089

Cohen, Z. (1997). "The chemicals of *Spirulina*.," in *Spirulina platensis (Arthrospira): Physiology, cell Biology and Biotechnology*, ed. A. Vonshak, (London: Taylor and Francis), 175–204.

Coleman, J. R., and Colman, B. (1981). Inorganic carbon accumulation and photosynthesis in a blue-green alga as a function of external pH. *Plant Physiol.* 67, 917–921. doi: 10.1104/pp.67.5.917

Davis, R., Aden, A., and Pienkos, P. T. (2011). Techno-economic analysis of autotrophic microalgae for fuel production. *Appl. Energy* 88, 3524–3531. doi: 10.1016/j.apenergy.2011.04.018

De Morais, M. G., and Costa, J. A. V. (2007). Biofixation of carbon dioxide by *Spirulina* sp. and Scenedesmus obliquus cultivated in a three-stage serial tubular photobioreactor. *J. Biotechnol.* 129, 439–445. doi: 10.1016/j.jbiotec.2007.01.009

De Oliveira, M. A. C. L., Monteiro, M. P. C., Robbs, P. G., and Leite, S. G. F. (1999). Growth and chemical composition of *Spirulina maxima* and *Spirulina platensis* biomass at different temperatures. *Aquac. Int.* 7, 261–275.

De Philippis, R., Colica, G., and Micheletti, E. (2011). Exopolysaccharide-producing cyanobacteria in heavy metal removal from water: molecular basis and practical applicability of the biosorption process. *Appl Microbiol. Biotechnol.* 92, 697–708. doi: 10.1007/s00253-011-3601-z

Del Campo, J. A., García-González, M., and Guerrero, M. G. (2007). Outdoor cultivation of microalgae for carotenoid production: current state and perspectives. *Appl. Microbiol. Biotechnol.* 74, 1163–1174. doi: 10.1007/s00253-007-0844-9

Dineshbabu, G., Uma, V. S., Mathimani, T., Deviram, G., Ananth, D. A., Prabaharan, D., et al. (2017). On-site concurrent carbon dioxide sequestration from flue gas and calcite formation in ossein effluent by a marine cyanobacterium *Phormidium valderianum* BDU 20041. *Energy Convers. Manag.* 141, 315–324. doi: 10.1016/j.enconman.2016.09.040

Doshi, A. (2017). *Economic Analyses of Microalgae Biofuels and Policy Implications in Australia*. Brisbane: Queensland University of Technology.

Dragone, G., Fernandes, B. D., Abreu, A. P., Vicente, A. A., and Teixeira, J. A. (2011). Nutrient limitation as a strategy for increasing starch accumulation in microalgae. *Appl. Energy* 88, 3331–3335. doi: 10.1016/j.apenergy.2011.03.012

Dubey, S. K., Dubey, J., Mehra, S., Tiwari, P., and Bishwas, A. J. (2011). Potential use of cyanobacterial species in bioremediation of industrial effluents. *Afr. J. Biotechnol,* 10, 1125–1132. doi: 10.1007/s10295-008-0452-4

El-Bestawy, E. (2008). Treatment of mixed domestic–industrial wastewater using cyanobacteria. *J. Indust. Microbiol. Biotechnol.* 35, 1503–1516. doi: 10.1007/s10295-008-0452-4

El-Sheekh, M. M., El-Shouny, W. A., Osman, M. E. H., and El-Gammal, E. W. E. (2005). Growth and heavy metals removal efficiency of *Nostoc muscorum* and *Anabaena subcylindrica* in sewage and industrial wastewater effluents. *Environ. Toxicol. Pharmacol.* 19, 357–365. doi: 10.1016/j.etap.2004.09.005

Fornarelli, R., Bahri, P. A., and Moheimani, N. (2017). *Utilization of Microalgae to Purify Waste Streams and Production of Value Added Products*. North Sydney: Australian Meat Processor Corporation.

Gelagutashvili, E., and Tsakadze, K. (2013). Effect of Hg(II) and Pb(II) ions on C-phycocyanin (*Spirulina platensis*). *Opt. Photonics J.* 3, 122–127. doi: 10.4236/opj.2013.31020

Giordano, M. (2001). Interactions between C and N metabolism in *Dunaliella salina* cells cultured at elevated CO2 and high N concentrations. *J Plant Physiol.* 158, 577–581. doi: 10.1078/0176-1617-00234

Gour, R., Kant, A., and Singh Chuahan, R. (2014). Screening of micro algae for growth and lipid accumulation properties. *J. Algal Biomass Util.* 5, 38–46.

Griffin, G. J., and Batten, D. F. (2013). The economics of producing biodiesel from micro-algae in the Asua Pacific region. *Int. J. Renew. Energy Deve.* 2, 105–113.

Gross, M., and Wen, Z. (2014). Yearlong evaluation of performance and durability of a pilot-scale revolving algal biofilm (RAB) cultivation system. *Bioresour. Technol.* 171, 50–58. doi: 10.1016/j.biortech.2014.08.052

Gupta, V., Ratha, S. K., Sood, A., Chaudhary, V., and Prasanna, R. (2013). New insights into the biodiversity and applications of cyanobacteria (blue-green algae)—Prospects and challenges. *Algal Res,* 2, 79–97. doi: 10.1016/j.algal.2013.01.006

Hall, D. O., Markov, S. A., Watanabe, Y., and Rao, K. K. (1995). The potential applications of cyanobacterial photosynthesis for clean technologies. *Photosynth. Res.* 46, 159–167. doi: 10.1007/BF00020426

Heimann, K. (2016). Novel approaches to microalgal and cyanobacterial cultivation for bioenergy and biofuel production. *Curr. Opini. Biotechnol.* 38, 183–189. doi: 10.1016/j.copbio.2016.02.024

Heimann, K., Cires, S., and Karthikeyan, O. P. (2015). "Cultivation of microalgae: Implications for the carbon footprint of aquaculture and agriculture industries," in *The Carbon Footprint Handbook*, ed. S. S. Muthu, (Boca Raton: CRC Press), 406–447.

Heimann, K., Karthikayan, O. P., and Cirés, S. (2013). Turning bad gas into good solids. *Qld. Min. Energy Bull. (Spring)* 92–96.

Ho, S.-H., Chen, C.-Y., Lee, D.-J., and Chang, J.-S. (2011). Perspectives on microalgal CO2-emission mitigation systems—a review. *Biotechnol. Adv.* 29, 189–198. doi: 10.1016/j.biotechadv.2010.11.001

Hoh, D., Watson, S., and Kan, E. (2016). Algal biofilm reactors for integrated wastewater treatment and biofuel production: a review. *Chem. Eng. J.* 287, 466–473. doi: 10.1016/j.biotechadv.2011.05.015

Issa, A. A., Abd-Alla, M. H., and Ohyama, T. (2014). "Nitrogen fixing cyanobacteria: future prospect," in *Advances in Biology and Ecology of Nitrogen Fixation*, ed. T. Ohyama, (london: e-book: InTech).

Ji, B., Zhang, W., Zhang, N., Wang, J., Lutzu, G. A., and Liu, T. (2014). Biofilm cultivation of the oleaginous microalgae *Pseudochlorococcum* sp. *Bioprocess Biosyst. Eng* 37, 1369–1375. doi: 10.1007/s00449-013-1109-x

Kao, C.-Y., Chiu, S.-Y., Huang, T.-T., Dai, L., Wang, G.-H., Tseng, C.-P., et al. (2012). A mutant strain of microalga *Chlorella* sp. for the carbon dioxide capture from biogas. *Biomass Bioenergy* 36, 132–140. doi: 10.1016/j.biombioe.2011.10.046

Karthikeyan, N., Prasanna, R., Nain, L., and Kaushik, B. D. (2007). Evaluating the potential of plant growth promoting cyanobacteria as inoculants for wheat. *Eur. J. Soil Biol.* 43, 23–30. doi: 10.1016/j.ejsobi.2006.11.001

Kumar, A. K., Sharma, S., Dixit, G., Shah, E., and Patel, A. (2020). Techno-economic analysis of microalgae production with simultaneous dairy effluent treatment using a pilot-scale High Volume V-shape pond system. *Renew. Energy* 145, 1620–1632. doi: 10.1016/j.renene.2019.07.087

Levitan, O., Rosenberg, G., Setlik, I., Setlikova, E., Grigel, J., Klepetar, J., et al. (2007). Elevated CO2 enhances nitrogen fixation and growth in the marine cyanobacterium *Trichodesmium*. *Global Change Biol.* 13, 531–538. doi: 10.1104/pp.110.159145

López, C. G., Fernández, F. A., Sevilla, J. F., Fernández, J. S., García, M. C., and Grima, E. M. (2009). Utilization of the cyanobacteria *Anabaena* sp. *ATCC* 33047 in CO2 removal processes. *Bioresour. Technol.* 100, 5904–5910. doi: 10.1016/j.biortech.2009.04.070

Markou, G., and Georgakakis, D. (2011). Cultivation of filamentous cyanobacteria (blue-green algae) in agro-industrial wastes and wastewaters: a review. *Appl. Energy* 88, 3389–3401. doi: 10.1016/j.apenergy.2010.12.042

Moheimani, N. R. (2016). *Tetraselmis suecica* culture for CO2 bioremediation of untreated flue gas from a coal-fired power station. *J. Appl. Phycol.* 28, 2139–2146. doi: 10.1007/s10811-015-0782-3

Moreno, J., Vargas, M. A., Olivares, H., Rivas, J., and Guerrero, M. G. (1998). Exopolysaccharide production by the cyanobacterium *Anabaena* sp. *ATCC* 33047 in batch and continuous culture. *J. Biotechnol.* 60, 175–182. doi: 10.1016/s0168-1656(98)00003-0

Osman, M. E. H., El-Sheekh, M. M., El-Naggar, A. H., and Gheda, S. F. (2010). Effect of two species of cyanobacteria as biofertilizers on some metabolic activities, growth, and yield of pea plant. *Biol. Fertil. Soils* 46, 861–875. doi: 10.1007/s00374-010-0491-7

Patil, L., and Kaliwal, B. (2017). Effect of CO2 concentration on growth and biochemical composition of newly isolated indigenous microalga *Scenedesmus bajacalifornicus* BBKLP-07. *Appl. Biochemi. Biotechnol.* 182, 335–348. doi: 10.1007/s12010-016-2330-2

Pereira, S., Micheletti, E., Zille, A., Santos, A., Moradas-Ferreira, P., Tamagnini, P., et al. (2011). Using extracellular polymeric substances (EPS)-producing cyanobacteria for the bioremediation of heavy metals: do cations compete for the EPS functional groups and also accumulate inside the cell? *Microbiology* 157, 451–458. doi: 10.1099/mic.0.041038-0

Pérez Sánchez, A., Singh, S., Pérez Sánchez, E. J., and Segura Silva, R. M. (2018). Techno-economic evaluation and conceptual design of a liquid biofertilizer plant. *Rev. Colomb. Biotecnol.* 20, 6–18.

Pierobon, S. C., Cheng, X., Graham, P. J., Nguyen, B., Karakolis, E. G., and Sinton, D. (2018). Emerging microalgae technology: a review. *Sustain. Energy Fuels* 2, 13–38. doi: 10.1039/c7se00236j

QLD (2016). *Soil Properties*. LAV. Management. Queensland: Queensland Government.

Querques, N., Cesta, M., Santos, R. M., and Chiang, Y. W. (2015). Microalgal phycocyanin productivity: strategies for phyco-valorization. *J. Chemi. Technol. Biotechnol.* 90, 1968–1982. doi: 10.1002/jctb.4796

Ravelonandro, P. H., Ratianarivo, D. H., Joannis-Cassan, C., Isambert, A., and Raherimandimby, M. (2011). Improvement of the growth of *Arthrospira* (*Spirulina*) *platensis* from Toliara (Madagascar): effect of agitation, salinity and CO2 addition. *Food Bioprod. Proce.* 89, 209–216. doi: 10.1016/j.fbp.2010.04.009

Roberts, D. A., Paul, N. A., Bird, M. I., and de Nys, R. (2015). Bioremediation for coal-fired power stations using macroalgae. *J f Environ. Manag.* 153, 25–32. doi: 10.1016/j.jenvman.2015.01.036

Roberts, G. W., Fortier, M.-O. P., Sturm, B. S. M., and Stagg-Williams, S. M. (2013). Promising pathway for algal biofuels through wastewater cultivation and hydrothermal conversion. *Energy Fuels* 27, 857–867. doi: 10.1021/ef3020603

Ruangsomboon, S., Chidthaisong, A., Bunnag, B., Inthorn, D., and Narumon, W. H. (2007). Lead (Pb2+) adsorption characteristics and sugar composition of capsular polysaccharides of cyanobacterium *Calothrix marchica*. *J. Sci. Technol.* 29, 529–541.

Ryckebosch, E., Bruneel, C., Muylaert, K., and Foubert, I. (2012). Microalgae as an alternative source of omega-3 long chain polyunsaturated fatty acids. *Lipid Technol.* 24, 128–130. doi: 10.1002/lite.201200197

Saunders, R. J., Paul, N. A., Hu, Y., and de Nys, R. (2012). Sustainable sources of biomass for bioremediation of heavy metals in waste water derived from coal-fired power generation. *PLoS One* 7:e36470. doi: 10.1371/journal.pone.0036470

Schenk, P. (2016). *On-farm Algal Ponds to Provide Protein for Northern Cattle*. North Sydney NSW: Meat and Lifestock Australia.

Schultze, L. K. P., Simon, M., Li, T., Langenbach, D., Podola, B., and Melkonian, M. (2015). High light and carbon dioxide optimize surface productivity in a twin-layer biofilm photobioreactor. *Algal Res.* 8, 37–44. doi: 10.1016/j.algal.2015.01.007

Setta, B. R. S., Barbarino, E., Passos, F. B., and Lourenço, S. O. (2017). An assessment of the usefulness of the cyanobacterium *Synechococcus subsalsus* as a source of biomass for biofuel production. *Latin Am. J. Aqu. Res.* 42, 364–375. doi: 10.3856/vol42-issue2-fulltext-7

Silva, P. G., and Silva, H. J. (2007). Effect of mineral nutrients on cell growth and self-flocculation of *Tolypothrix tenuis* for the production of a biofertilizer. *Bioresour. Technol.* 98, 607–611. doi: 10.1016/j.biortech.2006.02.026

Singh, J. S., Kumar, A., Rai, A. N., and Singh, D. P. (2016). Cyanobacteria: a precious bio-resource in agriculture, ecosystem, and environmental sustainability. *Front. Microbiol.* 7:529. doi: 10.3389/fmicb.2016.00529

Stock, A. (2014). "Australia's electricity sector," in *Ageing, Inefficient and Unprepared*, ed. C. Council, (Hobart: Australia Climate Council of Australian Ltd).

Tsuzuki, M., Ohnuma, E., Sato, N., Takaku, T., and Kawaguchi, A. (1990).). Effects of CO2 concentration during growth on fatty acid composition in microalgae. *Plant Physiol.* 93, 851–856. doi: 10.1104/pp.93.3.851

Velu, C., Cirés, S., Alvarez-Roa, C., and Heimann, K. (2015). First outdoor cultivation of the N2-fixing cyanobacterium *Tolypothrix* sp. in low-cost suspension and biofilm systems in tropical Australia. *J. Appli. Phycol.* 27, 1743–1753. doi: 10.1007/s10811-014-0509-x

Velu, C., Cirés, S., Brinkman, D. L., and Heimann, K. (2019). Effect of CO2 and metal-rich waste water on bioproduct potential of the diazotrophic freshwater cyanobacterium. *Tolypothrix* sp. *Heliyon* 5:e01549. doi: 10.1016/j.heliyon.2019.e01549

von Alvensleben, N., and Heimann, K. (2019). "The potential of microalgae for biotechnology: a focus on carotenoids," in *Blue Biotechnology: Production and Use of Marine Molecules*, eds S. La Barre, and S. Bates, (London: Wiley & Sons), 117–142. doi: 10.1002/9783527801718.ch4

von Alvensleben, N., Stookey, K., Magnusson, M., and Heimann, K. (2013). Salinity tolerance of *Picochlorum atomus* and the use of salinity for contamination control by the freshwater cyanobacterium *Pseudanabaena limnetica*. *PloS One* 8:e63569. doi: 10.1371/journal.pone.0063569

Vonshak, A., and Richmond, A. (1988). Mass production of the blue-green alga *Spirulina*: an overview. *Biomass* 15, 233–247. doi: 10.1016/0144-4565(88)90059-5

Wang, B., Li, Y., Wu, N., and Lan, C. Q. (2008). CO2 bio-mitigation using microalgae. *Appl. Microbiol. Biotechnol.* 79, 707–718. doi: 10.1007/s00253-008-1518-y

Watanabe, A. (1962). Effect of nitrogen-fixing blue-green alga: *Tolypothrix tenuis* on the nitrogenous fertility of paddy soil and on the crop yield of rice plant. *J. Gen. Appl. Microbiol.* 8, 85–91. doi: 10.2323/jgam.8.85

Watanabe, A., Nishigaki, S., and Konishi, C. (1951). Effect of nitrogen-fixing blue-green algae on the growth of rice plants. *Nature* 168:748. doi: 10.1038/168748b0

Weckesser, J., Hofmann, K., Jürgens, U. J., Whitton, B. A., and Raffelsberger, B. (1988). Isolation and chemical analysis of the sheaths of the filamentous cyanobacteria *Calothrix parietina* and *C. scopulorum*. *Microbiology* 134, 629–634. doi: 10.1099/00221287-134-3-629

Xia, J. R., and Gao, K. S. (2005). Impacts of elevated CO2 concentration on biochemical composition, carbonic anhydrase, and nitrate reductase activity of freshwater green algae. *J. Integ. Plant Biol.* 47, 668–675. doi: 10.1111/j.1744-7909.2005.00114.x

Zhang, K., Kurano, N., and Miyachi, S. (1999). Outdoor culture of a cyanobacterium with a vertical flat-plate photobioreactor: effects on productivity of the reactor orientation, distance setting between the plates, and culture temperature. *Appl. Microbiol. Biotechnol.* 52, 781–786. doi: 10.1007/s002530051591

Zhang, K., Miyachi, S., and Kurano, N. (2001). Photosynthetic performance of a cyanobacterium in a vertical flat-plate photobioreactor for outdoor microalgal production and fixation of CO2. *Biotechnol. Lett.* 23, 21–26.

Conflict of Interest: The authors declare that the research was conducted in the absence of any commercial or financial relationships that could be construed as a potential conflict of interest.

frontiers in Bioengineering and Biotechnology

BRIEF RESEARCH REPORT
published: 27 March 2020
doi: 10.3389/fbioe.2020.00204

Enhancing CO_2-Valorization Using *Clostridium autoethanogenum* for Sustainable Fuel and Chemicals Production

*James K. Heffernan[1†], Kaspar Valgepea[1,2†], Renato de Souza Pinto Lemgruber[1], Isabella Casini[3], Manuel Plan[4], Ryan Tappel[5], Sean D. Simpson[5], Michael Köpke[5], Lars K. Nielsen[1,4] and Esteban Marcellin[1,4]**

[1] Australian Institute for Bioengineering and Nanotechnology, The University of Queensland, Saint Lucia, QLD, Australia, [2] ERA Chair in Gas Fermentation Technologies, Institute of Technology, University of Tartu, Tartu, Estonia, [3] Center for Applied Geosciences, University of Tübingen, Tübingen, Germany, [4] Queensland Node of Metabolomics Australia, The University of Queensland, Saint Lucia, QLD, Australia, [5] LanzaTech Inc., Skokie, IL, United States

OPEN ACCESS

Edited by:
Christoph Herwig,
Vienna University of Technology, Austria

Reviewed by:
Claudio Martin Pereira De Pereira,
Federal University of Pelotas, Brazil
Frank Robert Bengelsdorf,
University of Ulm, Germany

***Correspondence:**
Esteban Marcellin
e.marcellin@uq.edu.au

[†]These authors have contributed equally to this work

Specialty section:
This article was submitted to Bioprocess Engineering, a section of the journal Frontiers in Bioengineering and Biotechnology

Received: 18 July 2019
Accepted: 02 March 2020
Published: 27 March 2020

Citation:
Heffernan JK, Valgepea K, de Souza Pinto Lemgruber R, Casini I, Plan M, Tappel R, Simpson SD, Köpke M, Nielsen LK and Marcellin E (2020) Enhancing CO_2-Valorization Using Clostridium autoethanogenum for Sustainable Fuel and Chemicals Production. Front. Bioeng. Biotechnol. 8:204. doi: 10.3389/fbioe.2020.00204

Acetogenic bacteria can convert waste gases into fuels and chemicals. Design of bioprocesses for waste carbon valorization requires quantification of steady-state carbon flows. Here, steady-state quantification of autotrophic chemostats containing Clostridium autoethanogenum grown on CO_2 and H_2 revealed that captured carbon (460 ± 80 mmol/gDCW/day) had a significant distribution to ethanol (54 ± 3 C-mol% with a 2.4 ± 0.3 g/L titer). We were impressed with this initial result, but also observed limitations to biomass concentration and growth rate. Metabolic modeling predicted culture performance and indicated significant metabolic adjustments when compared to fermentation with CO as the carbon source. Moreover, modeling highlighted flux to pyruvate, and subsequently reduced ferredoxin, as a target for improving CO_2 and H_2 fermentation. Supplementation with a small amount of CO enabled co-utilization with CO_2, and enhanced CO_2 fermentation performance significantly, while maintaining an industrially relevant product profile. Additionally, the highest specific flux through the Wood-Ljungdahl pathway was observed during co-utilization of CO_2 and CO. Furthermore, the addition of CO led to superior CO_2-valorizing characteristics (9.7 ± 0.4 g/L ethanol with a 66 ± 2 C-mol% distribution, and 540 ± 20 mmol CO_2/gDCW/day). Similar industrial processes are commercial or currently being scaled up, indicating CO-supplemented CO_2 and H_2 fermentation has high potential for sustainable fuel and chemical production. This work also provides a reference dataset to advance our understanding of CO_2 gas fermentation, which can contribute to mitigating climate change.

Keywords: gas fermentation, *Clostridium autoethanogenum*, carbon dioxide, valorization, carbon recycling, fuel and chemical platforms

INTRODUCTION

Gas fermentation has attractive waste carbon valorization properties, for which the need is intensifying (International Panel on Climate Change [IPCC], 2014; Emerson and Stephanopoulos, 2019). Recently, LanzaTech commercialized the first waste gas-to-ethanol process, efficiently incorporating the carbon from steel mill off-gas into fuel quality ethanol *via* the model acetogen

Clostridium autoethanogenum. The key carbon source—carbon monoxide (CO)—accounts for a significant portion of steel mill off-gas and synthesis gas (syngas), which can be generated from multiple high-volume, non-gaseous waste feedstocks (e.g., biomass, municipal solid waste) (Liew et al., 2016). Therefore, LanzaTech's process is significant in that it valorizes waste carbon by fusing two one-carbon gas molecules (C1) into liquid fuel. Furthermore, Handler et al. (2016) found that ethanol produced by LanzaTech's process reduced greenhouse gas emissions by 67 to 98% when compared to petroleum gasoline on an energy content and "cradle-to-grave" basis (feedstock dependent). Carbon dioxide (CO_2) represents a more diverse and plentiful waste stream compared to CO (International Panel on Climate Change [IPCC], 2014), thus embodying a feedstock with greater climate change mitigation and carbon recycling potential.

Increasing acetogenic carbon capture as CO_2 would build on the success of commercial gas fermentation and continue the expansion of the technology as a platform for sustainable chemical production (Redl et al., 2017; Bengelsdorf et al., 2018; Müller, 2019). Compared to other CO_2 valorization methods, acetogens are ideal candidates due to their high metabolic efficiency, ability to handle variable gas compositions, high product specificity, scalability, and low susceptibility to poisoning by sulfur, chlorine, and tars (Liew et al., 2016; Artz et al., 2018). However, metabolism of CO_2 requires an energy source, for which some see an appropriate solution is lacking (Emerson and Stephanopoulos, 2019).

Gas fermenting acetogens harbor the Wood-Ljungdahl pathway (WLP) (Drake et al., 2008), a non-photosynthetic C1-fixation metabolic pathway with the highest-known theoretical thermodynamic efficiency (Fast and Papoutsakis, 2012; Schuchmann and Müller, 2014; Müller, 2019). Various potential energy sources exist for metabolizing CO_2, primarily hydrogen, nitrates, sugars, and arginine. Yet, acetogenic CO_2 valorization, which is actively being developed for industrial implementation (Tizard and Sechrist, 2015), poses challenges along with promise. These include potential adenosine triphosphate (ATP) starvation in autotrophic conditions and carbon catabolite repression in hetero/mixotrophic conditions (Emerson and Stephanopoulos, 2019).

Hydrogen (H_2) is the most recognized energy source for CO_2 utilization—as metabolism of sugars or nitrates cause shifts in metabolism that result in lower CO_2 or H_2 utilization (Liew et al., 2016; Emerson and Stephanopoulos, 2019). H_2 production will also logically transition to renewable sources in the future, whereas production of sugars and nitrates are dependent on less-sustainable methods. Furthermore, levelized cost predictions for solar H_2 indicate a 30% reduction by 2030, potentially becoming competitive with the current levelized cost of fossil fuel derived H_2 by 2035 (Detz et al., 2018; Glenk and Reichelstein, 2019). This is in part due to rapidly decreasing solar electricity costs (IRENA, 2017) and projections of H_2 electrolysis technology development (Detz et al., 2018; Glenk and Reichelstein, 2019). Similarly, atmospheric CO_2 capture *via* direct air contact showed promising feasibility recently (Keith et al., 2018), which represents an essential development for carbon recycling (Otto et al., 2015). Various power-to-gas technologies are being discussed for mediating fluctuations in renewable power generation (Götz et al., 2016). By extension, gas fermentation to liquid products could couple mediation of renewable power fluctuations to carbon recycling (Redl et al., 2017). This provides an attractive new opportunity for bacterial artificial-photosynthesis, whereby renewable H_2 supplementation facilitates acetogenic CO_2 valorization (Claassens et al., 2016; Haas et al., 2018).

Continuous culture bioprocesses are preferable to batch or fed-batch fermentation bioprocesses (Hoskisson and Hobbs, 2005). Furthermore, systems-level quantification is essential for design-build-test-learn bioprocess optimization by metabolic engineering (Valgepea et al., 2017). Therefore, obtaining quantitative datasets from steady-state chemostat cultures, whose analyses are comparable between experiments, is important for development of these systems (Adamberg et al., 2015). Whilst Bengelsdorf et al. (2018) reviewed autotrophic acetogen growth on CO_2 and H_2 (CO_2/H_2), and Mock et al. (2015) provided notable insight into the CO_2/H_2 metabolism of *C. autoethanogenum*, the literature lacks a steady-state dataset where carbon flows in a CO_2/H_2 fermentation are quantified. Here we aimed to quantify steady-state CO_2/H_2 fermentation using fully instrumented chemostats and the model acetogen *C. autoethanogenum*. Subsequently, we showed that CO_2 is a promising feedstock alternative to CO, as more than half of the substrate CO_2 carbon was converted into ethanol. Furthermore, supplementation with CO at low concentrations improved fermentation performance significantly.

MATERIALS AND METHODS

Bacterial Strain, Growth Medium, and Continuous Culture Conditions

A derivate of *Clostridium autoethanogenum* DSM 10061 strain—DSM 19630—deposited in the German Collection of Microorganisms and Cell Cultures (DSMZ) was used in all experiments and stored as glycerol stocks at −80°C. This non-commercial strain was grown on CO_2/H_2 (∼23% CO_2, ∼67% H_2 and ∼10% Ar; BOC Australia) and $CO/CO_2/H_2$ (∼2% CO, ∼23% CO_2, ∼65% H_2, and ∼10% Ar; BOC Australia) in chemically defined medium (Valgepea et al., 2017). Cells were grown under strictly anaerobic conditions at 37°C and at a pH of 5 (maintained by 5 M NH_4OH). Chemostat continuous culture achieved steady-states at dilution rates (D) = 0.47 ± 0.01 (CO_2/H_2; specific growth rate (μ) = 0.0196 ± 0.0004 [average ± standard deviation]), 0.5 ± 0.01, and 1 ± 0.01 day^{-1} ($CO/CO_2/H_2$; μ = 0.021 ± 0.0004, and 0.042 ± 0.0008 h^{-1} respectively). See **Table 1** for steady-state gas-liquid mass transfer rate data. The steady-state results reported here were collected after optical density (OD), gas uptake and production rates had been stable in chemostat mode for at least three working volumes. See Valgepea et al. (2017) for details on equipment.

Experimental Analysis and Quantification

Biomass concentration (gDCW/L) was estimated, and extracellular metabolome analysis carried out as specified in Valgepea et al. (2018).

TABLE 1 | Summary of low-biomass *Clostridium autoethanogenum* fermentations.

Gas	y	F	N	BR	D	BC		Ace		EtOH	
	(Ar to 100%)	mL /min	rpm	#	day^{-1}	gDCW /L	±	g/L	±	g/L	±
CO[a]	60% CO	50	510	4	1	0.47	0.02	2.12	0.18	0.63	0.05
Syngas[a]	50 % CO, 20% CO_2, 20% H_2	50	500	2	1	0.48	0.04	4.35	0.12	0.61	0.06
CO/H_2[a]	15% CO, 45% H_2	50	650	4	1	0.46	0.04	0.69	0.07	4.46	0.41
$CO/CO_2/H_2$	2% CO, 23% CO_2, 65% H_2	30	1200	2	1	0.34	0.02	5.03	0.34	4.79	0.43
CO_2/H_2	23% CO_2, 67% H_2	32	500	3	0.5	0.18	0.02	2.51	0.42	2.36	0.25
$CO/CO_2/H_2$	2% CO, 23% CO_2, 65% H_2	30	800	2	0.5	0.54	0.01	5.97	0.98	9.69	0.39

[a]*Data from Valgepea et al. (2018).*

y, gas compositions; F, gas flowrate; N, stirrer speed; BR, biological replicates; D, dilution rate; BC, biomass concentration; Ace, acetate concentration; EtOH, ethanol concentration; ±, plus/minus standard deviation.

Bioreactor off-gas was analyzed by an online Hiden HPR-20-QIC mass spectrometer. The Faraday Cup detector monitored the intensities of H_2, CO, ethanol, H_2S, Ar, and CO_2 at 2, 14, 31, 34, 40, and 44 atomic mass units (amu), respectively, in the bioreactor off-gas. These masses were chosen so that each target compound would be represented by a unique signal. This was determined to be essential to achieve the highest confidence in quantification using preliminary experiments, as interferences from other compounds at a shared mass could not be reliably accounted for (e.g., the more intense signal from CO at 28 amu could not be used due to the uncertainty of interference at 28 amu from CO_2 fragmentation). Gas from the cylinder was used as the calibration gas for each MS-cycle (i.e., "online calibration") to achieve reliable off-gas analysis (Valgepea et al., 2017).

Gas uptake (CO, CO_2, and H_2) and production (ethanol) were determined using "online calibration" of the MS by analyzing the respective feed gas directly from the cylinder after each analysis cycle of the bioreactors. Specific rates (mmol/gDCW/h) were calculated by taking into account the exact composition of the respective gas, bioreactor liquid working volume, feed gas flow rate, off-gas flow rate (based on the fractional difference of the inert gas [Ar] in the feed and off-gas composition), the ideal gas molar volume, and the steady-state biomass concentration.

The carbon balances were determined at 116 ± 11%, 103 ± 12%, and 108 ± 11% for CO_2/H_2, and $CO/CO_2/H_2$ at D = 0.5 and 1 day^{-1} respectively (total C-mol products/total C-mol substrates), as specified in Valgepea et al. (2017).

Genome-Scale Metabolic Modeling With GEM iCLAU786

Model simulations were performed using genome scale model (GEM) iCLAU786 of *C. autoethanogenum* and flux balance analysis (FBA) (Orth and Palsson, 2011) as specified in Valgepea et al. (2018). Briefly, we used FBA to estimate intracellular fluxes (SIM1–26) by incorporating experimentally measured constraints (specific growth rate, and specific acetate, ethanol, cysteine, CO, CO_2, and H_2 consumption or production rates; **Table S3**) and employing maximization of ATP dissipation as the objective function. These values were validated by prediction of "optimal" growth phenotypes for experimental conditions (SIM27–48), which incorporated experimental constraints (specific cysteine, CO, CO_2, and H_2 consumption rates), ATP dissipation flux calculated above, and maximization of biomass yield as the objective function. Complete simulation results identified as SIMx (e.g., SIM1) in the text are in **Table S11**. SIM1-19, 27-41, and 49-55 are from Valgepea et al. (2018). Additional constraints were also used to improve the accuracy of predictive simulations were justifiable [SIM49-55; details described in Valgepea et al. (2018)]. Here, CO_2 reduction to formate was forced from the formate dehydrogenase (FdhA) reaction scheme (Reaction ID: rxn00103_c0) in SIM42-48, to the correct reaction scheme in SIM56-62, as identified by Mock et al. (2015)—FdhA/Hydrogenase ABCDE complex (HytABCDE; Reaction ID: rxn08518_c0). Additionally, since extracellular metabolome analysis did not detect excretion of pyruvate by the cells, we manually blocked pyruvate export in the model (rxn05469_c0) in SIM56-62. Reaction IDs comprising letters and numbers are labels corresponding to reactions in **Table S11** (follows reference to reaction/enzyme).

RESULTS

Clostridium autoethanogenum Steady-State Fermentation of Carbon Dioxide and Hydrogen

Clostridium autoethanogenum cells reached steady-state when growing on CO_2/H_2 in chemostats at dilution rate (D) ∼0.5 day^{-1} [specific growth rate (μ) ∼0.02 h^{-1}] with a biomass concentration of 0.18 ± 0.02 g dry cell weight (gDCW)/L (**Figure 1A**). It is important to note that attempts to reach a steady-state at D = 1 day^{-1} were unsuccessful. Unlike the chemostat cultures of *C. autoethanogenum* with CO (Valgepea et al., 2017, 2018) and CO_2/H_2 retentostat cultures (Mock et al., 2015), the CO_2/H_2 cultures could not reach stable biomass concentrations before the culture began oscillation cycles; previously observed above ∼1.6 gDCW/L (Valgepea et al., 2017). The physiological reason and mechanism for such oscillatory culture behavior are under investigation, but we assumed that cell recycling is a requirement for CO_2/H_2 culture stability. For example, Molitor et al. (2019) showed consistent, high-biomass

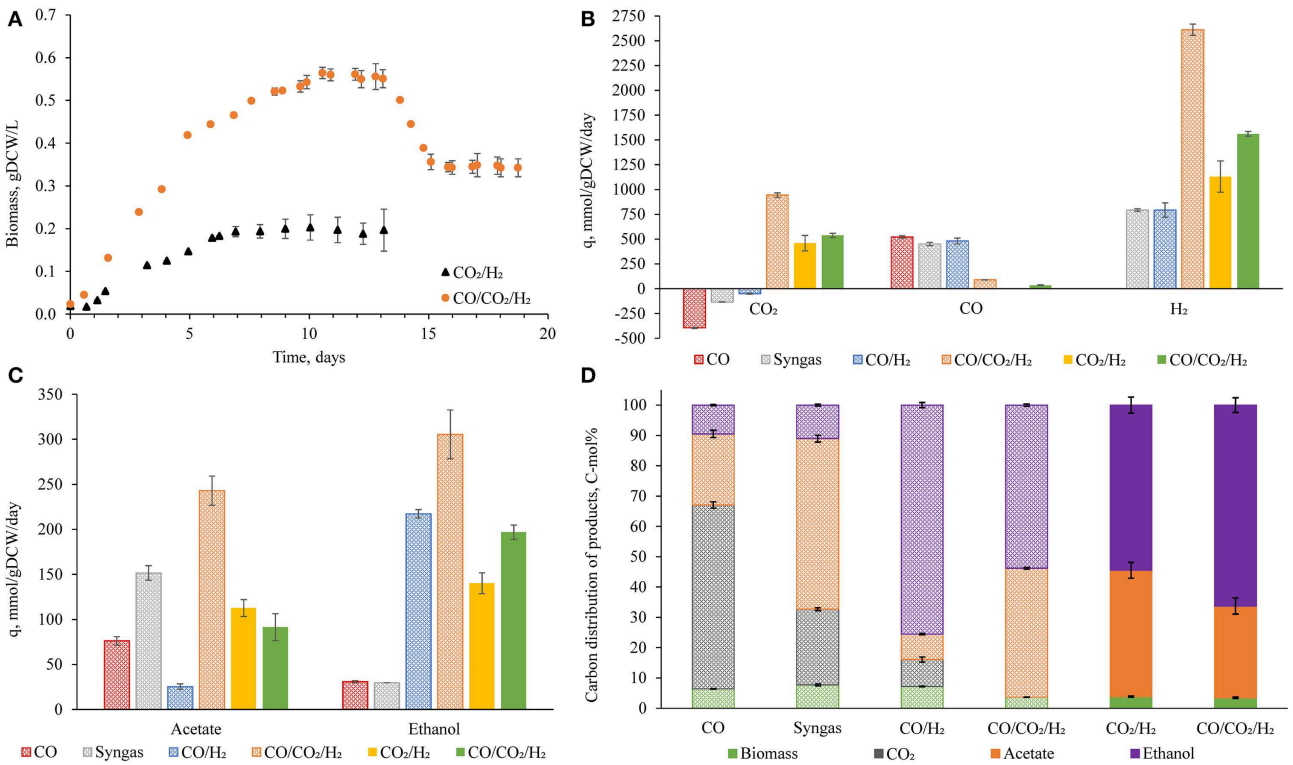

FIGURE 1 | Important fermentation characteristics of *Clostridium autoethanogenum* in autotrophic chemostats. Results from Valgepea et al. (2018) are also displayed **(B–D)**, the conditions of all fermentations are summarized in **Table 1**. Growth curves of novel fermentations with standard deviation at steady-state **(A)**. Specific rates of uptake **(B)** and production **(C)** for important metabolites. Product carbon balances **(D)**. Values represent the average ± standard deviation between biological replicates. Number of biological replicates, and detailed gas composition for each fermentation are available in **Table 1**. Patterned bars indicate a D of 1 day^{-1}, full bars indicate a D of 0.5 day^{-1} **(B–D)**. *q*, specific rate; *DCW*, dry cell weight.

concentration and high-acetate CO_2/H_2 fermentation with *Clostridium ljungdahlii* in a retentostat with complete recycling.

Despite the attempt to reach a steady-state at D = 1 day^{-1}, cells reached steady-state at dilution rate = 0.5 day^{-1}, with a specific rate of carbon incorporation (i.e., qCO_2) of 480 ± 80 mmol/gDCW/day (**Figure 1B**). Furthermore, the specific production rates of ethanol and acetate were 140 ± 10 and 113 ± 9 mmol/gDCW/day, respectively (**Figure 1C**). Strikingly, this meant around half of the captured carbon was converted to ethanol (54 ± 3 C mol%) (**Figure 1D** and **Table S4**). Fermentation conditions and titers are available in **Table 1**, showing an impressive ethanol concentration compared to previous fermentations where CO was the main carbon and energy source.

Despite the different dilution rate, the CO_2/H_2 results generated were compared to previously published chemostat cultures of *C. autoethanogenum* grown on CO, syngas, and CO/H_2 (Valgepea et al., 2018) at similar biomass concentrations (∼0.5 gDCW/L) (**Figures 1B–D**). Specific rates of acetate and ethanol production achieved here for CO_2/H_2 cultures fell between those for syngas (■) and CO/H_2 (■) cultures (**Figures 1B,D**). However, the specific rate of carbon incorporation was higher for CO_2/H_2 (**Figure 1C**). We found that more than half of the captured CO_2 was converted into ethanol (**Figure 1D**). These results were encouraging, especially as ethanol production has unfavorable stoichiometry compared to acetate (Mock et al., 2015). Furthermore, the H_2 specific uptake rate (1,130 ± 160 mmol/gDCW/day) showed that higher H_2 uptake rates are achievable (compared to old datasets). These results show that higher carbon yields are possible (Valgepea et al., 2018). To investigate further the metabolic demand and the feasibility of CO_2/H_2 fermentation, we utilized the measured specific consumption and production rates and specific growth rate from the steady-state dataset as constraints for the genome-scale metabolic model (GEM) to find candidate mechanisms for improving CO_2/H_2 fermentation using the metabolic model iCLAU786.

Metabolic Model of Carbon Dioxide and Hydrogen Fermentation

Estimation of intracellular processes constrained by *in vivo* datasets represents an important developmental step for progressing acetogenic CO_2 valorization. Here, we used the GEM to compare intracellular metabolic flux distributions on CO_2/H_2 and CO-containing gases (**Figure 2**). See **Figures S2, S3** and **Tables S8–S10** for further flux comparison summaries.

Intracellular metabolic fluxes estimated using the model iCLAU786 and flux balance analysis (FBA) (**Figure 2**) showed

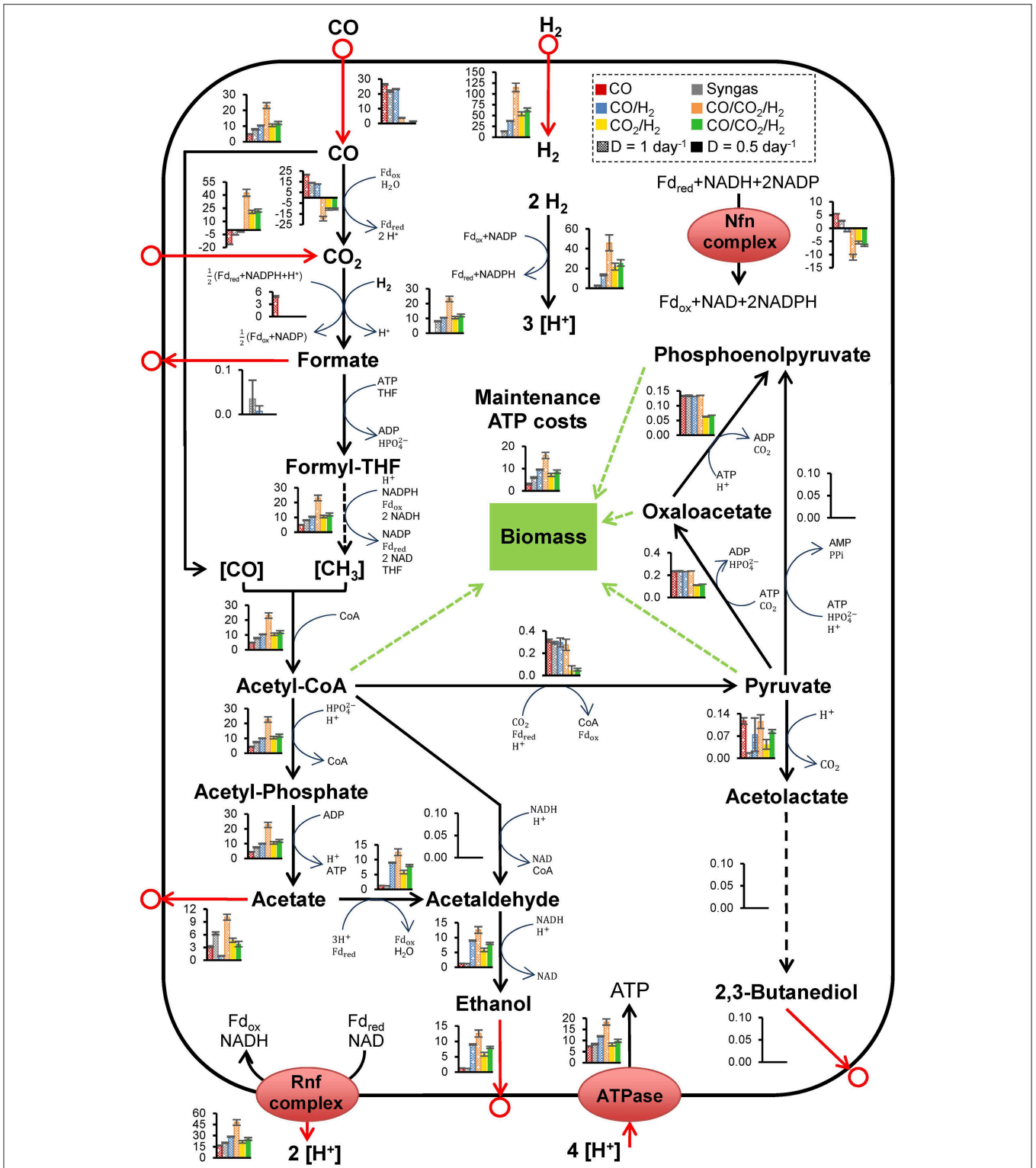

FIGURE 2 | Intracellular metabolic fluxes in *Clostridium autoethanogenum* growing on various gas mixes, estimated using the metabolic model iCLAU786 and flux balance analysis. Bar charts show specific flux rates (mmol/gDCW/h) from **Tables S10, S11** and represent the average ± standard deviation between biological Replicates from SIM: 1–4 (CO), 9–10 (Syngas), 13–15 (CO/H_2), 20–21 ($CO/CO_2/H_{21}$), 22–24 (CO_2/H_2), and 25–26 ($CO/CO_2/H_{20.5}$). Results for CO, syngas, and CO/H_2 are low biomass condition data from Valgepea et al. (2018), the conditions of these fermentations are summarized in **Table 1**. Number of biological replicates, and detailed gas composition for each fermentation are available in **Table 1**. Arrows show the direction of calculated fluxes; red arrows denote uptake or secretion, dashed arrows denote a series of reactions. Brackets denote metabolites bound by an enzyme. Refer to **Figures S1, S2** for enzyme involvement, metabolite abbreviations, and complete flux balance analysis datasets.

remarkable similarity to the combined theoretical stoichiometry of acetate and ethanol production (Mock et al., 2015) and indicated energetic cofactor circuits with mapping close to 1:1 (experimental:theoretical stoichiometry; **Figure S4**). Ethanol production likely occurred *via* acetaldehyde:ferredoxin oxidoreductase (AOR; ReactionID: leq000004; see Materials and Methods) under autotrophic conditions, with the HytABCDE (leq000001) and Nfn complex (leq000002) likely facilitating cofactor production *via* electron bifurcation (**Figure 2**) (Valgepea et al., 2018). This is a mechanism for minimization of free energy loss employed by *C. autoethanogenum* and may play a key role in sustaining proton motive force by balancing acetate, ethanol, and ATP production (Mock et al., 2015; Valgepea et al., 2018). Engineering acetogens to redirect this energy toward cellular growth, sacrificing some ethanol production, could be beneficial for CO_2 fermentation (Emerson and Stephanopoulos, 2019).

It was notable that, unlike CO fermentations, the intracellular pyruvate:ferredoxin oxidoreductase (PFOR; rxn05938_c0; acetyl-CoA ↔ pyruvate) flux was not significantly in the direction of pyruvate (**Figure 2**) (Valgepea et al., 2018). Under autotrophic conditions, PFOR links the WLP to anabolic pathways associated with biomass (Furdui and Ragsdale, 2000), and therefore this indicated high cell-specific energetic limitation. From this observation, we hypothesized that CO supplementation could provide a potential solution, as CO oxidation would generate additional Fd_{red}. Furthermore, an ATP/H_2 flux ratio of ∼0.15 was estimated using metabolic modeling here compared to an ATP/CO ratio of ∼0.28 in CO only fermentations (Valgepea et al., 2018). Considering CO/H_2 and CO_2/H_2 fermentations had equal carbon-flux through the WLP (∼10 mmol/gDCW/h; **Figure 2**), supplementation with renewable CO from CO_2 electrolysis could aid biomass formation and culture stability. A similar process (but CO fermentation) was detailed by Haas et al. (2018).

Clostridium autoethanogenum Steady-State Fermentation of Carbon Dioxide and Hydrogen Supplemented With Carbon Monoxide

To validate our modeling hypothesis, *Clostridium autoethanogenum* was cultured with a low concentration of carbon monoxide in addition to CO_2 and H_2 (CO/CO_2/H_2) in chemostats. A steady-state was reached at D = 0.5 day^{-1} (μ ∼0.02 h^{-1}), and at D =1 day^{-1} (μ ∼0.04 h^{-1}; **Figure 1A**; biomass concentrations of 0.54 ± 0.01 and 0.34 ± 0.02 gDCW/L respectively). CO/CO_2/H_2 fermentations at a D = 1 day^{-1} (CO/CO_2/H_{2^1}; superscript 1 denotes D of 1 day^{-1}) and at a D = 0.5 day^{-1} (CO/CO_2/$H_{2^{0.5}}$; superscript 0.5 denotes D of 0.5 day^{-1}) showed simultaneous uptake of CO (89 ± 2 and 36 ± 4 mmol/gDCW/day, respectively) and CO_2 (940 ± 20 and 540 ± 20 mmol/gDCW/day, respectively) (**Figure 1B**). The co-utilization of both C1 gases is, to the best of our knowledge, an unquantified phenomenon. This led to a specific carbon incorporation (CO/CO_2/H_{2^1} −1030 ± 30 mmol/gDCW/day) larger than any other gas type (maximum of ∼450 mmol/gDCW/day for fermentations with CO in Valgepea et al. (2018) or CO_2/H_2 in this work). This also resulted in significant improvements to culture performance compared to CO_2/H_2 fermentations.

Compared to CO_2/H_2, CO/CO_2/$H_{2^{0.5}}$ showed higher acetate and ethanol titers (**Table 1**) and specific productivities (**Figure 1C**), and a higher ethanol/acetate ratio (2.15 vs. 1.24 mol/mol respectively; **Tables S1, S2**). While at a similar biomass concentration (CO/CO_2/H_{2^1} best comparison due to similarity in dilution rate), acetate and ethanol titers (**Table 1**), and specific productivities (**Figure 1C**) are greater than during fermentation of other CO-containing gases. When comparing to high biomass (∼1.4 gDCW/L) CO cultures, CO-supplementation still performs impressively—CO/H_2 fermentation achieved a higher ethanol titer (11.6 ± 0.4 g/L), while CO and syngas fermentations were similar (3.9 ± 0.2 and 5.4 ± 0.3 g/L respectively; **Table S5**). Otherwise, all specific productivities were higher for CO/CO_2/H_{2^1} (**Figure S3**). Furthermore, the distribution of carbon to ethanol was still >50% (53.8 ± 0.4% and 66 ± 2% for CO/CO_2/H_{2^1} and CO/CO_2/$H_{2^{0.5}}$, respectively; **Figure 1D** and **Table S4**).

To understand the metabolic effects of supplementing CO, FBA was performed using the same conditions and alterations as for CO_2/H_2 (**Figure 2**). Notably, the WLP specific flux throughput for CO/CO_2/H_{2^1} was ∼2-fold greater than for any other gas type (including high-biomass Valgepea et al., 2018). Furthermore, for CO_2 fermentations, Nfn complex flux direction was opposite that of CO and syngas fermentations. CO/CO_2/$H_{2^{0.5}}$ also showed significantly greater flux through the AOR, whilst specific WLP productivity was insignificantly different compared to CO_2/H_2.

DISCUSSION

Achieving steady-state continuous cultures using CO_2/H_2 mixtures, without cell recycling here, was challenging. Yet, compared to other organisms fermenting CO_2/H_2 with continuous medium exchange, *Clostridium autoethanogenum* performs well (**Table 2**). No direct comparisons can be made to other experiments due to variations in conditions, but *C. autoethanogenum* clearly achieves the highest ethanol production, with comparable quantities of carbonous products also. *Acetobacterium woodii*, along with *Sporomusa ovata*, were shown to perform well when compared to a wide range of acetogens under batch CO_2/H_2 conditions (Groher and Weuster-Botz, 2016). Yet, as evidenced by omission of *S. ovata* from **Table 2**, few continuous culture characterizations of acetogens are available—an essential step for validation of industrial robustness in gas fermentation. As discussed by Molitor et al. (2019), the lack of yeast extract or $C_{\geq 2}$ substrates is also distinguishing between fermentations.

Notably, CO_2/H_2 cultures displayed higher variability between biological replicates compared to those of CO-containing gas mixtures (**Figure 1**) (Valgepea et al., 2017). This may indicate variable organism fitness, a trait previously discussed for *C. autoethanogenum* by Liew et al. (2016), who extensively covered numerous techniques used for enhancing gas fermentation including—coupling to other processes, adaptive

TABLE 2 | Summary of quantitative and continuous CO_2/H_2 fermentations.

Organism	Strain	Experimental conditions	Growth rate (day^{-1})	$C_{Product}$ g[DCW]/L	Productivity g/L/day, (g/gDCW/day)	Ref.
Acetobacterium woodii	DSM 1030	**1 L chemostat, D = 0.84 day^{-1}, 1,200 rpm, 30 L/h 17% CO_2, 40% H_2, 43% N_2, 1 atm, pH 7.0, 30°C, 4 g/L YE, *n* = 1**	**μ = 0.84**	**B = 1.1 A = 22.0**	**A = 19.1 (17.4)**	1
		1 L batch retentostat, D = 1.68 day^{-1}, 1,200 rpm, 30 L/h 17% CO_2, 40% H_2, 43% N_2, 1 atm, pH 7.0, 30°C, 4 g/L YE, *n* = 1		B = 6.0[a,b] A = 22.6	A = 40 (16.0[a,b])	1
		†D = 4.2 day^{-1}		B = 10.0[a,b] A = 23.5	A = 95 (18.5[a,b])	
		1 L batch retentostat, D = 8.4 day^{-1}, 1,200 rpm, 30 L/h 25% CO_2, 60% H_2, 15% N_2, 1 atm, pH 7.0, 30°C, 4 g/L YE, *n* = 1		B = 11.0 A = 17.6	A = 148 (20.3)	1[b,c]
	pMTL84151 _act_{thlA}	0.85 L batch retentostat, D = 1 day^{-1}, 800 rpm, 30 L/h 20% CO_2 and 80% H_2, pH 7.0, 30°C, 2 g/L YE, 10 g/L K-acetate, *n* = 1	μ = 0	B = 4.6[d] A = 48.6 Ac = 3.0	Ac = 0.6 (0.1)	2
Acetobacterium sp.	BR446	Semi-batch retentostat, D = 24 day^{-1}, CO_2 and H_2, medium not specified		B = 4.8 A = 3.0	A = 71.0 (14.7)	3
Clostridium autoethanogenum	DSM 19630	**0.75 L chemostat, D = 0.5 day^{-1}, 500 rpm, 1.92 L/h 23% CO_2, 67% H_2, 10% Ar, 1 atm, pH 5, 37°C, DM, *n* = 3**	**μ = 0.5**	**B = 0.2 A = 2.5 E = 2.4**	**B = 0.1 A = 1.3 (6.8) E = 1.2 (6.4)**	Here
		†800 rpm, 1.8 L/h 2% CO, 23% CO_2, 67% H_2, 10% Ar, *n* = 2	**μ = 0.5**	**B = 0.5 A = 6.0 E = 9.7**	**B = 0.3 A = 3.0 (5.5) E = 6.3 (11.6)**	
		†D = 1 day^{-1}, 1,200 rpm	**μ = 1.0**	**B = 0.3 A = 5.0 E = 4.8**	**B = 0.3 A = 5.0 (14.6) E = 6.2 (18.1)**	
	DSM 10061	1.3 L continuous retentostat, D = 4.9 day^{-1}, 21 L/h 23% CO_2, 65% H_2, 9.2% N_2, pH 5.3, 37°C, DM, 3.1 g/L ammonium acetate, *n* = 1	μ = 0.5	B = 1.8 A = 7.5 E = 6.3	A = 36.7 (20.0) E = 30.9 (16.9)	4
Clostridium ljungdahlii	DSM 13528	**0.5 L chemostat, D = 0.29 day^{-1}, 300 rpm, 1.8 L/h 20% CO_2 and 80% H_2, pH 5.5, 37°C, DM, *n* = 3**	**μ = 0.29**	**B = 0.2[e] A = 6.3 E = 1.8**	**A = 1.8 E = 0.5**	5
		†DM with $NaNO_3$ replacing NH_4Cl, *n* = 1	**μ = 0.29**	**B = 0.3[b,e] (pH 5.5) A = 13.4[b] (pH 6.0) E = 5.0[b] (pH 5.0)**	**A = 3.9 E = 1.4**	
		1 L batch retentostat, D = 0.96 day^{-1}, 300 rpm, 7.2 L/h 20% CO_2 and 80% H_2, pH 5.7, 35°C, DM, *n* = 1	μ = 0	B = 2.3[a] A = 18.5	A = 17.7	6
Moorella thermoacetica	ATCC 49707	1 L BCR, D = 2.16 day^{-1}, 72 L/h 33% CO_2 and 67% H_2, pH = 6.0, 60°C, 10 g/L YE, *n* = 1	μ = 0	B = 4.1[a] A = 25.0[a]	A = 54.0 (13.3)[f]	7
Moorella sp.	HUC22-1	0.5 L semi-continuous with cell retention, 500 rpm, continuous 20% CO_2 and 80% H_2, 3.6 L/h, pH 6.2, 55°C, 1 g/L YE, *n* = 1	μ = 0	B = 1.5 A = 22.0 E = 0.3	A = 6.9 (10.4)	8

Ref. 1–8: (Kantzow et al., 2015; Hoffmeister et al., 2016; Morinaga and Kawada, 1990; Mock et al., 2015; Klask et al., 2019; Molitor et al., 2019; Hu et al., 2016; Sakai et al., 2005).
$C_{Product}$, product concentration; D, dilution rate; YE, yeast extract; DM, defined medium; n, number of replicates; B, biomass; A, acetate; E, ethanol; Ac, acetone; BCR, bubble column reactor.
[a]estimated from graph, [b]not steady state (represented as maximum), [c]cell retention membrane was blocked before steady state was reached, [d]calculated using data from Kantzow et al. (2015), [e]calculated using data from Molitor et al. (2019), [f]calculated using estimated data.
†Similar to experiment above, only differences in conditions are listed. Bolded experiments are chemostats. Only biomass concentrations use gDCW/L.

laboratory evolution, and metabolic engineering of acetogens using genetic tools. CO-supplementation could be a valuable option for enhancement as it overcomes inherent problems linked to engineering acetogens. Supplementation of low quantities of CO here stabilized the culture, enabled culturing at D = 1 day^{-1}, and achieved higher biomass concentration with a carbon incorporation larger than any other gas type—all without compromising by-product distribution.

While, Valgepea et al. (2018) found that syngas fermentation lead to CO-only fermentation at steady-state, we observed co-utilization of CO and CO_2. Tizard and Sechrist (2015) have also shown co-utilization for *C. autoethanogenum* continuous cultures, and it seems that co-uptake may also occur for some points of syngas batch fermentation (Infantes et al., 2020). Co-utilization of sugars was found for *E. coli* in chemostats—where inhibition of consumption, but no change in induction time was observed (Standing et al., 1972). The WLP is most likely no different, in that metabolism of CO is preferential, yet the pathway can co-consume CO_2 under certain conditions.

Various efforts have been made toward enhancing $CO_2(+H_2)$ fermentation to $C_{\geq 2}$ products (**Table 2**) (Emerson and Stephanopoulos, 2019). Braun and Gottschalk (1981) first discovered the potential for enhancement when *Acetobacterium woodii* simultaneously consumed fructose and a headspace of CO_2/H_2 during batch cultivation. Growth and acetate production was high but no characterization of the headspace was performed. More recently, continuous glucose-supplemented CO_2/H_2 fermentation of *Moorella thermoacetica* by Park et al. (2019) did not lead to net uptake of CO_2. Furthermore, Jones et al. (2016) did not show net CO_2 uptake for a wide range of acetogens (not *A. woodii*) fermenting syngas and fructose. *A. woodii* generates a sodium ion (Na^+) gradient (Hess et al., 2013) rather than a proton (H^+) gradient for membranous ATP generation (Pierce et al., 2008; Poehlein et al., 2015; Bengelsdorf et al., 2018). This may highlight an important metabolic difference from other model acetogens—decoupling the resources of the WLP and membranous ATP generation pathways could facilitate fermentation of sugar and CO_2/H_2 simultaneously.

Other enhancements have also struggled to achieve net CO_2 uptake. Co-culture of *C. acetobutylicum* and *C. ljungdahlii* showed syntrophic metabolic coupling when fermenting glucose, fructose, and CO_2/H_2, but no net CO_2 uptake (Charubin and Papoutsakis, 2019). Addition of nitrate to batch CO_2/H_2 fermentation by *C. ljungdahlii*, increased biomass concentration and subsequently volumetric productivity of acetate (Emerson et al., 2019). However, the specific WLP productivity decreased, meaning lower utilization of CO_2. Other organisms not recognized as gas fermenters can also use mixotrophy to minimize carbon loss, such as *Clostridium beijerinckii* but have not displayed net CO_2 uptake either (Sandoval-Espinola et al., 2017). To the best of our knowledge, this is the first report where supplementation of a substrate other than H_2, increased productivities of continuous acetogenic CO_2 fermentation while maintaining net CO_2 utilization. Furthermore, the effect of CO supplementation on CO_2 utilization was superlinear, indicating a synergistic mechanism (Park et al., 2019). This is encouraging for development of bioprocesses valorizing CO_2.

Comparisons between fermentation datasets enables us to speculate about the positive effect of CO-supplementation on CO_2/H_2 fermentation. Although, addition of CO led to minimal metabolic shifts (**Figure 2**—CO_2/H_2 vs. $CO/CO_2/H_{2^{0.5}}$ and **Figure S2**), FBA showed that CO supplementation caused significant increases to the reduced ferredoxin consumption by AOR and Rnf complex (leq000004 and M002, respectively) compared to CO_2/H_2 (**Figure 2**). The overflow model proposed by Richter et al. (2016) suggests that high NADH production *via* Rnf and Nfn complexes (leq000002) is also important for reducing AOR product inhibition. In this way, NADH facilitates fast metabolism of acetaldehyde to ethanol *via* alcohol dehydrogenase (Adh(E); rxn00543_c0). Decreasing the acetate concentration reduces acidification and the ATP cost for excreting acetate (Valgepea et al., 2018). Including acetaldehyde conversion to ethanol and association to acetic acid, this also leads to consumption of 2 H^+ (4 here vs. 2 produced *via* CODH). Therefore, CO consumption decreases the intracellular H^+ pool, and following Le Chatelier's principle, drives HytABCDE activity. Indeed, the change in specific H_2 uptake relative to specific CO_2 uptake is greater than that of CO (for CO_2/H_2 vs. $CO/CO_2/H_{2^{0.5}}$, **Table S7**). Subsequently, the relative gain in free energy from H_2 is $\sim$ 4-fold greater than CO. We speculate this is ultimately responsible for the improved fitness of CO-supplemented CO_2/H_2 fermentation by *C. autoethanogenum*. We propose the following five critical factors to this enhanced metabolism: [1] metabolism of CO increases the intracellular pool of reduced ferredoxin; [2] this stimulates oxidation of ferredoxin, which if consumed by the AOR; [3] reduces ATP costs; and [4] decreases the H^+ pool/acidification; which therefore [5] drives H_2 uptake for further reduction of ferredoxin. Evidently, additional understanding of acetogenic redox metabolism, from a thermodynamic perspective, is important for developing acetogenic CO_2-valorization as a platform industrial bioprocess (Cueto-Rojas et al., 2015).

Physicochemical properties could also play a key role in CO-supplementation enabling to achieve a stable CO_2/H_2 chemostat culture at $D = 1\ day^{-1}$. Generation of a stable and large non-equilibrium is what drives microbial growth (Qian and Beard, 2005; Igamberdiev and Kleczkowski, 2009; Quéméner and Bouchez, 2014) and gas-liquid mass transfer (Ma et al., 2005). For continuous culture of gas fermenting microbes, an inherent relationship between substrate mass transfer and culture growth exists (**Supplementary Materials Note 2.1**). An important parameter for these systems is the Gibb's free energy of a system (Cueto-Rojas et al., 2015). This describes the thermodynamic favorability of the reaction system—termed spontaneity. Here, analysis of experimental flux and Gibbs free energy suggests that CO_2/H_2 fermentation is infeasible ($\Delta \dot{G}_{OR^0} = 5.4\ kJ/mol/day$), whereas CO-supplemented CO_2/H_2 fermentation is feasible ($\Delta \dot{G}_{OR^0} = -12.3\ kJ/mol/day$; **Table S6**). Though these calculations use standard conditions, they do indicate how close CO_2/H_2 fermentation is to the thermodynamic limit of metabolism. Theoretically, minute and unobservable changes to chemostat CO_2/H_2 fermentation can disrupt the culture (Henry and Martin, 2016). Thus, increasing the free energy of central metabolism with CO-supplementation appears to keep metabolism in a spontaneous and stable state by increasing reduced ferredoxin production.

The mechanisms for achieving the 2-fold higher specific WLP flux throughput for $CO/CO_2/H_{2^1}$ compared to others is less clear but appears to be linked to the difference in primary substrate. $CO/CO_2/H_{2^1}$ and CO/H_2 are the most similar CO_2 and CO fermentations, respectively ($D \sim 1\ day^{-1}$ and carbon to hydrogen feed ratio ($\sim$1:3); **Table 1**), and the maximum carbon incorporation per cell for CO/H_2 was roughly half of that of $CO/CO_2/H_{2^1}$ ($\sim$450 vs. $\sim$1,000 mmol/gDCW). Theoretically, cells will maximize carbon-to-redox metabolism by minimizing thermodynamic losses. CO supplementation to a CO_2/H_2 culture seems to facilitate this as $(H_2/carbon)_{feed}-(H_2/carbon)_{flux}$ was $\sim$0 mol/mol for $CO/CO_2/H_2$ fermentations only (**Table S2**)—an indication of the relative magnitude of carbon and redox metabolism. This suggests that high specific fluxes for $CO/CO_2/H_{2^1}$ may be a result of (close to) optimal co-factor recycling by *C. autoethanogenum*'s WLP and redox pathway.

Thus, the lower energy associated with CO_2 fermentation may, counterintuitively, stimulate specific WLP activity when in the presence of appropriate energy-containing substrates. Further quantifications of CO_2 metabolism and characterizations of enzyme activities are required to confirm these hypotheses (**Supplementary Materials Note 2.2**), as they assist our ability to engineer the links between redox and carbon metabolisms.

We established a dataset quantifying steady-state of the model acetogen *C. autoethanogenum* during autotrophic-CO_2/H_2 growth in chemostat cultures. This enabled analysis *via* FBA, and highlighted CO as a potential supplement. CO supplementation successfully improved metabolic stability and CO_2 utilization. This was the first time that intracellular fluxes for net uptake of CO_2 (with enhancement) where characterized. Industry is actively developing gas fermentation to valorize CO_2 (Tizard and Sechrist, 2015; Haas et al., 2018). Previously, genetic and process engineering of gas fermentation successfully developed the technology for industrial CO valorization (Liew et al., 2016). Therefore, progression to industrial CO_2 valorization is foreseeable, and CO supplementation may play a role in the continuing diversification of industrial gas fermentation.

DATA AVAILABILITY STATEMENT

All datasets generated for this study are included in the article/**Supplementary Material**.

AUTHOR CONTRIBUTIONS

All authors viewed and approved the manuscript and contributed significantly to the work. KV, EM, and LN conceived the project. JH, KV, and EM designed the experiments and analyzed the results. JH and KV performed experiments, supported by RS, IC, MP, and EM. JH wrote the manuscript with the help of KV, EM, RT, SS, MK, and LN.

FUNDING

This study was funded by a Grant from the Australian Research Council, partly funded by LanzaTech (ARC LP140100213).

ACKNOWLEDGMENTS

Elements of this research utilized equipment and support provided by the Queensland node of Metabolomics Australia, an initiative of the Australian Government being conducted as part of the NCRIS National Research Infrastructure for Australia. IC would like to acknowledge support from the German Academic Exchange Service (DAAD) through the DAAD Kurzstipendien für Doktoranden. We thank the following investors in LanzaTech's technology: Sir Stephen Tindall, Khosla Ventures, Qiming Venture Partners, Softbank China, the Malaysian Life Sciences Capital Fund, Mitsui, Primetals, CICC Growth Capital Fund I, L.P. and the New Zealand Superannuation Fund. There was no funding support from the European Union for the experimental part of the study. However, KV acknowledges support also from the European Union's Horizon 2020 research and innovation programme under grant agreement N810755.

SUPPLEMENTARY MATERIAL

The Supplementary Material for this article can be found online at: https://www.frontiersin.org/articles/10.3389/fbioe.2020.00204/full#supplementary-material

REFERENCES

Adamberg, K., Valgepea, K., and Vilu, R. (2015). Advanced continuous cultivation methods for systems microbiology. *Microbiology* 161, 1707–1719. doi: 10.1099/mic.0.000146

Artz, J., Müller, T. E., Thenert, K., Kleinekorte, J., Meys, R., Sternberg, A., et al. (2018). Sustainable conversion of carbon dioxide: an integrated review of catalysis and life cycle assessment. *Chem. Rev.* 118, 434–504. doi: 10.1021/acs.chemrev.7b00435

Bengelsdorf, F. R., Beck, M. H., Erz, C., Hoffmeister, S., Karl, M. M., Riegler, P., et al. (2018). Bacterial anaerobic synthesis gas (syngas) and $CO_2 + H_2$ fermentation. *Adv. Appl. Microbiol.* 103, 143–221. doi: 10.1016/bs.aambs.2018.01.002

Braun, K., and Gottschalk, G. (1981). Effect of molecular hydrogen and carbon dioxide on chemo-organotrophic growth of Acetobacterium woodii and Clostridium aceticum. *Arch. Microbiol.* 128, 294–298. doi: 10.1007/BF00422533

Charubin, K., and Papoutsakis, E. T. (2019). Direct cell-to-cell exchange of matter in a synthetic Clostridium syntrophy enables CO_2 fixation, superior metabolite yields, and an expanded metabolic space. *Metab. Eng.* 52, 9–19. doi: 10.1016/j.ymben.2018.10.006

Claassens, N. J., Sousa, D. Z., dos Santos, V. A. P. M., de Vos, W. M., and van der Oost, J. (2016). Harnessing the power of microbial autotrophy. *Nat. Rev. Microbiol.* 14, 692–706. doi: 10.1038/nrmicro.2016.130

Cueto-Rojas, H. F., van Maris, A. J., Wahl, S. A., and Heijnen, J. J. (2015). Thermodynamics-based design of microbial cell factories for anaerobic product formation. *Trends Biotechnol.* 33, 534–546. doi: 10.1016/j.tibtech.2015.06.010

Detz, R. J., Reek, J. N. H., and Van Der Zwaan, B. C. C. (2018). The future of solar fuels: when could they become competitive? *Energy Environ. Sci.* 11, 1653–1669. doi: 10.1039/C8EE00111A

Drake, H. L., Gößner, A. S., and Daniel, S. L. (2008). Old acetogens, new light. *Ann. N. Y. Acad. Sci.* 1125, 100–128. doi: 10.1196/annals.1419.016

Emerson, D. F., and Stephanopoulos, G. (2019). Limitations in converting waste gases to fuels and chemicals. *Curr. Opin. Biotechnol.* 59, 39–45. doi: 10.1016/j.copbio.2019.02.004

Emerson, D. F., Woolston, B. M., Liu, N., Donnelly, M., Currie, D. H., and Stephanopoulos, G. (2019). Enhancing hydrogen-dependent growth of and carbon dioxide fixation by Clostridium ljungdahli through nitrate supplementation. *Biotechnol. Bioeng.* 116, 294–306. doi: 10.1002/bit.26847

Fast, A. G., and Papoutsakis, E. T. (2012). Stoichiometric and energetic analyses of non-photosynthetic CO_2-fixation pathways to support synthetic biology strategies for production of fuels and chemicals. *Curr. Opin. Chem. Eng.* 1, 380–395. doi: 10.1016/j.coche.2012.07.005

Furdui, C., and Ragsdale, S. W. (2000). The role of pyruvate ferredoxin oxidoreductase in pyruvate synthesis during autotrophic growth by the Wood-Ljungdahl pathway. *J. Biol. Chem.* 275, 28494–28499. doi: 10.1074/jbc.M003291200

Glenk, G., and Reichelstein, S. (2019). Economics of converting renewable power to hydrogen. *Nat. Energy* 4, 216–222. doi: 10.1038/s41560-019-0326-1

Götz, M., Lefebvre, J., Mörs, F., McDaniel Koch, A., Graf, F., Bajohr, S., et al. (2016). Renewable power-to-gas: a technological and economic review. *Renew. Energy* 85, 1371–1390. doi: 10.1016/j.renene.2015.07.066

Groher, A., and Weuster-Botz, D. (2016). Comparative reaction engineering analysis of different acetogenic bacteria for gas fermentation. *J. Biotechnol.* 228, 82–94. doi: 10.1016/j.jbiotec.2016.04.032

Haas, T., Krause, R., Weber, R., Demler, M., and Schmid, G. (2018). Technical photosynthesis involving CO_2 electrolysis and fermentation. *Nat. Catal.* 1, 32–39. doi: 10.1038/s41929-017-0005-1

Handler, R. M., Shonnard, D. R., Griffing, E. M., Lai, A., and Palou-Rivera, I. (2016). Life cycle assessments of ethanol production via gas fermentation: anticipated greenhouse gas emissions for cellulosic and waste gas feedstocks. *Ind. Eng. Chem. Res.* 55, 3253–3261. doi: 10.1021/acs.iecr.5b03215

Henry, A., and Martin, O. C. (2016). Short relaxation times but long transient times in both simple and complex reaction networks. *J. R. Soc. Interface* 13:20160388. doi: 10.1098/rsif.2016.0388

Hess, V., Schuchmann, K., and Müller, V. (2013). The ferredoxin: NAD+ oxidoreductase (Rnf) from the acetogen acetobacterium woodii requires na+ and is reversibly coupled to the membrane potential. *J. Biol. Chem.* 288, 31496–31502. doi: 10.1074/jbc.M113.510255

Hoffmeister, S., Gerdom, M., Bengelsdorf, F. R., Linder, S., Flüchter, S., Öztürk, H., et al. (2016). Acetone production with metabolically engineered strains of *Acetobacterium woodii*. *Metab. Eng.* 36, 37–47. doi: 10.1016/j.ymben.2016.03.001

Hoskisson, P. A., and Hobbs, G. (2005). Continuous culture - making a comeback? *Microbiology* 151, 3153–3159. doi: 10.1099/mic.0.27924-0

Hu, P., Chakraborty, S., Kumar, A., Woolston, B. M., Liu, H., Emerson, D., et al. (2016). Integrated bioprocess for conversion of gaseous substrates to liquids. *Proc. Natl. Acad. Sci. U.S.A.* 113, 2–7. doi: 10.1073/pnas.1516867113

Igamberdiev, A. U., and Kleczkowski, L. A. (2009). Metabolic systems maintain stable non-equilibrium via thermodynamic buffering. *Bioessays* 31, 1091–1099. doi: 10.1002/bies.200900057

Infantes, A., Kugel, M., and Neumann, A. (2020). Effect of cysteine, yeast extract, pH regulation and gas flow on acetate and ethanol formation and growth profiles of clostridium ljungdahlii syngas fermentation. *BioRxiv[Preprint]*. doi: 10.1101/2020.01.13.904292

International Panel on Climate Change [IPCC] (2014). *Climate Change 2014: Mitigation of Climate Change*.

IRENA (2017). *Renewable Power Generation Costs in 2017*. Abu Dhabi: International Renewable Energy Agency.

Jones, S. W., Fast, A. G., Carlson, E. D., Wiedel, C. A., Au, J., Antoniewicz, M. R., et al. (2016). CO_2 fixation by anaerobic non-photosynthetic mixotrophy for improved carbon conversion. *Nat. Commun.* 7:12800. doi: 10.1038/ncomms12800

Kantzow, C., Mayer, A., and Weuster-Botz, D. (2015). Continuous gas fermentation by *Acetobacterium woodii* in a submerged membrane reactor with full cell retention. *J. Biotechnol.* 212, 11–18. doi: 10.1016/j.jbiotec.2015.07.020

Keith, D. W., Holmes, G., Angelo, D. St., and Heidel, K. (2018). A process for capturing CO_2 from the atmosphere. *Joule* 2, 1573–1594. doi: 10.1016/j.joule.2018.05.006

Klask, C., Kliem-kuster, N., Molitor, B., and Angenent, L. T. (2019). An open-source multiple-bioreactor system for replicable gas- fermentation experiments: nitrate feed results in stochastic inhibition events, but improves ethanol production of *Clostridium ljungdahlii* with CO_2 and H_2. *BioRxiv[Preprint]*. doi: 10.1101/2019.12.15.877050

Liew, F. M., Martin, E., Tappel, R., Heijstra, B., Mihalcea, C., and Köpke, M. (2016). Gas fermentation – a flexible platform for commercial scale production of low carbon fuels and chemicals from waste and renewable feedstocks. *Front. Microbiol.* 7:694. doi: 10.3389/fmicb.2016.00694

Ma, Y., Yu, G., and Li, H. Z. (2005). Note on the mechanism of interfacial mass transfer of absorption processes. *Int. J. Heat Mass Transf.* 48, 3454–3460. doi: 10.1016/j.ijheatmasstransfer.2005.03.008

Mock, J., Zheng, Y., Mueller, A. P., Ly, S., Tran, L., Segovia, S., et al. (2015). Energy conservation associated with ethanol formation from $H_2$and CO_2in *Clostridium autoethanogenum* involving electron bifurcation. *J. Bacteriol.* 197, 2965–2980. doi: 10.1128/JB.00399-15

Molitor, B., Mishra, A., and Angenent, L. T. (2019). Power-to-protein: converting renewable electric power and carbon dioxide into single cell protein with a two-stage bioprocess. *Energy Environ. Sci.* 12, 3515–3521. doi: 10.1039/C9EE02381J

Morinaga, T., and Kawada, N. (1990). The production of acetic acid from carbon dioxide and hydrogen by an anaerobic bacterium. *J. Biotechnol.* 14, 187–194. doi: 10.1016/0168-1656(90)90007-X

Müller, V. (2019). New horizons in acetogenic conversion of one-carbon substrates and biological hydrogen storage. *Trends Biotechnol.* 37, 1344–1354. doi: 10.1016/j.tibtech.2019.05.008

Orth, J. D., and Palsson, B. Ø. (2011). What is flux balance analysis? *Nat. Biotechnol.* 28, 245–248. doi: 10.1038/nbt.1614

Otto, A., Grube, T., Schiebahn, S., and Stolten, D. (2015). Closing the loop: captured CO_2 as a feedstock in the chemical industry. *Energy Environ. Sci.* 8, 3283–3297. doi: 10.1039/C5EE02591E

Park, J. O., Liu, N., Holinski, K. M., Emerson, D. F., Qiao, K., Woolston, B. M., et al. (2019). Synergistic substrate cofeeding stimulates reductive metabolism. *Nat. Metab.* 1, 643–651. doi: 10.1038/s42255-019-0077-0

Pierce, E., Xie, G., Barabote, R. D., Saunders, E., Han, C. S., Detter, J. C., et al. (2008). The complete genome sequence of Moorella thermoacetica (f. *Clostridium thermoaceticum). Environ. Microbiol.* 10, 2550–2573. doi: 10.1111/j.1462-2920.2008.01679.x

Poehlein, A., Cebulla, M., Ilg, M. M., Bengelsdorf, F. R., Schiel-bengelsdorf, B., Whited, G., et al. (2015). The complete genome sequence of *Clostridium aceticum*: a missing link between Rnf- and cytochrome-containing autotrophic acetogens. *MBio* 6:e01168-15. doi: 10.1128/mBio.01168-15

Qian, H., and Beard, D. A. (2005). Thermodynamics of stoichiometric biochemical networks in living systems far from equilibrium. *Biophys. Chem.* 114, 213–220. doi: 10.1016/j.bpc.2004.12.001

Quéméner, E. D. Le., and Bouchez, T. (2014). A thermodynamic theory of microbial growth. *ISME J.* 8, 1747–1751. doi: 10.1038/ismej.2014.7

Redl, S., Diender, M., Jensen, T. Ø., Sousa, D. Z., and Nielsen, A. T. (2017). Exploiting the potential of gas fermentation. *Ind. Crops Prod.* 106, 21–30. doi: 10.1016/j.indcrop.2016.11.015

Richter, H., Molitor, B., Wei, H., Chen, W., Aristilde, L., and Angenent, L. T. (2016). Ethanol production in syngas-fermenting Clostridium ljungdahlii is controlled by thermodynamics rather than by enzyme expression. *Energy Environ. Sci.* 9, 2392–2399. doi: 10.1039/C6EE01108J

Sakai, S., Nakashimada, Y., Inokuma, K., Kita, M., Okada, H., and Nishio, N. (2005). Acetate and ethanol production from H_2 and CO_2 by Moorella sp. using a repeated batch culture. *J. Biosci. Bioeng.* 99, 252–258. doi: 10.1263/jbb.99.252

Sandoval-Espinola, W. J., Chinn, M. S., Thon, M. R., and Bruno-Bárcena, J. M. (2017). Evidence of mixotrophic carbon-capture by n-butanol-producer Clostridium beijerinckii. *Sci. Rep.* 7, 1–13. doi: 10.1038/s41598-017-12962-8

Schuchmann, K., and Müller, V. (2014). Autotrophy at the thermodynamic limit of life: a model for energy conservation in acetogenic bacteria. *Nat. Rev. Microbiol.* 12, 809–821. doi: 10.1038/nrmicro3365

Standing, C. N., Fredrickson, A. G., and Tsuchiya, H. M. (1972). Batch- and continuous-culture transients for two substrate systems. *Appl. Microbiol.* 23, 354–359. doi: 10.1128/AEM.23.2.354-359.1972

Tizard, J. H., and Sechrist, P. A. (2015). *Carbon Capture in Fermentation*. U.S. Patent No 0,111,266. Washington, DC: U.S. Patent and Trademark Office. Available online at: https://patents.justia.com/patent/20150111266

Valgepea, K., De Souza Pinto Lemgruber, R., Abdalla, T., Binos, S., Takemori, N., Takemori, A., et al. (2018). H_2 drives metabolic rearrangements in gas-fermenting *Clostridium autoethanogenum*. *Biotechnol. Biofuels* 11:55. doi: 10.1186/s13068-018-1052-9

Valgepea, K., de Souza Pinto Lemgruber, R., Meaghan, K., Palfreyman, R. W., Abdalla, T., Heijstra, B. D., et al. (2017). Maintenance of ATP homeostasis triggers metabolic shifts in gas-fermenting acetogens. *Cell Syst.* 4, 505–515.e5. doi: 10.1016/j.cels.2017.04.008

Conflict of Interest: LanzaTech has interest in commercializing gas fermentation with C. autoethanogenum. RT, SS, and MK are employees of LanzaTech.

frontiers in Bioengineering and Biotechnology

REVIEW
published: 25 June 2020
doi: 10.3389/fbioe.2020.00632

Continuous Cultivation as a Tool Toward the Rational Bioprocess Development With *Pichia Pastoris* Cell Factory

*Miguel Angel Nieto-Taype, Xavier Garcia-Ortega, Joan Albiol, José Luis Montesinos-Seguí and Francisco Valero**

Department of Chemical, Biological and Environmental Engineering, School of Engineering, Universitat Autònoma de Barcelona, Bellaterra, Spain

The methylotrophic yeast *Pichia pastoris* (*Komagataella phaffii*) is currently considered one of the most promising hosts for recombinant protein production (RPP) and metabolites due to the availability of several tools to efficiently regulate the recombinant expression, its ability to perform eukaryotic post-translational modifications and to secrete the product in the extracellular media. The challenge of improving the bioprocess efficiency can be faced from two main approaches: the strain engineering, which includes enhancements in the recombinant expression regulation as well as overcoming potential cell capacity bottlenecks; and the bioprocess engineering, focused on the development of rational-based efficient operational strategies. Understanding the effect of strain and operational improvements in bioprocess efficiency requires to attain a robust knowledge about the metabolic and physiological changes triggered into the cells. For this purpose, a number of studies have revealed chemostat cultures to provide a robust tool for accurate, reliable, and reproducible bioprocess characterization. It should involve the determination of key specific rates, productivities, and yields for different C and N sources, as well as optimizing media formulation and operating conditions. Furthermore, studies along the different levels of systems biology are usually performed also in chemostat cultures. Transcriptomic, proteomic and metabolic flux analysis, using different techniques like differential target gene expression, protein description and ^{13}C-based metabolic flux analysis, are widely described as valued examples in the literature. In this scenario, the main advantage of a continuous operation relies on the quality of the homogeneous samples obtained under steady-state conditions, where both the metabolic and physiological status of the cells remain unaltered in an all-encompassing picture of the cell environment. This contribution aims to provide the state of the art of the different approaches that allow the design of rational strain and bioprocess engineering improvements in *Pichia pastoris* toward optimizing bioprocesses based on the results obtained in chemostat cultures. Interestingly, continuous cultivation is also currently emerging as an alternative operational mode in industrial biotechnology for implementing continuous process operations.

Keywords: *Pichia pastoris*, continuous cultivation, steady-state omics, physiological characterization, rational bioprocess development, bioreaction kinetics, heterologous protein production, systems microbiology

OPEN ACCESS

Edited by:
Manfred Zinn,
HES-SO Valais-Wallis, Switzerland

Reviewed by:
Dongming Xie,
University of Massachusetts Lowell, United States
Dirk Tischler,
Ruhr University Bochum, Germany

****Correspondence:***
Francisco Valero
francisco.valero@uab.cat

Specialty section:
This article was submitted to Bioprocess Engineering, a section of the journal Frontiers in Bioengineering and Biotechnology

Received: *27 September 2019*
Accepted: *22 May 2020*
Published: *25 June 2020*

Citation:
Nieto-Taype MA, Garcia-Ortega X, Albiol J, Montesinos-Seguí JL and Valero F (2020) Continuous Cultivation as a Tool Toward the Rational Bioprocess Development With Pichia Pastoris Cell Factory. Front. Bioeng. Biotechnol. 8:632. doi: 10.3389/fbioe.2020.00632

INTRODUCTION

In recent years, recombinant protein production (RPP) technology has given rise to a multibillion-dollar market offering products for a wide range of industrial activities such as food, detergent, paper, chemical, cosmetic, and pharmaceutical production. For example, more than 400 RPP-based pharmaceutical products are currently available on the market (Sanchez-Garcia et al., 2016; Vieira Gomes et al., 2018). In parallel, and derived from the RPP technology, metabolic engineering has opened the door to metabolic flux modification and new heterologous reactions. This enable the manufacture of a wide range of products of interest including vitamins, amino acids, ethanol, antimicrobials, enzyme inhibitors, and organic acids. The overall economic impact of RPP and metabolite productions was estimated at around 143.5 billion US dollars in 2014, with upward forecasts until 2020 (Porro et al., 2011; Singh et al., 2017).

Various organisms ranging from bacterial hosts to transgenic animals have been proposed as efficient cell factories for bioprocesses with the mentioned applications. For example, for RPP, most of the products including pharmaceuticals and industrial enzymes are obtained with the main considered workhorses, namely: *Escherichia coli*, *Saccharomyces cerevisiae* or Chinese hamster ovary (CHO) cells (Sørensen, 2010; Maccani et al., 2014). However, the use of non-conventional yeasts, which combine eukaryotic ability for protein processing and major microbial advantages, have lately started to be considered as promising alternatives. In general, the new choices offer many advantages in terms of pathway requirements, desired product profile, and gross physiology over *S. cerevisiae* (Wagner and Alper, 2016). Such is the case with *Schizosaccharomyces pombe*, *Hansenula polymorpha* (syn. *Ogataea polymorpha*), *Kluyveromyces lactis*, *Yarrowia lipolytica*, or *Komagataella phaffii (Pichia pastoris)* (Çelik and Çalik, 2012; Baghban et al., 2019). Actually, at present *Pichia pastoris* (recently classified as *Komagataella* spp.) has arisen as an efficient and versatile cell factory for obtaining a wide spectrum of biotechnological products including recombinant proteins and metabolites of diverse origins (Gasser et al., 2013; Peña et al., 2018).

The key features that make *P. pastoris* an outstanding host for the above-mentioned uses include fast growth at high densities in defined media, the availability of advanced tools for genetic modification (e.g., CRISPR/Cas9 system) and the ability to perform post-translational modifications as well as to secrete the products extracellularly (Vogl and Glieder, 2013; Gasser and Mattanovich, 2018; Weninger et al., 2018). Furthermore, the increasing knowledge on *P. pastoris* metabolism gathered over the last decades, together with the high RPP potential of this yeast, have strongly increased the interest in using this microbial cell factory to obtain a variety of compounds. Thus, strengthening *P. pastoris* as one of the most suitable chassis for the biotechnological industry.

Promoters have proved to be key regulators for RPP processes. For *P. pastoris*, the methanol inducible alcohol oxidase promoter (P_{AOX1}), a strong and tightly regulated promoter, was the first used obtaining efficient production rates of several proteins of interest (Cregg et al., 1993; Paulová et al., 2012; Ponte et al., 2016, 2018; Lee et al., 2017). Although P_{AOX1} affords outstanding RPP levels, using methanol has some relevant drawbacks, especially at production scale processes. These are mainly related with the increased costs and risk of storing and using methanol, as well as the increased oxygen demand and high heat production derived from methanol metabolization (Heyland et al., 2010; Prielhofer et al., 2013; Çalik et al., 2015). These shortcomings have given ground to dedicate important efforts to identify and to develop methanol-free alternatives, which can be classified in two categories: discovery of alternative efficient promoters for *P. pastoris* (P_{GAP}, P_{PGK}, P_{THI11}, P_{PYK}, P_{SDH}) (Periyasamy et al., 2013; Landes et al., 2016; Juturu and Wu, 2018; Massahi and Çalik, 2018; de Macedo Robert et al., 2019) and engineering or development of synthetic promoters (Ata et al., 2017; Wang et al., 2017; Prielhofer et al., 2018; Vogl et al., 2018b).

Nevertheless, not only is the promoter selection key in the strain engineering development to construct efficient cell factories, other relevant factors such as host strain background, gene engineering and dosage, protein processing helpers or secretion machinery also have a significant impact on the overall performance of the strain (Ahmad et al., 2014). Furthermore, it is crucial to combine the mentioned factors with an efficient bioprocess development from a bioprocess engineering approach (García-Ortega et al., 2019). For the latter, it should be essential to carry out a characterization producer clone used as a cell factory over different culture conditions to understand its performance and therefore, to design the rational based bioprocess strategies that allows to achieve the optimal performance for industrial bioprocesses (Yang and Zhang, 2018).

To obtain a proper characterization, cells should be kept under constant conditions in terms of both physico-chemical operating conditions as well as their metabolic state (Hoskisson and Hobbs, 2005). In this sense, continuous operation, which was first reported in 1920 (Cooney, 1979), is considered the most simple operational mode for this purpose. Continuous cultures are defined as a fermentation systems in which fresh medium is continuously added to the bioreactor and the components of the culture broth—cells and metabolites included—are continuously removed from the vessel (Fernandes et al., 2015); thereby forcing the cells to proliferate at a fixed rate and in a constant environment reaching the stationary state (Gramelsberger, 2018). The two main types of continuous cultures, chemostat, and turbidostat, are analogous and differ mainly in their cell growth control mechanism (Prielhofer et al., 2013; McGeachy et al., 2019). On one hand, chemostat is controlled through the continuous addition of culture medium in which a single nutrient is present at growth limiting conditions (Peebo and Neubauer, 2018). On the other hand, in turbidostat, the goal is to avoid nutrient limitation while growth is controlled by using an optical sensor which maintains a determined turbidity level by adding fresh medium through a feedback control loop. In this case, the resulting specific growth rate (μ) obtained is close to the maximum specific growth rate (μ_{max}) of the microorganism used (Gresham and Dunham, 2014; Fernandes et al., 2015).

Additional alternatives such as "changestats" have been proposed as a novel tool where an environmental parameter is

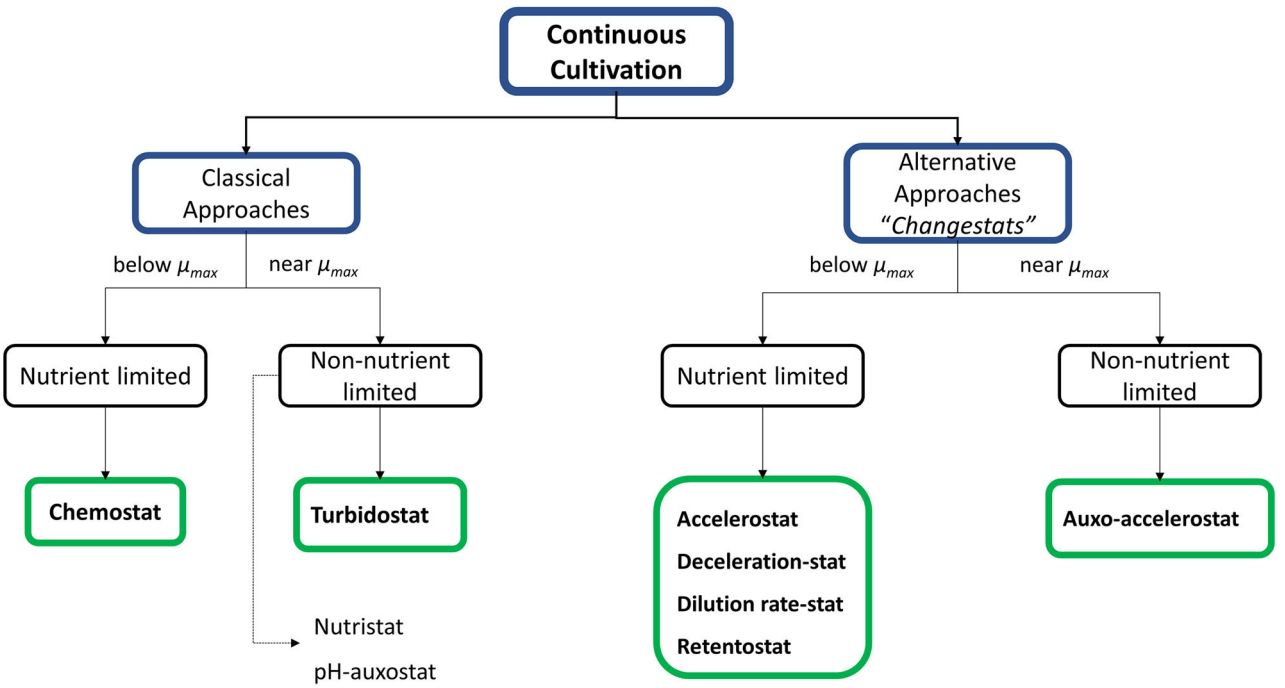

FIGURE 1 | Overview of different continuous cultivation strategies. They are divided in two main groups: the first, corresponding to the "classical" approaches which work at steady state conditions; whereas for the other hand, changestats are variations of classical strategies proposed to obtain similar results but at dynamic conditions allowing faster results.

continuously changed in a single experiment. These approaches provide quick information about the response of cells in front of determined environmental conditions under what has been called steady state growth space analysis (GSA) (chemostat or turbidostat-based approaches) (Adamberg et al., 2015). Several variants have been described in the literature and have been listed and classified below according to the limitation or not of a nutrient and it is summarized in **Figure 1**.

Nutrient-limited changestats:

- Accelerostats (A-stats) and deceleration-stats (De-stats), which are used to study the increase or decrease the specific growth rate, respectively (Nahku et al., 2010; Hoekema et al., 2014; Wagenen et al., 2015; Gerritzen et al., 2018).
- Dilution rate stats (D-stats), where an environmental parameter is continuously changed while the dilution rate is kept constant (Kasemets et al., 2003).
- Retentostats, where biomass is retained by means of internal or external filter devices. In prolonged retentostats, the energy derived from the consumed carbon source only allows to sustain the cellular maintenance but can no longer support biomass growth. This allows experiments to be performed at very low or near-zero specific growth rates (Herbert, 1961; Ercan et al., 2015a,b; Rebnegger et al., 2016).

Non-nutrient-limited changestats

- Auxo–accelerostats, allows to examine the effects of smooth environmental changes under nutrient-excess conditions (Nisamedtinov et al., 2008).
- Nutristats, where the dilution rate is a function of the set-point substrate concentration in the bioreactor (Curvers et al., 2002).
- Finally, as special case, adaptastats allow to operate under substrate-limiting conditions but, like turbidostats, work near μ_{max} (Tomson et al., 2006).

Although changestats have been presented as promising alternatives to classical continuous cultures, it should be noted that in these systems cells grow in a quasi-steady state because the absence of a total stabilization phase prevents them from reaching steady state (Subramanian et al., 2017). This is the reason why chemostats continue to be the main choice for characterizing microorganisms under substrate-limiting conditions (Ziv et al., 2013). In fact, first reported in 1950 (Monod, 1950), chemostat cultures have proved the best operational choice for precise kinetic and metabolic characterization; also, they have provided the most accurate quantitative understanding at whole-cell level (Hoskisson and Hobbs, 2005). Thus, the empirical knowledge obtained from this characterization allows the determination of several parameters at different conditions, which therefore can be used to identify the optimal culture conditions toward the maximization of product related parameters such as production rates and yields. The relation between cultures and production parameters is detailed through different examples in the following sections. On the other hand, the application of systems biology approaches based on continuous cultures has enabled the development of new highly sensitive analysis tools capable of detecting slight changes at different regulation points, which can be deemed

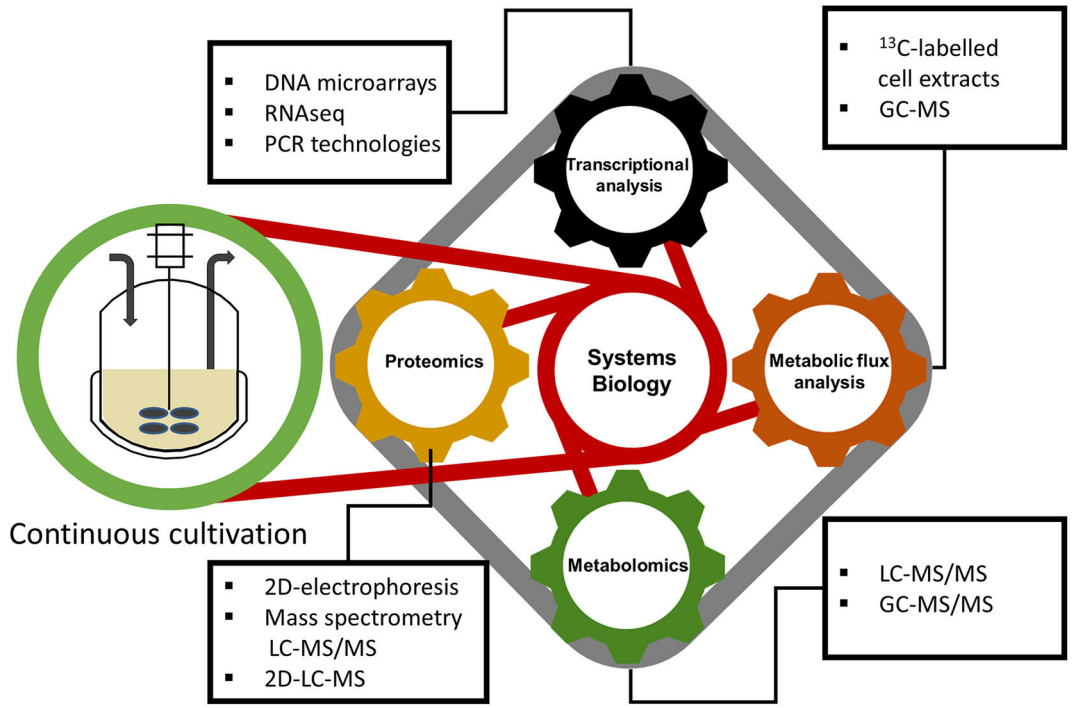

FIGURE 2 | Valuable information that gives continuous cultivation to systems biology for a deep understanding about cell physiology.

significant when integrating experimental results (Rebnegger et al., 2014).

The following sections describe the basis and uses of continuous cultivation with *Pichia pastoris*. Specifically, it has been focused on carbon-limited chemostat cultures, which according to the literature is the most used strategy for *Pichia pastoris* in continuous operation. The role of chemostat cultures has been reviewed as a powerful tool for the characterization of *P. pastoris* strains with a view to enabling the rational design of engineered cell factories and optimal operational strategies for maximal bioprocess efficiency.

CONTINUOUS CULTIVATION PROVIDES AN EXCELLENT TOOL FOR SYSTEMS BIOLOGY RESEARCH

Steady-State Omics, a Key Issue in the Renaissance of Research Into Continuous Cultures

The development of high-throughput molecular biology techniques in the post-genomic era has brought a renaissance of continuous cultures. At present, they are used not only in kinetic characterization and adaptive laboratory evolution (ALE) studies (Bull, 2010), but also as a powerful tool for gaining deeper insight into cell behavior thanks to the large amount of robust information they provide. In this sense, continuous cultivations have been used to understand cells response to internal traits such as those observed in engineered clones (using promoters engineering as an example) or to external stimuli such as operational strategies or environmental stress.

Transcriptomic, proteomic, metabolomics, and fluxomic data, can be jointly integrated into a systems biology approach (shown in **Figure 2**) in order to obtain an all-encompassing picture of a biological system used (Graf et al., 2009). A more detailed description is provided below in the next sections.

Transcriptional Studies

Transcriptional analysis is usually the first step in systems biology studies as it is also the first stage in the information flow from genomic data (Engstrom and Pfleger, 2017). Gene regulation can be examined by absolute or relative quantification of individual transcripts. Integrating this information enables further interpretation of data and reveals how the complex machinery behind a specific phenotype operates as a result of certain experimental conditions. The insight thus gained can be contrasted with knowledge derived from other structural levels of systems biology.

The contribution of transcriptional regulation to physiological outcomes is strongly dependent on the host employed. Thus, although 27% of all protein-coding genes in human cell lines are transcriptionally regulated (Vogel et al., 2010), the proportion amounts to 50% in *E. coli* and up to 70% in *S. cerevisiae* (Lu et al., 2007). These figures testify to the high significance of interpretations of transcriptional research in yeasts, where *P. pastoris* is taxonomically located.

Transcriptional data are typically acquired in either of two methodologies:

- One involves using specific primers for selected target genes either by real-time quantitative PCR (qPCR) (Landes et al., 2016) or droplet-digital PCR (ddPCR) analyses (Cámara et al., 2019). Both methods provide numerical results and hence quantitative data. Also, they are commonly used to examine the effects on the transcription regulation of certain genes of known sequence.
- However, other high-throughput technology methods such those using microarrays, based qualitative fluorescent detection, and/or RNA sequencing (RNAseq), which quantify the number of transcripts present in a sample by whole transcriptome sequencing, have arisen as helpful workhorses. In fact, these methods provide a robust overview of all transcripts (Baumann et al., 2010; Ata et al., 2018) and are thus especially useful when increased gene coverage is needed.

The selection of the method to be used in each case will be dictated by the specific objectives and information available about the studied system.

Continuous cultivation has proved useful for transcriptional analysis. Specifically, chemostats are frequently deemed the most suitable operational choice for this purpose, as seen with *S. cerevisiae* strains producing either recombinant proteins (Liu et al., 2013) or metabolites (Vos et al., 2015). As shown by several successful attempts described below, chemostat uses could be extended to *P. pastoris*, a similar cell factory related in the taxonomical group of yeasts.

Expression of heterologous proteins and metabolites in *P. pastoris* triggers many changes in cell physiology including stoichiometric drain of energy and cellular resources, or restrictions in the biochemical machinery responsible for bioproduct synthesis (Hesketh et al., 2013; Nocon et al., 2014). Identifying different points of regulation through transcriptional analysis can therefore allow useful information about cell performance to be obtained. Such information could be used to address new targets by strain engineering and to develop innovative, more efficient operational approaches by bioprocess engineering.

Puxbaum et al. (2015) provided a solid discussion about the potential limitations of RPP in *P. pastoris*; they found protein synthesis, folding, and secretion to be the main bottlenecks for the process. In this sense, Hesketh et al. (2013) directly observe stress arising during RPP by expressing under *AOX1* promoter two lysozyme variants differing in degree of misfolding in chemostat cultures. The effect on unfolded protein response (UPR) was examined by using the RNAseq SOLiD platform. In addition, further RT-PCR analysis showed a constitutive splicing of *HAC1* gene transcript across the different phases of RPP induction independent of the lysozyme misfolding level. The importance of this finding is based on the fact that Hac1p corresponds to a key transcription factor in the triggering of UPR response (Graf et al., 2008), and data obtained suggests that UPR is dependent on the transcript regulation of *HAC1* rather than on the splicing process. As a result, the genes *KAR2* and *PDI1*, which are further down the line in UPR, also exhibited high relative expression as revealed by RNAseq transcriptome analysis. Finally, a potential role of untranslated RNA molecules differentially regulated under different expressing conditions was suggested.

On the other hand, endoplasmic reticulum associated protein degradation (ERAD) is one other limiting factor for RPP (Dragosits et al., 2010; Adelantado et al., 2017). UPR and ERAD have been found to jointly control protein folding to a considerable extent and also, generally, heterologous protein synthesis, in *P. pastoris* (Delic et al., 2013; Zahrl et al., 2018). The relevance of both mechanisms as a response to RPP was confirmed by a microarray analysis intended to shed light on the transcriptional upregulation of these mechanisms in *P. pastoris* clones expressing a 2F5 Fab fragment relative to the wild type strain X-33 in chemostat cultures (Gasser et al., 2007).

Furthermore, it has been observed that transcriptional analysis provides useful information for characterizing native and engineered promoters. Thus, Landes et al. (2016) characterized the production of recombinant human serum albumin (HSA) by using an alternative promoter from the thiamine biosynthesis gene *THI11*, which is thiamine-repressible. An initial transcriptional assay on batch cultures using a specific transcriptional analysis with qPCR provided insight into the promoter performance under non-repressive conditions—absence of thiamine—and additional batch experiments allowed to define repression and de-repression effects of the thiamine concentration. Also, chemostat cultures were used to evaluate the performance of the same promoter under carbon-limited conditions at different specific growth rates in order to monitor production rates, and *THI11* and HSA gene transcription. Whereas, the specific production rate (q_{HSA}) improved with increasing specific growth rate (μ), gene transcription had no influence on the latter, indicating a constitutive nature of P_{THI11}.

In similar work intended to develop alternatives to the methanol-based expression system, Prielhofer et al. (2013) identified six novel promoters through microarray transcriptomics analysis under carbon non-limiting and limiting conditions (batch and chemostat cultivation, respectively). One of the promoters, P_{G1}, corresponding to a high-affinity glucose transporter (*GTH1*), exhibited strong and tight regulation under carbon-limiting conditions. Also, further characterization of this promoter at variable specific growth rates in chemostat cultures revealed the optimal specific production rate at a dilution rate $D = 0.07\ h^{-1}$.

As it was observed previously, the useful information derived from the production kinetics of recombinant *P. pastoris* producer clones growing at controlled specific growth rates in chemostat cultures have also enabled further transcriptional characterization and expansion of existing knowledge about the impact of this key parameter for improvement of the cell factory. Thus, Rebnegger et al. (2014) performed a transcriptional analysis using microarrays on *P. pastoris* clone expressing HSA under *GAP* promoter in chemostat cultures to examine the transcriptional response at different μ values. They found q_{HSA} and μ to be linearly related, and upregulation of ribosomal and translation-related genes in response to higher heterologous protein production. On the other hand, upregulation of UPR and secretory pathways at high μ levels suggested that, although high D rates resulted in no limitation in q_{HSA}, they caused

heterologous protein production-related stress. Furthermore, marked upregulation of transcriptional regulators involved in stress response as well as a carbon source and nitrogen responsive genes was observed at low μ levels, which suggest an adaptation to the carbon source limitation when the dilution rate was tuned. Finally, consistent with the widely reported Crabtree-negative effect on *P. pastoris* metabolism, mitochondrial transcripts were positively correlated to μ. It is worth mentioning that Crabtree effect corresponds to the respiro-fermentative phenotype widely reported for *S. cerevisiae*, however a similar phenomenon has been observed also in cancer cells (Warburg effect). In order to generate an alternative model for Warburg effect studies, Ata et al. (2018) convert Crabtree negative *P. pastoris* into a Crabtree positive. While determination of Crabtree phenotype was achieved using short- and long-term studies in chemostat cultures, RNASeq transcriptome and ^{13}C central metabolism flux analysis were performed in batch cultures. The use of chemostats for further transcriptional and metabolic studies could be proposed to provide new insight of *P. pastoris* as better model than *S. cerevisiae* for Warburg effect studies.

One other interesting use of molecular biology in strain engineering is to integrate multiple target expression cassettes in the *P. pastoris* genome, which usually leads to substantially increased production. Previous reports suggest that gene dosage considerably influences specific productivity (Schwarzhans et al., 2016; Vogl et al., 2018a). Thus, Cámara et al. (2017) evaluated the effect in chemostat cultures growing at $\mu = 0.10\ h^{-1}$ by using strains with multiple insertions of *Rhizopus oryzae* lipase (ROL) under *AOX1* promoter (0, 1, 2, 4, 8, and 15 copies). As confirmed by *ROL* transcriptional levels in a ddPCR analysis, optimal specific extracellular lipase activity was obtained with the 2C clone. By contrast, transcriptomic analyses with microarrays revealed constraints with increasing *ROL* gene dosage on the transcriptional machinery (specifically, in the methanol expression regulator 1, Mxr1p) (Cámara et al., 2017). This information was used to design new clones carrying several copies of *MXR1* and methanol-induced transcription factor (*MIT1*). As revealed by specific analysis with ddPCR, methanol uptake was found to have a positive effect on the transcriptional response; the effect, however, resulted in no increase in product activity (Cámara et al., 2019).

Not only strain engineering, but also new bioprocess strategies, have led to enhanced RPP. Therefore, better understanding the way cells adapt to different external conditions requires accurate physiological characterization (Baumann et al., 2008; Dragosits et al., 2010; Garcia-Ortega et al., 2016). Based on the positive effect of oxygen-limiting conditions on RPP (Baumann et al., 2008), the impact of these stress conditions was further examined by using transcriptional analysis with microarrays in samples obtained from chemostat cultures under normoxic, oxygen-limited and hypoxic conditions to study the expression of an antibody fragment (Fab) under the constitutive *GAP* promoter (Baumann et al., 2011). Supplementary proteomic and metabolic flux analyses, and lipid-profile analyses (lipidomics) support the findings obtained previously (Baumann et al., 2010; Adelantado et al., 2017). The ensuing information enabled thorough characterization of the oxygen-limiting effects observed in metabolism regulation, which included upregulation of genes associated to the glycolytic pathway, the oxidative branch of the pentose phosphate pathway (PPP), ergosterol and sphingolipid biosynthesis and UPR genes, while the tricarboxylic acid cycle (TCA) revealed transcriptional downregulation.

Osmotic stress has been reported to exert a beneficial effect on RPP. Thus, Dragosits et al. (2010) conducted a transcriptional analysis by using microarrays in combination with chemostat cultures and found increasing concentrations of KCl to result in upregulation of genes involved with UPR, ribosome biogenesis and translation, albeit only in the wild-type clone. Although a Fab-producing clone exhibited higher transcriptional levels than the wild-type strain, such levels were independent of the experimental conditions and no increase in product formation was observed at higher concentrations of KCl. This result suggests that upregulation of these genes as revealed by microarray analysis was previously triggered by a recombinant protein effect and that osmolarity induced no further increase.

Although most transcriptional analyses have been performed in chemostat cultures, some have been conducted in retentostats. Rebnegger et al. (2016) performed retentostat studies to outline the physiology and transcriptional response of *P. pastoris* under this operational condition at near-zero specific growth rates. Among the pool of genes that were differentially expressed in microarray hybridization for transcriptome analysis, upregulation in transcripts involved in alternative carbon source consumption (such as ethanol and methanol), global stress-related transcription factors and with nutrient responses reveal an adaptation of low substrate availability at near-zero growth rates. This finding reinforces the reduction observed in the maintenance coefficient (m_s), in comparison to chemostat cultures growing at higher μ. Otherwise, protein synthesis in retentostat cultures exhibited insubstantial transcriptional regulation, so further research, for example with RP-expressing clones, to determine whether the alternative cultures could be useful with *P. pastoris* and to outperform *S. cerevisiae* translational capacity at low μ is proposed.

Proteomic Studies

According to the central dogma of molecular biology, the protein level falls at the last stage of the information flow (van Hove et al., 2016; Engstrom and Pfleger, 2017). This, however, is no reason to underestimate the importance of the information it provides. Proteomics emerged in the mid-1990s as a new approach to determine the proportion of functional proteins containing information translated into the transcriptome pool. Such information is useful to contrast and supplement data obtained at other levels in systems biology in order to support and strengthen the conclusions of other studies (Szopinska and Morsomme, 2010).

Proteomic analysis with various microorganisms has provided interesting results (Brejning et al., 2005; Rossignol et al., 2009; Arvas et al., 2011; Dragosits et al., 2011). The use of proteomics on *P. pastoris* has been widely used in different cultivation modes including chemostat, batch and fed-batch cultures (Baumann et al., 2010; Dragosits et al., 2010; Pfeffer et al., 2012; Vanz

et al., 2012, 2014; Lin et al., 2013), though not so widely as in transcriptional analysis. This section focuses on applications involving continuous cultivation, specifically in chemostats.

The earliest example of proteome characterization was accomplished by Dragosits et al. (2009), who compared the effect of temperature changes on recombinant proteome. The greatest changes were observed at the highest and lowest temperature studied (20 and 30°C, respectively). In addition to increased specific productivity at 20°C, 2D-Gel electrophoresis followed by LC-ESI-QTOF tandem MS allowed the identification of 49 out of 150 spots that exhibited significant differences. Proteomic data revealed that some cellular processes were affected by low temperatures. On the one hand, energy metabolism, oxidative stress response, and protein folding protein levels occurred to a lesser extent; whereas, in amino acid metabolism and RNA/ribosomal biogenesis, an increase of protein levels might account for the positive effect on RPP at 20°C.

Dragosits et al. (2010) conducted a similar study to determine the effect of osmolarity on recombinant *P. pastoris* physiology. Thirty-seven out of the total spots detected, 300 for wild-type and 150 for recombinant clone, were successfully identified with significant changes. These results strengthen the findings of transcriptional analysis as regards energy metabolism and protein folding in both clones. On the other hand, as it was observed in transcriptional analysis, a positive effect on UPR response protein levels was observed at high osmolarity conditions, however it was only in control wild-type strain, whereas it was not the case for recombinant strain where no impact was exerted at different KCl concentrations. The author suggests that although osmolarity not exert a direct effect in producer clone, it could be used for preconditioning cells for RPP, and as outcome it can be considered on improved bioprocess and for generate novel routes for strain engineering.

Rußmayer et al. (2015) interpreted proteomic data at other levels of systems biology and demonstrated symbiosis by using multi-level analysis to expose the cellular processes involved in methanol metabolism. They found good positive correlation between transcriptomic and proteomic data, consistent with the strong transcriptional control over protein abundance in *S. cerevisiae* (Lu et al., 2007). Chemostat cultures on methanol–glycerol mixed feed revealed a positive correlation between protein production and transcripts from methanol metabolism, and also with peroxisome biogenesis. There was, however, no clear-cut relationship between the increased protein levels associated to the translation machinery and cytoskeleton organization, which were not reproduced at the transcriptional level.

The usefulness of proteomic analysis as a supplement to transcriptional and metabolic flux analysis can also be illustrated with the results under hypoxia conditions. Thus, Baumann et al. (2010) conducted an integrative multilevel study and found a strong positive correlation between transcriptional levels and protein data. This result provides support for the assumption that transcriptional regulation is stronger than post-transcriptional regulation in *P. pastoris*. In any case, proteomic data should never be considered irrelevant, particularly in those cases were transcript levels do not match protein expression and understanding the behavior of the cell factory is rather difficult as a result.

Metabolic Fluxes as Key Physiological Indicators

The physiological status of cells, which is directly reflected in their metabolic phenotypes, is a result of the interplay of various key cell processes and factors such as gene expression, protein production and kinetics, regulation and thermodynamic driving forces (metabolite concentrations). A metabolic phenotype is defined by the actual activities of the metabolic reactions in cells (viz., by reaction rates). Because they are rarely constant, reaction rates are usually determined under steady-state or pseudo-steady state conditions and commonly referred to as "metabolic fluxes," which are thus key indicators of the physiological status of cells.

Determining metabolic fluxes remains difficult despite major technological advances in quantifying all components involved. In fact, it is not always possible to determine the concentrations of all relevant components; also, *in vivo* values for kinetic parameters are usually unavailable. A number of techniques have thus been developed to quantify metabolic fluxes collectively that are known as "metabolic flux analysis" (MFA) or, simply, "fluxomics." Many of them have been applied to *P. pastoris* and the most salient are discussed below. Using those techniques for metabolic engineering improves existing knowledge of the physiological properties of biological systems, thus enabling the rational design of cell factories and efficient metabolic engineering cycles.

Metabolic Flux Analysis

As stated above, MFA is widely used for comprehensive analysis of the physiological effects of environmental changes or genetic engineering modifications. Metabolic fluxes (i.e., metabolic reaction rates in the steady state) provide an excellent operational picture of cell operation. A continuous culture provides a simple, convenient tool for maintaining a stable (in steady state) cell metabolism over long periods of time. Comparing metabolic flux distributions under different conditions allows a deeper understanding of the effects resulting from the genetic or environmental changes.

Although determining metabolic fluxes in continuous cultures has the advantage that cell inputs and outputs are stable, it is still a difficult task due to the large number of reactions taking place simultaneously in each cell. Because in steady state reaction rates are constant, it only requires considering the stoichiometry of the reactions to calculate metabolic fluxes. The mass balances for each metabolite involved in such reactions allow one to construct a linear metabolic model. Those metabolic models with a realistic degree of metabolic detail are known as Genome Scale Metabolic Models (GEMs). Using GEMs in combination with steady-state data should in theory allow one to calculate metabolic fluxes. Unfortunately, the intricate interconnections among metabolites, and the small number of flux measurements typically available (usually cell inputs and outputs only), prevent the accurate determination of most of the metabolic fluxes, which requires the combined use of mathematical models, optimization

methods and/or experimental techniques such as ^{13}C labeling (Ferrer and Albiol, 2014a,b).

Genome-scale metabolic models have become essential tools for MFA and rational-based strain engineering. These models are mathematically structured knowledge bases containing descriptions of all biochemical reactions, metabolites, and metabolic genes for a specific organism—a Biochemical, Genetic and Genomic (BiGG) knowledge base (King et al., 2016). GEMs can be used in a number of ways such as using their elementary modes or extreme pathways to predict phenotypic function, to improve understanding of the metabolism underlying structure, or using the well-known constraint-based modeling approach (Fong, 2014) to predict function, as examples.

Constructing so detailed BiGG knowledge bases is a continuously evolving process due to the still limited knowledge available on some cell details. The availability of the *P. pastoris* genome sequence allowed the development of the first metabolic reconstructions. Thus, the DSMZ70382 genome sequence, and the sequence from the GS115 strain, allowed the PpaMBEL1254 and iPP668 GEM, respectively, to be produced (Chung et al., 2010; Sohn et al., 2010). Although several improved versions of these *P. pastoris* GEMs have been reported (Ye et al., 2017; Tomàs-Gamisans et al., 2018), this is a continuously evolving field and new or upgraded versions of existing models are expected to appear in the near future.

The continuous cultivation methodology has been used to adjust and validate GEMs. Also, GEMs adapted to specific continuous culture conditions have been used with the latest algorithms and optimization techniques to determine metabolic fluxes under constrains derived from experimental data. This approach is highly useful for interpreting such data and also for designing effective metabolic engineering strategies. Its greatest advantage is that it can be used in any type of continuous culture experiment without the need for a special experimental technique such as ^{13}C labeling.

The most common alternative to using an optimization technique for metabolic flux calculations involves obtaining supplementary experimental information. Adding a carbon-labeled carbon source to the input medium of a continuous culture is one common method for this purpose. A typical experiment involves establishing a continuous culture and, once it has reached steady state, replace the input culture medium with another one containing a ^{13}C-labeled carbon source. The labeled substrate usually consists of a mixture of molecules labeled at different carbon positions in proportions that are selected according to the expected results. The information to be acquired can be either the distribution of the label once steady state is reached (Tomàs-Gamisans et al., 2019) or changes in the label during the transient labeling period (Heyland et al., 2011; Jordà et al., 2012, 2014b; Nocon et al., 2016). In either case, using this information jointly with steady-state input/output fluxes and a metabolic model allows one to calculate metabolic fluxes under specific conditions. Using GEMs in combination with ^{13}C labeling requires solving a very large number of equations. It is thus common to use manually or automatically constructed "context-specific" core models (Tomàs-Gamisans et al., 2019) to facilitate calculations and handling of data. These methodologies have been used in combination with chemostat cultures to examine the impact of heterologous protein production and the effects of different environmental conditions on *P. pastoris* metabolism.

Specific growth rate is one of the basic variables influencing the distribution of metabolic fluxes, and the macromolecular and elemental composition of biomass. This specific rate is easy to regulate in continuous cultures. In *P. pastoris*, the influence of the specific growth rate has been studied by applying ^{13}C labeling to chemostat cultures fed with various carbon sources (glycerol, methanol) or their mixtures (e.g., glycerol/methanol) (Jordà et al., 2014a; Tomàs-Gamisans et al., 2018). In general, the results were consistent with what is known as the "growth rate hypothesis" which states that increasing the specific growth rate increases the RNA and protein fractions of cells, thereby boosting protein synthesis and energy production at the expense of other fractions such as carbohydrates.

Biomass composition has also been found to depend on the particular carbon source. Thus, cells grown on methanol contain more protein than those grown on glycerol or glucose (Tomàs-Gamisans et al., 2018). This effect has also been seen with mixed glycerol/methanol or glucose/methanol feeds and can be ascribed to the methanol utilization pathway requiring an expanded metabolic machinery (Jordà et al., 2012, 2014a; Rußmayer et al., 2015). On the other hand, the amino acid composition of cells is virtually independent of their specific growth rate and only differs among carbon sources. Based on the foregoing, metabolic fluxes are calculated by using different biomass composition equations whichever the approach adopted (GEMs included). The environmental conditions also affect metabolic flux distribution. For example, altering the chemostat dilution rate or using a different carbon source alters the distribution of metabolic fluxes; as a result, specific consumption and production rates increase with increasing specific growth rate or by-products such as arabitol are formed (Jordà et al., 2014a; Tomàs-Gamisans et al., 2018). Interestingly, the amount of methanol directly dissimilated into CO_2 is influenced not only by the specific growth (dilution) rate, but also by the methanol fraction in mixed feeds. Experiments using chemostat cultures have shown environmental factors such as oxygen-limited conditions or low temperatures to have a strong impact on MFA (Mattanovich et al., 2004; Dragosits et al., 2009; Baumann et al., 2010; Carnicer et al., 2012).

The other most extensively studied factor in *P. pastoris* continuous cultures in addition to the environmental conditions is the impact of heterologous protein production on MFA. For this purpose, the effects of different model proteins on metabolic flux distribution relative to their non-productive counterparts is usually compared under identical cultivation conditions. The type of heterologous protein produced and, especially, the amount produced, have proved considerably influential on metabolic flux distributions. Thus, increased heterologous protein production has been shown to shift metabolism toward increased energy generation, reduction equivalents (ATP, NADH, NADPH) and building block production (enhanced pentose phosphate pathway, PPP, or TCA cycles) while reducing biomass yield (Heyland et al., 2011; Jordà et al., 2012, 2014b; Nocon

et al., 2016). Increased heterologous protein production has also been found to boost protein misfolding and, ultimately, trigger an unfolded protein response (UPR), thereby further draining resources and shifting metabolic fluxes (Graf et al., 2008). The effects of environmental factors and heterologous protein production on metabolic fluxes have fostered the development of *in silico* strategies to optimize metabolic engineering.

BIOPROCESS CHARACTERIZATION WITH CHEMOSTAT CULTURES

Microbial Physiology Studies/Physiological Characterization of the Cell Factory

Increasing the efficiency of a bioprocess (i.e., increasing yields and productivities with high-quality proteins) requires a deep physiological understanding of the cell factory. For the topic discussed in this review, such knowledge is expected to eventually allow the rational development of feasible and competitive bioprocesses with shorter times to market. The overall approach is usually not straightforward due to the complexity of the different interactions occurring at many cell physiology levels. Thus, since the interactions between the cell factory performance and the bioprocess conditions define key parameters of interest (KPI) of the production, an empirical determination of those are required. In this sense, to obtain this kind of information accurately, chemostats are considered the most usual continuous cultivation applied (Hoskisson and Hobbs, 2005). As pointed out in the Introduction section, variations of the continuous operating mode can be alternatively implemented to determine nutrient and environmental effects on metabolism and physiology.

Chemostat cultures provide important advantages over other alternatives such as batch and fed-batch cultures. The advantages arise from the fact that operating under steady-state conditions provides highly robust and reliable data, thus allowing one to assess the effect of a specific parameter while keeping all others constant. Therefore, several cultivation conditions such as medium composition, carbon and nitrogen sources, dilution rates, and others can be investigated to optimize their use. Moreover, some additional strain features and bioreaction kinetics can be thoroughly determined using chemostat cultures. Currently, these parameters are considered of capital importance toward bioprocess optimization for the development of improved industrial processes.

Traditionally, shake-flask cultures have been used to find optimal conditions of physical parameters (pH, T) and concretely, batch or fed-batch cultures to determine oxygen requirements (DO, pO2) However, currently, continuous cultivations should be considered a preferred option to assess the effect of any culture conditions. The fact of working in steady state conditions in whichever cell population is considered homogeneous allows to obtain very accurate and reliable results. In contrast, dynamic processes such as batch of fed-batch cultures are expected to be less robust and present more deviations due to possible drifts in culture conditions. Furthermore, also parameter determination such as kinetic rates and yields is also considered to be more complex in dynamic processes.

Operating Conditions and Media Optimization

Bioprocess performance is influenced by some physical conditions of cultures including temperature (T), pH and dissolved oxygen (DO). The optimum conditions for production may differ from those for growth due to their effect on several factors including protein-specific characteristics, kinetics and sensitivity of products to proteolytic degradation.

The optimum growth temperature for *P. pastoris* bioprocesses is about 30°C, above 32°C protein expression is suppressed and cell growth rapidly decays (Çalik et al., 2015). However, some authors have suggested that operating at lower temperatures of up to 20°C may significantly improve production of heterologous proteins (Surribas et al., 2007). Decreased operating temperatures have a double but opposite effect. On one hand, the solubility of oxygen is increased and consequently the oxygen transfer rate (OTR) is improved. On the contrary, bioreaction rates such as intracellular reactions, proteolysis and cell growth diminish. Reduced proteolysis at low temperatures is the result of decreased protease activity rather than decreased proteases production (Sirén et al., 2006). Thus, some studies have focused mainly on this cultivation parameter. Data obtained in chemostat cultures on the production of an antibody Fab fragment, indicates that folding stress is generally decreased at lower cultivation temperatures, therefore enabling a higher efficiency for protein processing and secretion (Dragosits et al., 2009). The specific productivity was 3-fold higher at the lower temperature of 20°C, observing also a reduction on the flux through the TCA cycle, jointly with lower oxidative stress response and less presence of molecular chaperones.

Berrios et al. (2017) examined the effect of using co-substrates with methanol in the production of *Rhyzopus oryzae* lipase (Rol) by *P. pastoris* in continuous cultures growing at the same μ but at different temperature (22 or 30°C). Overall, the lower temperature led to lower specific productivities irrespective of the co-substrate used. Strikingly, lowering temperature produced an increase in biomass concentration.

As a conclusion of the studies focused on the T effect, the efficiency of a low cultivation temperature depends on the target protein, so this effect should be studied for each case.

The pH of *P. pastoris* cultures is commonly set at 5.0–6.5 (Looser et al., 2015). pH values above 8 diminish cell viability, and can reduce protein activity and stability (Çalik et al., 2015). However, the optimum pH for RPP depends on the properties of the target protein, especially stability related with the isoelectric point (pI). Since the selection of the optimal pH should also consider the effect on the proteases, a pH value of 5.5 is thus often used to minimize this deleterious effect. In addition, an inappropriate pH can cause some components of the medium to precipitate, which should be avoided by choosing a low value in the working range (Cos et al., 2006).

The dissolved oxygen tension in *P. pastoris* cultivation is typically maintained at 20–30% (air saturation) by having the bioreactor operate at a constant agitation rate and using air or oxygen-enriched air as the inlet gas in order to ensure fully aerobic conditions (especially in high-cell density cultures). Chemostat cultures have been used to examine the

boosting effect of oxygen-limiting conditions on RPP. For example, Garcia-Ortega et al. (2017) compared different steady-states under oxygen-limiting conditions and found the optimum setting to provide a 3-fold increase in a specific production rate of the recombinant protein.

Using as simple and inexpensive media as possible is essential to reduce fermentation and protein purification costs for efficient RPP. The most common media for *P. pastoris* cultivation have been reviewed (Cos et al., 2006; Sreekrishna, 2010). However, some of them present important problems such as unbalanced composition, formation of precipitates, high ionic strength, etc.

One of the critical points in formulating cultivation media is the nitrogen source. In some cases, nitrogen is only supplied with the feed medium; in others, it is added when pH control is required. Nitrogen starvation produces an increase in protease activity which can be avoided by increasing the initial/inlet concentration of the nitrogen source. Protease inhibitors provide, in general, a more expensive alternative method to the use of protease-deficient strains in order to decrease the presence of proteolytic activity in culture broth (Shi et al., 2003; Sinha et al., 2005).

Cankorur-Cetinkaya et al. (2018) developed a new interesting medium formulation that provide an appropriate balance between cell growth and product formation in the synthesis of human lysozyme (HuLy) and the anti-idiotypic antibody 3H6 Fab in chemostat cultures of *P. pastoris*. Tyrosine supplementation increased productivity, but tryptophan addition had virtually no effect; also, phenylalanine addition increased HuLy expression but decreased 3H6 Fab expression.

The effect of biotin deficiency on the growth of *P. pastoris* producing a recombinant glycosylated avidin was studied in chemostat culture. Replacing biotin with aspartic acid and oleic acid, although they had a growth promoting effect, wash-out happened and avidin productivity decreased. The addition of small amounts of biotin provided stable chemostat cultures on methanol and enabled production of biotin-free avidin (Jungo et al., 2007b).

The composition of the cultivation medium also has a direct impact on osmolarity. Dragosits et al. (2010) examined the effect of osmolarity on cell physiology in wild-type and Fab fragment-producing strains of *P. pastoris* grown in carbon-limited chemostat cultures. Neither total protein nor specific Fab production was affected by osmolarity. However, proteins involved in energy metabolism and folding processes were affected by an increased osmolarity (especially with the wild-type strain). Also, a high osmolarity decreased biomass yield due to the increased energy maintenance requirements.

Carbon Sources

The main substrate for a recombinant production bioprocess is usually selected in terms of the promoter regulating the expression. With *P. pastoris* and constitutive promoters such as P_{GAP}, glycerol and glucose are widely used as carbon sources because they result in high specific growth rates that are usually accompanied by adequate specific production rates (Garcia-Ortega et al., 2013). In P_{AOX1}-driven systems, however, methanol is often the sole carbon source and inducer of protein expression (Barrigón et al., 2015).

Pichia strains exhibits a different phenotype regarding methanol assimilation. For Mut^S phenotype, cell growth is considerably slow relative to the standard strains, which are designated Mut^+ strains. Cell growth and productivity in bioprocesses involving Mut^S strains can be improved by using mixed substrates in combination with a co-feeding strategy (Arnau et al., 2010, 2011). This increases the total concentration of the carbon source and the amount of energy supplied reducing process times, as well as reducing heat production and oxygen requirements relative to Mut^+ bioprocesses. Glycerol and sorbitol are the most commonly used co-substrate jointly to methanol (Jungo et al., 2007a,c), although in repressed classical systems, glycerol may lead to lower specific production rates (Arnau et al., 2011; Potvin et al., 2012). New, unrepressed promoters allow glycerol and glucose to be used in combination with methanol to substantially increase RPP efficiency (García-Ortega et al., 2019).

The continuous strategy provides a powerful tool for assessing the potential impact of using co-substrates. The design of this system is usually based on the selection of a dilution rate (D) far enough from μ_{max}, which should ensure that no accumulation of substrates apart from methanol is produced. Moreover, the methanol concentration used should be high enough to allow efficient induction of the target protein, but not so high as to inhibit cell growth or protein production.

D'Anjou and Daugulis (2001) used a substrate mixture of methanol and glycerol with a Mut^+ strain for P_{AOX1}-driven heterologous production of a sea raven antifreeze protein. The specific product formation rate (q_P) and product-based volumetric productivity (Q_V) increased throughout the range of dilution rates used (0.01–0.10 h^{-1}). Similarly, Boze et al. (2001) studied the production of recombinant porcine follicle-stimulating hormone (rFSH) with mixed substrates of sorbitol and methanol. Neither protein production nor Q_V or q_P increased relative to the use of methanol as sole carbon source at the same dilution rate (0.01 h^{-1}). However, the substrate concentration ratio was not optimized in either study.

Jungo et al. (2007a) studied the influence of the methanol fraction in the feed medium on recombinant avidin productivity and specific alcohol oxidase activity by using a glycerol–methanol mixed substrate to grow a *P. pastoris* Mut^+ strain expressing recombinant avidin at a constant dilution rate $D = 0.06\,h^{-1}$. With methanol fractions higher than 0.6 C-mol C-mol^{-1}, q_P was like cultures performed with methanol as sole carbon source.

Canales et al. (2015) used the production of *Rhizopus oryzae* lipase (Rol) as a model system to investigate the application of methanol-glycerol feeding mixtures in the *P. pastoris* Mut^+ producer clone. Cultures were grown in a simple chemostat system and response surface methodology was used to evaluate the effects of D and the methanol/glycerol ratio in the feed as experimental variables. The optimum conditions provided q_P values similar to, and Q_V values higher than those of processes using methanol alone as substrate. Furthermore, Berrios et al. (2017) compared the effect of glycerol and sorbitol as co-substrates for methanol in continuous cultures growing at the

same rate. Higher Q_V, but lower q_P and volumetric methanol consumption rates were observed using glycerol as a co-substrate at either 22 or 30°C.

Paulová et al. (2012) used a mixture of glucose and methanol in continuous cultures of a Mut^+ *P. pastoris* strain to obtain recombinant trypsinogen. No repressive effect of glucose on methanol was observed under conditions far enough from μ_{max}. The product was synthesized throughout the D range, with enhanced productivity at intermediate D values that was significantly higher than with methanol alone in the feed.

Niu et al. (2013) used a co-feeding strategy based on a methanol–sorbitol mixture with the aim of reducing the high oxygen demand at large-scale operation. Thus, they used transient continuous cultures of a Mut^+/P_{AOX1}-lacZ strain at a fixed dilution rate. While a linear change of methanol fraction was conducted, cell growth and metabolism, including O_2 consumption, CO_2 and heat production were analyzed. Based on the results, decreasing the methanol fraction in the feeding medium reduced the specific oxygen uptake rate and maintained maximal ß-galactosidase q_P. Production was optimal with methanol fractions over the range of 0.45–0.75 C-mol C-mol^{-1}.

Although glucose and sorbitol have also been tested as co-substrates jointly with methanol for Mut^+ phenotype, glycerol is the most selected co-substrate to improve the productivity and to reduce the specific oxygen uptake rate and heat generation in continuous cultures in comparison with the sole use of methanol as a substrate. However, the methanol:glycerol ratio and the operating dilution rate must be empirically optimized for each target protein.

Bioreaction Kinetics

The physiological characterization of the producer strains, production rates and yields included, is currently considered critical for bioprocess development. Environmental factors affect cell factories in terms such as rearrangement of central carbon, amino acid metabolism and other basic functions, all of which have a direct impact on cell growth, folding stress, and vesicular transport, and also potential implications in protein secretion and other phenomena influencing production rates and yields (Baumann et al., 2010; Zahrl et al., 2017).

Continuous cultivation is the most frequently used operational mode to obtain accurate physiological data for reliable characterization. By contrast, fed-batch cultures are usually deemed less robust, and more laborious and time-consuming (García-Ortega et al., 2019). Also, stress conditions associated to high-cell density cultures can eventually occur and render them unsuitable for accurate physiological studies.

On the other hand, the use of dynamic process conditions for fast physiological strain characterization in order to reduce experimental time associated to conventional fed-batch and/or continuous cultivation has been reviewed (Spadiut et al., 2013). Moreover, the use of transient continuous cultures in order to reduce the time-consuming steady-state experiments was also implemented in the quantitative study of using mixed feeds (Jungo et al., 2007a).

Table 1 summarizes the continuous cultures used so far to characterize the bioreaction kinetics involved in some RPP processes with *P. pastoris*. The table shows the target protein, strain, promoter, substrate, operating strategy, and product formation kinetics. As can be seen, chemostat cultivation was the norm, but alternative strategies based on S-stats (nutriostats) (Curvers et al., 2002) or DO-stats were also used (Yamawaki et al., 2007).

The most common types of kinetics reported for cell growth (μ), substrate uptake (q_S), and product formation (q_P) are Monod for cell growth, *Pirt*'s as a maintenance energy model and *Luedeking–Piret* as linear μ-dependence for substrate uptake and product formation, respectively. However, saturation patterns, non-monotonic behaviors or bell-shaped types have also been observed, especially in substrate-inhibited systems for cell growth and non-constitutive RPP (Barrigón et al., 2015).

The kinetics of oxygen uptake, carbon dioxide production, and substrate uptake can usually be fitted to a linear model thanks to the rather linear relationship between specific rates and the specific growth rate. These have been widely discussed in several studies on chemostat cultures of *P. pastoris* (Maurer et al., 2006; Rebnegger et al., 2014; Looser et al., 2015; Garcia-Ortega et al., 2016).

Because production kinetics is influenced by a number of physiological interactions, the overall balance of the different steps from gene transcription to product secretion is usually considered instead. As discussed by some authors, the correlation between q_P and μ is specific for each case, so it must be determined experimentally for each individual strain and protein under fixed operating conditions (Looser et al., 2015). The data of **Table 1** confirm that production kinetics is not only influenced by the promoter used with each strain but also, often, protein-specific. For this reason, the most widely used expression systems (viz., that driven by methanol-inducible P_{AOX1} and the constitutive glycolytic P_{GAP}) usually exhibit different production kinetics. Thus, the P_{AOX1}-driven expression system often exhibits non-monotonic kinetics, possibly as a consequence of the metabolic burden resulting from methanol uptake and/or protein processing, and from secreting limitations due to outstanding expression levels (García-Ortega et al., 2019). In this situation, maximizing bioprocess efficiency entails using intermediate μ values far from μ_{max}. On the other hand, a growth-coupled increasing correlation between μ and q_P has been observed in constitutive expression systems relying on glycolytic promoters such as *GAP* or *PGK* (Rebnegger et al., 2014; Garcia-Ortega et al., 2016; de Macedo Robert et al., 2019), and also with the thiamine sensitive *THI11* promoter (Landes et al., 2016), q_P peaking at higher μ values closer to μ_{max}.

For most proteins, however, q_P is related to μ by a growth-coupled production model (D'Anjou and Daugulis, 2001; Rebnegger et al., 2014; Garcia-Ortega et al., 2016) and even, possibly, by a *Luedeking–Piret* or μ-linear model (Curvers et al., 2002; Jungo et al., 2006; Khasa et al., 2007; Tang et al., 2010). Other, partially growth-dependent, exhibit a μ-saturated production pattern (Maurer et al., 2006; Buchetics et al., 2011) or fit a bell-shaped model (Yamawaki et al., 2007). For example, Yamawaki et al. (2007) found q_P for scFv to exhibit either a saturation behavior on μ or bell-shaped kinetics depending on the operational mode used (continuous or fed-batch cultivation).

TABLE 1 | Summary of continuous cultures used as a tool toward the rational based bioprocess development with *P. pastoris* cell factory.

Protein expressed	Strain	Promoter	Substrate	Continuous strategy	Production kinetics	Optimization approach	References
Fab fragment (anti-HIV antibody 2F5)	X-33	*GAP*	Glucose	Chemostat	Growth-coupled μ-saturated	Optimized feeding from continuous data	Maurer et al., 2006
Fab fragment (anti-HIV antibody 3H6)	X-33	*GAP*	Glucose	Chemostat	Growth-coupled μ-saturated	Optimized feeding from continuous data	Buchetics et al., 2011
Fab fragment (anti-HIV antibody 2F5)	X-33	*GAP*	Glucose	Chemostat	Growth-coupled	Optimal D at continuous mode	Garcia-Ortega et al., 2016
hGM-CSF (human)	GS115 Mut$^+$	*GAP*	Glucose	Chemostat	Linear	Fed-batch designed from continuous data	Khasa et al., 2007
phytase	X-33	*GAP*	Glucose	Chemostat	Linear	Fed-batch designed from continuous data	Tang et al., 2010
srAFP	GS115 Mut^S	*AOX*	Glycerol/methanol	Chemostat	Growth-coupled	Fed-batch designed from continuous data	D'Anjou and Daugulis, 2001
°scFv	GS115 Mut$^+$	*AOX*	Methanol	DO-stat S-stat	Bell shaped μ-saturated	Trade-off between fed-batch and continuous	Yamawaki et al., 2007
hCTRB	GS115 Mut$^+$	*AOX*	Methanol	Nutriostat	Linear	Optimal D at continuous mode	Curvers et al., 2002
rHV2	GS115 Mut$^+$	*AOX*	Methanol	Chemostat	Bell shaped	Fed-batch designed from continuous data	Zhou and Zhang, 2002
Porcine trypsinogen	X-33	*AOX*	Glucose/methanol	Chemostat	Bell shaped	Optimal D at continuous mode	Paulová et al., 2012
Avidin	GS115 Mut$^+$	*AOX*	Methanol/glycerol/ sorbitol	Chemostat	Linear	Fed-batch designed from continuous data	Jungo et al., 2006, 2007a,c
CalB	X-33	*PGK*	Glycerol	Chemostat	Linear	Trade-off between fed-batch and continuous	de Macedo Robert et al., 2019
Serum albumin (human)	X-33	*THI11*	Glucose	Chemostat	Growth-coupled	Optimized feeding from continuous data	Landes et al., 2016

For other proteins, studies performed in chemostat (Paulová et al., 2012) or fed-batch cultures (Zhou and Zhang, 2002; Zhang et al., 2005) have shown them to fit μ non-monotonically increasing or bell-shaped models.

In **Table 2** a comparison of q_P and $Y_{P/X}$ according to the μ reached in continuous and fed-batch bioprocesses is presented. This table includes results obtained with different target proteins, promoters, gene dosage, substrates, and feeding strategies. In continuous mode, $Y_{P/X}$ normally decreases when μ increases, but in contrast q_P increases along with μ, except in the production of hSA where $Y_{P/X}$ increases when μ increases, which is probably associated with the high gene dosage (6 copies) (Landes et al., 2016). In general, this linear behavior between q_P and μ is related with the commonly observed μ-dependence in *P. pastoris* bioprocesses, which indicates that the product formation is growth-dependent.

When the data obtained in both, continuous and fed-batch mode are compared, the analysis is often difficult because not all the examples have been studied for coincident μ's. However, the q_P behavior is quite similar for the two operating modes, only for the case of rHV2 and Crl1 production regulated by P_{AOX1}, which q_P presents a maximum at intermediate μ for the fed-batch cultivation not following a product formation growth-dependent pattern. On the other hand, there is not a common trend in reference to $Y_{P/X}$ behavior in front of μ, observing different positive and negative linear relationships, bell-shaped and saturation patterns.

In terms of absolute values, only in the case of Fab 3H6 and hSA production, the specific production rate (q_P) and the $Y_{P/X}$ values were always higher in continuous mode at similar μ comparing to those obtained in fed-batch cultivation.

Additionally, since productivities could be one of the main performance criteria from an industrial point of view, volumetric productivity (Q_V) has been also included in **Table 2**. Nevertheless, the comparison could not be made in a suitable way because the biomass concentration and the reactor volume may not be equivalent in the two operating modes. Moreover, for a proper comparison it had to be also considered a time window of several weeks in order to take into account the unproductive time between consecutive fed-batches. For instance, taking these factors into consideration, overall CalB production was reported as 5.8 times greater in continuous culture (de Macedo Robert et al., 2019).

The results of this experimental approach, which is mostly performed in chemostat cultures, provide a wealth of knowledge to tailor rational strategies with a view to optimizing bioprocess

TABLE 2 | Comparison of specific production rates (q_P), product yields ($Y_{P/X}$), and volumetric productivities (Q_v) between continuous and fed-batch operating modes with different proteins produced, promoters/gene dosage, substrates, specific growth rates (μ), and feeding strategies used.

			Continuous				Fed-batch				References
Protein	**Promoter/gene dosage**	**Substrate**	μ h^{-1}	q_P AU/(g_X·h)	$Y_{P/X}$ AU/g_X	Q_v AU/(L·h)	μ h^{-1}	q_P AU/(g_X·h)	$Y_{P/X}$ AU/g_X	Q_v AU/(L·h)	
Crl1	P_{GAP}	Glucose	0.056	78.2	1,400	1,924	0.048	77	1,610	2,195	Nieto-Taype et al., 2020
	Sc		0.081	89.1	1,093	2,410	0.087	149	1,700	3,246	
			0.136	126	930	3,108	0.133	292	2,190	10,442	
Crl1	P_{AOX}	MetOH	0.020	118	6,017	2,291	0.028	364	13,155	2,291	Garrigós-Martínez et al., 2019
	sc		0.050	271	5,398	5,564	0.053	588	11,299	5,564	
			0.079	310	3,939	6,874	0.084	326	3,911	6,874	
CalB	P_{PGK}	Glucose	0.050	20.4	449	449	0.060	19.4	323	402	de Macedo Robert et al., 2019
	Sc		0.090	38.4	423	864	0.110	47.5	423	796	
			0.160	59.1	377	1,331	0.140	52.3	377	868	
Phytase	P_{GAP}	Glucose	0.050	480	9,600	nd	DFP 0.118	567	4,800	20,900	Tang et al., 2010
			0.150	820	5,500	nd	DFP 0.125	586	4,680	17,400	
			0.300	1,420	4,700	nd	DFP 0.125	628	5,020	18,700	
Protein	**Promoter/gene dosage**	**Substrate**	μ h^{-1}	q_P $\mu g/(g_X \cdot h)$	$Y_{P/X}$ mg/g_X	Q_v mg/(L·h)	μ h^{-1}	q_P $\mu g/(g_X \cdot h)$	$Y_{P/X}$ mg/g_X	Q_v mg/(L·h)	**References**
Human FAB 2F5	P_{GAP}	Glucose	0.050	17.2	0.33	0.34	0.050	7.7	0.15	0.24	Garcia-Ortega et al., 2013, 2016
	sc		0.100	32.4	0.32	0.70	0.101	25.7	0.25	0.64	
			0.150	45.7	0.30	1.04	0.146	35.2	0.24	0.73	
Human FAB 2F5	P_{GAP}	Glucose	0.060	25.1	0.42	0.62	CFR	10.0	0.48	0.39	Maurer et al., 2006
	sc		0.100	34.0	0.34	0.94					
			0.150	41.4	0.28	1.14	OFR	30.0	0.48	0.67	
Human FAB 3H6 CLB2	P_{GAP}	Glucose	0.190	45.6	0.24	1.38					Buchetics et al., 2011
	sc		0.050	48.1	0.96	1.32					
			0.100	60.5	0.60	1.66	OFR	10	0.45	nd	
			0.150	66.1	0.44	1.82					
rHV2	P_{AOX}	MetOH 0.4 g/L	0.017	nd	nd	nd	0.01	0.03	3.0	nd	Zhou and Zhang, 2002
		MetOH 0.6 g/L	0.020	nd	nd	nd	0.02	0.20	9.8	nd	
		MetOH 1.5 g/L	0.040	nd	nd	nd	0.04	0.08	2.0	nd	
						CLC 0.018	0.17	9.6	14		
hSA	P_{THI11}	Glucose	0.050	0.003	0.06	0.05					Landes et al., 2016
	6 copies		0.075	0.017	0.22	0.30					
			0.100	0.050	0.50	1.00					
			0.125	0.119	0.95	2.38					
			0.150	0.180	1.20	3.60	0.150	0.023	0.88	2.60	
Avidin	P_{AOX}	*MS-MS 6	0.03	0.003	0.11	0.03					Jungo et al., 2007c
		(% Methanol 25	0.03	0.013	0.42	0.13					
		C-mol) 43	0.03	0.016	0.54	0.16	0.027	0.049	1.78	3.24	
		65	0.03	0.016	0.52	0.13					
		100	0.03	0.016	0.54	0.12					

*SC: Single Copy; nd: not determined; All the fed-batch cultures were carried out by implementing open-loop feeding strategies except: DFP, Different Feeding Profile; CFR, Constant Feed Rate; OFR, Optimized Feed Rate; CLC, Closed Loop Control; *Mixed-substrates Methanol-Sorbitol. Some values have been estimated from the values indicated in the references or directly from the figures. For rHV2, hSA, and avidin, q_P is expressed as mg/(g_X·h).*

operating conditions for increased production rates and yields. Although production patterns are expected to be similar when using the same expression system to produce different target proteins, the outcome usually depends on both. Therefore, optimal bioprocess development requires using similar experiments not only to maximize production rates, but also to identify the most suitable conditions for testing other strains with industrial potential. Chemostats therefore provide an effective platform for easily characterizing production strains and elucidating production kinetics by the obtention of accurate and robust data.

Bioprocess Optimization and Process Development

Most of the bioprocesses currently used for recombinant protein or metabolite production are performed in the fed-batch mode on the grounds of the high cell concentrations it affords, and the increased amounts of product obtained as a result. Therefore, using the data obtained from chemostats with fed-batch cultures requires that the latter operate in a pseudo-stationary state or balanced growth in order to maintain the overall μ value rather constant during the process. This can be accomplished by using a fed-batch strategy based on pre-programed exponential feeding

derived from mass balances. Under these conditions, if μ is kept constant and the biomass-to-substrate yield rather constant throughout the cultivation period, the substrate can be assumed to reach a pseudo-stationary state.

Table 1 summarizes works with continuous cultures as a tool for further rational process development based on the physiological characterization of the producer strains. As can be seen, three main approaches have been used for optimal RPP. One involves identifying the optimum D conditions under continuous operation for key parameters of interest (KPIs) including productivities (Curvers et al., 2002; Paulová et al., 2012). Another uses a trade-off between fed-batch and continuous operation for yields or productivities depending on the particular design or performance criteria (Yamawaki et al., 2007). The third is a sequential approach to bioprocess design (i.e., fed-batch operation is designed and implemented on the basis of production kinetics or productivity data obtained under continuous operation) (Zhou and Zhang, 2002; Jungo et al., 2007a,c; Khasa et al., 2007; Tang et al., 2010).

Garcia-Ortega et al. (2016) characterized the recombinant production of Fab fragment 2F5 driven by the constitutive promoter P_{GAP} in chemostat cultures. A positive effect of high μ levels on productivity was observed, which confirmed that production was growth-coupled.

de Macedo Robert et al. (2019) compared *Candida antarctica* lipase (CalB) production with the constitutive promoter *PGK* in continuous and fed-batch cultures. They found volumetric and specific productivity to peak at the highest μ levels, which indicated a direct correlation between growth and production.

Production kinetic profiles for other proteins have also been obtained in other continuous cultures that were used as references to develop optimal feeding strategies adjusted to cell factory performance. The result was a marked increase in production in terms of volumetric productivity and product titer for some Fab fragments (Maurer et al., 2006; Buchetics et al., 2011) and human serum albumin (Landes et al., 2016).

D'Anjou and Daugulis (2001) used glycerol–methanol mixtures as co-substrates for continuous cultures to obtain sea raven antifreeze protein (srAFP). They elucidated the relationship of μ to the yield on methanol, q_S on methanol and q_P and then used data collected under continuous operation to predict cell growth and RPP, as well as to develop an exponential feeding strategy for fed-batch cultures with the same two carbon sources. The outcome was increased product yield and productivity relative to a heuristic approach.

IS CONTINUOUS CULTIVATION A REAL ALTERNATIVE FOR ITS USE IN INDUSTRIAL *PICHIA PASTORIS* PROCESSES?

The Transition of Industrial Biotechnology From Batch/Fed-Batch Mode to Continuous Manufacturing

The main current trend in bioprocess optimization is to move away from standard, fixed protocols toward concepts enabling the operator to adapt particular recommendations to any specific clones, strains or bioreactors (Looser et al., 2015). This requires combining effective strains and bioprocess engineering approaches for optimal results, and also avoiding complex media to reduce costs and facilitate downstream processes with a view to increasing economic viability of the bioprocess (Sreekrishna, 2010; Potvin et al., 2012). In this sense, due to the relevant advantages of the continuous manufacturing, as once pioneered in the oil and chemical industry, many industrial bioprocesses are expected to eventually evolve from batch or fed-batch to continuous processes (Croughan et al., 2015).

Currently, continuous biomanufacturing processes based on the application of continuous fermentation are being carried out in different industries including ethanol, lactic acid, and numerous biopharmaceutical productions. Mears et al. (2017) discussed some of these examples performed with continuous microbial systems at industrial scale to evaluate the expected wide implementation in biopharmaceutical biomanufacturing processes. Actually, the US FDA has encouraged the development of continuous processing for biopharmaceuticals manufacturing (Croughan et al., 2015). In this sense, it is worth mentioning that Novo Nordisk implemented the continuous insulin production with the yeast *S. cerevisiae* since the 1990's (Peebo and Neubauer, 2018). And currently, several commercial biopharmaceuticals such as monoclonal antibodies or therapeutic proteins are recombinantly produced in continuous perfusion cultures of mammalian cell lines (Mears et al., 2017).

Industrially, switching from batch to continuous operation can have several advantages such as reduced processing costs, increased productivity, and product quality, and the ability to integrate upstream and downstream in a continuous manner (Cankorur-Cetinkaya et al., 2018). However, bottlenecks in industrial bioprocesses are generally product-specific and must be identified on a case-by-case basis with provision for economic constraints (Yang and Zhang, 2018).

Continuous cultures growing under steady-state conditions are, in theory, more effective in this mode than are batch or fed-batch cultures. In this mode, which is usually performed at a constant μ, most of the factors involved in the RPP as well as a large fraction of the transcriptome, proteome and fluxome can be considered constant, since it has been reported that they are coordinated by μ (Peebo and Neubauer, 2018). Therefore, continuous cultivations where μ can be easily fixed, simplifies significantly the interpretation and control of the bioprocess. In this way, bioprocesses should be easier to characterize, understand, control and maintain under optimal conditions over long periods. Furthermore, the lag and dead times, intrinsically associated to batch and fed-batch operation, result in considerably diminished productivity. Hence, continuous biomanufacturing processes allow reducing running costs, minimizing equipment size, integrating upstream and downstream steps, increasing product quality, ensuring constant product recovery, and making processes scalable are additional advantages of continuous cultures over batch and fed-batch cultures (Peebo and Neubauer, 2018).

However, continuous cultivation also has some drawbacks arising from the need to ensure long-term stability and sterility in the cultures, and to shorten average long development times (Croughan et al., 2015). Specifically, the genetic instability of

recombinant strains may limit the length of RPP bioprocesses; especially for with *P. pastoris* strains. Clone stability can be confirmed by testing productivity over a large number of generations under steady states (about 20–30 residence times) in chemostat cultures growing under a steady state. Alternatively, it can also be assured with periodic changes in dilution rate or the aeration conditions (Cankorur-Cetinkaya et al., 2018). Additionally, and concretely for multi-copy strains, the gene dosage conservation in continuous cultures maintained over long periods is important to be checked.

Challenges to Be Addressed in *Pichia Pastoris* Continuous Cultivations

An important requirement with continuous bioprocesses is to develop effective alternative promoters to replace the classical P_{AOX1}, which is widely used efficiently in fed-batch processes but is not recommended for continuous RPP. In fact, identifying strong and constitutively expressed promoters, and testing them in continuous cultures currently still remains a major goal (Cankorur-Cetinkaya et al., 2018). Obviously, efficiently exploiting the potential advantages of continuous cultivation requires integrating upstream and downstream bioprocess flows. Thus, the implementation of new approaches is a challenge for biotechnology companies in order to reach short process development times jointly with minimal risks in the context of possible hard quality/regulatory requirements (Rathore et al., 2015). At this point a question arises: is continuous cultivation a real alternative to fed-batch cultures for its use in industrial biotechnology based on the *Pichia pastoris* cell factory?

Gasser and Mattanovich (2018) reported some interesting guidelines to transform this yeast from an efficient cell factory to a useful chassis for the production of recombinant proteins and biochemicals as a real alternative to *Saccharomyces cerevisiae*. Furthermore, Moser et al. (2017) investigated the impact of long-term carbon source adaptation toward improved cell growth in RPP processes with *P. pastoris* in the context of Adaptive Laboratory Evolution (ALE). Adaptation of the yeast to growth on methanol over 250 generations was examined and observed a complex correlation among carbon source, cell growth and RPP. Increased specific growth rates on rich and minimal growth media was studied at the level of both population and single clone. Selected clones displayed strain-dependent variations for the yield of P_{AOX1}-based recombinant protein expression, one showing up to 2-fold increase in terms product titer.

From a bioprocess engineering perspective, process variability often results in issues arising from changes in critical process parameters (CPPs), key parameters of interest (KPIs), or critical material attributes (CMAs), all of which in turn affect critical quality attributes (CQAs). CPPs can change throughout a culture and require using appropriate control strategies to reduce process variability. Advances in process analytical technology (PAT) and quality by design (QbD) approaches have substantially reduced times for process development. According to Hernandez (2015), in the context of transition to continuous bioprocesses it is essential to adapt these methodologies from batch to continuous cultures.

It has been stated that continuous bioprocesses require real-time monitoring of process variability in order to identify eventual deviations and to ensure consistent performance (Rajamanickam et al., 2018). Variability in KPIs (e.g., cell growth, yields, production rates) is especially important because it has a direct impact on process performance and product quality. Thus, continuous bioprocesses require real-time monitoring with standard sensors for direct measurements, or soft sensors that

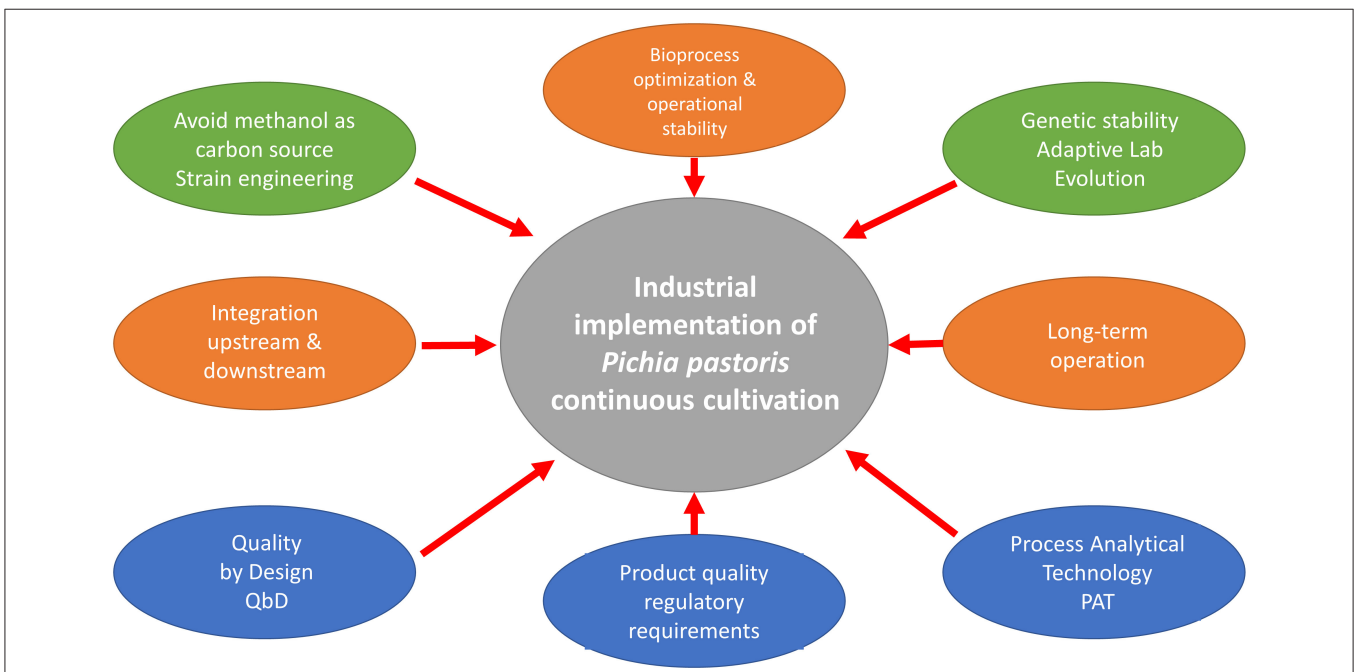

FIGURE 3 | Mean features in the industrial implementation of *Pichia pastoris* continuous cultivation.

allow the indirect determination of parameters ensuring a high bioprocess efficiency. Recent advances in the monitoring of various cell factories, including soft-sensors, have been reviewed by several authors (Valero and López-Santín, 2017; Veloso and Ferreira, 2017; Randek and Mandenius, 2018). Nevertheless, most of the reported monitoring applications for *P. pastoris* have been described for batch and fed-batch operations. Besides the common sensors used for the monitoring and control of culture conditions and gas analysis, just scarce applications have been reported for continuous mode (Jungo et al., 2007a; Fazenda et al., 2013). In this scenario, further implementing PAT and QbD in *P. pastoris* continuous cultures has been deemed essential for industrial processes.

How Far Is the Implementation of *Pichia pastoris* Continuous Manufacturing Processes?

Several RPP industrial processes are currently performed with *P. pastoris*. Including both industrial enzymes and biopharmaceuticals, the www.pichia.com website provides a list of products manufactured with *Pichia* which are on the market of late stage development. However, according to the open literature, there are no reported in detail continuous biomanufacturing processes implemented with *P. pastoris*. Nevertheless, taking into consideration the state of the art discussed in this section, some long terms continuous examples described in the literature could eventually become interesting candidates for continuous manufacturing with *P. pastoris*.

A chemostat process producing recombinant hepatitis B small surface antigen (rHBsAg) was maintained working for 2 weeks reaching similar levels of product titer than at the end of a fed-batch culture. Specifically, Q_V and q_P were, respectively, about 1.5 and 1.3 times higher, than in fed-batch mode. Interestingly, no contamination issues or/and genome instability were detected after those 2 weeks of continuous operation (Rahimi et al., 2019). In another study, the performance of continuous cultures designed as a combination of turbidostat/chemostat modes at constant cell concentration was evaluated (Wang et al., 2012). As a relevant outcome, it was reported that feeding the system with methanol resulted in high recombinant polygalacturonate lyase PGL expression and a substantial performance improvement relative to conventional fed-batch cultures. Moreover, a chemostat producing lipase B from *Candida antarctica* (CalB) was running 6 weeks at $\mu = 0.14\ h^{-1}$. In this case, considering the unproductive time spent in setting up, draining out, cleaning and reassembling in fed-batch operation, the overall CalB production was 5.8 times greater than the fed-batch process (de Macedo Robert et al., 2019).

Finally, a summary including the main items required to address toward the industrial implementation of continuous cultivation with the cell factory *P. pastoris* is presented in **Figure 3**.

CONCLUSIONS

The yeast *P. pastoris* is considered an outstanding cell factory alternative for its industrial use in production processes of both

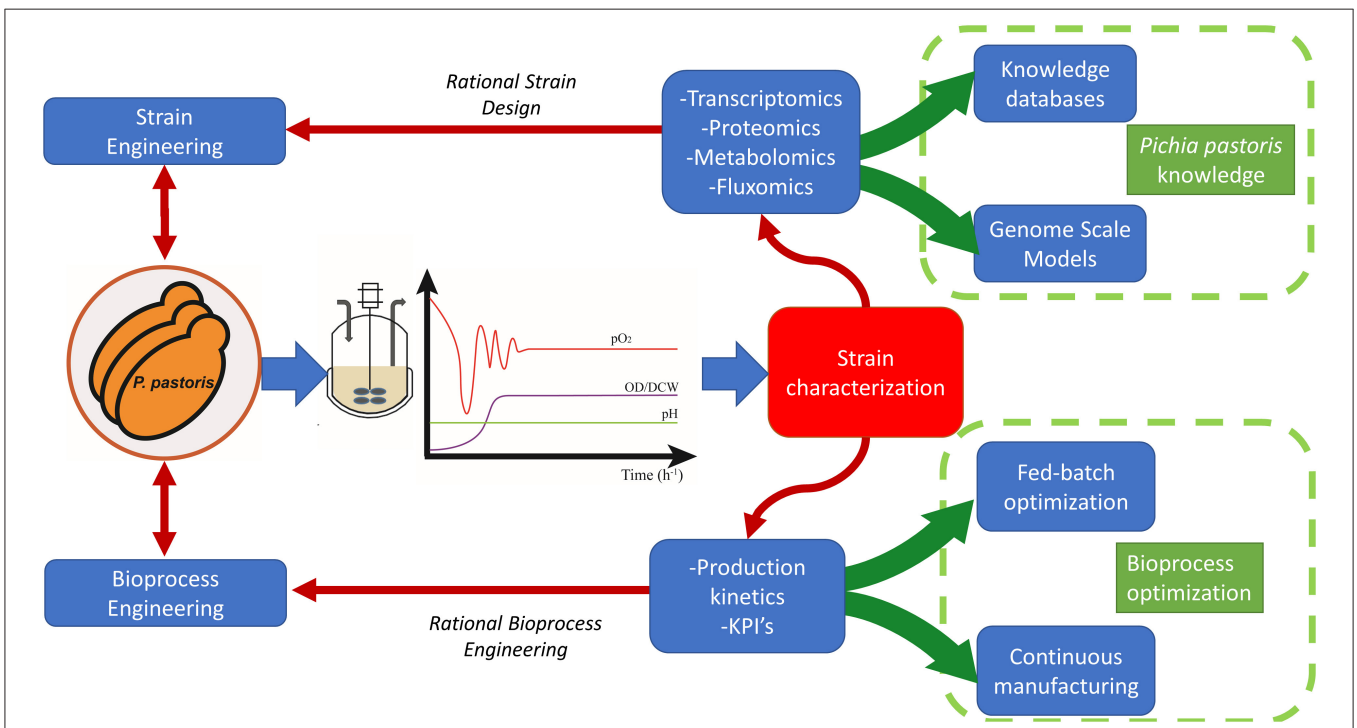

FIGURE 4 | Use of continuous cultivation as a tool toward the rational bioprocess development with *Pichia pastoris* cell factory by combining strain and bioprocess engineering.

metabolites and recombinant proteins. Despite the excellent features of this host, in general, most of the bioprocesses based on fermentation technology are considered still far from achieving the maturity of other industries. In this sense, the present trends toward their optimization are provided by two complementary approaches: Strain development and bioprocess engineering. In order to achieve relevant progresses in the long road to bioprocess optimization it is essential to acquire robust and reliable knowledge of the system used. This knowledge is considered with the objective to be able to design and implement rational developments from any of the both approaches mentioned. In this context, continuous cultivation emerges as an excellent tool to accurately characterize the performance of the cell factory in terms of physiological and production parameters. Furthermore, the steady state conditions achieved during the continuous cultures and the high degree of cell population homogeneity makes this operational mode, an excellent tool toward the development of a wide range of systems biology studies including transcriptomics, proteomics, metabolomics and other cutting edge "-omics" studies.

In **Figure 4** is summarized how continuous cultivation can be used as a tool toward the rational development of bioprocesses with *P. pastoris*. It illustrates the different approaches that, based on the results obtained in continuous cultivation (chemostat), allow to achieve rational improvements at both strain and bioprocess engineering level.

Besides, the current trends of industrial biotechnology is promoting the transition from batch/fed-batch-based processes toward the continuous biomanufacturing due to the numerous advantages that present this operation mode in terms of ensuring a robust and very high product quality as well as, among others, to reduce running costs and minimizing equipment requirements. The potential implementation of biomanufacturing processes with *P. pastoris* has the most relevant challenges with the identification of efficient and methanol-free alternative promoters, the integration of upstream and downstream, reaching short process development times with minimal risks on quality/regulatory requirements through PAT and QbD approaches and, finally, to evaluate the impact of long-term continuous operation on genetic stability and cell physiology.

AUTHOR CONTRIBUTIONS

MN-T and XG-O contributed writing the Abstract and the Introduction sections. MN-T and JA wrote the section: Continuous cultivations provide an excellent tool for systems biology research. JM-S and FV wrote the section: Bioprocess characterization with chemostat cultures. XG-O, JM-S, and FV wrote the section: Is continuous cultivation a real alternative for its use in industrial Pichia pastoris processes? XG-O, JM-S, and FV wrote the Conclusions section. All authors read, reviewed, and approved the submitted version.

FUNDING

This work was funded by MINECO and FEDER under Project CTQ2016-74959-R. The authors' group is member 2017-SGR-1462 and the Reference Network in Biotechnology (XRB) of Generalitat de Catalunya.

ACKNOWLEDGMENTS

MN-T acknowledges award by the National Council of Science Technology and Technological Innovation (CONCYTEC) through its executing unit and the National Fund for Scientific, Technological and Technological Innovation Development (FONDECYT).

REFERENCES

Adamberg, K., Valgepea, K., and Vilu, R. (2015). Advanced continuous cultivation methods for systems microbiology. *Microbiology* 161, 1707–1719. doi: 10.1099/mic.0.000146

Adelantado, N., Tarazona, P., Grillitsch, K., García-Ortega, X., Monforte, S., Valero, F., et al. (2017). The effect of hypoxia on the lipidome of recombinant *Pichia pastoris*. *Microb. Cell Fact*. 16:86. doi: 10.1186/s12934-017-0699-4

Ahmad, M., Hirz, M., Pichler, H., and Schwab, H. (2014). Protein expression in *Pichia pastoris*: recent achievements and perspectives for heterologous protein production. *Appl. Microbiol. Biotechnol.* 98, 5301–5317. doi: 10.1007/s00253-014-5732-5

Arnau, C., Casas, C., and Valero, F. (2011). The effect of glycerol mixed substrate on the heterologous production of a *Rhizopus oryzae* lipase in *Pichia pastoris* system. *Biochem. Eng. J.* 57, 30–37. doi: 10.1016/j.bej.2011.08.004

Arnau, C., Ramon, R., Casas, C., and Valero, F. (2010). Optimization of the heterologous production of a *Rhizopus oryzae* lipase in *Pichia pastoris* system using mixed substrates on controlled fed-batch bioprocess. *Enzyme Microb. Technol.* 46, 494–500. doi: 10.1016/j.enzmictec.2010.01.005

Arvas, M., Pakula, T., Smit, B., Rautio, J., Koivistoinen, H., Jouhten, P., et al. (2011). Correlation of gene expression and protein production rate - a system wide study. *BMC Genomics* 12:616. doi: 10.1186/1471-2164-12-616

Ata, Ö., Prielhofer, R., Gasser, B., Mattanovich, D., and Çalik, P. (2017). Transcriptional engineering of the glyceraldehyde-3-phosphate dehydrogenase promoter for improved heterologous protein production in *Pichia pastoris*. *Biotechnol. Bioeng.* 114, 2319–2327. doi: 10.1002/bit.26363

Ata, Ö., Rebnegger, C., Tatto, N. E., Valli, M., Mairinger, T., Hann, S., et al. (2018). A single Gal4-like transcription factor activates the Crabtree effect in *Komagataella phaffii*. *Nat. Commun.* 9:4911. doi: 10.1038/s41467-018-07430-4

Baghban, R., Farajnia, S., Rajabibazl, M., Ghasemi, Y., Mafi, A., Hoseinpoor, R., et al. (2019). Yeast expression systems: overview and recent advances. *Mol. Biotechnol.* 61, 365–384. doi: 10.1007/s12033-019-00164-8

Barrigón, J. M., Valero, F., and Montesinos, J. L. (2015). A macrokinetic model-based comparative meta-analysis of recombinant protein production by *Pichia pastoris* under AOX1 promoter. *Biotechnol. Bioeng.* 112, 1132–1145. doi: 10.1002/bit.25518

Baumann, K., Carnicer, M., Dragosits, M., Graf, A. B., Stadlmann, J., Jouhten, P., et al. (2010). A multi-level study of recombinant *Pichia pastoris* in different oxygen conditions. *BMC Syst. Biol.* 4:141. doi: 10.1186/1752-0509-4-141

Baumann, K., Dato, L., Graf, A. B., Frascotti, G., Dragosits, M., Porro, D., et al. (2011). The impact of oxygen on the transcriptome of recombinant *S. cerevisiae* and *P. pastoris* - a comparative analysis. *BMC Genomics* 12:218. doi: 10.1186/1471-2164-12-218

Baumann, K., Maurer, M., Dragosits, M., Cos, O., Ferrer, P., and Mattanovich, D. (2008). Hypoxic fed-batch cultivation of *Pichia pastoris* increases specific and volumetric productivity of recombinant proteins. *Biotechnol. Bioeng.* 100, 177–183. doi: 10.1002/bit.21763

Berrios, J., Flores, M.-O., Díaz-Barrera, A., Altamirano, C., Martínez, I., and Cabrera, Z. (2017). A comparative study of glycerol and sorbitol as co-substrates in methanol-induced cultures of *Pichia pastoris*: temperature effect and scale-up simulation. *J. Ind. Microbiol. Biotechnol.* 44, 407–411. doi: 10.1007/s10295-016-1895-7

Boze, H., Laborde, C., Chemardin, P., Richard, P., Venturin, C., Combarnous, Y., et al. (2001). High-level secretory production of recombinant porcine follicle-stimulating hormone by *Pichia pastoris*. *Process Biochem.* 36, 907–913. doi: 10.1016/S0032-9592(00)00296-X

Brejning, J., Arneborg, N., and Jespersen, L. (2005). Identification of genes and proteins induced during the lag and early exponential phase of lager brewing yeasts. *J. Appl. Microbiol.* 98, 261–271. doi: 10.1111/j.1365-2672.2004.02472.x

Buchetics, M., Dragosits, M., Maurer, M., Rebnegger, C., Porro, D., Sauer, M., et al. (2011). Reverse engineering of protein secretion by uncoupling of cell cycle phases from growth. *Biotechnol. Bioeng.* 108, 2403–2412. doi: 10.1002/bit.23198

Bull, A. T. (2010). The renaissance of continuous culture in the post-genomics age. *J. Ind. Microbiol. Biotechnol.* 37, 993–1021. doi: 10.1007/s10295-010-0816-4

Çalik, P., Ata, Ö., Güneş, H., Massahi, A., Boy, E., Keskin, A., et al. (2015). Recombinant protein production in *Pichia pastoris* under glyceraldehyde-3-phosphate dehydrogenase promoter: from carbon source metabolism to bioreactor operation parameters. *Biochem. Eng. J.* 95, 20–36. doi: 10.1016/j.bej.2014.12.003

Cámara, E., Landes, N., Albiol, J., Gasser, B., Mattanovich, D., and Ferrer, P. (2017). Increased dosage of AOX1 promoter-regulated expression cassettes leads to transcription attenuation of the methanol metabolism in *Pichia pastoris*. *Sci. Rep.* 7:44302. doi: 10.1038/srep44302

Cámara, E., Monforte, S., Albiol, J., and Ferrer, P. (2019). Deregulation of methanol metabolism reverts transcriptional limitations of recombinant *Pichia pastoris* (*Komagataella* spp) with multiple expression cassettes under control of the AOX1 promoter. *Biotechnol. Bioeng.* 116, 1710–1720. doi: 10.1002/bit.26947

Canales, C., Altamirano, C., and Berrios, J. (2015). Effect of dilution rate and methanol-glycerol mixed feeding on heterologous *Rhizopus oryzae* lipase production with *Pichia pastoris* Mut + phenotype in continuous culture. *Biotechnol. Prog.* 31, 707–714. doi: 10.1002/btpr.2069

Cankorur-Cetinkaya, A., Narraidoo, N., Kasavi, C., Slater, N. K. H., Archer, D. B., and Oliver, S. G. (2018). Process development for the continuous production of heterologous proteins by the industrial yeast, *Komagataella phaffii*. *Biotechnol. Bioeng.* 115, 2962–2973. doi: 10.1002/bit.26846

Carnicer, M., ten Pierick, A., van Dam, J., Heijnen, J. J., Albiol, J., van Gulik, W., et al. (2012). Quantitative metabolomics analysis of amino acid metabolism in recombinant *Pichia pastoris* under different oxygen availability conditions. *Microb. Cell Fact.* 11:83. doi: 10.1186/1475-2859-11-83

Çelik, E., and Çalik, P. (2012). Production of recombinant proteins by yeast cells. *Biotechnol. Adv.* 30, 1108–1118. doi: 10.1016/j.biotechadv.2011.09.011

Chung, B. K., Selvarasu, S., Andrea, C., Ryu, J., Lee, H., Ahn, J., et al. (2010). Genome-scale metabolic reconstruction and in silico analysis of methylotrophic yeast *Pichia pastoris* for strain improvement. *Microb. Cell Fact.* 9:50. doi: 10.1186/1475-2859-9-50

Cooney, C. L. (1979). Continuous culture of microorganisms: an overview and perspective. *Ann. N.Y. Acad. Sci.* 326, 295–314. doi: 10.1111/j.1749-6632.1979.tb14170.x

Cos, O., Ramón, R., Montesinos, J. L., and Valero, F. (2006). Operational strategies, monitoring and control of heterologous protein production in the methylotrophic yeast *Pichia pastoris* under different promoters: a review. *Microb. Cell Fact.* 5:17. doi: 10.1186/1475-2859-5-17

Cregg, J. M., Vedvick, T. S., and Raschke, W. C. (1993). Recent advances in the expression of foreign genes in *Pichia pastoris*. *Nat. Biotechnol.* 11, 905–910. doi: 10.1038/nbt0893-905

Croughan, M. S., Konstantinov, K. B., and Cooney, C. (2015). The future of industrial bioprocessing: batch or continuous? *Biotechnol. Bioeng.* 112, 648–651. doi: 10.1002/bit.25529

Curvers, S., Linnemann, J., Klauser, T., Wandrey, C., and Takors, R. (2002). Recombinant protein production with *Pichia pastoris* in continuous fermentation – kinetic analysis of growth and product formation. *Eng. Life Sci.* 2:229. doi: 10.1002/1618-2863(20020806)2:8<229::AID-ELSC229>3.0.CO;2-9

D'Anjou, M. C., and Daugulis, A. J. (2001). A rational approach to improving productivity in recombinant *Pichia pastoris* fermentation. *Biotechnol. Bioeng.* 72, 1–11. doi: 10.1002/1097-0290(20010105)72:1<1::AID-BIT1>3.0.CO;2-T

de Macedo Robert, J., Garcia-Ortega, X., Montesinos-Seguí, J. L., Guimaraes Freire, D. M., and Valero, F. (2019). Continuous operation, a realistic alternative to fed-batch fermentation for the production of recombinant lipase B from *Candida antarctica* under the constitutive promoter PGK in *Pichia pastoris*. *Biochem. Eng. J.* 147, 39–47. doi: 10.1016/j.bej.2019.03.027

Delic, M., Valli, M., Graf, A. B., Pfeffer, M., Mattanovich, D., and Gasser, B. (2013). The secretory pathway: exploring yeast diversity. *FEMS Microbiol. Rev.* 37, 872–914. doi: 10.1111/1574-6976.12020

Dragosits, M., Frascotti, G., Bernard-Granger, L., Vázquez, F., Giuliani, M., Baumann, K., et al. (2011). Influence of growth temperature on the production of antibody Fab fragments in different microbes: a host comparative analysis. *Biotechnol. Prog.* 27, 38–46. doi: 10.1002/btpr.524

Dragosits, M., Stadlmann, J., Albiol, J., Baumann, K., Maurer, M., Gasser, B., et al. (2009). The effect of temperature on the proteome of recombinant *Pichia pastoris*. *J. Proteome Res.* 8, 1380–1392. doi: 10.1021/pr8007623

Dragosits, M., Stadlmann, J., Graf, A., Gasser, B., Maurer, M., Sauer, M., et al. (2010). The response to unfolded protein is involved in osmotolerance of *Pichia pastoris*. *BMC Genomics* 11:207. doi: 10.1186/1471-2164-11-207

Engstrom, M. D., and Pfleger, B. F. (2017). Transcription control engineering and applications in synthetic biology. *Synth. Syst. Biotechnol.* 2, 176–191. doi: 10.1016/j.synbio.2017.09.003

Ercan, O., Bisschops, M. M. M., Overkamp, W., Jørgensen, T. R., Ram, A. F., Smid, E. J., et al. (2015a). Physiological and transcriptional responses of different industrial microbes at near-zero specific growth rates. *Appl. Environ. Microbiol.* 81, 5662–5670. doi: 10.1128/AEM.00944-15

Ercan, O., Wels, M., Smid, E. J., and Kleerebezem, M. (2015b). Molecular and metabolic adaptations of Lactococcus lactis at near-zero growth rates. *Appl. Environ. Microbiol.* 81, 320–331. doi: 10.1128/AEM.02484-14

Fazenda, M. L., Dias, J. M., Harvey, L. M., Nordon, A., Edrada-Ebel, R., LittleJohn, D., et al. (2013). Towards better understanding of an industrial cell factory: investigating the feasibility of real-time metabolic flux analysis in *Pichia pastoris*. *Microb. Cell Fact.* 12:51. doi: 10.1186/1475-2859-12-51

Fernandes, B. D., Mota, A., Teixeira, J. A., and Vicente, A. A. (2015). Continuous cultivation of photosynthetic microorganisms: approaches, applications and future trends. *Biotechnol. Adv.* 33, 1228–1245. doi: 10.1016/j.biotechadv.2015.03.004

Ferrer, P., and Albiol, J. (2014a). "13C-based metabolic flux analysis in yeast: the *Pichia pastoris* case," in *Methods in Molecular Biology*, ed V. Mapelli (New York, NY: Humana Press Inc.), 209–232. doi: 10.1007/978-1-4939-0563-8_13

Ferrer, P., and Albiol, J. (2014b). "13C-Based metabolic flux analysis of recombinant *Pichia pastoris*," in *Metabolic Flux Analysis*, eds J. O. Krömer, L. K. Nielsen, and L. M. Blank (New York, NY: Humana Press Inc.), 291–313. doi: 10.1007/978-1-4939-1170-7_17

Fong, S. S. (2014). Computational approaches to metabolic engineering utilizing systems biology and synthetic biology. *Comput. Struct. Biotechnol. J.* 11, 28–34. doi: 10.1016/j.csbj.2014.08.005

Garcia-Ortega, X., Adelantado, N., Ferrer, P., Montesinos, J. L., and Valero, F. (2016). A step forward to improve recombinant protein production in *Pichia pastoris*: from specific growth rate effect on protein secretion to carbon-starving conditions as advanced strategy. *Process Biochem.* 51, 681–691. doi: 10.1016/j.procbio.2016.02.018

García-Ortega, X., Cámara, E., Ferrer, P., Albiol, J., Montesinos-Seguí, J. L., and Valero, F. (2019). Rational development of bioprocess engineering strategies for recombinant protein production in *Pichia pastoris* (*Komagataella phaffi*) using the methanol free GAP promoter. Where do we stand? *N. Biotechnol.* 53, 24–34. doi: 10.1016/j.nbt.2019.06.002

Garcia-Ortega, X., Ferrer, P., Montesinos, J. L., and Valero, F. (2013). Fed-batch operational strategies for recombinant Fab production with *Pichia pastoris* using the constitutive GAP promoter. *Biochem. Eng. J.* 79, 172–181. doi: 10.1016/j.bej.2013.07.013

Garcia-Ortega, X., Valero, F., and Montesinos-Seguí, J. L. (2017). Physiological state as transferable operating criterion to improve recombinant protein production in *Pichia pastoris* through oxygen limitation. *J. Chem. Technol. Biotechnol.* 92, 2573–2582. doi: 10.1002/jctb.5272

Garrigós-Martínez, J., Nieto-Taype, M. A., Gasset, A., Montesinos-Seguí, J. L., Garcia-Ortega, X., and Valero, F. (2019). Specific growth rate governs AOX1 gene expression, affecting the production kinetics of *Pichia pastoris* (*Komogataella phaffii*) PAOX1-driven recombinant producer strains with different target gene dosage. *Microb. Cell Fact.* 181:87. doi: 10.1186/s12934-019-1240-8

Gasser, B., and Mattanovich, D. (2018). A yeast for all seasons – is *Pichia pastoris* a suitable chassis organism for future bioproduction? *FEMS Microbiol. Lett.* 365:181. doi: 10.1093/femsle/fny181

Gasser, B., Maurer, M., Rautio, J., Sauer, M., Bhattacharyya, A., Saloheimo, M., et al. (2007). Monitoring of transcriptional regulation in *Pichia pastoris* under protein production conditions. *BMC Genomics* 8:179. doi: 10.1186/1471-2164-8-179

Gasser, B., Prielhofer, R., Marx, H., Maurer, M., Nocon, J., Steiger, M., et al. (2013). *Pichia pastoris*: protein production host and model organism for biomedical research. *Future Microbiol.* 8, 191–208. doi: 10.2217/fmb.12.133

Gerritzen, M. J. H., Maas, R. H. W., Van Den Ijssel, J., Van Keulen, L., Martens, D. E., Wijffels, R. H., et al. (2018). High dissolved oxygen tension triggers outer membrane vesicle formation by *Neisseria meningitidis*. *Microb. Cell Fact.* 17:157. doi: 10.1186/s12934-018-1007-7

Graf, A., Dragosits, M., Gasser, B., and Mattanovich, D. (2009). Yeast systems biotechnology for the production of heterologous proteins. *FEMS Yeast Res.* 9, 335–348. doi: 10.1111/j.1567-1364.2009.00507.x

Graf, A., Gasser, B., Dragosits, M., Sauer, M., Leparc, G. G., Tüchler, T., et al. (2008). Novel insights into the unfolded protein response using *Pichia pastoris* specific DNA microarrays. *BMC Genomics* 9:390. doi: 10.1186/1471-2164-9-390

Gramelsberger, G. (2018). Continuous culture techniques as simulators for standard cells: Jacques Monod's, Aron Novick's and Leo Szilard's quantitative approach to microbiology. *Hist. Philos. Life Sci.* 40:23. doi: 10.1007/s40656-017-0182-x

Gresham, D., and Dunham, M. J. (2014). The enduring utility of continuous culturing in experimental evolution. *Genomics* 104, 399–405. doi: 10.1016/j.ygeno.2014.09.015

Herbert, D. (1961). "A theoretical analysis of continuous culture systems," in *Continuous Culture of Microorganisms, Microbiology Group Symposium Papers*, eds D. W. Henderson, J. J. H. Hastings, B. A. Southgate, and P. W. Brian (London: Society of Chemical Industry; University College), 51–53.

Hernandez, R. (2015). Continuous manufacturing: a changing processing paradigm. *BioPharm Int.* 28, 20–41.

Hesketh, A. R., Castrillo, J. I., Sawyer, T., Archer, D. B., and Oliver, S. G. (2013). Investigating the physiological response of Pichia (Komagataella) pastoris GS115 to the heterologous expression of misfolded proteins using chemostat cultures. *Appl. Microbiol. Biotechnol.* 97, 9747–9762. doi: 10.1007/s00253-013-5186-1

Heyland, J., Fu, J., Blank, L. M., and Schmid, A. (2010). Quantitative physiology of *Pichia pastoris* during glucose-limited high-cell density fed-batch cultivation for recombinant protein production. *Biotechnol. Bioeng.* 107, 357–368. doi: 10.1002/bit.22836

Heyland, J., Fu, J., Blank, L. M., and Schmid, A. (2011). Carbon metabolism limits recombinant protein production in *Pichia pastoris*. *Biotechnol. Bioeng.* 108, 1942–1953. doi: 10.1002/bit.23114

Hoekema, S., Rinzema, A., Tramper, J., Wijffels, R. H., and Janssen, M. (2014). Deceleration-stats save much time during phototrophic culture optimization. *Biotechnol. Bioeng.* 111, 792–802. doi: 10.1002/bit.25131

Hoskisson, P. A., and Hobbs, G. (2005). Continuous culture - making a comeback? *Microbiology* 151, 3153–3159. doi: 10.1099/mic.0.27924-0

Jordà, J., De Jesus, S. S., Peltier, S., Ferrer, P., and Albiol, J. (2014a). Metabolic flux analysis of recombinant *Pichia pastoris* growing on different glycerol/methanol mixtures by iterative fitting of NMR-derived 13C-labelling data from proteinogenic amino acids. *N. Biotechnol.* 31, 120–132. doi: 10.1016/j.nbt.2013.06.007

Jordà, J., Jouhten, P., Cámara, E., Maaheimo, H., Albiol, J., and Ferrer, P. (2012). Metabolic flux profiling of recombinant protein secreting *Pichia pastoris* growing on glucose: methanol mixtures. *Microb. Cell Fact.* 11:57. doi: 10.1186/1475-2859-11-57

Jordà, J., Rojas, H. C., Carnicer, M., Wahl, A., Ferrer, P., and Albiol, J. (2014b). Quantitative metabolomics and instationary 13C-metabolic flux analysis reveals impact of recombinant protein production on trehalose and energy metabolism in *Pichia pastoris*. *Metabolites* 4, 281–299. doi: 10.3390/metabo4020281

Jungo, C., Marison, I., and von Stockar, U. (2007a). Mixed feeds of glycerol and methanol can improve the performance of *Pichia pastoris* cultures: a quantitative study based on concentration gradients in transient continuous cultures. *J. Biotechnol.* 128, 824–837. doi: 10.1016/j.jbiotec.2006.12.024

Jungo, C., Rérat, C., Marison, I. W., and von Stockar, U. (2006). Quantitative characterization of the regulation of the synthesis of alcohol oxidase and of the expression of recombinant avidin in a *Pichia pastoris* Mut+ strain. *Enzyme Microb. Technol.* 39, 936–944. doi: 10.1016/j.enzmictec.2006.01.027

Jungo, C., Schenk, J., Pasquier, M., Marison, I. W., and von Stockar, U. (2007c). A quantitative analysis of the benefits of mixed feeds of sorbitol and methanol for the production of recombinant avidin with *Pichia pastoris*. *J. Biotechnol.* 131, 57–66. doi: 10.1016/j.jbiotec.2007.05.019

Jungo, C., Urfer, J., Zocchi, A., Marison, I., and von Stockar, U. (2007b). Optimisation of culture conditions with respect to biotin requirement for the production of recombinant avidin in *Pichia pastoris*. *J. Biotechnol.* 127, 703–715. doi: 10.1016/j.jbiotec.2006.08.001

Juturu, V., and Wu, J. C. (2018). Heterologous protein expression in *Pichia pastoris*: latest research progress and applications. *ChemBioChem* 19, 7–21. doi: 10.1002/cbic.201700460

Kasemets, K., Drews, M., Nisamedtinov, I., Adamberg, K., and Paalme, T. (2003). Modification of A-stat for the characterization of microorganisms. *J. Microbiol. Methods* 55, 187–200. doi: 10.1016/S0167-7012(03)00143-X

Khasa, Y. P., Khushoo, A., Srivastava, L., and Mukherjee, K. J. (2007). Kinetic studies of constitutive human granulocyte-macrophage colony stimulating factor (hGM-CSF) expression in continuous culture of *Pichia pastoris*. *Biotechnol. Lett.* 29, 1903–1908. doi: 10.1007/s10529-007-9473-8

King, Z. A., Lu, J., Dräger, A., Miller, P., Federowicz, S., Lerman, J. A., et al. (2016). BiGG models: a platform for integrating, standardizing and sharing genome-scale models. *Nucleic Acids Res.* 44, D515–D522. doi: 10.1093/nar/gkv1049

Landes, N., Gasser, B., Vorauer-Uhl, K., Lhota, G., Mattanovich, D., and Maurer, M. (2016). The vitamin-sensitive promoter PTHI11 enables pre-defined autonomous induction of recombinant protein production in *Pichia pastoris*. *Biotechnol. Bioeng.* 113, 2633–2643. doi: 10.1002/bit.26041

Lee, J. Y., Chen, H., Liu, A., Alba, B. M., and Lim, A. C. (2017). Auto-induction of *Pichia pastoris* AOX1 promoter for membrane protein expression. *Protein Expr. Purif.* 137, 7–12. doi: 10.1016/j.pep.2017.06.006

Lin, X. Q., Liang, S. L., Han, S. Y., Zheng, S. P., Ye, Y. R., and Lin, Y. (2013). Quantitative iTRAQ LC-MS/MS proteomics reveals the cellular response to heterologous protein overexpression and the regulation of HAC1 in *Pichia pastoris*. *J. Proteomics* 91, 58–72. doi: 10.1016/j.jprot.2013.06.031

Liu, Z., Hou, J., Martínez, J. L., Petranovic, D., and Nielsen, J. (2013). Correlation of cell growth and heterologous protein production by *Saccharomyces cerevisiae*. *Appl. Microbiol. Biotechnol.* 97, 8955–8962. doi: 10.1007/s00253-013-4715-2

Looser, V., Bruhlmann, B., Bumbak, F., Stenger, C., Costa, M., Camattari, A., et al. (2015). Cultivation strategies to enhance productivity of *Pichia pastoris*: a review. *Biotechnol. Adv.* 33, 1177–1193. doi: 10.1016/j.biotechadv.2015.05.008

Lu, P., Vogel, C., Wang, R., Yao, X., and Marcotte, E. M. (2007). Absolute protein expression profiling estimates the relative contributions of transcriptional and translational regulation. *Nat. Biotechnol.* 25, 117–124. doi: 10.1038/nbt1270

Maccani, A., Landes, N., Stadlmayr, G., Maresch, D., Leitner, C., Maurer, M., et al. (2014). *Pichia pastoris* secretes recombinant proteins less efficiently than Chinese hamster ovary cells but allows higher space-time yields for less complex proteins. *Biotechnol. J.* 9, 526–537. doi: 10.1002/biot.201300305

Massahi, A., and Çalik, P. (2018). Naturally occurring novel promoters around pyruvate branch-point for recombinant protein production in *Pichia pastoris* (*Komagataella phaffii*): pyruvate decarboxylase- and pyruvate kinase-promoters. *Biochem. Eng. J.* 138, 111–120. doi: 10.1016/j.bej.2018.07.012

Mattanovich, D., Gasser, B., Hohenblum, H., and Sauer, M. (2004). Stress in recombinant protein producing yeasts. *J. Biotechnol.* 113, 121–135. doi: 10.1016/j.jbiotec.2004.04.035

Maurer, M., Kühleitner, M., Gasser, B., and Mattanovich, D. (2006). Versatile modeling and optimization of fed batch processes for the production of secreted heterologous proteins with *Pichia pastoris*. *Microb. Cell Fact.* 5:37. doi: 10.1186/1475-2859-5-37

McGeachy, A. M., Meacham, Z. A., and Ingolia, N. T. (2019). An accessible continuous-culture turbidostat for pooled analysis of complex libraries. *ACS Synth. Biol.* 8, 844–856. doi: 10.1021/acssynbio.8b00529

Mears, L., Feldman, H., Falco, F. C., Bach, C., Wu, M., Nørregaard, A., et al. (2017). "Continuous fermentation for biopharmaceuticals?," in *Continuous Manufacturing of Pharmaceuticals*, eds P. Kleinebudde J. Khinast, and J. Rantanen (Chichester: John Wiley & Sons, Ltd), 227–246.

Monod, J. (1950). La technique de culture continue, theorie et applications. *Ann. l'Institut Pasteur* 79, 390–410.

Moser, J. W., Prielhofer, R., Gerner, S. M., Graf, A. B., Wilson, I. B. H., Mattanovich, D., et al. (2017). Implications of evolutionary engineering for growth and recombinant protein production in methanol-based growth media in the yeast *Pichia pastoris*. *Microb. Cell Fact.* 16:49. doi: 10.1186/s12934-017-0661-5

Nahku, R., Valgepea, K., Lahtvee, P.-J., Erm, S., Abner, K., Adamberg, K., et al. (2010). Specific growth rate dependent transcriptome profiling of *Escherichia coli* K12 MG1655 in accelerostat cultures. *J. Biotechnol.* 145, 60–65. doi: 10.1016/j.jbiotec.2009.10.007

Nieto-Taype, M. A., Garrigós-Martínez, J., Sánchez-Farrando, M., Valero, F., Garcia-Ortega, X., and Montesinos-Seguí, J. L. (2020). Rationale-based selection of optimal operating strategies and gene dosage impact on recombinant protein production in *Komogataella phaffii* (*Pichia pastoris*). *Microb. Biotechnol.* 13, 315–327. doi: 10.1111/1751-7915.13498

Nisamedtinov, I., Lindsey, G. G., Karreman, R., Orumets, K., Koplimaa, M., Kevvai, K., et al. (2008). The response of the yeast *Saccharomyces cerevisiae* to sudden vs. gradual changes in environmental stress monitored by expression of the stress response protein Hsp12p. *FEMS Yeast Res.* 8, 829–838. doi: 10.1111/j.1567-1364.2008.00391.x

Niu, H., Jost, L., Pirlot, N., Sassi, H., Daukandt, M., Rodriguez, C., et al. (2013). A quantitative study of methanol/sorbitol co-feeding process of a *Pichia pastoris* Mut+/pAOX1-lacZ strain. *Microb. Cell Fact.* 12:33. doi: 10.1186/1475-2859-12-33

Nocon, J., Steiger, M., Mairinger, T., Hohlweg, J., Rußmayer, H., Hann, S., et al. (2016). Increasing pentose phosphate pathway flux enhances recombinant protein production in *Pichia pastoris*. *Appl. Microbiol. Biotechnol.* 100, 5955–5963. doi: 10.1007/s00253-016-7363-5

Nocon, J., Steiger, M. G., Pfeffer, M., Sohn, S. B., Kim, T. Y., Maurer, M., et al. (2014). Model based engineering of *Pichia pastoris* central metabolism enhances recombinant protein production. *Metab. Eng.* 24, 129–138. doi: 10.1016/j.ymben.2014.05.011

Paulová, L., Hyka, P., Branská, B., Melzoch, K., and Kovar, K. (2012). Use of a mixture of glucose and methanol as substrates for the production of recombinant trypsinogen in continuous cultures with *Pichia pastoris* Mut+. *J. Biotechnol.* 157, 180–188. doi: 10.1016/j.jbiotec.2011.10.010

Peebo, K., and Neubauer, P. (2018). Application of continuous culture methods to recombinant protein production in microorganisms. *Microorganisms* 6:56. doi: 10.3390/microorganisms6030056

Peña, D. A., Gasser, B., Zanghellini, J., Steiger, M. G., and Mattanovich, D. (2018). Metabolic engineering of *Pichia pastoris*. *Metab. Eng.* 50, 2–15. doi: 10.1016/j.ymben.2018.04.017

Periyasamy, S., Govindappa, N., Sreenivas, S., and Sastry, K. (2013). Isolation, characterization and evaluation of the *Pichia pastoris* sorbitol dehydrogenase promoter for expression of heterologous proteins. *Protein Expr. Purif.* 92, 128–133. doi: 10.1016/j.pep.2013.09.008

Pfeffer, M., Maurer, M., Stadlmann, J., Grass, J., Delic, M., Altmann, F., et al. (2012). Intracellular interactome of secreted antibody Fab fragment in *Pichia pastoris* reveals its routes of secretion and degradation. *Appl. Microbiol. Biotechnol.* 93, 2503–2512. doi: 10.1007/s00253-012-3933-3

Ponte, X., Barrigón, J. M., Maurer, M., Mattanovich, D., Valero, F., and Montesinos-Seguí, J. L. (2018). Towards optimal substrate feeding for heterologous protein production in *Pichia pastoris* (*Komagataella* spp) fed-batch processes under PAOX1 control: a modelling aided approach. *J. Chem. Technol. Biotechnol.* 93, 3208–3218. doi: 10.1002/jctb.5677

Ponte, X., Montesinos-Seguí, J. L., and Valero, F. (2016). Bioprocess efficiency in *Rhizopus oryzae* lipase production by *Pichia pastoris* under the control of PAOX1 is oxygen tension dependent. *Process Biochem.* 51, 1954–1963. doi: 10.1016/j.procbio.2016.08.030

Porro, D., Gasser, B., Fossati, T., Maurer, M., Branduardi, P., Sauer, M., et al. (2011). Production of recombinant proteins and metabolites in yeasts: when are these systems better than bacterial production systems? *Appl. Microbiol. Biotechnol.* 89, 939–948. doi: 10.1007/s00253-010-3019-z

Potvin, G., Ahmad, A., and Zhang, Z. (2012). Bioprocess engineering aspects of heterologous protein production in *Pichia pastoris*: a review. *Biochem. Eng. J.* 64, 91–105. doi: 10.1016/j.bej.2010.07.017

Prielhofer, R., Maurer, M., Klein, J., Wenger, J., Kiziak, C., Gasser, B., et al. (2013). Induction without methanol: novel regulated promoters enable high-level expression in *Pichia pastoris*. *Microb. Cell Fact.* 12:5. doi: 10.1186/1475-2859-12-5

Prielhofer, R., Reichinger, M., Wagner, N., Claes, K., Kiziak, C., Gasser, B., et al. (2018). Superior protein titers in half the fermentation time: promoter and process engineering for the glucose-regulated GTH1 promoter of *Pichia pastoris*. *Biotechnol. Bioeng.* 115, 2479–2488. doi: 10.1002/bit.26800

Puxbaum, V., Mattanovich, D., and Gasser, B. (2015). Quo vadis? The challenges of recombinant protein folding and secretion in *Pichia pastoris*. *Appl. Microbiol. Biotechnol.* 99, 2925–2938. doi: 10.1007/s00253-015-6470-z

Rahimi, A., Hosseini, S. N., Karimi, A., Aghdasinia, H., and Arabi Mianroodi, R. (2019). Enhancing the efficiency of recombinant hepatitis B surface antigen production in *Pichia pastoris* by employing continuous fermentation. *Biochem. Eng. J.* 141, 112–119. doi: 10.1016/j.bej.2018.10.019

Rajamanickam, V., Herwig, C., and Spadiut, O. (2018). Data science, modeling, and advanced PAT tools enable continuous culture. *Bioprocess Int.* 16, 20–25.

Randek, J., and Mandenius, C.-F. (2018). On-line soft sensing in upstream bioprocessing. *Crit. Rev. Biotechnol.* 38, 106–121. doi: 10.1080/07388551.2017.1312271

Rathore, A. S., Agarwal, H., Sharma, A. K., Pathak, M., and Muthukumar, S. (2015). Continuous processing for production of biopharmaceuticals. *Prep. Biochem. Biotechnol.* 45, 836–849. doi: 10.1080/10826068.2014.985834

Rebnegger, C., Graf, A. B., Valli, M., Steiger, M. G., Gasser, B., Maurer, M., et al. (2014). In *Pichia pastoris*, growth rate regulates protein synthesis and secretion, mating and stress response. *Biotechnol. J.* 9, 511–525. doi: 10.1002/biot.201300334

Rebnegger, C., Vos, T., Graf, A. B., Valli, M., Pronk, J. T., Daran-Lapujade, P., et al. (2016). *Pichia pastoris* exhibits high viability and a low maintenance energy requirement at near-zero specific growth rates. *Appl. Environ. Microbiol.* 82, 4570–4583. doi: 10.1128/AEM.00638-16

Rossignol, T., Kobi, D., Jacquet-Gutfreund, L., and Blondin, B. (2009). The proteome of a wine yeast strain during fermentation, correlation with the transcriptome. *J. Appl. Microbiol.* 107, 47–55. doi: 10.1111/j.1365-2672.2009.04156.x

Rußmayer, H., Buchetics, M., Gruber, C., Valli, M., Grillitsch, K., Modarres, G., et al. (2015). Systems-level organization of yeast methylotrophic lifestyle. *BMC Biol.* 13:80. doi: 10.1186/s12915-015-0186-5

Sanchez-Garcia, L., Martín, L., Mangues, R., Ferrer-Miralles, N., Vázquez, E., and Villaverde, A. (2016). Recombinant pharmaceuticals from microbial cells: a 2015 update. *Microb. Cell Fact.* 15:33. doi: 10.1186/s12934-016-0437-3

Schwarzhans, J.-P., Wibberg, D., Winkler, A., Luttermann, T., Kalinowski, J., and Friehs, K. (2016). Integration event induced changes in recombinant protein productivity in *Pichia pastoris* discovered by whole genome sequencing and derived vector optimization. *Microb. Cell Fact.* 15:84. doi: 10.1186/s12934-016-0486-7

Shi, X., Karkut, T., Chamankhah, M., Alting-Mees, M., Hemmingsen, S. M., and Hegedus, D. (2003). Optimal conditions for the expression of a single-chain antibody (scFv) gene in *Pichia pastoris*. *Protein Expr. Purif.* 28, 321–330. doi: 10.1016/S1046-5928(02)00706-4

Singh, R., Kumar, M., Mittal, A., and Mehta, P. K. (2017). Microbial metabolites in nutrition, healthcare and agriculture. *3 Biotech* 7:15. doi: 10.1007/s13205-016-0586-4

Sinha, J., Plantz, B. A., Inan, M., and Meagher, M. M. (2005). Causes of proteolytic degradation of secreted recombinant proteins produced in methylotrophic yeast *Pichia pastoris*: case study with recombinant ovine interferon-? *Biotechnol. Bioeng.* 89, 102–112. doi: 10.1002/bit.20318

Sirén, N., Weegar, J., Dahlbacka, J., Kalkkinen, N., Fagervik, K., Leisola, M., et al. (2006). Production of recombinant HIV-1 Nef (negative factor) protein using *Pichia pastoris* and a low-temperature fed-batch strategy. *Biotechnol. Appl. Biochem.* 44:151. doi: 10.1042/BA20060001

Sohn, S. B., Graf, A. B., Kim, T. Y., Gasser, B., Maurer, M., Ferrer, P., et al. (2010). Genome-scale metabolic model of methylotrophic yeast *Pichia pastoris* and its

use for *in silico* analysis of heterologous protein production. *Biotechnol. J.* 5, 705–715. doi: 10.1002/biot.201000078

Sørensen, H. P. (2010). Towards universal systems for recombinant gene expression. *Microb. Cell Fact.* 9:27. doi: 10.1186/1475-2859-9-27

Spadiut, O., Rittmann, S., Dietzsch, C., and Herwig, C. (2013). Dynamic process conditions in bioprocess development. *Eng. Life Sci.* 13, 88–101. doi: 10.1002/elsc.201200026

Sreekrishna, K. (2010). "Pichia, optimization of protein expression," in *Encyclopedia of Industrial Biotechnology*, ed M. C. Flickinger (Hoboken, NJ: John Wiley & Sons, Inc.), 16.

Subramanian, G., Erm, S., Abner, K., Seiman, A., Adamberg, K., and Vilu, R. (2017). "Study of cells in the steady-state growth space," in *Continuous Biomanufacturing - Innovative Technologies and Methods*, ed G. Subramanian (Weinheim: Wiley-VCH Verlag GmbH & Co. KGaA), 233–258.

Surribas, A., Stahn, R., Montesinos, J. L., Enfors, S.-O., Valero, F., and Jahic, M. (2007). Production of a *Rhizopus oryzae* lipase from *Pichia pastoris* using alternative operational strategies. *J. Biotechnol.* 130, 291–299. doi: 10.1016/j.jbiotec.2007.04.009

Szopinska, A., and Morsomme, P. (2010). Quantitative proteomic approaches and their application in the study of yeast stress responses. *Omi. A J. Integr. Biol.* 14, 639–649. doi: 10.1089/omi.2010.0045

Tang, S., Potvin, G., Reiche, A., and Zhang, Z. (2010). Modeling of phytase production by cultivation of *Pichia pastoris* under the control of the GAP promoter. *Int. J. Chem. React. Eng.* 8:11. doi: 10.2202/1542-6580.2144

Tomàs-Gamisans, M., Ferrer, P., and Albiol, J. (2018). Fine-tuning the *P. pastoris* iMT1026 genome-scale metabolic model for improved prediction of growth on methanol or glycerol as sole carbon sources. *Microb. Biotechnol.* 11, 224–237. doi: 10.1111/1751-7915.12871

Tomàs-Gamisans, M., Ødum, A. S. R., Workman, M., Ferrer, P., and Albiol, J. (2019). Glycerol metabolism of *Pichia pastoris* (*Komagataella* spp.) characterised by 13C-based metabolic flux analysis. *N. Biotechnol.* 50, 52–59. doi: 10.1016/j.nbt.2019.01.005

Tomson, K., Barber, J., and Vanatalu, K. (2006). Adaptastat—a new method for optimising of bacterial growth conditions in continuous culture: interactive substrate limitation based on dissolved oxygen measurement. *J. Microbiol. Methods* 64, 380–390. doi: 10.1016/j.mimet.2005.05.014

Valero, F., and López-Santín, J. (2017). "Online analysis for industrial bioprocesses: gas analysis" in *Current Developments in Biotechnology and Bioengineering*, eds Ch. Larroche, M. A. Sanromán, G. Du, and A. Pandey (Amsterdam: Elsevier), 649–678. doi: 10.1016/B978-0-444-63663-8.00022-7

van Hove, B., Love, A. M., Ajikumar, P. K., and De Mey, M. (2016). "Programming biology: expanding the toolset for the engineering of transcription," in *Synthetic Biology*, eds A. Glieder, Ch. P. Kubicek, D. Mattanovich, B. Wiltschi, and M. Sauer (Cham: Springer International Publishing), 1–64.

Vanz, A. L., Lünsdorf, H., Adnan, A., Nimtz, M., Gurramkonda, C., Khanna, N., et al. (2012). Physiological response of *Pichia pastoris* GS115 to methanol-induced high level production of the hepatitis B surface antigen: catabolic adaptation, stress responses, and autophagic processes. *Microb. Cell Fact.* 11:103. doi: 10.1186/1475-2859-11-103

Vanz, A. L., Nimtz, M., and Rinas, U. (2014). Decrease of UPR- and ERAD-related proteins in *Pichia pastoris* during methanol-induced secretory insulin precursor production in controlled fed-batch cultures. *Microb. Cell Fact.* 13, 1–10. doi: 10.1186/1475-2859-13-23

Veloso, A. C., and Ferreira, E. C. (2017). "Online analysis for industrial bioprocesses: broth analysis" in *Current Developments in Biotechnology and Bioengineering*, eds Ch. Larroche, M. A. Sanromán, G. Du, and A. Pandey (Amsterdam: Elsevier), 679–704. doi: 10.1016/B978-0-444-63663-8.00023-9

Vieira Gomes, A., Souza Carmo, T., Silva Carvalho, L., Mendonça Bahia, F., and Parachin, N. (2018). Comparison of yeasts as hosts for recombinant protein production. *Microorganisms* 6:38. doi: 10.3390/microorganisms6020038

Vogel, C., De Sousa Abreu, R., Ko, D., Le, S.-Y., Shapiro, B. A., Burns, S. C., et al. (2010). Sequence signatures and mRNA concentration can explain two-thirds of protein abundance variation in a human cell line. *Mol. Syst. Biol.* 6:400. doi: 10.1038/msb.2010.59

Vogl, T., Gebbie, L., Palfreyman, R. W., and Speight, R. (2018a). Effect of plasmid design and type of integration event on recombinant protein expression in *Pichia pastoris*. *Appl. Environ. Microbiol.* 84, e02712–e02717. doi: 10.1128/AEM.02712-17

Vogl, T., and Glieder, A. (2013). Regulation of *Pichia pastoris* promoters and its consequences for protein production. *N. Biotechnol.* 30, 385–404. doi: 10.1016/j.nbt.2012.11.010

Vogl, T., Sturmberger, L., Fauland, P. C., Hyden, P., Fischer, J. E., Schmid, C., et al. (2018b). Methanol independent induction in *Pichia pastoris* by simple derepressed overexpression of single transcription factors. *Biotechnol. Bioeng.* 115, 1037–1050. doi: 10.1002/bit.26529

Vos, T., de la Torre Cortés, P., van Gulik, W. M., Pronk, J. T., and Daran-Lapujade, P. (2015). Growth-rate dependency of de novo resveratrol production in chemostat cultures of an engineered *Saccharomyces cerevisiae* strain. *Microb. Cell Fact.* 14:133. doi: 10.1186/s12934-015-0321-6

Wagenen, J., Van Pape, M. L., and Angelidaki, I. (2015). Characterization of nutrient removal and microalgal biomass production on an industrial waste-stream by application of the deceleration-stat technique. *Water Res.* 75, 301–311. doi: 10.1016/j.watres.2015.02.022

Wagner, J. M., and Alper, H. S. (2016). Synthetic biology and molecular genetics in non-conventional yeasts: current tools and future advances. *Fungal Genet. Biol.* 89, 126–136. doi: 10.1016/j.fgb.2015.12.001

Wang, H., Li, J., Liu, L., Li, X., Jia, D., Du, G., et al. (2012). Increased production of alkaline polygalacturonate lyase in the recombinant *Pichia pastoris* by controlling cell concentration during continuous culture. *Bioresour. Technol.* 124, 338–346. doi: 10.1016/j.biortech.2012.08.027

Wang, J., Wang, X., Shi, L., Qi, F., Zhang, P., Zhang, Y., et al. (2017). Methanol-independent protein expression by AOX1 promoter with trans-acting elements engineering and glucose-glycerol-shift induction in *Pichia pastoris*. *Sci. Rep.* 7:41850. doi: 10.1038/srep41850

Weninger, A., Fischer, J. E., Raschmanová, H., Kniely, C., Vogl, T., and Glieder, A. (2018). Expanding the CRISPR/Cas9 toolkit for *Pichia pastoris* with efficient donor integration and alternative resistance markers. *J. Cell. Biochem.* 119, 3183–3198. doi: 10.1002/jcb.26474

Yamawaki, S., Matsumoto, T., Ohnishi, Y., Kumada, Y., Shiomi, N., Katsuda, T., et al. (2007). Production of single-chain variable fragment antibody (scFv) in fed-batch and continuous culture of *Pichia pastoris* by two different methanol feeding methods. *J. Biosci. Bioeng.* 104, 403–407. doi: 10.1263/jbb.104.403

Yang, Z., and Zhang, Z. (2018). Engineering strategies for enhanced production of protein and bio-products in *Pichia pastoris*: a review. *Biotechnol. Adv.* 36, 182–195. doi: 10.1016/j.biotechadv.2017.11.002

Ye, R., Huang, M., Lu, H., Qian, J., Lin, W., Chu, J., et al. (2017). Comprehensive reconstruction and evaluation of *Pichia pastoris* genome-scale metabolic model that accounts for 1243 ORFs. *Bioresour. Bioprocess.* 4:22. doi: 10.1186/s40643-017-0152-x

Zahrl, R. J., Mattanovich, D., and Gasser, B. (2018). The impact of ERAD on recombinant protein secretion in *Pichia pastoris* (Syn *Komagataella* spp.). *Microbiology* 164, 453–463. doi: 10.1099/mic.0.000630

Zahrl, R. J., Peña, D. A., Mattanovich, D., and Gasser, B. (2017). Systems biotechnology for protein production in *Pichia pastoris*. *FEMS Yeast Res.* 17:fox068. doi: 10.1093/femsyr/fox068

Zhang, W., Sinha, J., Smith, L. A., Inan, M., and Meagher, M. M. (2005). Maximization of production of secreted recombinant proteins in *Pichia pastoris* fed-batch fermentation. *Biotechnol. Prog.* 21, 386–393. doi: 10.1021/bp049811n

Zhou, X.-S., and Zhang, Y.-X. (2002). Decrease of proteolytic degradation of recombinant hirudin produced by *Pichia pastoris* by controlling the specific growth rate. *Biotechnol. Lett.* 24, 1449–1453. doi: 10.1023/A:1019831406141

Ziv, N., Brandt, N. J., and Gresham, D. (2013). The use of chemostats in microbial systems biology. *J. Vis. Exp.* 80:50168. doi: 10.3791/50168

Conflict of Interest: The authors declare that the research was conducted in the absence of any commercial or financial relationships that could be construed as a potential conflict of interest.

Advantages of publishing in Frontiers

OPEN ACCESS
Articles are free to read for greatest visibility and readership

FAST PUBLICATION
Around 90 days from submission to decision

HIGH QUALITY PEER-REVIEW
Rigorous, collaborative, and constructive peer-review

TRANSPARENT PEER-REVIEW
Editors and reviewers acknowledged by name on published articles

Frontiers
Avenue du Tribunal-Fédéral 34
1005 Lausanne | Switzerland

Visit us: www.frontiersin.org
Contact us: frontiersin.org/about/contact

REPRODUCIBILITY OF RESEARCH
Support open data and methods to enhance research reproducibility

DIGITAL PUBLISHING
Articles designed for optimal readership across devices

FOLLOW US
@frontiersin

IMPACT METRICS
Advanced article metrics track visibility across digital media

EXTENSIVE PROMOTION
Marketing and promotion of impactful research

LOOP RESEARCH NETWORK
Our network increases your article's readership